The velvet protein Vel1 controls initial plant root colonization and conidia formation for xylem distribution in Verticillium wilt

Dissertation
For the award of the degree
“Doctor rerum naturalium”
of the Georg-August-Universität Göttingen

within the doctoral program
“Genes and Development”
of the Georg-August University School of Science (GAUSS)

submitted by
Annalena Maria Höfer
from Duderstadt

October 2020

Thesis Committee and Members of the Examination Board

Referee: **Prof. Dr. Gerhard Braus**
Department of Molecular Microbiology and Genetics
Georg-August-Universität Göttingen

2nd referee: **Prof. Dr. Andrea Polle**
Department of Forest Botany and Tree Physiology
Georg-August-Universität Göttingen

3rd referee: **Prof. Dr. Rolf Daniel**
Department of Genomic and Applied Microbiology
Georg-August-Universität Göttingen

Prof. Dr. Stefanie Pöggeler
Department of Genetics of Eukaryotic Microorganisms
Georg-August-Universität Göttingen

Prof. Dr. Kai Heimel
Department of Molecular Microbiology and Genetics
Georg-August-Universität Göttingen

PD Dr. Michael Hoppert
Department of General Microbiology
Georg-August-Universität Göttingen

Date of oral examination: 8th January 2021

Declaration of Independence:

Herewith I declare that the dissertation entitled “The velvet protein Vel1 controls initial plant root colonization and conidia formation for xylem distribution in Verticillium wilt*”* was written on my own and independently without any other aids and sources than indicated.

Annalena Maria Höfer

Göttingen, 2020

This work was accomplished in the group of Prof. Dr. Gerhard H. Braus, at the Department of Molecular Microbiology and Genetics at the Institute of Microbiology and Genetics, Georg-August-Universität Göttingen.

Parts of this work are published in:

Nesemann K, Braus-Stromeyer SA, Harting R, **Höfer A**, Kusch H, Ambrosio AB, Timpner C, Braus GH. 2018. Fluorescent pseudomonads pursue media-dependent strategies to inhibit growth of pathogenic Verticillium fungi. *Applied Microbiology and Biotechnology* 102: 817-831.

Höfer A, Harting R, Aßmann NF, Gerke J, Schmitt K, Starke J, Bayram Ö, Tran VT, Valerius O, Braus-Stromeyer SA, Braus GH. 2021. The velvet protein Vel1 controls initial plant root colonization and conidia formation for xylem distribution in Verticillium wilt. *PLoS Genetics* **17**: e1009434.

Table of Contents

Summary

The velvet family of regulatory proteins is well-conserved in fungi and links developmental processes and secondary metabolite production. These proteins comprise a velvet domain for DNA binding and dimerization with structural similarity to the Rel homology domain of the mammalian NF-κB transcription factor. Functions of homologs of all velvet domain protein encoding genes in the fungal life cycle were systematically characterized in the plant pathogen *Verticillium dahliae*. These velvet proteins are required in different phases of fungal growth, development, secondary metabolite formation and pathogenicity. The Vel1-Vel2, Vel2-Vos1 and Vel3-Vos1 heterodimers are present during vegetative hyphal growth. Except from Vel3, all velvet proteins additionally interact with other non-velvet proteins. During filamentous growth Vel1, Vel3 and Vos1 are predominately localized to the nucleus. Vel2 is mainly localized to the nucleus but subpopulations are also present in the cytoplasm. The soil-borne *V. dahliae* plant pathogenic fungus is responsible for Verticillium wilt disease of many crops. Fungal diseases in crop plants are an emerging threat for human nutrition in connection with the increasing world population. *Verticillium* spp. start infection by colonizing and invading the roots. One of the major novel findings of this thesis is that the velvet domain protein Vel1 is required for the initial plant root colonization and entry into the host xylem. Inside the plant the fungus forms conidia which are distributed by the sap stream. Together with Vel3, Vel1 promotes conidiation and propagation *in planta*. Germinating conidia colonize the whole host and finally lead to the induction of disease symptoms. Vel1 is needed for disease symptom induction in tomatoes. In the senescent plant, the fungus forms microsclerotia as resting structures in order to survive until the next growing season. Formation of microsclerotia is positively regulated by Vel1 and in a light-dependent manner by Vel2. Vel3 has opposite functions during formation of these resting structures. Microsclerotia contain the pigment melanin. The synthesis of the melanin precursor scytalone and other secondary metabolites is promoted by Vel1 and Vel2 but negatively regulated by Vel3. So far, the function of Vos1 in *V. dahliae* remains ambiguous. Fungicides either harm the environment or are useless once the fungus has entered the plant xylem. Inhibition of fungal growth, conidiation and resting structure formation are strategies to combat the pathogen. Vel1 is the most important among the four *V. dahliae* velvet proteins with a wide variety of functions during all phases of the fungal life cycle *in* as well as *ex planta* making it a potential target to combat the fungus. A combined application with antagonistic bacteria might be a strategy to persistently harm the fungus, because we could show in pilot studies that fluorescent pseudomonads, which have the genomic requirements to produce different secondary metabolites, are able to inhibit conidia germination and growth of the plant pathogen *V. dahliae* in a media-dependent manner.

Zusammenfassung

Die Familie der regulatorischen Velvet-Proteine ist in Pilzen gut konserviert und verbindet Entwicklungsprozesse und die Bildung von Sekundärmetaboliten. Diese Proteine besitzen eine Velvet-Domäne mit strukturellen Ähnlichkeiten zur Rel-Homologie-Domäne des NF-κB-Transkriptionsfaktors von Säugetieren. Diese wird für die Bindung von DNA und Bildung von Proteindimeren benötigt. Alle homologen Velvet-Protein-kodierenden Gene wurden systematisch hinsichtlich ihrer Funktionen im pilzlichen Lebenszyklus des Pflanzenpathogens *Verticillium dahliae* untersucht. Die Velvet-Proteine werden in verschiedenen Phasen des Pilzwachstums, der Entwicklung, der Bildung von Sekundärmetaboliten sowie für die Pathogenität benötigt. Die Heterodimere Vel1-Vel2, Vel2-Vos1 und Vel3-Vos1 kommen während des vegetativen Hyphenwachstums vor. Mit Ausnahme von Vel3 interagieren alle Velvet-Proteine zusätzlich mit Proteinen aus anderen Familien. Während des filamentösen Wachstums sind Vel1, Vel3 und Vos1 hauptsächlich im Zellkern lokalisiert. Vel2 ist überwiegend im Zellkern lokalisiert, Subpopulationen sind aber auch im Zytoplasma vorhanden. Der im Boden persistierende pflanzenpathogene Pilz *V. dahliae* ist für die in zahlreichen Kulturpflanzen vorkommende Verticillium-Welke verantwortlich. Pilzkrankheiten in Kulturpflanzen sind eine aufkommende Bedrohung im Zusammenhang mit der Ernährung der wachsenden Weltbevölkerung. Die Infektion des Wirtes durch *Verticillium* spp. beginnt mit der Kolonisierung und Penetration der Pflanzenwurzel. Eine wichtige neue Erkenntnis dieser Arbeit ist, dass das Velvet-Domänen Protein Vel1 für die initiale Kolonisierung der Pflanzenwurzel und den Eintritt in das Xylem benötigt wird. Innerhalb der Pflanze bildet der Pilz Konidien, die vom Strom des Xylemsafts verteilt werden. Vel1 und Vel3 beeinflussen die Sporenbildung und somit auch die Ausbreitung des Pilzes in der Pflanze. Auskeimende Konidien besiedeln den gesamten Wirt und induzieren schließlich Krankheitssymptome. Vel1 wird für die Induktion von Krankheitssymptomen in Tomatenpflanzen benötigt. In der seneszenten Pflanze bildet der Pilz Mikrosklerotien als Überdauerungsstrukturen um bis zur nächsten Vegetationsperiode zu überleben. Die Mikrosklerotienbildung wird durch Vel1 und abhängig vom Licht auch durch Vel2 positiv reguliert. Im Gegensatz dazu hat Vel3 während der Bildung dieser Überdauerungsstrukturen eine hemmende Wirkung. Mikrosklerotien enthalten das Pigment Melanin. Die Synthese des Melaninvorläufers Scytalon und anderer Sekundärmetabolite wird durch Vel1 und Vel2 positiv beeinflusst, während Vel3 einen gegenteiligen Effekt hat. Die Funktion von Vos1 in *V. dahliae* bleibt unklar. Fungizide sind entweder umweltschädigend oder wirkungslos sobald der Pilz in das Xylem der Pflanze eingedrungen ist. Die Hemmung des Pilzwachstums sowie die Bildung von Sporen und Überdauerungsstrukturen sind geeignete Strategien zur Bekämpfung des Pilzes. Vel1 ist das wichtigste der vier Velvet-Proteine in *V. dahliae* mit einer Vielzahl von Funktionen in den verschiedenen Phasen des pilzlichen Lebenszyklus innerhalb und außerhalb der Pflanze und stellt somit einen potenziellen Angriffspunkt bei der Bekämpfung des Pilzes dar. Eine kombinierte Anwendung mit Bakterien, die das Pilzwachstum hemmen, ist möglicherweise eine geeignete Strategie den Pilz dauerhaft und nachhaltig zu schädigen, denn in ersten Versuchen konnten wir zeigen, dass fluoreszierende Pseudomonaden, die die genomische Voraussetzung haben verschiedene Sekundärmetabolite zu produzieren, die Sporenkeimung und das Pilzwachstum vom Pflanzenpathogen *V. dahliae* abhängig vom Medium verringern.

1 INTRODUCTION

1.1 Plant pathogenic *Verticillium* spp. inducing Verticillium wilt

1.1.1 The genus *Verticillium*

The fungal kingdom includes an omnipresent group of eukaryotic microorganisms with beneficial as well as harmful representatives (Naranjo-Ortiz & Gabaldón, 2019). One large phylum of fungi is the Ascomycota, which comprise an asexual life cycle but sexual propagation is not described for most members (Berlanger & Powelson, 2000; Naranjo-Ortiz & Gabaldón, 2019). Within this phylum different subphyla and classes can be distinguished with *Verticillium* belonging to the class of Sordariomycetes (Fradin & Thomma, 2006; Naranjo-Ortiz & Gabaldón, 2019). Members of the genus *Verticillium* are plant pathogenic and induce Verticillium wilt in a broad range of different host plants. Within this study *V. dahliae* was used as model organism.

In former days, classification of strains was conducted according to the formation of different resting structures, but phylogenetic analysis including genomic data of five *Verticillium* strains revealed that four of them cluster together in one group and just one forms a separate group (Zare *et al.*, 2007; Inderbitzin *et al.*, 2011a). Hence, Inderbitzin and co-workers tried to establish a new taxonomic framework and were able to identify five new *Verticillium* species (Inderbitzin *et al.*, 2011a). In total, a set of ten different *Verticillium* strains was identified with *Verticllium alfalfae*, *Verticillium isaacii*, *Verticillium klebahnii*, *Verticillium nonalfalfae* and *Verticillium zaregamsianum* as newly described species and *Verticillium albo-atrum*, *Verticillium dahliae*, *Verticillium longisporum*, *Verticillium nubilum* and *Verticillium tricorpus* as already known ones.

V. dahliae was first described by Klebahn, is found world-wide in temperate and subtropical regions and has a wide host range with over 200 different hosts as for instance tomato, pepper, eggplant, strawberry, olive, potato and cotton making it the most influential pathogen within the genus *Verticillum* (Klebahn, 1913; Fradin & Thomma, 2006; Klosterman *et al.*, 2009; Inderbitzin *et al.*, 2011a).

Although the haploid stage is most dominant in ascomycetes, *Verticillium* spp. have one exception with *V. longisporum* being the only species which is amphidiploid (Ingram, 1968; Karapapa *et al.*, 1997; Collins *et al.*, 2003; Inderbitzin *et al.*, 2011b; Tran *et al.*, 2013; Depotter *et al.*, 2016). Interestingly, *V. longisporum* arose independently three times by hybridization of four different lineages with three parental species and *V. dahliae* as only known parental strain of two hybridization events (Ingram, 1968; Inderbitzin *et al.*, 2011b). Even though the two mating idiomorphs *MAT1-1* and *MAT1-2* were identified in *V. dahliae*, the fungus may exhibit

just a cryptic sexual stage and *V. longisporum* presumably arose from a parasexual cycle by anastomosis (Klosterman *et al.*, 2009; Short *et al.*, 2014). Microsclerotia and conidia of *V. longisporum* are morphologically similar to *V. dahliae* but longer in comparison to the parental strain (Ingram, 1968; Karapapa *et al.*, 1997; Inderbitzin *et al.*, 2011a). The hybridization event also changed the host range as the amphidiploid strain mainly infects *Brassicaceae* as for example oilseed rape, whereas *V. dahliae* mostly infects dicotyledonous species (Karapapa *et al.*, 1997; Zeise & von Tiedemann, 2002; Fradin & Thomma, 2006; Eynck *et al.*, 2007; Inderbitzin & Subbarao, 2014).

The diverse set of *Verticillium* strains is able to infect a large number of potential host plants and thereby causes a high degree of destroyed crops, which are often economically important crops and high valuable ornamental plants (Fradin & Thomma, 2006; Klosterman *et al.*, 2009; Inderbitzin *et al.*, 2011a; Inderbitzin & Subbarao, 2014). Hence, the economic loss induced by *Verticillium* spp. is severe (EFSA PLH Panel (EFSA Panel on Plant Health), 2014; Depotter *et al.*, 2016). Breeding of resistant cultivars was successful for some crops as for example cotton but was overcome in a few years for others as for instance tomato (Klosterman *et al.*, 2009).

1.1.2 Life cycle of *Verticillium dahliae*

Verticillium wilt occurs once in a growing season, hence it is a monocyclic disease (Fradin & Thomma, 2006; Depotter *et al.*, 2016). The life cycle of *Verticillium* spp. comprises a dormant, biotrophic and necrotrophic phase, which means that the fungus is hemibiotroph (Fradin & Thomma, 2006; Reusche *et al.*, 2012) (Figure 1).

During the dormant phase, microsclerotia of *V. dahliae* remain in the soil (Klosterman *et al.*, 2009) (Figure 1a). As long-term resting structure they can persist there for several years without a suitable host (Wilhelm, 1955). Germination of microsclerotia is inhibited until root exudates of potential hosts are perceived (Berlanger & Powelson, 2000; Fradin & Thomma, 2006; Eynck *et al.*, 2007). If root exudates are present in the rhizosphere, germination starts and hyphae grow towards the potential host plant. One microsclerotium consists of many cells, that are all able to germinate and thereby enhance a successful infection (Fradin & Thomma, 2006; Klosterman *et al.*, 2009).

At the root, *Verticillium* spp. use the tip or sites of lateral root formation for penetration because at these positions the endodermis is not fully developed (Fradin & Thomma, 2006; Klosterman *et al.*, 2009). The endodermis functions as barrier but if it is damaged, for instance by nematodes, the fungus can also penetrate there (Fradin & Thomma, 2006). Invasion takes place by the formation of hyphopodia, which are the swollen tips of hyphae (Reusche *et al.*, 2014; Zhao *et al.*, 2014) (Figure 1b,c). Some plants use structural barriers as a dark gum or cell wall appositions of lignin and lignin tubers to prevent infection (Klosterman *et al.*, 2009). Although a single microsclerotium can germinate several times, in most cases the fungus does

not reach the vascular tissue. Therefore, the position of initial colonization seems to be more important than the number of colonization events (Klosterman *et al.*, 2009). Once inside the plant, the whole root is colonized and the biotrophic phase is established (Figure 1b).

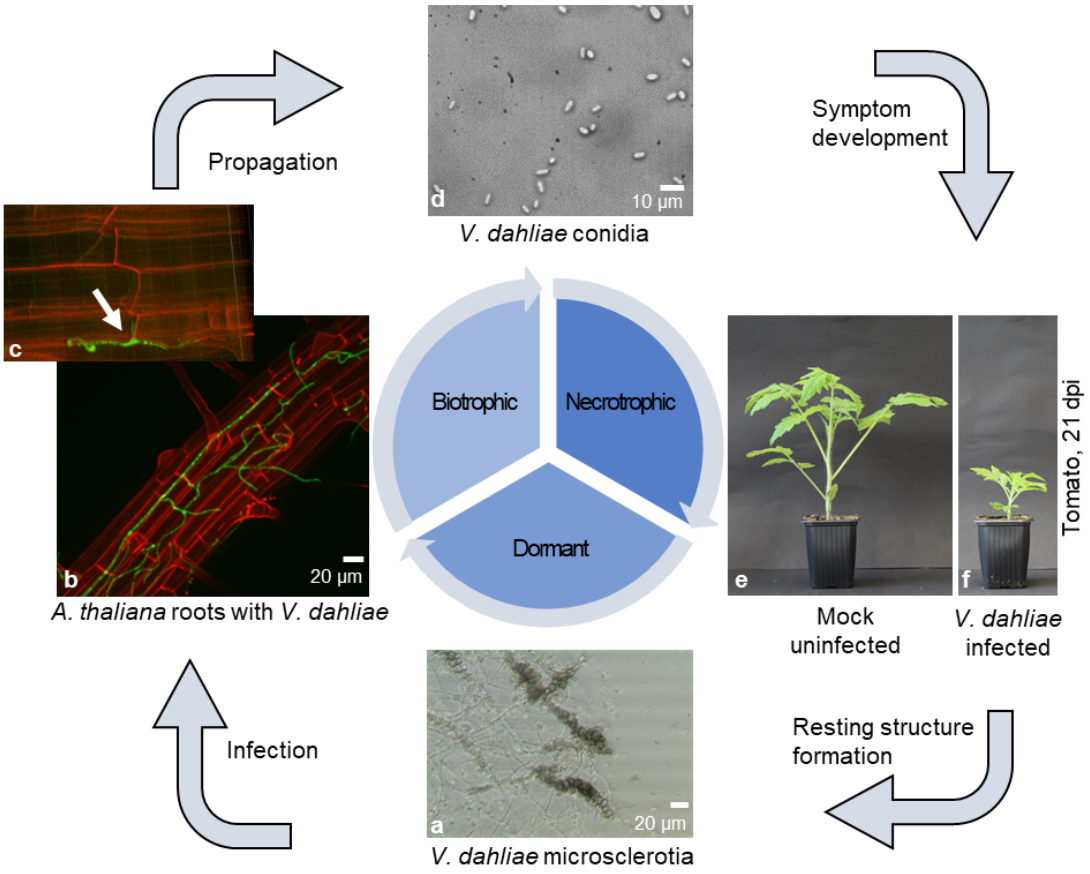

Figure 1: Life cycle of *V. dahliae*. The life cycle of *V. dahliae* consists of three different phases: dormant, biotrophic and necrotrophic. **(a)** Within the dormant phase black melanized microsclerotia remain in the soil until they recognize a suitable host due to the perception of root exudates. After microsclerotia germination, hyphae grow towards the plant. **(b)** The fungus enters the biotrophic phase and colonization of the whole root starts. Infection takes place where the endodermis is damaged or has not yet developed. **(c)** *Verticillium* spp. form hyphopodia, which are swollen tips of hyphae (indicated by white arrow) and allow the entry into roots. The images show *Arabidopsis thaliana* roots five days after infection with *V. dahliae* spores expressing free GFP. The root was stained with 0.0025 % propidium iodide and 0.005 % silwet. **(d)** Within the plant *V. dahliae* propagates via the formation of conidia in the xylem sap. The conidia are carried by the sap stream and trapped in pit cavities or vessel ends. At this position, the conidia germinate and plug the xylem. Nutrients and water are no more transported due to the plugging and/or initiation of defense reactions by the plant. **(e and f)** As consequence symptom development starts and the fungus reaches the necrotrophic phase. Infected plants show disease symptoms as for instance stunted growth. The picture shows an uninfected tomato plant (Mock, e) and a tomato plant infected with spores of *V. dahliae* wild type (f) by root dipping 21 days post infection (dpi). In the senescent plant *V. dahliae* starts to produce microsclerotia as resting structures again, which remain in the soil for several years until a suitable host is present. The figure is based on information from the following papers: Wilhelm, 1955; Berlanger & Powelson, 2000; Fradin & Thomma, 2006; Klosterman *et al.*, 2009; Reusche *et al.*, 2012, 2014.

Within the vascular tissue, conidiation starts and *Verticillium* uses the sap stream for propagation inside the plant (Klosterman *et al.*, 2009; EFSA PLH Panel (EFSA Panel on Plant

Health), 2014) (Figure 1d). The xylem sap contains some organic acids and low concentrations of amino acids and requires the fungal cross-pathway control for growth (Singh *et al.*, 2010; Timpner *et al.*, 2013). Conidia germinate in trapping sites as pit cavities or vessel ends. There, growing hyphae invade neighboring cells where more conidia are produced (Fradin & Thomma, 2006; Klosterman *et al.*, 2009). By the colonization of the vascular and cortical tissue the transpiration stream is plugged and the induction of disease symptoms starts due to a lack of nutrients and water (Berlanger & Powelson, 2000; Klosterman *et al.*, 2009). Furthermore, a defense reaction is initiated by the plant, which stops the transport of water and nutrients to the shoots as well (Fradin & Thomma, 2006; Kamble *et al.*, 2013; Carroll *et al.*, 2018).
Now, the necrotrophic phase starts with the induction of disease symptoms like stunted growth, necrosis, chlorosis and wilting (Fradin & Thomma, 2006; EFSA PLH Panel (EFSA Panel on Plant Health), 2014) (Figure 1f). When the fungus recognizes that the plant is senescent, it forms large amounts of microsclerotia, which are released into the soil with the fading plant and remain there until a new host is present (Wilhelm, 1955; Berlanger & Powelson, 2000; Fradin & Thomma, 2006; EFSA PLH Panel (EFSA Panel on Plant Health), 2014; Carroll *et al.*, 2018).

1.1.3 *Verticillium* spp. adhesion, infection and propagation via conidia

The initial steps of a fungal infection are to adhere, colonize and penetrate the surface of the host plant (Braun & Howard, 1994; Tran *et al.*, 2014; Zhao *et al.*, 2016; Bui *et al.*, 2019). Defects in these crucial steps often make an infection unfeasible or inefficient. Examples for proteins involved in root colonization of *V. dahliae* are the Verticillium transcription activator of adhesion (VTA) proteins Vta2 and Vta3, as well as Som1, which is a homolog of the flocculation protein Flo8 that is involved in adhesion in *Saccharomyces cerevisiae* (Brückner & Mösch, 2012; Tran *et al.*, 2014; Bui *et al.*, 2019). *VTA2* and *VTA3* were identified during a screen for adhesive genes in a nonadherent *FLO8*-deficient yeast strain (Tran *et al.*, 2014). Another gene identified within this screen was *VTA1*, which also rescues adhesion but is dispensable for root colonization (Tran *et al.*, 2014; Harting *et al.*, 2020). For human pathogenic fungi as *Aspergillus fumigatus*, adhesion to host surfaces is also crucial. The homolog of *V. dahliae SOM1* is as well required for adhesion and virulence in this organism (Lin *et al.*, 2015). Taken these results into account, colonization of host surfaces by fungi relies on adhesive proteins, that are the first crucial factor within disease induction and virulence.
Not just the ability to adhere to the root, but also the formation of a penetration structure like a hyphopodium is needed for a successful root infection (Reusche *et al.*, 2014; Zhao *et al.*, 2014). Often adhesion and developmental processes are controlled by reactive oxygen species (ROS) as for instance hydrogen peroxide (Aguirre *et al.*, 2005; Gessler *et al.*, 2007). In *V. dahliae NoxB* and *Pls1* are localized in hyphopodia and produce ROS to induce

penetration peg formation by activation of the transcription factor Crz1. Deletion strains of these genes developed defective hyphopodia without formation of a penetration peg (Zhao *et al.*, 2016).

When the fungus has finally reached the vascular system, it has to propagate by the formation of conidia to colonize the whole plant. Conidia of *V. dahliae* are ovoid and develop on phialides arranged around the conidiophores (Berlanger & Powelson, 2000; Fradin & Thomma, 2006). The size of conidia is approximately 6.5 µm x 3 µm (Inderbitzin *et al.*, 2011a; EFSA PLH Panel (EFSA Panel on Plant Health), 2014). Conidia are no long-term survival structures although they are also produced on the root surface where a successful infection took place and in dead plants, leading to the assumption that a second infection and colonization of other plants is expedite particularly if crops are grown again on the same field (Vallad & Subbarao, 2008; Klosterman *et al.*, 2009). Several studies in plant pathogenic fungi revealed a connection between pathogenicity and conidiation. For instance in *V. dahliae VTA2*, *VTA3* and *SOM1* are not only needed for plant root colonization but also to produce conidia and induce disease symptoms (Tran *et al.*, 2014; Bui *et al.*, 2019). Furthermore, these three proteins control the expression of genes involved in conidiation such as *CON8* and *ABA1* (Tran *et al.*, 2014; Bui *et al.*, 2019). Accordingly, increased conidiation of *V. dahliae* strains correlates with the virulence of the fungal strain, which shows the importance of conidia production during the disease (Schnathorst, 1963; EFSA PLH Panel (EFSA Panel on Plant Health), 2014).

1.1.4 Induction of pathogenicity in plant hosts

Different *Verticillium* strains not just slightly differ in their appearance and host range, they also lead to induction of different disease symptoms (Fradin & Thomma, 2006; Inderbitzin *et al.*, 2011a). Although the disease induced by the plant pathogenic fungus is named Verticillium wilt, wilting of the host plant does not always occur (Berlanger & Powelson, 2000). For instance, in tomato plants the most prominent symptom of an infection with *V. dahliae* is stunted growth (Figure 1f) and oilseed rape infected with *V. longisporum* display stem striping at the end of the growing season (Depotter *et al.*, 2016). As *Verticillium* spp. enter the plant via the roots, the infection is acropetal and symptoms are first observed in the oldest parts of a leaf. In other cases, the fungus induces yellow spots that later become necrotic. Most commonly, symptoms like chlorosis, necrosis, vascular discoloration, stunting, wilting and vein clearing are observed but may vary between different *Verticillium* strains (Berlanger & Powelson, 2000; Fradin & Thomma, 2006). The exact properties making *Verticillium* spp. a plant pathogen are still under investigation, but cell-wall-degrading enzymes, elicitors, toxins and effectors that are secreted by the fungus seem to be crucial components for disease induction (Fradin & Thomma, 2006).

During plant colonization *Verticillium* spp. often have to degrade polysaccharides as pectin, cellulose and hemicellulose to access the plant root and enter the xylem (Waldron *et al.*, 2003). Pectin-degrading enzymes and carbohydrate-active enzymes are therefore more often found in the genome of *Verticillium* spp. in comparison to other fungi (Fradin & Thomma, 2006; Klosterman *et al.*, 2011). Hence, the presence of these enzymes highly contributes to the pathogenesis of *Verticillium* spp. (Klosterman *et al.*, 2011). In many fungi other factors are known to be crucial for pathogenesis, for example the lysin motif (LysM) effectors and the necrosis and ethylene-inducing like proteins (NLP) (Pemberton & Salmond, 2004; Gijzen & Nürnberger, 2006; Qutob *et al.*, 2006; Bolton *et al.*, 2008; de Jonge & Thomma, 2009; de Jonge *et al.*, 2010). Most fungi contain approximately three LysM effectors and the same number of NLP genes. In contrast, *V. dahliae* contains seven LysM effectors and eight NLP genes (Klosterman *et al.*, 2011). NLP proteins are especially toxic towards dicotyledonous plants, which is in agreement with the fact that *V. dahliae* mainly infects this plant species (Pemberton & Salmond, 2004; Gijzen & Nürnberger, 2006; Qutob *et al.*, 2006; Fradin & Thomma, 2006). Studies in *V. dahliae* JR2 showed that solely deletion strains of *NLP1*, *NLP2* and *NLP3* are impaired in plant infection (Santhanam *et al.*, 2013; Leonard *et al.*, 2020).

In contrast to other *Verticillium* spp., *V. dahliae* infects many different plants and can adapt quickly to new hosts (Klosterman *et al.*, 2009). It is therefore assumed that the secreted proteins of *V. dahliae* are another factor making it a successful pathogen. These proteins might have redundant functions or are host-specific, which is supported by the fact that single effector deletion strains often did not affect virulence (Leonard *et al.*, 2020). Furthermore, adaptation to different hosts might be facilitated by highly flexible lineage-specific (LS) regions (Klosterman *et al.*, 2011; Depotter *et al.*, 2019). Analysis of an LS region present in the pathogenic *V. longisporum* isolate Vl43 but absent in the asymptomatic isolate Vl32, led to the suggestion that virulence might be extenuated by this region in order to use the full capacity of the host plant (Starke, 2019). Taking this into account, LS regions may tightly control the aggressiveness of plant pathogenic fungi for optimal growth conditions inside the infected plant dependent on the host.

The sophisticated interplay between cell wall degrading enzymes, effectors, elicitors and toxins, as well as the highly flexible regions in the genome make *V. dahliae* a successful and destructive pathogen with high economic impact. Another important factor for the induction of Verticillium wilt and the resulting losses are the resting structures called microsclerotia, which can remain in the soil for several years (Wilhelm, 1955).

1.1.5 Microsclerotia as long-term *Verticillium* spp. resting structures

Verticillium spp. form melanized hyphae or microsclerotia as resting structures (Klosterman *et al.*, 2009; Inderbitzin *et al.*, 2011a). In the senescent plant *V. dahliae* already prepares itself

for the next cycle of disease by the formation of microsclerotia, which are the primary inoculum of the fungus (Fradin & Thomma, 2006). These resting structures are formed by swelling of hyphae, which than septate and can remain in the soil for several years (Wilhelm, 1955; Griffiths, 1970; Fradin & Thomma, 2006). Microsclerotia are round or elongated and have a size of 25-100 µm (Inderbitzin *et al.*, 2011a; EFSA PLH Panel (EFSA Panel on Plant Health), 2014).

The fungus requires during growth in the plant host protection against oxidative stress, especially also in the late phase of disease (Singh *et al.*, 2012; Hoppenau *et al.*, 2014). The dark pigment melanin facilitates the long-term survival of the resting structure in the soil as it protects against environmental stresses as for example radiation, extreme temperatures and reactive oxygen species but also attacks of other microorganisms (Bell & Wheeler, 1986; Belozerskaya *et al.*, 2017; Casadevall *et al.*, 2017; Fan *et al.*, 2020).

There are two pathways for melanin biosynthesis in fungi with either 1,8-dihydroxynaphthalene (DHN) or L-3,4-dihydroxyphenylalanine (L-DOPA) as intermediates (Eisenman & Casadevall, 2012). *Verticillium* spp. generally use the pentaketide pathway with DHN intermediates to produce melanin (Bell *et al.*, 1976; Bell & Wheeler, 1986; Pegg & Brady, 2002). Acetyl CoA and malonyl CoA are converted to 1,3,6,8-tetrahydroxynaphthalene (1,3,6,8-THN) by a polyketide synthase. Next, this intermediate product is reduced to scytalone and afterwards dehydrated to 1,3,8-tetrahydroxynaphthalene (1,3,8-THN) by the scytalone dehydratase. Subsequently, the product is reduced to vermelone, which is later oxidized and polymerized by a laccase to DHN melanin (Bell & Wheeler, 1986; Wang *et al.*, 2018) (Figure 2). To better understand the formation of melanized structures, RNA-seq analysis of microsclerotia from *V. dahliae* Ls17 was conducted and revealed over 200 differentially regulated genes as for instance a tetrahydroxynapthalene reductase, a scytalone dehydratase and genes associated within a 48.8 kb-long gene cluster presumably connected to melanin biosynthesis (Duressa *et al.*, 2013).

Signaling elements of the high osmolarity glycerol (HOG)- mitogen activated protein kinase (MAPK) pathway contribute to melanin biosynthesis as deletion strains of the genes for the kinase Hog1 and the kinase kinase Pbs2 have defects in melanization and genes associated with melanin biosynthesis were down-regulated in these strains (Tian *et al.*, 2016; Wang *et al.*, 2016, 2018). From other fungi as for example *M. oryzea* and *B. cinerea*, Cmr1 type transcription factors are known to regulate melanin expression (Schumacher, 2016; Wang *et al.*, 2018). In *V. dahliae* an ortholog of this gene is up-regulated in the previously mentioned melanin biosynthesis gene cluster (Duressa *et al.*, 2013; Wang *et al.*, 2018). Analysis of Cmr1 exhibited that the transcription factor positively regulates the polyketide synthase Pks1 and the polyketide chain shortening enzyme Vayg1 but inhibits the laccase Lac1 (Wang *et al.*, 2018) (Figure 2). Other studies identified the MADS-box transcription factor Mcm1 as global regulator

with a diverse set of functions in pathogenicity, secondary metabolism, conidiation as well as formation of microsclerotia and furthermore indicate it as second regulator of Cmr1 expression (Xiong *et al.*, 2016; Wang *et al.*, 2018).

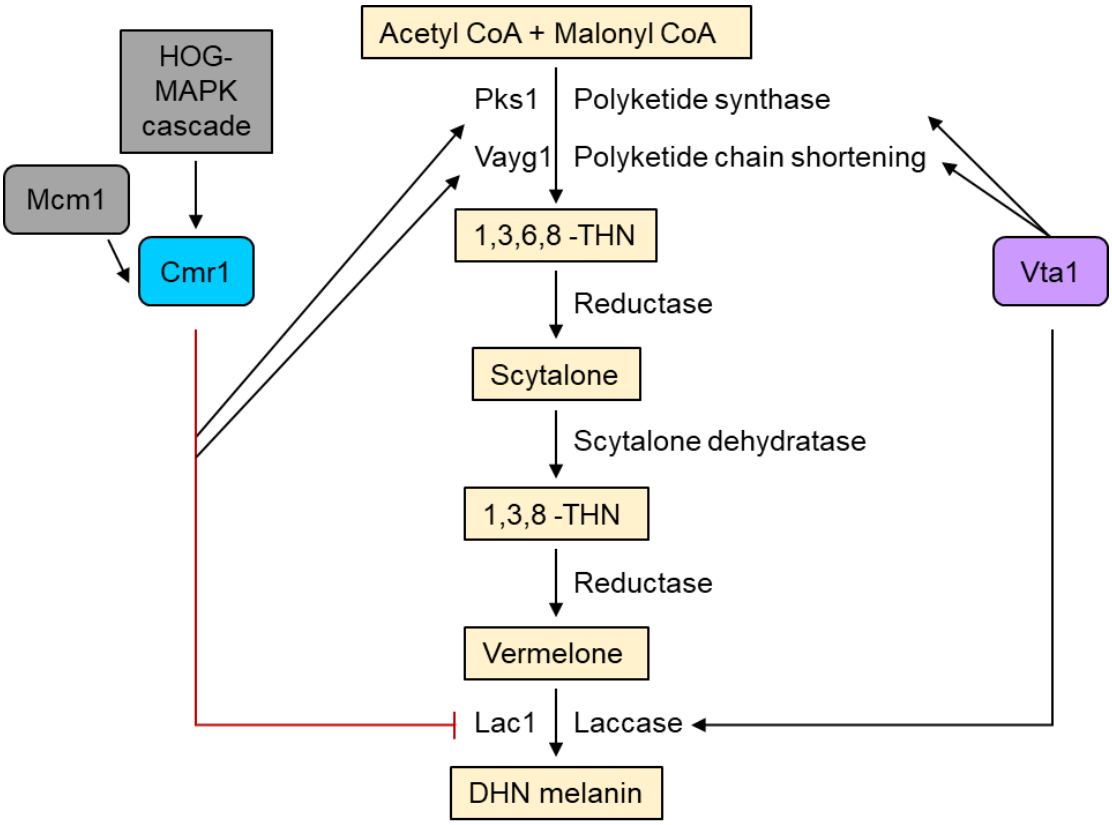

Figure 2: DHN melanin biosynthesis pathway and control in *V. dahliae*. Illustrated are the products and key enzymes in DHN melanin biosynthesis. *Verticillium* spp. synthesize DHN melanin by converting acetyl CoA and malonyl CoA to 1,3,6,8-THN. In two reduction steps vermelone is produced and finally oxidized to DHN melanin. The production of DHN melanin is controlled by the HOG-MAPK cascade and the transcription factor Cmr1, which is also regulated by Mcm1. A second control network for melanin biosynthesis is regulated by the transcription factor Vta1, which also controls Pks1, Vayg1 and Lac1. The figure was modified according to Wang *et al.* (2018).

An additional control level for melanin biosynthesis is provided by the transcription factor Vta1, which is also located within the melanin biosynthesis cluster and controls the expression of melanogenesis associated genes as *PKS1*, *VAYG1* and *LAC1*. Vta1 has no effect on *CMR1*, which equally has no impact on *VTA1* (Duressa *et al.*, 2013; Wang *et al.*, 2018; Harting *et al.*, 2020) (Figure 2). Also, a putative THN-reductase and a scytalone dehydrogenase are controlled by Vta1, suggesting a direct or indirect control by Vta1. Both transcription factors differentially control *LAC1*, maybe due to activity of the two transcription factors under different conditions (Harting *et al.*, 2020).

The formation of melanized microsclerotia as major inoculum of *V. dahliae* is tightly controlled and regulated by a complex network of signaling cascades. A better understanding of the

interplay of the involved genes could therefore be a first step in identification of potential sites for fungal control and Verticillium wilt reduction.

1.2 The velvet family of regulatory proteins and fungal light sensing

1.2.1 The velvet proteins in *A. nidulans*

Besides melanin, fungi have the potential to produce multiple secondary metabolites (Gerke & Braus, 2014; Macheleidt *et al.*, 2016). These metabolites can be beneficial as for instance antibiotics like penicillin or harmful such as aflatoxin (Gerke & Braus, 2014). In fungi secondary metabolism is connected to development (Calvo *et al.*, 2002; Yu & Keller, 2005; Brakhage, 2013; Keller, 2019). This connection is well-studied in the filamentous model fungus *A. nidulans* (Bayram & Braus, 2012). Depending on the environmental conditions and internal stimuli, *A. nidulans* undergoes asexual or sexual development after the vegetative hyphae have reached a competence state (Etxebeste *et al.*, 2010; Bayram & Braus, 2012; Noble & Andrianopoulos, 2013) (Figure 3).

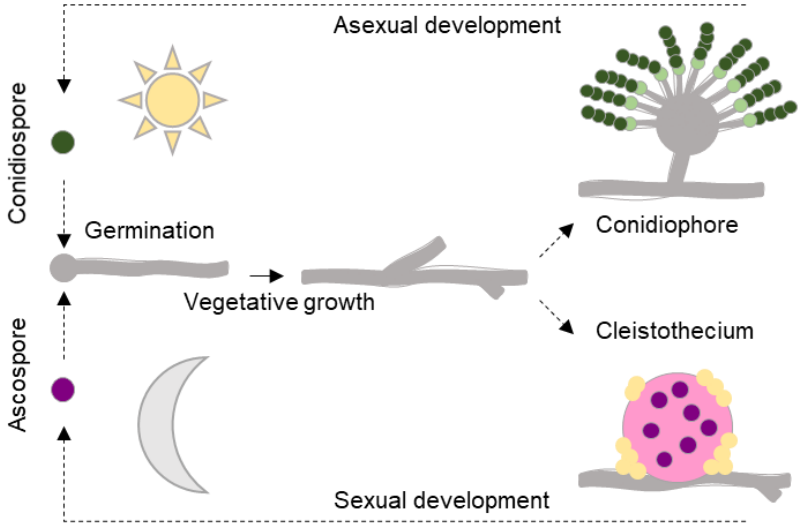

Figure 3: Life cycle of *A. nidulans*. The germinating spore forms a vegetative hypha, which has reached developmental competence after 12-20 hours. Environmental signals such as light and darkness induce either asexual or sexual development. Asexual development is favored in light and air-borne conidiospores are formed. In darkness mainly sexual development is performed, which results in the formation of a cleistothecium with ascospores surrounded by Hülle cells. The figure was modified according to Bayram & Braus (2012).

In light sexual development is reduced whereas asexual development is promoted. This leads to the development of a conidiophore with air-borne conidiospores. Without illumination asexual development is delayed, whereas sexual development is predominantly initiated. The hyphae develop multinuclear Hülle cells, which function as nuclear storage and developmental backup (Troppens *et al.*, 2020). In addition, they nurse and surround the young closed fruiting body (cleistothecium), that develops sexual ascospores inside (Figure 3). This cleistothecium is the overwintering structure of the fungus in the soil (Bayram & Braus, 2012; Bayram *et al.*,

2016). During both developmental programs *A. nidulans* produces secondary metabolites (Bayram & Braus, 2012; Brakhage, 2013). Secondary metabolites have a low molecular weight and are known as natural bioactive substances (Bayram & Braus, 2012). They are not required for normal growth but involved in transcription, development as well as communication and play crucial roles as virulence factors (Brakhage, 2013; Macheleidt *et al.*, 2016).

Secondary metabolism and development are connected by the velvet family of regulatory proteins (Kato *et al.*, 2003). In *A. nidulans* more than half a century ago the first velvet family member, velvet A (VeA), was identified during a random mutagenesis screening and described as a strain with a point mutation in VeA that produces more conidia but fewer fruiting bodies (Käfer, 1965). Later this strain was named *veA1* (Mooney *et al.*, 1990) and more research revealed that the point mutation led to a shift in translation initiation, which consequently leads to a protein missing the first 36 amino acids (Kim *et al.*, 2002). Wild type strains of *A. nidulans* require red light for conidiation. In contrast, the *veA1* strain produced conidia in the absence of light, which means that VeA is important for conidiation induced by red light (Mooney & Yager, 1990). The interaction of VeA with the red-light receptor FphA and the blue-light receptors LreA and LreB supported the light-dependence of VeA (Purschwitz *et al.*, 2008) (Figure 4).

Construction of a complete deletion and an overexpression strain of VeA identified this protein as positive regulator of sexual development and suppressor of asexual development (Kim *et al.*, 2002). Later, VeA was identified as linker between development and secondary metabolism as it is required for the expression of the transcription factor *aflR*, which is needed in the production of the aflatoxin precursor sterigmatocystin. Furthermore, VeA is involved in the transcription of the synthase genes *ipnA* and *acvA*, which both are participating in penicillin production (Kato *et al.*, 2003). Localization studies in light and dark revealed a VeA enrichment in the nucleus in darkness, which approves a light-dependent function of VeA (Stinnett *et al.*, 2007; Bayram *et al.*, 2008b).

In total, four members of the velvet family are described in *A. nidulans*: VeA, velvet like B (VelB), velvet like C (VelC) and viability of spores A (VosA) (Käfer, 1965; Ni & Yu, 2007; Bayram *et al.*, 2008b; Sarikaya-Bayram *et al.*, 2010) (Figure 4).

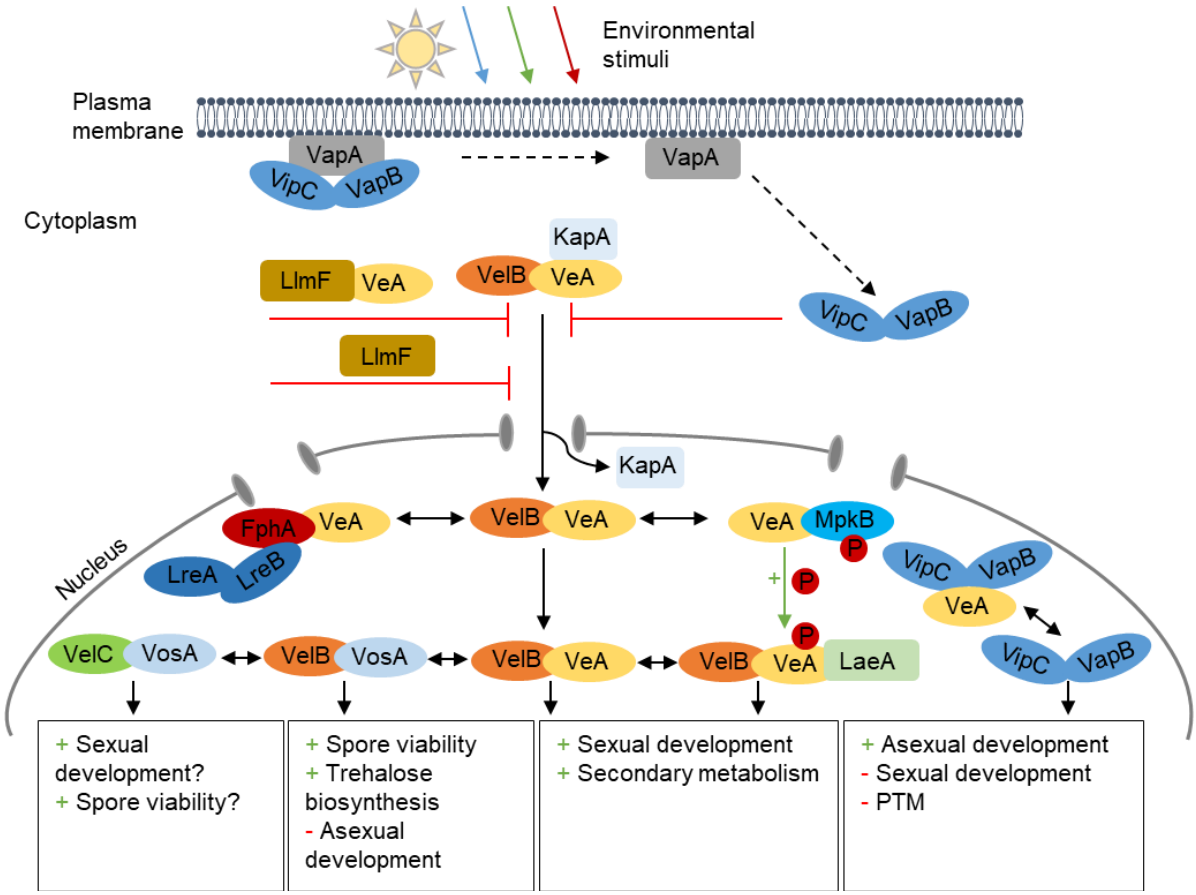

Figure 4: Interactions of velvet family proteins in *A. nidulans*. The two methyltransferases VipC and VapB are bound to the plasma membrane by VapA. Environmental signals such as light, pH, oxygen or starvation result in the release of the two methyltransferases and their transfer to the nucleus, which inhibits nuclear entry of VeA. The nuclear entry of VeA is also hindered by the methyltransferase LlmF. The α-importin KapA facilitates nuclear entry of the VeA-VelB heterodimer, which is reduced in light. Inside the nucleus the VeA-VelB heterodimer has different options. VeA is able to interact with the red-light receptor protein phytochrome FphA, that furthermore can interact with the two blue-light receptors LreA and LreB. VeA also can interact with the mitogen activated protein kinase (MAPK) MpkB. MpkB phosphorylates VeA, which improves the interaction to VelB. Together with the methyltransferase LaeA the VeA-VelB heterodimer forms the trimeric velvet complex. The heterodimer or the trimeric complex activate genes for sexual development and secondary metabolite gene clusters. Moreover, LaeA might induce posttranslational modifications (PTM) of the velvet proteins and thereby control developmental processes. The two methyltransferase VipC and VapB can also interact with VeA. Alone or together with VeA, the methyltransferases decrease posttranslational modifications and activate asexual development as well as repress sexual development. Free VelB interacts with VosA, which influences spore viability, trehalose biosynthesis and asexual reproduction. By interacting with VelC, VosA might also regulate sexual development and spore viability. The figure was modified according to Sarikaya-Bayram *et al.* (2015).

Similar as VeA, VelB of *A. nidulans* is light-dependent and present during sexual development as well as involved in secondary metabolism and positively influences asexual development (Bayram *et al.*, 2008b; Park *et al.*, 2012b). The localization of VelB to the nucleus and the cytoplasm is not affected by illumination. VelB possess no conventional nuclear localization signal (NLS) and accumulates in the cytoplasm if VeA is absent, VeA might transport VelB to the nucleus. Tandem affinity purification with VeA, revealed that it interacts with VelB in darkness (Bayram *et al.*, 2008b). Furthermore, the methyltransferase loss of *aflR* expression

A (LaeA), which is a regulator of secondary metabolism in *Aspergillus* spp. (Bok & Keller, 2004) and the α-importin KapA were identified as interaction partners of VeA (Bayram *et al.*, 2008b). Yeast-two hybrid experiments and bimolecular fluorescence complementation revealed interactions of VeA and VelB in the nucleus and the cytoplasm whereas VeA and LaeA are only interacting in the nucleus, suggesting that the VeA-VelB heterodimer migrates into the nucleus with the help of KapA and is released there (Figure 4). An interaction of VelB and LaeA was not observed, assuming a bridging function of VeA between the proteins, which leads to the formation of the trimeric velvet complex consisting of VeA-VelB-LaeA in the nucleus that links light-responsive development and secondary metabolism (Bayram *et al.*, 2008b). Accordingly, the trimeric velvet complex of VelB-VeA-LaeA or the VeA-VelB heterodimer activate sexual development and positively regulate secondary metabolite production (Bayram *et al.*, 2008b; Sarikaya-Bayram *et al.*, 2015). There are hints that LaeA might coordinate fungal development and secondary metabolism by posttranslational modifications as for instance methylation of the histone 3 (Sarikaya-Bayram *et al.*, 2015). The nuclear entry of the velvet complex is not just regulated by light but also by the LaeA like methyltransferase LlmF binding to VeA (Figure 4). LlmF hence negatively regulates the production of sterigmatocystin and sexual development (Palmer *et al.*, 2013).

A. nidulans VelC is less extensively studied than VeA and VelB. VelC is a positive regulator of sexual development but also functions in asexual development as it controls asexual specific genes and negatively influences conidiation (Park *et al.*, 2014). Moreover, VelC seems to interact with another member of the velvet family, VosA (Park *et al.*, 2014), which is involved in spore viability, trehalose biosynthesis, represses asexual development and controls genes for secondary metabolism (Ni & Yu, 2007; Kim *et al.*, 2020), but the function of the heterodimer remains ambiguous, although functions in sexual development and spore viability are assumed (Sarikaya-Bayram *et al.*, 2015). VosA also interacts with VelB supposing that there is a competition for VelB between the velvet complex and the VelB-VosA dimer or another carrier to the nucleus (Bayram *et al.*, 2008b; Sarikaya-Bayram *et al.*, 2010; Park *et al.*, 2012b). The VelB-VosA heterodimer controls spore viability and trehalose biosynthesis and represses asexual sporulation when conditions are unsuitable (Park *et al.*, 2012b; Sarikaya-Bayram *et al.*, 2015).

In order to respond to environmental stimuli such as light, nutrition or oxygen, fungi possess different signal transduction pathways (Bayram & Braus, 2012; Macheleidt *et al.*, 2016). Often external signals are received at the plasma membrane as for instance by the membrane-bound VapA-VipC-VapB complex (Figure 4). The methyltransferases VeA interacting protein C (VipC) and VipC associated protein B (VapB) of the trimeric complex are bound to the plasma membrane by the FYVE-like zinc finger protein known as VipC associated protein A (VapA). If the complex is bound to the plasma membrane, the velvet complex consisting of VelB-VeA-

LaeA can activate sexual development. Environmental signals mediate the release of VipC-VapB from VapA and inhibit nuclear entry of VeA as well as reduce the proteins stability. Moreover, in the nucleus VipC and VapB interact with VeA and reduce the amount of the velvet complex. By decreasing histone 3 methylation, the methyltransferase VipC-VapB might also activate asexual development (Sarikaya-Bayram *et al.*, 2014).

There is a considerable fungal potential to form various homo- and heterodimers of velvet domain proteins, which can associate with additional proteins as e.g. methyltransferases, which presumably changes during development in different cell types depending on gene expression, protein turnover control and surveillance mechanisms (Gerke & Braus, 2014).

1.2.2 Structure of the velvet proteins and features of the velvet domain

All members of the velvet family comprise a velvet domain with a size of approximately 150 amino acids (aa), which exhibits no sequence similarity to other known domains but contains proline residues in the middle of the velvet motif (Bayram & Braus, 2012) (Figure 5).

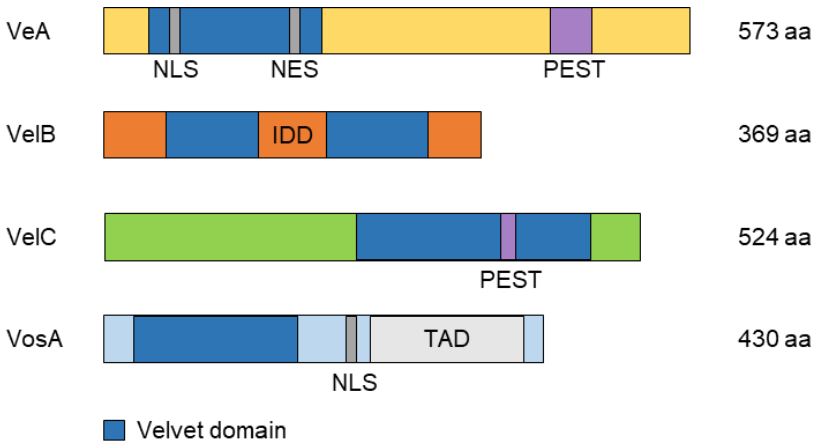

Figure 5: Domain structure of the velvet proteins in *A. nidulans*. The four velvet proteins VeA, VelB, VelC and VosA are depicted. Nuclear localization signals (NLS), nuclear export signals (NES), PEST regions, intrinsically disordered domain (IDD) and transcription activation domain (TAD) are shown. The figure was adapted from Bayram & Braus (2012).

In *A. nidulans*, only VeA and VosA comprise a nuclear localization signal (NLS), which enables them to enter the nucleus. In addition, VeA has a nuclear export signal (NES), which makes it possible for VeA to leave the nucleus. In the VeA and the VelC proteins a PEST motif rich in proline (P), glutamic acid (E), serine (S) and threonine (T) is predicted (Bayram & Braus, 2012; Park *et al.*, 2014). This region is often found in unstable proteins or polypeptides that have to be rapidly degraded suggesting this motif is a degradation signal (Rechsteiner & Rogers, 1996). Only in VosA a transcription activation domain (TAD) is present, which led to the assumption that it might function as a transcription factor (Ni & Yu, 2007). VelB neither has an NLS, NES nor a PEST motif or a TAD, but the velvet domain of VelB is interrupted by 99 amino acids (Ahmed *et al.*, 2013). This interruption is assumed to be an intrinsically disordered region.

In order to crystalize VelB the full-length protein was used, but the insertion was not visible in the crystal structure maybe as result of proteolytic cleavage (Ahmed *et al.*, 2013). Interestingly, this interruption is conserved in ascomycetes including *V. dahliae* and basidiomycetes, although the amino acid sequence is highly different between the examined fungi (Thieme, 2018). In general, most protein domains are structured but also intrinsically disordered domains (IDD) due to small amounts of large hydrophobic amino acids are known (van der Lee *et al.*, 2014; Wright & Dyson, 2015). Disordered regions are common in eukaryotic proteins. Proteins with an IDD are often posttranslationally modified and involved in DNA, RNA as well as protein binding (van der Lee *et al.*, 2014; Wright & Dyson, 2015). Hence, and due to their flexibility, they are interacting with diverse proteins and influence different signaling processes (Wright & Dyson, 2015). A more detailed analysis of the IDD of VelB in *A. nidulans* showed that it destabilizes the VelB protein, is required to form a VelB homodimer and a VelB-VosA heterodimer. Furthermore, the IDD is required for conidiation and control of secondary metabolism (Thieme, 2018).

Analysis of the *A. nidulans* velvet domain structure revealed no similarity to known protein structures, but crystallization of a truncated VosA and the VelB-VosA heterodimer show similarity of the velvet domain with the Rel homology domain (RHD) of the transcription factor NF-κB in mammalians. However, the overall amino acid sequence similarity of the two domains is just 13.7 % (Ahmed *et al.*, 2013). NF-κB transcription factors are a crucial signaling system during inflammation, immune response and differentiation (O'Dea & Hoffmann, 2010; Oeckinghaus *et al.*, 2011). In mammals five NF-κB family members can form 15 homo- and heterodimers (O'Dea & Hoffmann, 2010). Dimerization and DNA binding occurs at the RHD. Similar as the velvet proteins, the NF-κB transcription factors are involved in signaling pathways (O'Dea & Hoffmann, 2010; Oeckinghaus *et al.*, 2011). Hence, one can speculate if both proteins have a common ancestor (Gerke & Braus, 2014).

The structural information on velvet proteins suggests that they are DNA binding transcription factors (Ni & Yu, 2007; Ahmed *et al.*, 2013) with a protein-protein interaction domain which enables the formation of different homo- and heterodimers with velvet and non-velvet proteins (Bayram *et al.*, 2008b; Sarikaya-Bayram *et al.*, 2010, 2015; Bayram & Braus, 2012). Their broad spectrum of interactions exposes the velvet proteins as key players in different cellular processes, which are linked to diverse signaling pathways (Bayram & Braus, 2012).

1.2.3 Velvet proteins as key factors for correct fungal development

A. nidulans VosA is binding to over 1500 promoter sequences, especially promoters of genes involved in asexual development as for instance *brlA*, *wetA* and trehalose biosynthesis genes such as *tpsA* and *treA*. Further experiments revealed that VosA is binding to an 11-nucleotide consensus DNA sequence (Ahmed *et al.*, 2013). One promoter sequence that VosA is binding

to, is the one of the zinc cluster transcription factor SclB, which activates asexual development and spore viability in *A. nidulans* independent of light. SclB activates BrlA, which induces conidiation by promoting AbaA and WetA. Together with RcoA, SclB is an activator of secondary metabolism. SclB also positively effects CatA, TrxR and RsmA in order to promote oxidative stress response and secondary metabolism. AbaA and WetA induce activation of VosA to repress SclB (Thieme *et al.*, 2018). The interplay of VosA and SclB is one example of how interwoven the velvet proteins are in fungal development and secondary metabolism.

Because of the important velvet protein functions in cellular development, tight control mechanisms and extensive links to signaling pathways are required. Presence or absence of VeA dramatically alters fungal development (Figure 4). Correct levels of VeA are therefore required, which are controlled by the deubiquitinase UspA (Meister *et al.*, 2019). In a *uspA* deletion mutant VeA is not properly degraded, which leads to prolonged multicellular development in the deletion strain. Fbox proteins bind their substrates for ubiquitin-mediated degradation by the proteasome (Kipreos & Pagano, 2000). Deletion of Fbox23 increased the amount of VeA as shown for the *uspA* deletion strain. Hence, the Fbox protein might label VeA for ubiquitination. VeA is normally present in early fungal development and the protein amount decreases within the first 24 h of development. This suggests VeA is important during establishing developmental competence and initial steps of fungal development (Meister *et al.*, 2019).

MAPK cascades are conserved in signal transduction of eukaryotes (Widmann *et al.*, 1999; Saito, 2010). In the yeast *Saccharomyces cerevisiae* the MAPK pathway is involved in sexual reproduction and activated by mating pheromones. Central components of the pathway are the MAP3K Ste11, MAP2K Ste7 and MAPK Fus3, which are connected by the scaffold protein Ste5 (Bardwell, 2005; Saito, 2010). The homolog of Fus3 in *A. nidulans* is MpkB. It enters the nucleus where it phosphorylates VeA in order to enhance the formation of the VeA-VelB heterodimer for sexual development and secondary metabolism (Bayram *et al.*, 2012) (Figure 4). Phosphorylation of VeA occurs at different phosphorylation sites indicating a complex regulation of interacting proteins (Rauscher *et al.*, 2016). In other fungi as for instance *Fusarium oxysporum* or *V. dahliae*, MAPK pathways are also involved in pathogenicity (Husaini *et al.*, 2018; Starke, 2019).

The velvet proteins might also be connected to other pathways involved in development and secondary metabolism as for instance the protein kinase A (PKA) pathway or the protein kinase C (PKC) pathway by yet unknown mechanisms as these pathways are involved in development and secondary metabolism as well (Bayram & Braus, 2012).

1.2.4 Velvet proteins are part of a complex fungal light control of development

Velvet domain controlled fungal developmental programs are often regulated by environmental signals such as light of different wavelengths (Yu & Fischer, 2019). The life cycle of *A. nidulans* discriminates between illumination and darkness (Figure 3). The *A. nidulans* trimeric velvet complex controlled coordination between development and secondary metabolism reacts to an interplay of external signals for the availability of nutrients, the presence of pheromones, the ratio between carbon dioxide and oxygen in the air and is regulated by light as it reduces the amount of the trimeric complex in the nucleus (Bayram *et al.*, 2008b; Bayram & Braus, 2012) (Figure 4). The default mode without illumination results in high sexual development and delayed asexual development, whereas light reduces sexual but promotes the asexual program (Bayram *et al.*, 2016). *A. nidulans* possess a red-light sensing phytochrome FphA, two blue-light receptors LreA and LreB, a putative green-light sensing opsin and a cryptochrome/photolyase CryA (Bayram *et al.*, 2010). Inside the nucleus VeA, directly interacts with the red-light phytochrome receptor protein FphA, which is connected to the blue-light receptors LreA and LreB (Purschwitz *et al.*, 2008; Bayram *et al.*, 2010) (Figure 4). The cryptochrome CryA does not directly interact with VeA, but negatively influences the transcription of *veA* mRNA and thereby hinders the formation of Hülle cells and sexual development (Bayram *et al.*, 2008a).

The best studied fungal light control system is the Sordariomycete *Neurospora crassa*, which is related to *V. dahliae* (Chen *et al.*, 2010; Maharachchikumbura *et al.*, 2016). The blue-light receptors LreA and LreB of *A. nidulans* correspond to white collar 1 (WC-1) and white collar 2 (WC-2) in *N. crassa* and coordinate light control to the circadian rhythm of the fungus (Purschwitz *et al.*, 2008; Chen *et al.*, 2010). Little is known about light-sensing abilities and circadian rhythm of *V. dahliae*, which carries genes for WC-1 and WC-2 as well as the circadian clock regulator Frq in its genome (Salichos & Rokas, 2010; Leonard, 2019). *V. dahliae* recognizes the presence or absence of light during incubation in alternating light/dark cycles as it forms more microsclerotia in darkness and more aerial hyphae during constant illumination resulting in a ring-like structure. Incubation in constant conditions abolished this effect (Leonard, 2019). The circadian clock component Frq presumably represses microsclerotia formation in light and promotes conidiation and fungal growth. These developmental programs might be connected to fungal virulence, but might not require a free-running circadian system in *V. dahliae* (Leonard, 2019; Cascant-Lopez *et al.*, 2020).

1.2.5 Velvet proteins in different fungi connect developmental processes and secondary metabolism

Velvet proteins are fungal specific and conserved in ascomycetes and basidiomycetes (Ni & Yu, 2007). Many *Aspergillus* spp. have been studied for their velvet protein functions leading

to the assumption that their role in fungal development and secondary metabolism is conserved, which is supported by cross-complementation experiments between *A. nidulans* and *A. fumigatus* as well as *A. nidulans* and *N. crassa* (Bayram *et al.*, 2008c; Park *et al.*, 2012a; Sarikaya-Bayram *et al.*, 2019). In *V. dahliae* the formation of microsclerotia as resting structures is an important process as they are the long-term survival structures and major inoculum source of the fungus (Fradin & Thomma, 2006). A similar process in *Aspergillus* spp. is the formation of sclerotia, which relies on VeA and VelB in *A. flavus* and on VeA in *A. parasiticus* (Calvo *et al.*, 2004; Amaike & Keller, 2009; Duran *et al.*, 2009; Chang *et al.*, 2013; Eom *et al.*, 2018). Often, secondary metabolites such as the carcinogenic aflatoxin are produced by different *Aspergillus* spp. for defense and communication (Amaike & Keller, 2011; Brakhage, 2013). The production of secondary metabolites is connected to *A. flavus* VeA, VelB and VelD as well as to VeA in *A. fumigatus* and *A. parasiticus* (Calvo *et al.*, 2004; Duran *et al.*, 2007; Amaike & Keller, 2009; Duran *et al.*, 2009; Dhingra *et al.*, 2012; Eom *et al.*, 2018). Fungi propagate by the formation of conidia, which are distributed by air or water (Bayram & Braus, 2012). Especially VeA promotes conidiation in *A. niger* and *A. parasiticus* (Calvo *et al.*, 2004; Wang *et al.*, 2015). Spore production in *A. flavus* is favored by VeA and VelB (Amaike & Keller, 2009; Duran *et al.*, 2009; Eom *et al.*, 2018). In contrast to that *A. fumigatus* VeA, VelB and VosA are negative regulators of conidiation (Park *et al.*, 2012a). Trehalose is a stress protectant and energy reserve for fungal spores (Perfect *et al.*, 2017). The VelB-VosA heterodimer of *A. nidulans* is involved in trehalose biosynthesis and spore viability (Sarikaya-Bayram *et al.*, 2010; Park *et al.*, 2012b). Similar roles were assigned to VelB and VosA in *A. fumigatus* and *A. flavus* (Park *et al.*, 2012a; Eom *et al.*, 2018). The formation of trehalose in *A. niger* in contrast is connected to VeA (Wang *et al.*, 2015).

A sophisticated interplay between development and secondary metabolite production as known for the velvet proteins is also required in plant pathogenic fungi. As these fungi induce destructive diseases with high economical losses (Dean *et al.*, 2012), velvet proteins might be a starting point to combat fungal plant infections. Velvet proteins have been studied in the filamentous ascomycete *Magnaporthe oryzae* inducing the rice blast disease, which is the most detrimental disease of rice worldwide. They have also been analyzed in the necrotrophic plant pathogenic fungus *Botrytis cinerea* that infects over 1000 different species worldwide or in the soil-borne destructive pathogen *Fusarium oxysporum*, which attacks more than 100 different plants but also immunocompromised humans (Wilson & Talbot, 2009; Dean *et al.*, 2012; Husaini *et al.*, 2018; Petrasch *et al.*, 2019). Similar to *Aspergillus* spp., the velvet domain proteins of the mentioned plant pathogens are connected to developmental processes such as conidiation or sclerotia formation. In *M. oryzae VEA*, *VELB* and *VELC* are required for conidiation. *VEA* and *VELB* are needed for conidia germination whereas *VELC* is important for the morphology of conidia (Kim *et al.*, 2014). In *B. cinerea* all velvet homologs are expressed

during all phases of the fungal life cycle: conidiation in light, development of sclerotia in darkness and infection of plants. Light-dependent processes such as macroconidia and sclerotia formation as well as melanin biosynthesis are regulated by *B. cinerea* VEL1 (Schumacher *et al.*, 2012). In *F. oxysporum* f. sp. *lycopersici* homologs of *A. nidulans* VeA, VelB and VelC were identified (López-Berges *et al.*, 2009, 2013). Especially VeA and VelB but to a minor extend also VelC of *F. oxysporum* are negative regulators of conidiation and influence the shape and size of microconidia (López-Berges *et al.*, 2013). Velvet proteins of the different fungi are also connected to plant infection and virulence. *M. oryzae* infects its host by the formation of melanized appressoria (Wilson & Talbot, 2009). Within this major step of disease induction *M. oryzae VEA* is required for appressorium formation and *VELC* for plant cell penetration (Kim *et al.*, 2014). *B. cinerea* VEL1 is dispensable for plant penetration but required for colonization of leaves and hence needed for full virulence, but is not important for the production of the two virulence-related secondary metabolites botcinic acid and botrydial (Schumacher *et al.*, 2012). However, *B. cinerea* VEL1 regulates the expression of genes related to secondary metabolism such as PKS-encoding genes, which are needed for melanin biosynthesis (Kroken *et al.*, 2003; Schumacher *et al.*, 2014, 2015). VeA is crucial for virulence of *F. oxysporum* in mammals and plants whereas VelB is only involved in plant virulence. The mycotoxin beauvericin is produced during infection of *F. oxysporum* in plants and mammals. *In planta*, both, VeA and VelB, are required for the production of this mycotoxin (López-Berges *et al.*, 2013). Hence, a connection between secondary metabolism and velvet genes is also present in plant pathogenic fungi.

In summary, the role of velvet domain proteins in different ascomycetes is often related to fungal development and differentiation as well as secondary metabolism and virulence. However, the role of velvet domain proteins differs considerably in different fungi, which makes it important to understand the specific mechanistic function of all velvet proteins in a vascular pathogenic fungus as *Verticillium*. So far nothing is known about velvet domain proteins in *Verticillium* spp. and it remains to be examined whether these proteins are potential targets to control fungal growth and to fight plant diseases caused by the pathogen.

1.3 Microbial interactions in the rhizosphere

In the senescent plant *V. dahliae* forms microsclerotia as resting structures, which survive until the next growing season in the soil. They have to germinate in the rhizosphere of a suitable host plant and grow towards the roots to start a novel disease cycle. Antifungal chemicals are mostly useless once the fungus has entered the plant xylem and might be applied *ex planta* in the rhizosphere. Fungal growth is additionally controlled by other inhabitants of the rhizosphere.

1.3.1 Composition of the plant rhizosphere

The soil around a plant root is considered as rhizosphere. This region is influenced by root exudates and plant-derived carbon and contains a high amount of microbial biomass (Fierer, 2017; Gouda *et al.*, 2018). Conditions in the soil as well as microbial communities are highly diverse (Raaijmakers & Mazzola, 2012; Fierer, 2017). Within the soil eukaryotes, bacteria, archaea and viruses are present with bacteria and fungi as the most abundant groups (Fierer, 2017). These microorganisms can be beneficial or detrimental for the plant (Mendes *et al.*, 2013). Beneficial microorganism as for instance *Pseudomonas* spp., *Bacillus* spp. or *Trichoderma* spp. promote plant growth and protect plants against pathogens (Mendes *et al.*, 2013; Woo *et al.*, 2014; Deketelaere *et al.*, 2017). In contrast, plant pathogens such as *Ralstonia solanacearum*, *Fusarium oxysporum* and *V. dahliae* lead to yield losses in economically important crops (Dean *et al.*, 2012; Mendes *et al.*, 2013; Deketelaere *et al.*, 2017). Opportunistic human pathogens as for example *P. aeruginosa* are also present in the soil (Mendes *et al.*, 2013). Among these pathogens is also the saprophytic ascomycete *A. fumigatus*, which can lead to aspergillosis in immunocompromised patients and has a high mortality rate (Latgé & Chamilos, 2019). Different other *Aspergillus* spp. like the well-studied species *A. nidulans*, which is frequently used as model organism, are present in the soil as well (de Vries *et al.*, 2017).

The different soil-inhabiting microorganisms can communicate, interact and compete for example for space and nutrients. Due to these competitions the environment including plants can also be affected.

1.3.2 Bacterial and fungal relations and their impact on plants

Due to the increasing world population, the need for higher crop yields has grown for ages. In general, nearly enough food is available, but especially low-income countries and poor people suffer from malnutrition and famine (Alexandratos & Bruinsma, 2012). Monocultures and increased international trade have led to more virulent strains, which are often tolerant to pesticides (Syed Ab Rahman *et al.*, 2018). In recent years, the usage of chemical toxins against plant pathogens or other microorganisms enhanced crop quality and output, but also led to environmental damages, resistances of pathogens and moreover has disadvantages for human health. Hence, alternatives which are useful and environmentally acceptable are required (Deketelaere *et al.*, 2017; Syed Ab Rahman *et al.*, 2018; Keswani *et al.*, 2019). An alternative method to chemical compounds can be microbes as for example fungi or bacteria, which often live as endophytes, symbionts or colonize the root surface. They are beneficial for the plant, environmentally safe and economically favorable regarding development, registration and market demand (Egamberdieva *et al.*, 2017; Gouda *et al.*, 2018; Syed Ab Rahman *et al.*, 2018; Keswani *et al.*, 2019; Yan *et al.*, 2019).

Beneficial effects of fungi and bacteria against pathogens are diverse and helpful during biotic stress like pathogen attack as well as abiotic stress like drought, temperature changes, salinity, UV radiation and heavy metals (Yan *et al.*, 2019). Microbial biocontrol organisms apply four different main modes of action against pathogens: induced resistance and priming, competition for infection site, space and nutrients, hyperparasitism/mycoparasitism and antibiosis using antimicrobial metabolites. Often these mechanisms are combined and therefore the single mechanisms are not always clear to distinguish (Deketelaere *et al.*, 2017; Köhl *et al.*, 2019).

Verticillium wilt can lead to approximately 50 % yield losses in high crops as cotton, olive and strawberry (EFSA PLH Panel (EFSA Panel on Plant Health), 2014). Hence, environmentally acceptable control mechanism against this disease are required. Depending on the medium, strains of *Pseudomonas fluorescens* and *Pseudomonas protegens* isolated from the plant rhizosphere can inhibit growth of *V. dahliae* and *V. longisporum* on plate (Nesemann *et al.*, 2018). Other studies revealed that also *Bacillus thuringiensis* and *Bacillus weihenstephanensis*, which were isolated from the rhizosphere of field-grown tomatoes, inhibit growth of *V. dahliae* and to a smaller extent also *V. longisporum* (Hollensteiner *et al.*, 2017).

In order to control Verticillium wilt, soil fumigation with a mixture of methyl bromide and chloropicrin was applied before planting but due to high costs and environmental burden alternatives are required (Ajwa *et al.*, 2002; Duniway, 2002; Martin, 2003; Klosterman *et al.*, 2009). One aim in disease control is the reduction of long-living microsclerotia as infection source (Klosterman *et al.*, 2009; Inderbitzin & Subbarao, 2014). In some cases resting structure reduction could already be achieved by crop rotation as for instance with planting broccoli and strawberry in alternation, but for many other crops the broad host range of *Verticillium* spp. and the longevity of microsclerotia make rotation inefficient (Njoroge *et al.*, 2009; Klosterman *et al.*, 2009; Wheeler *et al.*, 2019). Hence, mutually antagonistic microorganisms inhibiting resting structure formation or their germination are a promising alternative. In addition to the afore mentioned *Bacillus* spp. and *Pseudomonas* spp. also non-pathogenic *Verticillium* strains, *Trichoderma* spp. and *Fusarium* spp. are useful against *Verticillium* spp. as well (Deketelaere *et al.*, 2017). By comparing several studies on Verticillium wilt control, Deketelaere and co-workers identified modes of action desirable for a promising antagonist against *Verticillium* spp. (Deketelaere *et al.*, 2017). These mechanisms include the general effects as mentioned before and can be direct or indirect. Furthermore, the mechanisms were extended by Deketelaere and co-workers as biocontrol agents should aid the plant by growth promotion and reduce germination of the inoculum (Deketelaere *et al.*, 2017) (Figure 6).

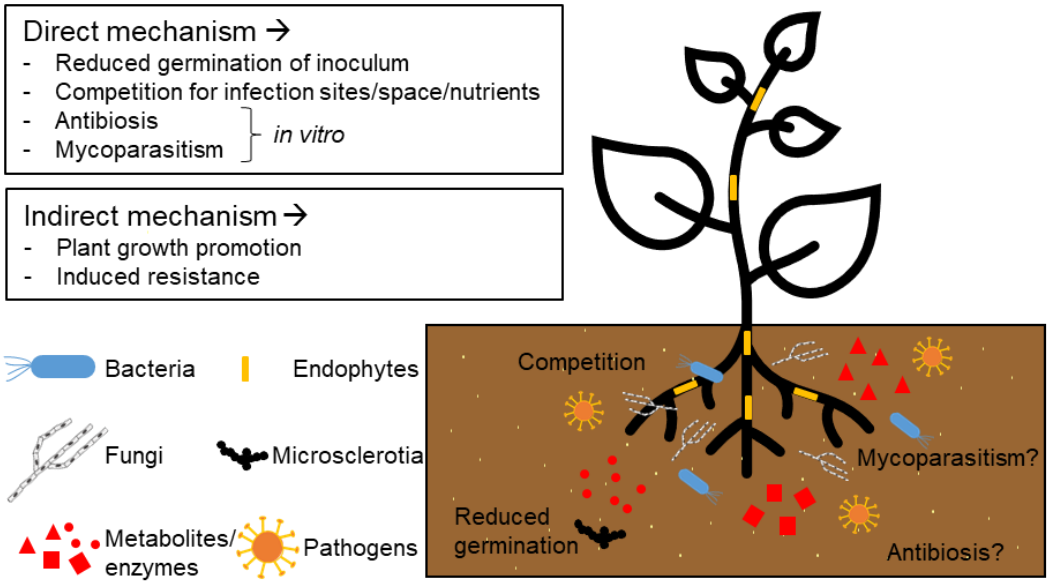

Figure 6: Antagonistic fungi and bacteria alter plant defense reactions against *Verticillium* spp. Microorganisms work direct and indirect against Verticillium wilt. Mutually antagonistic microorganisms are directly reducing germination of inoculum as for instance microsclerotia, compete with pathogens for infection sites, space and nutrients and presumably induce antibiosis by production of metabolites and mycoparasitism by secretion of lytic enzymes. In an indirect way, the microorganisms promote plant growth and induce resistance against pathogens. The figure was composed with information derived from Deketelaere *et al.*, 2017.

Microsclerotia are the primary inoculum of *V. dahliae* and remain in the soil for several years (Wilhelm, 1955), which make Verticillium wilt a recurrent problem. By diminishing the amount of germinating microsclerotia the disease is reduced (Klosterman *et al.*, 2009; Inderbitzin & Subbarao, 2014; Deketelaere *et al.*, 2017; Fan *et al.*, 2020). Verticillium wilt is often accompanied by reduced growth. Applying growth promoting microbes can counteract this effect (Deketelaere *et al.*, 2017). These microorganisms often fix nutrients and nitrogen, solubilize phosphate and potassium, induce the production of phytohormones, siderophores and exopolysaccharides and contribute to rhizoremediation, which leads to plant growth promotion (Naraghi *et al.*, 2012; Gouda *et al.*, 2018). Positions to infect the plant as well as space on the root and nutrients are limited. Hence, the competition for these reduces pathogens. Considering that *Verticillium* spp. are vascular plant pathogens (Reusche *et al.*, 2014), especially microorganisms that colonize the xylem are vitally important (Deketelaere *et al.*, 2017). Many microbes have a mutually antagonistic effect on *Verticillium* spp. *in vitro*, which may be due to antibiosis by antimicrobial metabolites and mycoparasitism by secretion of cell wall degrading enzymes but *in planta* data is mostly lacking (Deketelaere *et al.*, 2017). Another frequently effect caused by the presence of antagonistic microbes is the induction of resistance in the host due to expression of defense related genes, defense pathways dependent on salicylic and jasmonic acid as well as pathogen- and damage-associated molecular pattern-triggered immunity (Deketelaere *et al.*, 2017).

As the rhizosphere composition and the environmental conditions differ, the antagonistic ability of microorganisms can be altered (Gouda *et al.*, 2018). Mutually antagonistic microbes that are functional in sterile soil or in *in vitro* systems are often failing to function in the field due to complex conditions in the natural habitat (Stadler & von Tiedemann, 2014; Deketelaere *et al.*, 2017; Köhl *et al.*, 2019). In order to achieve the optimal results of microbe application, the mode of action has to be understood and application methods have to be taken into account (Deketelaere *et al.*, 2017; Köhl *et al.*, 2019). Today, research in biotechnology and nanotechnology has produced nanomaterials, biosensors and nano-fertilizers, that are starting to be used in order to bring antagonistic microorganisms close to the position where they reach their full potential (Gouda *et al.*, 2018). Beside all these advantages and chances of microorganisms as control agent, one should also keep adverse effects of microbes in mind as they can lead to a delay in growth, survival of natural enemies in the rhizosphere, can act as latent pathogens and might have toxic effects or lead to resistances when antimicrobial metabolites are applied in large scale (Köhl *et al.*, 2019; Yan *et al.*, 2019).

Fungi induce a diverse set of reactions in bacteria and *vice versa* bacteria induce biochemical reactions in fungi as the cross-pathway control system for supply of amino acids (Fischer *et al.*, 2018). This control system is required for pathogenicity in *Verticillium* spp. (Timpner *et al.*, 2013) and important for developmental programs as the formation of fruiting bodies as resting structures of *A. nidulans* (Hoffmann *et al.*, 2000, 2001).

During this study, the soil-borne plant pathogen *V. dahliae* was investigated. In the soil the fungus can encounter different pseudomonads. Hence, the interaction of *V. dahliae* and these bacteria was elucidated in more detail.

1.3.3 Fluorescent pseudomonads and their bioactive compounds

The antagonistic effect of fluorescent pseudomonads, which belong to the group of γ-proteobacteria, towards fungi is known for several decades (Weller *et al.*, 2002; Haas & Défago, 2005). The bacteria produce antifungal substances, impede pathogenicity factors of the fungus and can also induce systemic resistance in potential host plants (Haas & Défago, 2005; Pieterse *et al.*, 2014). Pseudomonads are able to produce different substances with antifungal potential as for instance phenazines, 2,4-diacetylphloroglucinol (DAPG), pyoluteorin, and hydrogen cyanide (Haas & Défago, 2005; Raaijmakers & Mazzola, 2012) (Figure 7).

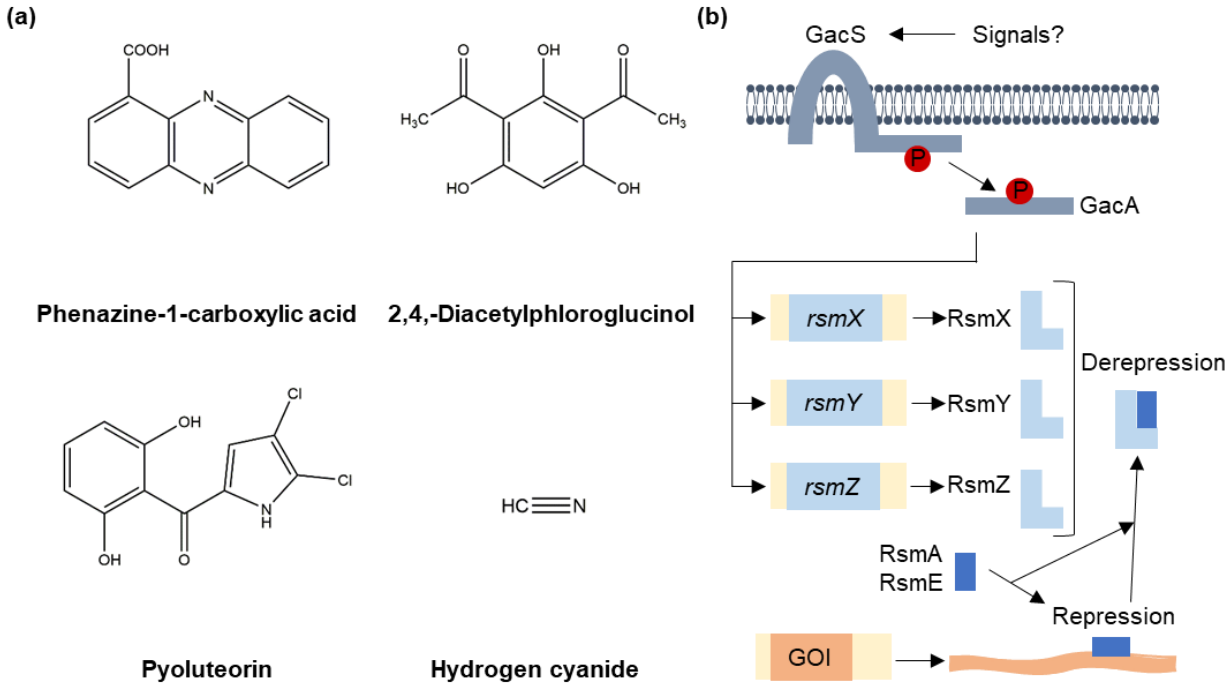

Figure 7: Chemical structures of antibiotic compounds and the GacS/GacA two-component system. (a) Depicted are examples of biocontrol substances produced by pseudomonads. **(b)** Model of the GacS/GacA two-component system. The sensor kinase GacS is stimulated by an unknown signal, which leads to autophosphorylation. The phosphate group is transferred to GacA and the transcription of *rsmX*, *rsmY* and *rsmZ* is activated. The proteins RsmA and RsmE bind to the small RNAs, which leads to posttranscriptional repression of biocontrol genes (here shown as gene of interest, GOI).The figure is modified according to Haas & Défago (2005) and Keswani *et al.* (2020).

The production of heterocyclic nitrogen-containing phenazines is reported for many *Pseudomonas* spp. and other bacteria (Mavrodi *et al.*, 2006; Biessy & Filion, 2018). With antagonistic effects, which rely on their redox activity leading to reactive oxygen species and oxidative stress, they affect a broad spectrum of other microorganisms including pathogenic fungi, bacteria and oomycetes (Mavrodi *et al.*, 2006; Mousa & Raizada, 2015; Biessy & Filion, 2018). Phenazine production is regulated in all strains by the gene cluster *phzABCDEFG*, but so far chemical synthesis of phenazines was not efficient due to low yield and toxic side products (Biessy & Filion, 2018; Keswani *et al.*, 2020). The phenolic antibiotic DAPG also has a broad working spectrum against fungi, bacteria and parasites, controls plant diseases and is produced by many *Pseudomonas* spp. worldwide (Weller *et al.*, 2007; Keswani *et al.*, 2020). Chemical synthesis of DAPG is possible, but the substance is instable in sunlight and phytotoxic in high concentrations, which makes it unattractive for commercial use (Haas & Défago, 2005; Keswani *et al.*, 2020). The chlorinated polyketide pyoluteorin is also produced by pseudomonads and controls many soil-borne diseases (Keswani *et al.*, 2020). However, the mode of action of this substance is unknown (Haas & Défago, 2005). The volatile compound hydrogen cyanide is produced in different Gram-negative bacteria including pseudomonads and inhibits the cytochrome C oxidase as well as other metalloproteins, which

makes it extremely poisonous and a suppressor of plant diseases (Mousa & Raizada, 2015; Keswani *et al.*, 2020).

In addition, in many Gram-negative bacteria the GacS/GacA two-component system controls the expression of secondary metabolites and extracellular enzymes, including the above mentioned substances (Heeb & Haas, 2001; Haas & Défago, 2005). The sensor kinase GacS is autophosphorylated by an unknown signal and the phosphate group is transferred to the response regulator GacA, which than activates the transcription of the small non-coding RNA genes *rsmX*, *rsmY* and *rsmZ*. The small RNAs bind to RsmA and RsmE, which are posttranscriptional repressors of some biocontrol genes (Haas & Défago, 2005).

Pseudomonads fulfil the genomic requirements to produce diverse bioactive compounds that are differentially useful antagonists against soil pathogens such as *V. dahliae* or *V. longisporum in vitro* (Nesemann *et al.*, 2018). Different *Pseudomonas* strains might additionally be capable of antagonizing human pathogens, however, interactions between different pseudomonads and the opportunistic pathogen *P. aeruginosa* are not well studied. Chatterjee and co-workers discovered that environmental pseudomonads isolated from soil and water exhibit antagonistic activity on a plate assay against *P. aeruginosa,* which leads to severe infections of the lung in patients with cystic fibrosis (Chatterjee *et al.*, 2017). As resistance against antibiotics is increasing, pseudomonads may also provide novel bioactive substances as treatment for human infections. Due to the positive effects regarding this lung-inhabiting bacterium, it may be interesting to investigate if pseudomonads have an antagonistic effect on other pathogens inhabiting the lung as for instance *A. fumigatus*.

Besides the beneficial effects of pseudomonads, one should also keep in mind that application in the field or greenhouse might be complicated as the bacteria are not viable during storage for several weeks, which makes commercial use difficult (Haas & Défago, 2005). Hence, antagonistic strains that produce spores as for instance *Bacillus* spp. are also under investigation and commercially available (Haas & Défago, 2005; Hollensteiner *et al.*, 2017). Many studies regarding antibiotic producing bacteria are just conducted *in vitro* or had no effect when tested *in planta* (Deketelaere *et al.*, 2017). Therefore, it is questionable if the bacteria are producing these substances in the soil as well and if concentrations are high enough to harm other organisms (Köhl *et al.*, 2019).

1.4 Aims of the study

Verticillium wilt occurs in many valuable crop plants and hence induces the damage of agricultural products as well as financial losses. The use of fungicides against *Verticillium* spp. is difficult as they are often harmful towards the environment and difficult in application as the fungus is mainly localized *in planta*. In addition, long-term resting structures of the fungus remain in the soil for several years (Wilhelm, 1955), which make this disease recurrent. The life cycle of *V. dahliae* is complex as it requires different developmental programs in order to colonize the plant root by the formation of hyphopodia, distribute *in planta* by conidia and produce melanized microsclerotia in the fading plant to survive harsh conditions in the soil. Especially for the formation of microsclerotia secondary metabolites like melanin have to be produced to ensure shelter of the survival structures.

The velvet proteins can coordinate fungal developmental processes and secondary metabolite production (Kato *et al.*, 2003). The conservation of velvet proteins in ascomycetes and basidiomycetes (Ni & Yu, 2007) suggests important roles for members of this family in different species, which have to be adapted to the life cycle of the respective fungus. The formation of different homo- and heterodimers with other velvet and non-velvet proteins suggests a complex function of the velvet domain proteins in diverse biological processes (Sarikaya-Bayram *et al.*, 2015). Previous studies of the velvet family in some plant pathogenic fungi have not yet revealed their exact regulatory functions during pathogenicity and any corresponding study with *Verticillium* spp. is missing. It is yet unknown, whether velvet domain proteins affect the formation of microsclerotia.

Microsclerotia are present in the soil in the rhizosphere were microorganisms such as pseudomonads produce different metabolites with an antagonistic effect on fungal growth (Haas & Défago, 2005; Deketelaere *et al.*, 2017). Microorganism in the soil communicate by the formation of metabolites or influence developmental processes in the life cycle of other microorganisms (Macheleidt *et al.*, 2016). Microsclerotia germination and growth towards a host plant is affected by the microbiome of the plant rhizosphere.

The primary goal of this thesis was to systematically examine the molecular role of all four genes encoding velvet domain proteins during *V. dahliae* vegetative growth, fungal development, infection of plants, growth and propagation within the plant and the formation of microsclerotia as long-lasting survival and resting structures. This includes to examine whether any of the velvet domain encoding genes might be promising targets to control *V. dahliae* as pathogen of important crops in our agriculture.

A second goal of this thesis was to analyze the interplay of soil-borne *V. dahliae* with different fluorescent pseudomonads isolated from the plant rhizosphere. This includes the

efficiency and persistence to inhibit conidia germination and the impact of the presence of bacteria on fungal growth during different cultivation conditions.

2 MATERIALS AND METHODS

2.1 Laboratory materials

Media, solutions and buffers used within this study were prepared using products from AppliChem GmbH (Darmstadt, Germany), BD Biosciences (Heidelberg, Germany), Biozym Scientific GmbH (Hessisch Oldendorf, Germany), Carl Roth GmbH & Co. KG (Karlsruhe, Germany), Fluka (Neu-Ulm, Germany), Invitrogen (Carlsbad, CA, USA), Merck KGaA (Darmstadt, Germany), Oxoid Deutschland GmbH (Wesel, Germany), Roche Diagnostics GmbH (Mannheim, Germany), Serva Electrophoresis GmbH (Heidelberg, Germany), Sigma-Aldrich Chemie GmbH (St. Louis, MO, USA), Th. Geyer GmbH & Co. KG (Renningen, Germany), Thermo Fisher Scientific (Schwerte, Germany) and VWR International GmbH (Darmstadt, Germany).

For determination of the pH value a WTW bench pH/mV Routine meter pH 526 (Sigma-Aldrich Chemie GmbH, St. Louis, MO, USA) was used.

Plastic consumables such as pipet tips, reaction tubes, petri dishes were purchased from Sarstedt AG & Co. KG (Nümbrecht, Germany), StarLab GmbH (Hamburg, Germany) and Nerbe Plus GmbH (Winsen/Luhe, Germany). The 1.5 ml and 2 ml reaction tubes were centrifuged in Heraeus™ Biofuge Fresco and Heraeus™ Pico™ centrifuges from Heraeus Instruments GmbH (Hanau, Germany) as well as in Centrifuge 5417 R from Eppendorf AG (Hamburg, Germany) and in a Heraeus Fresco™ 17 centrifuge (Thermo Fisher Scientific, Schwerte, Germany). For centrifugation of 15 ml and 50 ml tubes Centrifuge 5804 R from Eppendorf AG (Hamburg, Germany) was utilized. Larger cultures were centrifuged with the Sorvall® RC-5B Plus Superspeed Centrifuge (Thermo Fisher Scientific, Schwerte, Germany). For incubation with constant agitation the GFL shaking water bath 1086 (GFL, Burgwedel, Germany), the Orbital shaker 3005, Orbital shaker 3020 and the Rotamax 120 (Heidolph, Schwabach, Germany) and the compact shaker KS-15 A control (Edmund Bühler GmbH, Bodelshausen, Germany) were applied. For constant agitation of reaction tubes with a volume of 1.5 ml the VXR basic Vibrax® equipped with VX 2E extension (IKA®-Werke GmbH & Co. KG, Staufen, Germany) was used.

For selection of microorganisms, ampicillin (Carl Roth GmbH & Co. KG, Karlsruhe, Germany), kanamycin (AppliChem GmbH, Darmstadt, Germany), carbenicillin disodium salt (Fluka, Neu-Ulm, Germany), chloramphenicol (AppliChem GmbH, Darmstadt, Germany), doxycycline (Sigma-Aldrich Chemie GmbH, St. Louis, MO, USA), clonNAT nourseothricin dihydrogen sulfate (Werner Bioagents GmbH, Jena, Germany), cefotaxime (Wako Chemicals GmbH,

Neuss, Germany), hygromycin B (InvivoGen, San Diego, CA, USA) and G 418 disulfate salt (geneticin) (Sigma-Aldrich Chemie GmbH, St. Louis, MO, USA) were used.

Sterile filtration of small volumes was conducted by using Filtropur filters with a size of 0.2 µm (Sarstedt AG & Co. KG, Nümbrecht, Germany).

By using Miracloth (Calbiochem Merck, Darmstadt, Germany) fungal spores and mycelium were separated. Fungal spores were diluted in Coulter Isoton II Diluent and counted with the Coulter Particle Count and Size Analyzer Z2 (Beckman Coulter, Krefeld, Germany).

Primers were purchased either from Eurofins Genomics GmbH (Ebersberg, Germany) or Sigma-Aldrich Chemie GmbH (St. Louis, MO, USA). Restriction enzymes, polymerases and appropriate buffers as well as deoxynucleotides were obtained from Thermo Fisher Scientific (Schwerte, Germany) and New England Biolabs (Ipswich, MA, USA). Polymerase chain reactions were performed in T Professional Standard 96, T Professional Trio 48 and T Professional Standard 96 Gradient thermocyclers of Biometra GmbH (Göttingen, Germany).

For purification of DNA the NucleoSpin® Plasmid Kit or the NucleoSpin® Gel and PCR Clean-up Kit from Macherey-Nagel (Düren, Germany) were used. For extraction of RNA the Direct-zol™ RNA MiniPrep Kit (Zymo Research, Freiburg im Breisgau, Germany) was used.

A NanoDrop™ ND-1000 spectrophotometer from PeqLab Biotechnology GmbH (Erlangen, Germany) was utilized for measuring DNA and RNA concentrations. Concentrations of proteins were measured with the Infinite M200 microplate reader using the Magellan software (Tecan Trading AG, Männedorf, Schweiz).

The GeneRuler™ 1 kb DNA ladder and GeneRuler™ 100 bp DNA ladder (Thermo Fisher Scientific, Schwerte, Germany) were used to determine the size of DNA on agarose gels. For determination of the protein size on-gel the PageRuler™ Prestained Protein Ladder 10-180 kDA (Thermo Fisher Scientific, Schwerte, Germany) was applied. For agarose gel electrophoresis Mini-Sub® Cell GT chambers were utilized. Sodium dodecyl sulfate (SDS) - polyacrylamide gel electrophoresis was conducted with Mini-Protean® Tetra Cell and Mini Trans-Blot® Electrophoretic Cell. Both, agarose gels and SDS-polyacrylamide gels, were run with a Power Pac™ 3000 power supply (BIO-RAD Laboratories, Hercules, CA, USA). The RNase A was obtained from AppliChem (Darmstadt, Germany).

For blotting DNA from an agarose gel, the Amersham™ Hybond-N™ nylon membrane was used. To blot proteins from SDS-polyacrylamide gels the Amersham™ Protran™ 0.45 µm NC nitrocellulose membrane was applied. Both membranes were obtained from GE Healthcare life sciences (München, Germany). Southern hybridization was conducted with the Amersham™ AlkPhos Direct™ Labeling and Detection System (GE Healthcare life sciences, München, Germany). Labelled DNA fragments were visualized using the CDP-*Star*® Detection Reagent (GE Healthcare life sciences, München, Germany). For detection of chemiluminescent signals of Southern and western hybridizations the Amersham™

Hyperfilm™-ECL (GE Healthcare life sciences, München, Germany) and the Optimax® X-ray Film Processor from Protec GmbH & Co. KG (Oberstenfeld, Germany) were utilized. Incubation of the nylon membrane was conducted in a HERAhybrid 12 hybridization oven (Heraeus Instruments GmbH, Hanau, Germany). For western hybridization the chemiluminescent signals were also detected by applying the Fusion SL chemiluminescence detector (PeqLab, Erlangen, Germany) operated with Fusion 15.18 (Vilber Lourmat Deutschland GmbH, Eberhardzell, Germany). For western hybridization the α-GFP antibody sc-9996 (Santa Cruz Biotechnology, Dallas, TX, USA) was used as primary antibody. As secondary antibody the mouse 115-035-003 antibody coupled to a horseradish peroxidase (Jackson ImmunoResearch, West Grove, PA, USA) was applied.

In order to conduct protein pull downs, GFP-Trap® Agarose beads from ChromoTek GmbH (Planegg-Martinsried, Germany) were used. Proteins were purified with Poly-Prep® Chromatography Columns (BIO-RAD Laboratories, Hercules, CA, USA). To enhance the enzymatic reaction RapiGest™ SF Surfactant (Waters Corporation, Milford, MA, USA) was applied. Trypsin from Serva Electrophoresis GmbH (Heidelberg, Germany) was utilized afterwards.

In order to concentrate samples, the Savant SPD 111V SpeedVac Concentrator (Thermo Fisher Scientific, Schwerte, Germany) was used. For cloning, the GeneArt® Seamless Cloning and Assembly Kit and CloneJET™ PCR Cloning Kit were utilized (Thermo Fisher Scientific, Schwerte, Germany). Ligation of fragments was conducted with the T4 DNA-Ligase (Thermo Fisher Scientific, Schwerte, Germany).

Fluorescence microscopy was conducted in µ-Slide 8 Well microscopy chambers of ibidi GmbH (Gräfelfing, Germany). The Zeiss Observer Z1 microscope (Zeiss, Oberkochen, Germany) with a CSU-X1 A1 confocal scanner unit (Yokogawa, Ratingen, Germany) and QuantEM:512SC digital camera (Photometrics, Tuscon, AZ, USA) was used with the SlideBook 6.0 digital microscopy software (Intelligent Imaging Innovations, Göttingen, Germany).

For scanning plates from phenotypical analysis, the Epson Perfection V600 Photo Scanner (Epson, Suwa, Japan) was used. Colonies were phenotypically examined and discoloration of the hypocotyl was observed by using the binocular microscope SZX12-ILLB2-200 (Olympus Deutschland GmbH, Hamburg, Germany) illuminated with the KL1500-LCD light source (Olympus Deutschland GmbH, Hamburg, Germany). Microsclerotia from fungal colonies were analysed with the Axiolab light microscope (Zeiss, Oberkochen, Germany). Binocular microscope and light microscope were equipped with SC30 cameras (Olympus Deutschland GmbH, Hamburg, Germany) and used with the cellSens Dimension software version 1.4 (Olympus Deutschland GmbH, Hamburg, Germany).

For plant experiments pots with a size of 70x70x80 mm were obtained from Soparco GmbH (Saarbrücken, Germany). A mixture of Fruhstorfer Erde Typ T Struktur 1-fein- (Archut GmbH & Co. KG, Lauterbach, Germany) and crystal silica sand 0.4-0.8 mm (Dorsilit, Hirschau, Germany) was used. Plants were incubated in a BrightBoy GroBank (CLF PlantClimatics, Emersacker, Germany). Phenotypical analysis of fungal strains was conducted in a growth chamber APT.line™ KBW 400 (Binder GmbH, Tuttlingen, Germany).
The concentration of bacterial cells was measured with an Eppendorf BioPhotometer® D30 (Hamburg, Germany).
Materials and instruments not referred to in this part are mentioned in the following chapters.

2.2 Cultivation of microorganisms

Media and supplemented substances were prepared using deionized water. For sterilization media were either autoclaved at 121 °C and 2 bar for 20 min or filtered through a 0.2 µm pore size membrane if the compound was heat-sensitive. Temperature-sensitive compounds were added to the media after autoclaving.

2.2.1 Cultivation of bacterial strains

For cultivation of *Escherichia coli*, *Agrobacterium tumefaciens*, *Pseudomonas fluorescens*, *Pseudomonas synxantha* (formerly *P. fluorescens*) and *Pseudmonas protegens* strains lysogeny broth (LB) medium was used (Bertani, 1951) [1 % (w/v) bacto-tryptone, 0.5 % (w/v) yeast extract, 1 % (w/v) NaCl, pH 7.5, 2 % agar for solid medium]. Liquid cultures were placed on a rotary shaker at 37 °C for *E. coli* strains and 25 °C for *A. tumefaciens* strains. Pseudomonas strains were incubated at 30 °C.
For transformation of chemically competent *E. coli* or *A. tumefaciens* cells liquid SOC medium (2 % bacto-tryptone, 0.5 % yeast extract, 10 mM NaCl, 2.5 mM KCl, 10 mM $MgCl_2$, 10 mM $MgSO_4$; 20 mM glucose were added after autoclaving) was used. For selection, solid LB medium was supplemented with either 100 µg/ml ampicillin or 100 µg/ml kanamycin. For conservation of plasmids equal amounts of bacterial overnight culture and 100 % glycerol were mixed. Plasmids were stored at -80 °C.

2.2.2 Cultivation of *Aspergillus nidulans* and *Aspergillus fumigatus*

Conidia of *A. nidulans* and *A. fumigatus* were both grown on solid minimal medium [1% (w/v) glucose, 1 x AspA solution (70 mM $NaNO_3$, 7 mM KCl, 11.2 mM KH_2PO_4, pH 5.5 with KOH), 1 x (v/v) trace element solution (18 µM $FeSO_4$, 174 µM EDTA, 76 µM $ZnSO_4$, 178 µM H_3BO_3, 25 µM $MnCl_2$, 7.1 µM $CoCl_2$, 6.4 µM $CuSO_4$, 6.2 µM $(NH_4)_6Mo_7O_{24}$; pH 6.5 with KOH) (Hill & Käfer, 2001), 2 mM $MgSO_4$, 2 % agar]. *A. nidulans* was incubated at 37 °C in light; *A. fumigatus* was incubated at 37 °C in darkness. Conidia were collected in sodium-tween

solution [0.96 % (w/v) NaCl, 0.05 % (v/v) Tween80] and stored at 4 °C. To determine the spore concentration the Coulter Particle Count and Size Analyzer Z2 (Beckman Coulter, Krefeld, Germany) and the corresponding Coulter Isoton II Diluent were used. Particles between 1.9 to 4.5 µm were counted.

2.2.3 Cultivation of *Verticillium dahliae*

For conidiospore formation the conidia of *V. dahliae* were cultivated in liquid simulated xylem medium (SXM) modified according to Neumann & Dobinson (2003) as previously described by Hollensteiner *et al.* (2017). In order to obtain fungal mycelium for genomic DNA extraction, the conidia were inoculated in liquid potato dextrose medium (PDM) [2.65 % (w/v) Potato Dextrose broth (Carl Roth GmbH & Co. KG)]. Both types of cultures were incubated at 25 °C under constant agitation at 120 rpm.

The mycelium from PDM or SXM cultures was separated from the liquid with Miracloth filters (Calbiochem Merck, Darmstadt, Germany) and washed with 0.96 % (w/v) NaCl. Mycelium was used for DNA extraction, protein extraction and RNA extraction.

The conidia from SXM cultures were filtered by using sterile Miracloth filters (Calbiochem Merck, Darmstadt, Germany). Conidia were washed with sterile water twice, resuspended in sterile water and stored at 4 °C. For determination of the spore concentration the Coulter Particle Count and Size Analyzer Z2 (Beckman Coulter, Krefeld, Germany) and the corresponding Coulter Isoton II Diluent were used. Particles between 1.9 to 4.5 µm were measured.

For selection of transformants PDM plates [3.9 % (w/v) potato extract glucose agar (Carl Roth GmbH & Co. KG, Karlsruhe, Germany), 0.5 % (w/v) agar] were supplemented with the antimycotics clonNAT nourseothricin dihydrogen sulfate (72 µg/ml), hygromycin B (50 µg/ml), geneticin (50 µg/ml) and the antibiotic cefotaxime (300 µg/ml) as required.

In order to conserve fungal spores, the freshly harvested spores were resuspended in sodium-tween solution [0.96 % (w/v) NaCl, 0.05 % (v/v) Tween80], set to a concentration of $2x10^7$ spores/ml and mixed with the equal volume of 50 % glycerol. The fungal strains were afterwards stored at -80 °C.

2.3 Strains, plasmids and primers

2.3.1 Bacterial strains

For cloning and plasmid construction the *E. coli* strain DH5α (Invitrogen, Carlsbad, CA, USA) was used. *A. tumefaciens*-mediated transformation (ATMT) of *V. dahliae* was performed using the *A. tumefaciens* strain AGL1 (Lazo *et al.*, 1991). Different *Pseudomonas* spp. were used for co-cultivation experiments. All bacterial strains used in this study are indicated in Table 1.

Table 1: Bacterial strains used in this study.

Strain name	Description	Reference
Agrobacterium tumefaciens		
AGL1	Used for A. *tumefaciens*-mediated transformation of *V. dahliae*	(Lazo *et al.*, 1991)
Escherichia coli		
DH5α	Used for cloning and extraction of plasmid DNA	Invitrogen
***Pseudomonas* spp.**		
P_rhizo (DSMZ: DSM8569)	*P. fluorescens*, wild type, isolated from rape seed rhizosphere	(Berg & Ballin, 1994)
P_phen (2-79, B-15132)	*P. synxantha* (formerly *P. fluorescens*), wild type, i.a. phenazine production	(Weller & Cook, 1983)
P_DAPG (CHA0, DSMZ: DSM19095)	*P. protegens*, wild type, i.a DAPG production	(Stutz *et al.*, 1986)

DSMZ = "Deutsche Sammlung von Mikroorganismen und Zellkulturen", Germany; DAPG = 2,4-diacetylphloroglucinol

2.3.2 *Verticillium* strains

Verticillium strains used and generated within this study are listed in Table 2. *V. dahliae* JR2 (Fradin *et al.*, 2009) served as wild type and background strain for construction of other strains.

Table 2: *Verticillium dahliae* strains used in this study.

Strain name	Description	Reference
JR2 (VGB39)	Wild type isolate from *Solanum lycopersicum*	(Fradin *et al.*, 2009)
VGB18 (Δ*LAE1*)	Δ*LAE1::NAT^{R}*	(Nesemann *et al.*, 2018)
VGB22 (WT/*HISTONE-RFP*)	*^{P}GPDA:H2B:RFP:TRPC^{T}:^{P}GPDA:NAT^{R}*	This study
VGB45 (WT/*OE-GFP*)	*^{P}GPDA:GFP:TRPC^{T}:^{P}GPDA:HYG^{R}:TRPC^{T}*	(Tran *et al.*, 2014)
VGB58/VGB59 (Δ*VEL2*)	Δ*VEL2::^{P}GPDA:NAT^{R}*	This study
VGB64/VGB65 (Δ*VOS1*)	Δ*VOS1::^{P}GPDA:NAT^{R}*	This study
VGB219/VGB220 (*OE-VOS1-GFP*/*HISTONE-RFP*)	*^{P}GPDA:H2B:RFP:TRPC^{T}:^{P}GPDA:NAT^{R};* *^{P}GPDA:VOS1:GFP:TRPC^{T}:^{P}GPDA:HYG^{R}:TRPC^{T}*	This study
VGB223 (*OE-VEL2-GFP*/*HISTONE RFP*)	*^{P}GPDA:H2B:RFP:TRPC^{T}:^{P}GPDA:NAT^{R};* *^{P}GPDA:VEL2:GFP:TRPC^{T}:^{P}GPDA:HYG^{R}:TRPC^{T}*	This study
VGB234/VGB235 (Δ*VEL3*)	Δ*VEL3::^{P}GPDA:NAT^{R}:TRPC^{T}*	This study
VGB241/VGB242 (Δ*VOS1*)	Δ*VOS1::^{P}GPDA:HYG^{R}:TRPC^{T}*	This study

Table 2: *Verticillium dahliae* strains used in this study, continued.

Strain name	Description	Reference
VGB246/VGB247 (Δ*VEL1*)	Δ*VEL1::^{P}GPDA:HYG^{R}:TRPC^{T}*	This study
VGB281/VGB282 (Δ*VEL1*/Δ*VEL2*)	Δ*VEL2::^{P}GPDA:NAT^{R};* Δ*VEL1::^{P}GPDA:HYG^{R}:TRPC^{T}*	This study
VGB289/VGB290 (Δ*VEL3*/Δ*VEL1*)	Δ*VEL1::^{P}GPDA:HYG^{R}:TRPC^{T};* Δ*VEL3::^{P}GPDA:NAT^{R}:TRPC^{T}*	This study
VGB297 (*OE-VEL1*)	*^{P}GPDA:VEL1:GFP:TRPC^{T}:^{P}GPDA:HYG^{R}:TRPC^{T}*	This study
VGB362 (Δ*VEL2/OE-VEL1-GFP*)	Δ*VEL2::^{P}GPDA:NAT^{R};* *^{P}GPDA:VEL1:GFP:TRPC^{T}:^{P}GPDA:HYG^{R}:TRPC^{T}*	This study
VGB364 (*OE-VEL1-GFP*/*HISTONE-RFP*)	*^{P}GPDA:H2B:RFP:TRPC^{T}:^{P}GPDA:NAT^{R};* *^{P}GPDA:VEL1:GFP:TRPC^{T}:^{P}GPDA:HYG^{R}:TRPC^{T}*	This study
VGB373 (Δ*VOS1*/Δ*VEL3*)	Δ*VEL3::^{P}GPDA:NAT^{R}:TRPC^{T};* Δ*VOS1::^{P}GPDA:HYG^{R}:TRPC^{T};*	This study
VGB375 (Comp. *VEL2*)	Δ*VEL2::^{P}VEL2:VEL2:GFP:^{P}GPDA:HYG^{R}:TRPC^{T}:VEL2^{T}*	This study
VGB392 (WT/*OE-GFP*)	*^{P}GPDA:GFP:TRPC^{T}:^{P}GPDA:NAT^{R}:TRPC^{T}*	(Starke *et al.*, 2020)
VGB443/VGB444 (Δ*VEL1*/*OE-GFP*)	Δ*VEL1::^{P}GPDA:HYG^{R}:TRPC^{T};* *^{P}GPDA:GFP:TRPC^{T}:^{P}GPDA:NAT^{R}:TRPC^{T}*	This study
VGB445/VGB446 (Comp. *VEL3*)	Δ*VEL3::^{P}VEL3:VEL3:^{P}GPDA:HYG^{R}:TRPC^{T}:VEL3^{T}*	This study
VGB447 (*VEL1-GFP*)	*^{P}VEL1:VEL1:GFP:^{P}GPDA:HYG^{R}:TRPC^{T}:VEL1^{T}*	This study
VGB450 (*VEL2-GFP*)	*^{P}VEL2:VEL2:GFP:^{P}GPDA:HYG^{R}:TRPC^{T}:VEL2^{T}*	This study
VGB451 (*VEL3-GFP*)	*^{P}VEL3:VEL3:GFP:^{P}GPDA:HYG^{R}:TRPC^{T}:VEL3^{T}*	This study
VGB453 (*VOS1-GFP*)	*^{P}VOS1:VOS1:GFP:^{P}GPDA:HYG^{R}:TRPC^{T}:VOS1^{T}*	This study
VGB468 (*VEL2$^{\Delta IDD}$-GFP*)	*^{P}VEL2:VEL2$^{\Delta 210\text{-}325}$:GFP:^{P}GPDA:HYG^{R}:TRPC^{T}:VEL2^{T}*	This study
VGB474 (Comp. *VEL1*)	Δ*VEL1::^{P}VEL1:VEL1^{P}GPDA:NAT^{R}:TRPC^{T}:VEL1^{T}*	This study
VGB477 (WT/*HISTONE-RFP*)	*^{P}GPDA:H2B:RFP:TRPC^{T}:^{P}GPDA:GEN^{R}:TRPC^{T}*	(Starke *et al.*, 2020)
VGB495 (Δ*VEL1*/*HISTONE-RFP*)	*^{P}GPDA:H2B:RFP:TRPC^{T}:^{P}GPDA:GEN^{R}:TRPC^{T};* Δ*VEL1::^{P}GPDA:NAT^{R}:TRPC^{T}*	This study
VGB496/VGB497 (Δ*VEL1*/*OE-VEL2-GFP*/*HISTONE-RFP*)	*^{P}GPDA:H2B:RFP:TRPC^{T}:^{P}GPDA:GEN^{R}:TRPC^{T};* Δ*VEL1::^{P}GPDA:NAT^{R}:TRPC^{T}* *^{P}GPDA:VEL2:GFP:TRPC^{T}:^{P}GPDA:HYG^{R}:TRPC^{T}*	This study
VGB498/VGB499 (Δ*VEL2*/*OE-VEL1-GFP*/*HISTONE-RFP*)	Δ*VEL2::^{P}GPDA:NAT^{R};* *^{P}GPDA:VEL1:GFP:TRPC^{T}:^{P}GPDA:HYG^{R}:TRPC^{T};* *^{P}GPDA:H2B:RFP:TRPC^{T}:^{P}GPDA:GEN^{R}:TRPC^{T}*	This study
VGB501/VGB502 (*OE-VEL3-GFP*/*HISTONE-RFP*)	*^{P}GPDA:H2B:RFP:TRPC^{T}:^{P}GPDA:NAT^{R};* *^{P}GPDA:VEL3:GFP:TRPC^{T}:^{P}GPDA:HYG^{R}:TRPC^{T}*	This study

^{P}=promoter, ^{T}=terminator, *NAT^{R}*=nourseothricin resistance marker, *HYG^{R}*=hygromycin B resistance marker, *GEN^{R}*= geneticin resistance marker

2.3.3 *Aspergillus* strains

Within this study the *A. nidulans* wild type strain A4 and the *A. fumigatus* wild type strain AfS35 were used. Further information about the *Aspergillus* strains is indicated in Table 3.

Table 3: *Aspergillus nidulans* and *Aspergillus fumigatus* strains used in this study.

Strain name	Description	Reference
Aspergillus niduans		
A4	wild type	Fungal Genetic Stock Center (McCluskey *et al.*, 2010)
Aspergillus fumigatus		
AfS35	wild type with deletion of *akuA*	Derivative of AfS28 (Krappmann *et al.*, 2006)

2.3.4 Plants

Plants used within this study were obtained as seeds and are listed in Table 4. All plants were grown in climate chambers at long day conditions (16 h, 25 °C: 8 h, 22 °C, light: dark; light: fluorescence: 60, GroLEDs: 100, illumination: 95 µmol).

Table 4: Plants used in this study.

Strain name	Description	Reference
Arabidopsis thaliana		
Columbia-0	thale cress, family: *Brassicaceae*, used for root colonization of *V. dahliae*	Notthingham Arabidopsis Stock Centre, stock no. N1902
Solanum lycopersicum		
Moneymaker	tomato, family: Solanaceae, used as host for *V. dahliae*	Bruno Nebelung GmbH & Co. Kniepenkerl-Pflanzenzüchtung (Everswinkel, Germany)

2.3.5 Plasmid and strain construction

For amplification of DNA fragments either the Q5® High-Fidelity DNA Polymerase (New England Biolabs, Ipswich, MA, USA) or the Phusion™ High-Fidelity DNA Polymerase (Thermo Fisher Scientific, Schwerte, Germany) were applied. Primers and plasmids were designed and verified with Lasergene SeqBuilder (DNASTAR, Inc.,Madison,WI, USA). Primers and plasmids used within this study are listed below in Table 5 and Table 6.

2.3.5.1 Primers

The oligonucleotides used in this study are listed in Table 5. Oligonucleotides were either obtained from Eurofins Genomics Germany GmbH (Ebersberg, Germany) or Sigma-Aldrich Chemie GmbH (St. Louis, MO, USA). In order to calculate the annealing temperature of a primer pair, the NEB Tm calculator v1.12.0 was used (New England Biolabs, Ipswich, MA, USA). Primers used for seamless cloning reactions were constructed with a 15 bp overhang

complementary to the adjacent fragment. Primers used for ligation were created with a restriction site.

Table 5: Primers used in this study.

Primer name	Sequence 5' to 3'	Size	Overhang to/ restriction site
AO3	ATG GAC CGA CCC TCG AAT C	19 mer	-
AO11	ATG TCC GCC ACC ACC AT	17 mer	-
AO12	TCA TTT TGT GAA AAT AGG CGT GT	23 mer	-
AO13	AAC CCT TCT TCT GCG CT	17 mer	-
AO14	ACC ACC GCT ACC ACC TTT TGT GAA AAT AGG CGT GTA CT	38 mer	Linker
AO15	TGA GCA GAC ATC ACC ATG TCC GCC ACC ACC AT	32 mer	*GPDA* promoter
AO18	GTA TGT TGT GTG GAA CCT TAC CGC AAG CAT CTC GG	35 mer	pME4564
AO19	AGA TCC CCG GGT ACC GGT GTC TGG CGT CAG AAT GTG	36 mer	*GPDA* promoter
AO20	AGG TAA TCC TTC TTT TGC AGC ACC TTG TGA TGC G	34 mer	*TRPC* terminator
AO21	CAC AGT ACA CGA GGA TGG AGT TTG TTG CTT CTC CT	35 mer	pME4564
AO24	GAG CGA CGC CTC TTG CTT G	19 mer	-
AO25	GCT GGA TAT CCC TCT CGG G	19 mer	-
AO28	TGA GCA GAC ATC ACC ATG GAC CGA CCC TCG AAT CC	35 mer	*GPDA* promoter
AO29	ACC ACC GCT ACC ACC AAC CCT TCT TCT GCG CTT CT	35 mer	Linker
AO30	GTA TGT TGT GTG GAA AAC TAG CCC CCA TCG AC	32 mer	pME4564
AO31	ACC GGT CAC TGT ACA GGT GGA GGG GAC ACC AAG	33 mer	*GPDA* promoter
AO32	AGG TAA TCC TTC TTT TTG GGA TAT ACA GGA CTA TTT G	37 mer	*TRPC* terminator
AO33	CAC AGT ACA CGA GGA ATC GGC CAG AGT ACG TC	32 mer	pME4564
AO74	TGC TTG CCA TCT TGC TAC ACC	21 mer	-
AO75	GTA CAT CCC CTG AGG GTG GCG GAC GAG GTT CAC CT	35 mer	VEL2 after IDD
AO76	CCT CAG GGG ATG TAC ACG	18 mer	-
AO77	CTA ATA ATC GTC ATC GTC GT	20 mer	pPK2 (*Eco*RV)

Table 5: Primers used in this study, continued.

Primer name	Sequence 5' to 3'	Size	Overhang to/ restriction site
AO78	TTT TCT AGA ATG AGG CGC TGG TCA TTC AA	29 mer	*Xba*I restriction site
AO79	TAG TCT AGA TGC ATC TTC AGA CAC GCA AA	29 mer	*Xba*I restriction site
AO101	ATT CTT AAT TAA GAT CCT TAC CGC AAG CAT CTC G	34 mer	pME4564
AO136	ACC GGT CAC TGT ACA TCA TTT TGT GAA AAT AGG CGT	36 mer	*GPDA* promoter
AO137	AGG TAA TCC TTC TTT TGC AGC ACC TTG TGA TG	32 mer	*TRPC* terminator
AO138	AGG ACT TCT AGA AGG CTT GAC AAG CCA AGT CGT TG	35 mer	pME4564
AO140	AGG TAA TCC TTC TTT TGC AGC ACC TTG TGA TG	32 mer	*TRPC* terminator
AO157	ATT CTT AAT TAA GAT AAC TAG CCC CCA TCG AC	32 mer	pME4564
AO158	AAG ATC CCC GGG TAC TCA AAC CCT TCT TCT GCG	33 mer	*GPDA* promoter
AO159	AGG TAA TCC TTC TTT TTG GGA TAT ACA GGA CTA TTT	36 mer	*TRPC* terminator
AO160	AGG ACT TCT AGA AGG ATC GGC CAG AGT ACG TC	32 mer	pME4564
AO165	GGT GGT AGC GGT GGT GT	17 mer	-
AO166	ACC ACC GCT ACC ACC TTT TGT GAA AAT AGG CGT GTA CT	38 mer	Linker
AO167	ATT CTT AAT TAA GAT TGC TTG CCA TCT TGC TAC ACC	36 mer	pME4564
AO168	ACC ACC GCT ACC ACC ATA ATC GTC ATC GTC GTC A	34 mer	Linker
AO169	AGG TAA TCC TTC TTT CTA GAA TGA GGC GCT GGT	33 mer	*TRPC* terminator
AO170	AGG ACT TCT AGA AGG TGC ATC TTC AGA CAC GCA	33 mer	pME4564
AO171	ACC ACC GCT ACC ACC AAC CCT TCT TCT GCG CT	32 mer	Linker
AO174	AGG ACT TCT AGA AGG TGG AGT TTG TTG CTT CTC	33 mer	pME4564
AO175	ACC GGT CAC TGT ACA GGT GTC TGG CGT CAG AA	32 mer	*GPDA* promoter
AO176	ATT CTT AAT TAA GAT CCT GGA GTA CTC TGC GCA	33 mer	pME4564
AO177	ACC ACC GCT ACC ACC GGA GTA GTC CCG ACC CCA	33 mer	Linker
AO178	AGG TAA TCC TTC TTT TGA TGT TAC TTG CGA GAC TCG	36 mer	*TRPC* terminator
AO179	AGG ACT TCT AGA AGG AAG CTT CCC GTC CGT TGA	33 mer	pME4564
AO191	ACC GGT CAC TGT ACA CTT GTC AAG CAA CGG CCT	33 mer	*GPDA* promoter

Table 5: Primers used in this study, continued.

Primer name	Sequence 5' to 3'	Size	Overhang to/ restriction site
ML1	TTC CAC ACA ACA TAC GAG CC	20 mer	-
ML2	TCC TCG TGT ACT GTG TAA GC	20 mer	-
ML8	AAA GAA GGA TTA CCT CTA AAC AA	23 mer	-
ML9	TGT ACA GTG ACC GGT GAC	18 mer	-
ML30	GGT GGT AGC GGT GGT ATG GTG AGC AAG GGC GAG	33 mer	Linker
ML31	GGT GAT GTC TGC TCA AGC GG	20 mer	-
PC4	TGT ACA GTG ACC GGT GAC TC	20 mer	-
RH514	ACC GGT CAC TGT ACA TTA CTT GTA CAG CTC GTC CAT	36 mer	*GPDA* promoter
RH590	TGT ACA GTG ACC GGT GA	17 mer	-
RO3	GGT ACC CGG GGA TCT TTC G	19 mer	-
RO4	AAA GAA GGA TTA CCT CTA AAC AA	23 mer	-
SZ19	ACC TCT GGA GGC AAG GCT T	19 mer	-
SZ20	GCT TGG CCT TCT TCT TCT GC	20 mer	-
VEL2gfp-F	GGG CTC GAG ATG AGC TAC GAC CAG CAC CA	29 mer	*Xho*I restriction site
VEL2gfp-R	GGG GGT ACC ATA ATC GTC ATC GTC GTC ATC C	31 mer	*Kpn*I restriction site
VEL2-P1	GGG TTA ATT AAT GCT TGC CAT CTT GCT ACA C	31 mer	*Pac*I restriction site
VEL2-P2	GGG ACT AGT TAC TTT GGC CGA CTC TTG CT	29 mer	*Spe*I restriction site
VEL2-P3	GGG TCT AGA GCG AGG GAG GTA GAA AAG GT	29 mer	*Xba*I restriction site
VEL2-P4	GGG CCT GCA GGG CAT CTT CAG ACA CGC AAA A	31 mer	*Sbf*I restriction site
VELB-F1	ATG AGC TAC GAC CAG CAC C	19 mer	-
VELB-R1	ATA ATC GTC ATC GTC GTC AT	20 mer	-
VOS1-P1	GGG TTA ATT AAT GTC AGG CTC CTC TCG ATT T	31 mer	*Pac*I restriction site
VOS1-P2	GGG GAT ATC GAT GTT GAA GTT CCG CTG GT	29 mer	*Eco*RV restriction site
VOS1-P3	GGG GGA TCC GCG AGA CTC GAA GTT GGA CA	29 mer	*Bam*HI restriction site
VOS1-P4	GGG GGG CCC GCC AGA GAT ACA GCG TGT GA	29 mer	*Apa*I restriction site

Table 5: Primers used in this study, continued.

Primer name	Sequence 5' to 3'	Size	Overhang to/ restriction site
Vos1orf-E1	GGG CTC GAG ATG GCA GGT CTT GCC AAT	27 mer	*Xho*I restriction site
Vos1orf-E2	GGG GGT ACC GGA GTA GTC CCG ACC CCA	27 mer	*Kpn*I restriction site
ZQY3	CTG CAG GAA TTC GAT GTG ACC GGT GAC TCT TTC TG	35 mer	pBlueScript II KS
ZQY7	ATC GAT AAG CTT GAT CGA GTG GAG ATG TGG AGT GG	35 mer	pBlueScript II KS
ZQY8	GTG ACC GGT GAC TCT TTC TG	20 mer	-
ZQY9	CGA GTG GAG ATG TGG AGT GG	20 mer	-

2.3.5.2 Plasmids

Plasmids were constructed by using the GeneArt® Seamless Cloning and Assembly Kit as indicated by the manufacturer. Alternatively, the T4 DNA-Ligase (Thermo Fisher Scientific, Schwerte, Germany) was used with appropriate restriction enzymes for plasmid construction. In order to use the GeneArt® Seamless Cloning and Assembly Kit, a 15 bp overhang to the favored neighboring fragments was amplified from genomic DNA (gDNA) or complementary DNA (cDNA) of the wild type JR2 or previously designed plasmids. For integration at the genomic locus a flanking region with a size of 1-2 kb up-and downstream of the gene of interest was amplified. If necessary fragments were fused by fusion PCR (Szewczyk *et al.*, 2006). Long fusion constructs were pre-cloned. The achieved fragments were purified with the NucleoSpin® Gel and PCR Clean-up Kit (Macherey-Nagel, Düren, Germany) and used for transformation of *E. coli*. Transformants were tested for positive ones by using the *Taq* DNA Polymerase (Thermo Fisher Scientific, Schwerte, Germany). Plasmids from positive transformants were furthermore digested with restriction enzymes (New England Biolabs and Thermo Fisher Scientific) for confirmation. All plasmids were sequenced by Microsynth Seqlab GmbH (Göttingen, Germany).

For selection of transformants the nourseothricin resistance marker (NAT^R), the hygromycin B resistance marker (HYG^R) and the geneticin resistance marker (GEN^R) were used. Upstream of all markers the strong promoter glyceraldehyde-3-phosphate dehydrogenase *gpdA* from *A. nidulans* FGSC A4 (AN8041) is present (Punt *et al.*, 1988; David *et al.*, 2008). Downstream of the markers the tryptophane biosynthesis gene *trpC* from *A. nidulans* FGSC A4 (AN0648) is attached as terminator (Käfer, 1977; David *et al.*, 2008). This combination of promoter and terminator was also used for the construction of ectopically integrated overexpressions with GFP. If required, the *trpC* promoter from *A. nidulans* FGSC A4 (AN0648) was applied.

Plasmids used and constructed within this study are listed in Table 6.

Table 6: Plasmids used in this study.

Plasmid name	Description	Reference
pBlueScript II KS	Cloning vector, *AMP^R*	Fermentas
pGreen2	*^{P}GPDA:GFP:TRPC^T:^{P}GPDA:HYG^R:TRPC^T; KAN^R* Cloning vector with left and right border for ATMT, *Eco*RV restriction site	(Tran *et al.*, 2014)
pME5062 (pKO2)	*^{P}GPDA:NAT^R; KAN^R* Cloning vector with left and right border for ATMT *Eco*RV restriction site	(Leonard *et al.*, 2020)
pPK2	*^{P}GPDA:HYG^R:TRPC^T; KAN^R* Cloning vector with left and right border for ATMT, *Eco*RV restriction site	(Covert *et al.*, 2001)
pME4548	*^{P}TRPC:NAT^R; KAN^R* Cloning vector with left and right border for ATMT,	(Bui *et al.*, 2019)
pME4564	*^{P}TRPC:HYG^R; KAN^R* Cloning vector with left and right border for ATMT, Amplify backbone with ML1 and ML2 or exchange *^{P}TRPC:HYG^R* by digestion with *Eco*RV and *Stu*I with desired fragment	(Leonard *et al.*, 2020)
pME4815	*^{P}GPDA:NAT^R:TRPC^T* in pME4564	(Starke *et al.*, 2020)
pME4819	*^{P}GPDA:GFP:TRPC^T* in pME4815	(Starke *et al.*, 2020)
pME4975	*^{P}GPDA:RFP:H2B:TRPC^T* in pPK2, left and right border for ATMT	(Starke *et al.*, 2020)
pME4976	*^{P}GPDA:RFP:H2B:TRPC^T* in pCOM (with *GEN^R*), left and right border for ATMT	(Starke *et al.*, 2020)
pME4990	*^{P}GPDA:NLP3:GFP:TRPC^T:^{P}GPDA:HYG^R:TRPC^T* in pPK2, left and right border for ATMT	(Leonard *et al.*, 2020)
pME5063	*^{P}VEL1:^{P}GPDA:HYG^R:TRPC^T:VEL1^T* in pME4564, left and right border for ATMT	This study
pME5064	*^{P}VEL1:VEL1:^{P}GPDA:NAT^R:TRPC^T:VEL1^T* in pME4564, left and right border for ATMT	This study
pME5065	*^{P}VEL1:^{P}GPDA:NAT^R:TRPC^T:VEL1^T* in pME4564, left and right border for ATMT	This study
pME5066	*^{P}VEL2:^{P}TRPC:NAT^R:VEL2^T* in pME4548, left and right border for ATMT	This study
pME5067	*^{P}VEL2:VEL2:GFP:^{P}GPDA:HYG^R:TRPC^T:VEL2^T* in pME4564, left and right border for ATMT	This study
pME5068	*^{P}VEL3:^{P}GPDA:NAT^R:TRPC^T:VEL3^T* in pME4564, left and right border for ATMT	This study
pME5069	*^{P}VEL3:VEL3:^{P}GPDA:HYG^R:TRPC^T:VEL3^T* in pME4564, left and right border for ATMT	This study
pME5070	*^{P}VOS1:^{P}GPDA:NAT^R:VOS1^T* in pKO2, left and right border for ATMT	This study
pME5071	*^{P}VOS1:^{P}GPDA:HYG^R:TRPC^T:VOS1^T* in pME4564, left and right border for ATMT	This study
pME5072	*^{P}VEL1:VEL1:GFP:^{P}GPDA:HYG^R:TRPC^T:VEL1^T* in pME4564, left and right border for ATMT	This study
pME5073	*^{P}VEL3:VEL3:GFP:^{P}GPDA:HYG^R:TRPC^T:VEL2^T* in pME4564, left and right border for ATMT	This study

Table 7: Plasmids used in this study, continued.

Plasmid name	Description	Reference
pME5074	*^{P}VOS1:VOS1:GFP:^{P}GPDA:HYG^{R}:TRPC^{T}:VOS1^{T}* in pME4564, left and right border for ATMT	This study
pME5075	*^{P}VEL2:VEL2ΔIDD:^{P}GPDA:HYG^{R}:TRPC^{T}* in pPK2, left and right border for ATMT	This study
pME5076	*^{P}VEL2:VEL2ΔIDD:^{P}GPDA:HYG^{R}:TRPC^{T}:VEL2^{T}* in pME5075 left and right border for ATMT	This study
pME5077	*^{P}VEL2:VEL2ΔIDD:GFP:^{P}GPDA:HYG^{R}:TRPC^{T}:VEL2^{T}* in pME4564, left and right border for ATMT	This study
pME5078	*^{P}GPDA:VEL1:GFP:TRPC^{T}* in pGreen2, left and right border for ATMT	This study
pME5079	*^{P}GPDA:VEL1:GFP:TRPC^{T}:^{T}TRPC:HYG^{R}:GPDA^{P}* in pPK2, left and right border for ATMT	This study
pME5080	*^{P}GPDA:HYG^{R}:TRPC^{T}:^{P}GPDA:VEL2:GFP:TRPC^{T}* in pGreen2, left and right border for ATMT	This study
pME5081	*^{P}GPDA:VEL3:GFP:TRPC^{T}* in pGreen2, left and right border for ATMT	This study
pME5082	*^{P}GPDA:VEL3:GFP:TRPC^{T}* in pBlueScript II KS	This study
pME5083	*^{P}GPDA:VEL3:GFP:TRPC^{T}:^{P}GPDA:HYG^{R}:TRPC^{T}* in pPK2, left and right border for ATMT	This study
pME5084	*^{P}GPDA:HYG^{R}:TRPC^{T}:^{P}GPDA:VOS1:GFP:TRPC^{T}* in pGreen2, left and right border for ATMT	This study

ATMT=*Agrobacterium tumefaciens*-mediated transformation, ^{P}=promoter, ^{T}=terminator, *NAT^{R}*=nourseothricin resistance marker, *HYG^{R}*=hygromycin B resistance marker, *AMP^{R}*=ampicillin resistance marker, *GEN^{R}*=geneticin resistance marker, *KAN^{R}*=kanamycin resistance marker

2.3.5.3 Cloning strategies

2.3.5.3.1 Transformation of *Escherichia coli*

The chemically competent *E. coli* strain DH5α was used for cloning reactions. Chemically competent cells were generated as previously described by Bui (2017). Transformation was conducted by the heat shock method according to Inoue *et al.* (1990) and Hanahan *et al.* (1991). On ice 200 µl of competent *E. coli* cells were thawed and mixed with the ligation mixture. Afterwards the solution was incubated on ice for 30 min. In the next step, a heat shock was conducted for 1 min at 42 °C. The cells were stored on ice for 2 min and 800 µl SOC medium [2 % (w/v) bacto-tryptone, 0.5 % (w/v) yeast extract, 10 mM NaCl (w/v), 2.5 mM KCl (w/v), 10 mM $MgCl_2$ (w/v), 10 mM $MgSO_4$ (w/v), 20 mM glucose (w/v)] was added. Next, the cells were incubated 50 min at 37 °C under constant agitation to induce cell growth. The cells were distributed on LB plates supplemented with kanamycin (100 µg/ml) or ampicillin (100 µg/ml) for selection of positive transformants. The plates were incubated at 37 °C overnight. Transformants were tested by colony PCR using the *Taq* DNA Polymerase (Thermo Fisher Scientific, Schwerte, Germany) for successful transformation.

2.3.5.3.2 Transformation of *Agrobacterium tumefaciens*

The AGL-1 strain was used for *A. tumefaciens*-mediated transformation of *V. dahliae*. Competent cells of *A. tumefaciens* were generated by incubating cells overnight in LB medium supplemented with carbenicillin (50 µg/ml) at 28 °C shaking. Cells were grown until OD_{600} reached 0.8. Then the cells were kept on ice for 15 min and centrifuged at 4000 rpm for 10 min at 4 °C. The obtained pellet was resuspended in 20 ml cold and sterile 100 mM $MgCl_2$ solution and incubated for 1 h on ice. Next, the solution was centrifuged again at 4000 rpm for 10 min at 4 °C and the pellet was resuspended in 20 ml cold and sterile 20 mM $CaCl_2$ solution. Lastly, the cells were incubated on ice for 4 to 5 hours and mixed with glycerol to a final concentration of 20 %. Aliquots were frozen in liquid nitrogen and stored at -80 °C.

Transformation of *A. tumefaciens* was done using the freeze-thaw method (Jyothishwaran *et al.*, 2007). On ice 200 µl competent cells were thawed and mixed with 1 µg of plasmid DNA. The mixture was incubated for 10 min on ice and frozen for 10 min in liquid nitrogen. Next, the heat shock was performed at 37 °C for 5 min. The cells were afterwards mixed with 800 µl SOC medium and incubated for 1 h in a shaking water bath with 28 °C. Later the cells were distributed on LB plates supplemented with kanamycin (100 µg/ml) for selection of positive transformants and incubated for three days at 25 °C. Clones were tested for positive transformants by using the *Taq* DNA Polymerase (Thermo Fisher Scientific, Schwerte, Germany).

2.3.5.3.3 Transformation of *Verticillium dahliae*

V. dahliae was transformed by *A. tumefaciens*-mediated transformation according to Mullins *et al.* (2001). *A. tumefaciens* cultures were inoculated in LB medium supplemented with kanamycin (100 µg/ml) and grown overnight at 25 °C on a rotary shaker. On the next day, 20 ml induction medium (IM) [1xMM salts (2.5 stock: 3.625 g/l KH_2PO_4, 5.125 g/l K_2HPO_4, 0.375 g/l NaCl, 1.25 g/l $MgSO_4x7H_2O$, 0.165 g/l $CaCl_2x2H_2O$, 6.2 mg/l $FeSO_4x7H_2O$, 1.25 g/l $(NH_4)_2SO_4$), 10 mM glucose, 0.5 % glycerol, 40 mM 2-(*N*-morpholino)ethanesulfonic acid (MES), supplemented freshly with 200 µM acetosyringone (AS)] were inoculated with 0.5 to 1 ml overnight culture and incubated in a water bath at 28 °C under constant agitation for 4 to 5 hours. Afterwards the culture was mixed in a 1:1 ratio with *V. dahliae* spores (concentration: $1x10^6$ spores/ml). From the mixture 200 µl were spread on filter paper (Ø 85 mm, Sartorius, Göttingen, Germany) put on solid induction medium [1xMM salts, 5 mM glucose, 0.5 % (v/v) glycerol, 40 mM MES,10 mM AS, 1.5 % (w/v) agar]. The plates were incubated at 25 °C in darkness for three days. Then the filter paper was transferred to PDM plates supplemented with cefotaxime (300 µg/ml) and antifungal agents required for selection of positive transformants (50 µg/ml hygromycin B, 72 µg/ml nourseothricin, 50 µg/ml geneticin). After approximately seven days the filters were removed from the plates and clones were separated

two times on PDM plates supplemented with required antifungal drugs. In order to obtain fungal spores, single colonies were inoculated in liquid SXM supplemented with cefotaxime (300 µg/m) and grown as previously described.

2.3.5.4 Construction of plasmids and *Verticillium* strains

Construction of *VEL1* deletion (*HYG^R*) and corresponding complementation strain

For a *VEL1* (VDAG_JR2_Chr7g04890) deletion strain, the 5' and 3' flanking regions of the gene were amplified from wild type gDNA. The 5' region was amplified with the primers AO18 and AO19 (1280 bp) and the 3' region with the primer pair AO20 and AO21 (1185 bp). The hygromycin resistance cassette was obtained from pPK2 using RO3 and RO4 (3942 bp). The backbone was amplified from pME4564 with the primers ML1 and ML2 (6728 bp). All fragments were ligated and resulted in pME5063. This plasmid was used for transformation of the wild type (VGB39). The received deletion transformants were tested by Southern hybridization. Cutting of the genomic DNA obtained from wild type and deletion transformants with *Xho*I and labbeling with the 3' flanking region as probe revealed correct integration of the deletion cassette (Figure A1). The two deletion transformants were named VGB246 and VGB247.
For construction of the complementation strain, the *VEL1* 5' flanking region and the gene were amplified with AO101 and AO136 (2998 bp) from gDNA of the wild type. The 3' flanking region was amplified with the primers AO137 and AO138 (1080 bp). The nourseothricin resistance cassette was amplified from pME4815 using ML8 and ML9 (2194 bp). Plasmid pME4564 was treated with *Eco*RV and *Stu*I (6804 bp) and served as backbone. The fragments were ligated and the resulting plasmid was named pME5064. The plasmid was used to transform VGB246. The received transformants were tested by Southern hybridization for correct integration at the locus by using the 3' flanking region as probe and cutting the gDNA with *Xho*I (Figure A1). VGB474 was confirmed as correct complementation strain.

Construction of *VEL2* deletion and corresponding complementation strain

For construction of a *VEL2* (VDAG_JR2_Chr3g06150a) deletion strain, the 5' region of *VEL2* was amplified with the primers VEL2-P1 and VEL2-P2 and ligated to *Pac*I/*Spe*I cut vector pME4548. Next, the vector was cut with *Xba*I/*Sbf*I and ligated to the 3' flanking region, which was amplified by VEL2-P3 and VEL2-P4. The resulting plasmid was named pME5066. Transformation of the wild type (VGB39) with the plasmid resulted in deletion transformants VGB58 and VGB59. The gDNA of the transformants was cut with *Bgl*II and correct integration of the deletion cassette was confirmed by Southern hybridization using the 3' flanking region as probe (Figure A2).
To construct a corresponding complementation strain with GFP fused to the C-terminus, the primers AO167 and AO168 were used to amplify the 5' flanking region and the *VEL2* gene

without stop codon (3550 bp) from wild type gDNA. The 3' flanking region was amplified with the primers AO169 and AO170 (2014 bp). The hygromycin marker was amplified from the plasmid pME4990 with RH590 and RO4 (2641 bp). Also, *GFP* (lacking the start codon) together with a 15 bp flexible linker (protein sequence GGSGG) was amplified from pME4990 by using AO165 and RH514 (747 bp). Subsequently, the hygromycin marker and *GFP* were fused by PCR using the primers AO165 and RO4 (3388 bp). The three fragments were ligated into pME4564 cut with *Eco*RV and *Stu*I (6804 bp). The constructed plasmid was named pME5067. The plasmid was used to transform the deletion strain VGB58. The resulting strain VGB375 was tested by Southern hybridization for correct integration of the complementation cassette at the locus by using the same enzyme and probe as for the deletion strain (Figure A2).

Construction of *VEL3* deletion and corresponding complementation strain

The *VEL3* (VDAG_JR2_Chr6g00630a) deletion strain was constructed by amplifying the 5' flanking region (AO30 and AO31, 1011 bp) and the 3' flanking region (AO32 and AO33, 1530 bp) from wild type gDNA. The nourseothricin resistance cassette was amplified from pME4815 with the primer pair ML8 and ML9 (2194 bp). The plasmid pME4564 was used to amplify the backbone with the primers ML1 and ML2 (6728 bp). Ligation of the fragments resulted in pME5068, which was used for wild type (VGB39) transformation. The resulting transformants VGB234 and VGB235 were tested for correct integration by Southern hybridization with the 5' flanking region as probe and *Xho*I to treat the gDNA (Figure A3).

To construct the corresponding complementation strain, the 5' flanking region and *VEL3* were amplified from gDNA with the primers AO157 and AO158 (2323 bp). The 3' flanking region was amplified from gDNA with the primers AO159 and AO160 (1548 bp). From the plasmid pPK2 the hygromycin resistance cassette was amplified with the primers RO3 and RO4 (3942 bp). As backbone pME4564 was cut with *Eco*RV and *Stu*I (6804 bp). The fragments were ligated and resulted in the plasmid pME5069. VGB234 was transformed with the construct. The obtained complementation transformants VGB445 and VGB446 were tested by Southern hybridization for correct integration at the locus by using the same enzyme and probe as for the deletion strains (Figure A3).

Construction of *VOS1* (*NAT^R*) deletion strain

For construction of a *VOS1* deletion strain with a nourseothricin marker, the *VOS1* 3' flanking region was amplified with the primers VOS1-P3 and VOS1-P4 and inserted into the *Bam*HI/*Hin*dIII restriction site of pME5062 (pKO2). The 5' flanking region was amplified with the primers VOS1-P1 and VOS1-P2 and ligated into the *Pac*I/*Eco*RV restriction sites. The resulting plasmid was named pME5070. The wild type (VGB39) was transformed with the generated plasmid resulting in deletion transformants VGB64 and VGB65. gDNA of the generated strains was cut with *Bgl*I to test the strains by Southern hybridization using the 3' flanking region as probe (Figure A4).

Construction of *VOS1* (*HYG^R*) deletion strain

The *VOS1* deletion strain was also constructed with a hygromycin resistance cassette. Therefore, the 5' flanking region of the gene was amplified from gDNA using AO176 and AO191 (1444 bp). The 3' flanking region was amplified from gDNA with the primers AO178 and AO179 (1210 bp). The hygromycin resistance cassette was amplified from pME5074 with the primers RH590 and RO4 (2641 bp). All fragments were ligated to *Eco*RV and *Stu*I-treated plasmid pME4564 (6804 bp). The resulting plasmid pME5071 was used for transformation of the wild type. The received transformants VGB241 and VGB242 were verified by Southern hybridization of gDNA cut with *Bgl*I and the 3' flanking region as probe (Figure A4).

Construction of *VEL1*/*VEL2* double deletion strain

To obtain a double deletion strain of *VEL1* and *VEL2*, the single deletion strain of *VEL2* (VGB58) was used as parental strain. The plasmid pME5063 was used to transform VGB58. The resulting double deletion transformants VGB281 and VGB282 were confirmed by Southern hybridization in the same way as the single deletion strains (Figure A1 and A2).

Construction of *VEL3*/*VEL1* double deletion strain

For construction of a *VEL3* and *VEL1* double deletion strain, the *VEL1* single deletion strain (VGB246) was transformed with pME5068. The resulting *VEL1* and *VEL3* double deletion transformants VGB289 and VGB290 were tested by Southern hybridization with the same enzyme and probe as the single deletion strains (Figure A1 and Figure A3).

Construction of *VOS1*/*VEL3* double deletion strain

A *VOS1* and *VEL3* double deletion strain was constructed by using the single deletion strain of *VEL3* (VGB234) as parental strain. The plasmid pME5071 was used for transformation of the *VEL3* deletion strain resulting in VGB373. Southern hybridization was conducted as for the *VOS1* and *VEL3* single deletion strains to confirm the double deletion strain (Figure A3 and A4).

Construction of *VEL1* deletion strain overexpressing *GFP*

For examination of root colonization, the plasmid pME4819, which ectopically overexpresses GFP, was introduced into the *VEL1* deletion strain (VGB246). Resulting transformants were named VGB443 and VGB444. A screening for green fluorescence was conducted in 15 µ-Slide 8 Well microscopy chambers (ibidi GmbH, Gräfelfing, Germany). The strains were, furthermore, tested by Southern hybridization for correct integration of the deletion cassette. gDNA was cut with *Bgl*I and *Xho*I and the 3' flanking region was used as probe. Additionally, the 5' flanking region was used as probe for gDNA cut with *Bgl*I.

Construction of a strain with *VEL1-GFP* at the endogenous locus

A strain with GFP fused to the C-terminus of Vel1 was constructed by amplifying the *VEL1* 5' flanking region and the gene without stop codon with the primer pair AO101 and AO166 (2995 bp) from gDNA. The 3' flanking region of *VEL1* was amplified from gDNA with AO140 and AO138 (1080 bp). The plasmid pME4990 was used to amplify the hygromycin resistance marker with the primers RH590 and RO4 (2641 bp). Furthermore, *GFP* (without start codon) and a 15 bp flexible linker (protein sequence GGSGG) were amplified from the same plasmid with AO165 and RH514 (747 bp). In a fusion PCR the hygromycin resistance cassette and *GFP* were linked by using AO165 and RO4 (3388 bp). pME4564 cut with *Eco*RV and *Stu*I was used as backbone (6804 bp). The constructed plasmid was named pME5072. The plasmid was used to transform the wild type (VGB39) resulting in VGB447. gDNA of the strain was cut with *Bam*HI and Southern hybridization was performed to confirm correct integration at the locus with the 3' flanking region as probe. The presence of the fusion protein was tested by western analysis. The strain was additionally phenotypically examined for wild type-like functionality.

Construction of a strain with *VEL2-GFP* at the endogenous locus

VEL2 was fused with *GFP* and introduced at the endogenous locus of the *VEL2* deletion strain to construct a *VEL2-GFP* complementation strain as described afore. The wild type (VGB39) was also transformed with the plasmid pME5067 resulting in VGB450. The strain was tested for correct integration at the locus by Southern hybridization. Therefore, gDNA was cut with

*Hinc*II and the 5' flanking regions were used as probe. The presence of the fusion protein was confirmed by western experiments. The strain was also checked by phenotypical analysis for wild type-like functionality.

Construction of a strain with *VEL3-GFP* at the endogenous locus

For construction of a strain coding for Vel3 C-terminally fused to GFP, the primers AO157 and AO171 were used to amplify the *VEL3* 5' flanking region and the gene without stop codon (2323 bp) from gDNA. The 3' flanking region of *VEL3* was amplified with AO159 and AO160 (1548 bp) from gDNA. The hygromycin resistance cassette was amplified from pME4990 with the primers RH590 and RO4 (2641 bp). *GFP* (lacking the start codon) and a 15 bp flexible linker (protein sequence GGSGG) were amplified from pME4990 using AO165 and RH514 (747 bp). The hygromycin resistance cassette and *GFP* were fused by PCR with AO165 and RO4 (3388 bp). The plasmid pME4564 was cut with *Eco*RV and *Stu*I (6804 bp) and used as backbone. The fragments were ligated and the resulting plasmid was named pME5073. The plasmid was used for transformation of the wild type (VGB39) and the received strain was named VGB451. gDNA of the constructed strain was cut with *Pst*I and integration at the locus was confirmed by Southern hybridization with the 3' flanking region as probe. Furthermore, the strain was tested by western experiments for presence of the fusion protein and phenotypically analyzed for wild type-like functionality.

Construction of a strain with *VOS1-GFP* at the endogenous locus

In order to construct a strain coding for Vos1 C-terminally fused to GFP, the *VOS1* 5' flanking region and *VOS1* without stop codon were amplified with the primer pair AO176 and AO177 (2683 bp) from gDNA. For amplification of the 3' flanking region of the gene from gDNA, AO178 and AO179 were used (1210 bp). To amplify *GFP* (without start codon) together with a 15 bp flexible linker (protein sequence GGSGG) from the plasmid pME4990, the primers AO165 and RH514 were used (747 bp). From the same plasmid also the hygromycin resistance cassette was amplified with RH590 and RO4 (2641 bp). Next, the two fragments were fused by PCR using AO165 and RO4 (3388 bp). The plasmid pME4564 was cut with *Eco*RV and *Stu*I to obtain the backbone (6804 bp). The above-mentioned fragments were ligated and the received plasmid was named pME5074. The plasmid was used to transform the wild type (VGB39) resulting in VGB453. The strain was tested by Southern hybridization. Therefore, gDNA was cut with *Pst*I and *Xho*I and tested for correct integration using the 3' flanking region as probe. Furthermore, the gDNA was cut with *Aat*II and tested by Southern hybridization with the 5' flanking region as probe. The strain was also verified by western experiments and phenotypically analyzed for wild type-like functionality.

Construction of a strain with *VEL2$^{\Delta IDD}$-GFP* at the endogenous locus

The construction of a *VEL2* strain without *IDD* fused to *GFP* was conducted in several steps. In the first step, the primers AO74 and AO75 were used to amplify the 5' flanking region of the gene and *VEL2* until the start of the *IDD* (2674 bp) from gDNA. In another PCR, AO76 and AO77 were utilized to amplify the part of *VEL2* downstream of the *IDD* (463 bp) from gDNA. As AO75 was constructed with an overhang to *VEL2* after the *IDD*, the two fragments were fused by PCR using AO74 and AO77 (3137 bp). The fragment was ligated in the *Eco*RV-linearized pPK2 and the resulting plasmid was named pME5075. In the next step, pME5075 was cut with *Xba*I and the 3' flanking region of *VEL2* was amplified with AO78 and AO79 (1997 bp). Ligation of pME5075 and the PCR fragment resulted in a plasmid named pME5076. In the last step, the 5' flanking region and *VEL2* without *IDD* and stop codon were amplified with AO167 and AO168 (3149 bp) from pME5076. The 3' flanking region was amplified with the primers AO169 and AO170 (2014 bp). *GFP* (without start codon) and a flexible linker (protein sequence GGSGG) were amplified from pME4990 with AO165 and RH514 (747 bp). The hygromycin resistance cassette was amplified from the same plasmid with the primers RH590 and RO4 (2641 bp). The *GFP*-linker fragment and the hygromycin marker were fused by PCR with the primers AO165 and RO4 (3388 bp). The three generated fragments were ligated into pME4564 cut with *Eco*RV and *Stu*I (6804 bp). The created plasmid was named pME5077. The wild type (VGB39) was transformed with the plasmid resulting in VGB468. The gDNA of the constructed strain was treated with *Hinc*II and *Pst*I and tested by Southern hybridization with the 5' flanking region as probe. The strain was also confirmed by cutting the gDNA with *Eco*RI and conducting a Southern hybridization with the 3' flanking region as probe. In addition, the strain was tested by western experiments and phenotypically analyzed.

Construction of a strain with *HISTONE-RFP* fluorescence

In order to construct a strain with red fluorescent nuclei, the histone H2B was tagged with RFP and named pME4975 (Starke *et al.*, 2020). The wild type (VGB39) was transformed with pME4975 and the resulting strain was named VGB22.

Construction of *VEL1-GFP* overexpression strain

For the construction of a strain overexpressing Vel1 fused to GFP C-terminally, the primers ML30 and ML31 were used to amplify the backbone of pGreen2 including *GFP*. *VEL1* was amplified from cDNA with the primer pair AO15 and AO14 (1686 bp) without stop codon. The resulting plasmid was named pME5078. In the next step, pPK2 was cut with *Eco*RV. The *GPDA* promoter, *VEL1-GFP* and the *TRPC* terminator were amplified from pME5078 with PC4 and ML8 (4049 bp). The PCR fragment was ligated into pPK2 resulting in pME5079. The wild type (VGB39) was transformed with pME5079 resulting in VGB297. This strain was confirmed

by western experiments for the presence of Vel1-GFP. Furthermore, VGB22 was transformed with pME5079 for localization studies. The resulting transformants were named VGB364 and VGB365 and were checked for presence of the fusion protein by western analysis.

Construction of *VEL2-GFP* overexpression strain

To construct a strain overexpressing Vel2 with GFP fused to its C-terminus, the plasmid pGreen2 was used as backbone. *VEL2* was amplified from cDNA without stop codon using VEL2gfp-F and VEL2gfp-R (1380 bp) and inserted into the vector at the *Xho*I/*Kpn*I restriction site. The constructed plasmid was named pME5080. For localization studies, VGB22 was transformed with pME5080. The resulting strain was named VGB223 and was checked by western analysis for presence of the fusion protein.

Construction of *VEL3-GFP* overexpression strain

The construction of a Vel3 overexpression strain C-terminally fused to GFP was conducted in several steps. In the first step, the primers AO28 and AO29 were used to amplify *VEL3* from cDNA (1341 bp) without stop codon. The primers ML30 and ML31 were used to amplify the backbone including *GFP* with a 15 bp flexible linker (protein sequence GGSGG) from pGreen2. The fragment was ligated into the backbone and the resulting plasmid was named pME5081. The primers ZQY3 and ZQY7 were used to amplify the *GPDA* promoter, *VEL3*-GFP and the *TRPC* terminator from pME5081 (3734 bp). In the next step, pBlueScript II KS was treated with *Eco*RV and ligated with the previously generated fragment. The resulting construct was named pME5082. Lastly, pPK2 was linearized with *Eco*RV and the primers ZQY8 and ZQY9 were used to amplify the *GPDA* promoter, *VEL3-GFP* and the *TRPC* terminator from pME5082 (3704 bp). The fragments were ligated and the resulting plasmid was named pME5083. To examine the localization of *VEL3*, pME5083 was used to transform VGB22. The generated transformants were named VGB501 and VGB502. Western analysis was conducted to check the presence of the fusion protein.

Construction of *VOS1-GFP* overexpression strain

In order to construct an overexpression strain of VOS1 fused C-terminally with GFP, the primers Vos1orf-E1 and Vos1orf-E2 were used to amplify *VOS1* from cDNA (1137 bp) without stop codon. The plasmid pGreen2 was treated with *Xho*I/*Kpn*I to serve as backbone and was ligated to *VOS1*. The resulting plasmid was named pME5084. VGB22 was transformed with pME5084 for localization studies. The resulting transformants were named VGB219 and VGB220. The presence of the fusion protein was examined by western analysis.

Construction of a *VEL1-GFP* overexpression strain with *VEL2* deletion and *HISTONE-RFP* expression

For the construction of a *VEL1-GFP* overexpression strain in the *VEL2* deletion background, the plasmid pME5079 was used to transform the deletion strain of *VEL2* (VGB58). The resulting strain was named VGB362. In the next step, VGB362 was transformed with pME4976 to generate a strain with red fluorescent nuclei for localization studies. The resulting transformants VGB498 and VGB499 were verified by Southern hybridization. The presence of the Vel1-GFP fusion protein was confirmed via western analysis.

Construction of a *VEL2-GFP* overexpression strain with *VEL1* deletion and *HISTONE-RFP* expression

For construction of a *VEL2-GFP* overexpression strain in the *VEL1* deletion background, the *VEL1* deletion strain was constructed with a nourseothricin resistance cassette. Therefore, the 5' flanking region of *VEL1* was amplified with AO101 and AO175 (1280 bp) and the 3' flanking region with the primers AO140 and AO174 (1185 bp) from wild type gDNA. The nourseothricin resistance marker was amplified from pME4815 with ML8 and ML9 (2194 bp). As backbone pME4564 was cut with *Eco*RV and *Stu*I (6804 bp). The fragments were ligated and the resulting plasmid was named pME5065. VGB477, which expresses histones tagged with RFP, was transformed with the plasmid resulting in VGB495. Next, VGB495 was transformed with pME5080, which is an overexpression strain of *VEL2-GFP*, leading to VGB496 and VGB497. The transformants were tested by Southern hybridization for correct integration of the deletion cassette. Western analysis was carried out to check the presence of the fusion protein.

2.4 Nucleic acid methods

2.4.1 Nucleic acid purification

2.4.1.1 Isolation of plasmid DNA from *Escherichia coli*

To obtain plasmid DNA from *E. coli*, the strain of interest was inoculated in 5 ml LB medium supplemented with either kanamycin (100 µ/ml) or ampicillin (100 µg/ml) and grown over night at 37 °C on a rotary shaker. The NucleoSpin® Plasmid Kit (Macherey-Nagel, Düren, Germany) was used as indicated by the manufacturer to purify the plasmid DNA. Pre-warmed dH_2O was used to eluate the plasmid DNA from spin columns.

2.4.1.2 Isolation of genomic DNA from *Verticillium dahliae*

Spores of *V. dahliae* were grown in liquid PDM at 25 °C under constant agitation for three to seven days to obtain fungal mycelium. gDNA of *V. dahliae* was isolated according to a modified method from Kolar *et al.* (1988). The mycelium was collected in Miracloth filters (Calbiochem

Merck, Darmstadt, Germany) and washed with 0.96 % (w/v) NaCl. Afterwards it was dried and ground in liquid nitrogen to a fine powder. The powder was vigorously mixed with 800 µl lysis buffer [50 mM Tris pH 7.5, 50 mM EDTA pH 8.0, 3 % (w/v) SDS, 1 % (v/v) β-mercaptoethanol]. The mixture was incubated for 1 h at 65 °C. Afterwards, 800 µl phenol were added and the mixture was centrifuged for 20 min at 13000 rpm at 4 °C. Within the centrifugation step the phases separated and the upper one was then transferred into a new reaction tube. For denaturation of proteins, 500 µl chloroform were added and the mixture was centrifuged for 10 min at 13000 rpm at 4 °C. Again, the upper phase was transferred into a new reaction tube and mixed with 400 µ isopropanol. For precipitation of the gDNA, the reaction tube was centrifuged for 2 min at 13000 rpm. After removing the supernatant, 300 µl 70 % (v/v) ethanol were used to wash the gDNA by centrifugation for 1 min at 13000 rpm. The liquid was removed and the pellet left at 65 °C until it has dried. Later the gDNA was dissolved in 50-100 µl dH_2O supplemented with RNase A (10 mg/ml) and incubated at 65 °C for approximately 30 min. The quality and concentration of the gDNA was checked by agarose gel electrophoresis.

2.4.2 Polymerase chain reaction

Fragments of DNA for plasmid construction, as probes for Southern hybridization or to confirm the presence and correctness of fungal genes were amplified by polymerase chain reaction (PCR) (Saiki *et al.*, 1988). Colony PCRs were conducted to identify positive clones of *E. coli* and *A. tumefaciens* transformants (Bergkessel & Guthrie, 2013). The Q5® High-Fidelity DNA Polymerase (New England Biolabs, Ipswich, MA, USA), the Phusion™ High-Fidelity DNA Polymerase (Thermo Fisher Scientific, Schwerte, Germany) and the *Taq* DNA Polymerase (Thermo Fisher Scientific, Schwerte, Germany) were used. Oligonucleotides and PCR programs were created as indicated by the manufacturer. The annealing temperature was determined by using NEB Tm calculator v1.12.0 (New England Biolabs, Ipswich, MA, USA).

2.4.3 Agarose gel electrophoresis

DNA and RNA fragments were separated according to their size by agarose gel electrophoresis. Samples were mixed with 6 x loading dye [0.25 % (w/v) bromophenol blue, 0.25 % (v/v) xylene cyanol FF, 40 % (w/v) sucrose, pH 8.0] and load on a 1 % agarose gel [1 % (w/v) agarose (Biozym Scientific GmbH, Hessisch Oldendorf, Germany), 1 x TAE buffer (40 mM Tris-acetate, 20 mM sodium acetate, 2 mM EDTA, pH 8.3), 0.0001 mg/ml ethidium bromide] in 1 x TAE buffer. The GeneRuler™ 1 kb DNA ladder or GeneRuler™ 100 bp DNA ladder (Thermo Fisher Scientific, Schwerte, Germany) were used as size standard. Separation of the fragments was conducted with an electric field of 90 V. By exposure to UV light (λ = 254 mm) using the Gel iX20 Imager with Intas GDS gel documentation software (Intas Science Imaging Instruments GmbH, Göttingen, Germany) or the TFX-20 MX Vilber Lourmat

Super Bright transilluminator (Sigma-Aldrich Chemie GmbH, St. Louis, MO, USA) visualization of DNA and RNA fragments in gel was accomplished.

2.4.4 Isolation of DNA from agarose gels

DNA fragments for cloning, probes for Southern hybridization or fragments cut with restriction enzymes were separated according to their size by agarose gel electrophoresis. Desired fragments were cut out of the gel and purified with the NucleoSpin® Gel and PCR Clean-up Kit from Macherey-Nagel (Düren, Germany) according to the instruction manual. Pre-warmed dH_2O was used to eluate the DNA from spin columns.

2.4.5 Southern hybridization

In order to confirm the correct integration of DNA, *V. dahliae* strains were tested by Southern hybridization (Southern, 1975). Isolated gDNA was cut with appropriate restriction enzymes overnight to achieve fragments, which are distinguishable from the used parental strain. The cut DNA was separated on a 1 % agarose gel and subsequently washed in three steps to depurinate, denature and neutralize the DNA: 10 min washing buffer I (0.25 M HCl), 25 min washing buffer II (0.5 M NaOH, 1.5 M NaCl), 30 min washing buffer III (1.5 M NaCl, 0.5 M Tris, pH 7.4). Next, the DNA was transferred by dry-blotting for at least 90 min to Amersham™ Hybond-N™ nylon membrane (GE Healthcare life sciences, München, Germany). The membrane was dried for 10 min at 70 °C and DNA was crosslinked to the membrane by exposure to UV light (λ = 254 nm) for 3 min from both sides of the membrane. Pre-hybridization and probe labelling with Amersham™ AlkPhos Direct™ Labelling Reagents (GE Healthcare life sciences, München, Germany) were done according to the manufacturer's instructions. The membrane was incubated with the probe overnight at 60 °C in a HERAhybrid 12 hybridization oven (Heraeus Instruments GmbH, Hanau, Germany). The next day, the membrane was washed twice in pre-warmed washing buffer [2 M urea, 50 mM SDS, 50 mM Na_3PO_4, 150 mM NaCl, 1 mM $MgCl_2$, 2 % (w/v) blocking reagent] for 10 min at 60 °C in the rotation oven. Afterwards, the membrane was washed twice in another washing buffer (1 M Tris Base, 2 M NaCl, pH 10; freshly added 2 mM $MgCl_2$) for 5 min at room temperature under constant agitation. The labelled DNA fragments were detected using the CDP-*Star*® Detection Reagent (GE Healthcare life sciences, München, Germany) as indicated by the manufacturer. The membrane was exposed to an Amersham™ Hyperfilm™-ECL (GE Healthcare life sciences, München, Germany). The film was developed using the Optimax® X-ray Film Processor from Protec GmbH & Co. KG (Oberstenfeld, Germany).

2.4.6 RNA extraction from *V. dahliae*

Fungal mycelium was used to obtain RNA by applying the Direct-zol™ RNA MiniPrep Kit (Zymo Research, Freiburg im Breisgau, Germany) as indicated by the manufacturer. The mycelium was washed with 0.96 % NaCl, dried and ground to a fine powder in liquid nitrogen. A 15 ml tube was filled with 1 ml of the powder and 1 ml TRIzol (Ambion and life technologies, Carlsbad, CA, USA) and frozen in liquid nitrogen. For cutting of remaining DNA, DNase I was applied onto the columns according to the instructions. The isolated RNA was eluted with pre-warmed DNase/RNase free water. The concentration and quality of the RNA was checked using agarose gel electrophoresis to examine appearance of bands for ribosomal RNAs at ~2.3 kb (28S) and ~1.1 kb (18S). Furthermore, the quality and concentration of RNA was tested by applying the NanoDrop™ ND-1000 spectrophotometer (PeqLab Biotechnology GmbH, Erlangen, Germany). RNA was diluted 1:10 and should reveal absorption rations at 260 nm/280 nm (~1.8) and 260 nm/230 nm (~2.0-2.2). The purified DNA was subsequently used for cDNA synthesis.

2.4.7 Complementary DNA synthesis

The QuantiTect Reverse Transcription Kit from Qiagen (Hilden, Germany) was used according to the manufacturer's instructions. From the purified RNA 0.8 µg were reversely transcribed to cDNA. The absence of genomic DNA in the created cDNA was tested by using the primers SZ19 and SZ20 and the gene *H2A* as control because this combination allows a clear differentiation between cDNA and gDNA.

2.4.8 Sequencing

Plasmid DNA, gDNA, cDNA or PCR fragments were sequenced according to Sanger by Microsynth Seqlab GmbH (Göttingen, Germany). The sequences were evaluated by using Lasergene SeqBuilder (DNASTAR, Inc.,Madison,WI, USA). Annotations were made according to the Ensembl Fungi database (Kersey *et al.*, 2018).

2.4.9 Verification of gene annotations

Annotations from the Ensembl Fungi database (Kersey *et al.*, 2018) were verified by cDNA amplification from wild type JR2 (Fradin *et al.*, 2009) and subsequent sequencing. To verify the annotation of *VEL1* the primers AO11 and AO12 were used. The annotation of *VEL2* was confirmed by VelB-F1 and VelB-R1. *VEL3* annotation was confirmed by using the primers AO3 and AO13. The *VOS1* annotation was verified by using Vos1orf-E1 and Vos1orf-E2.
Ensembl Fungi annotations for *VEL1*, *VEL2* and *VEL3* could be confirmed. The correct annotation of *VOS1* starts already 528 base pairs upstream from the start codon predicted by

Ensembl Fungi as confirmed by amplification and sequencing of cDNA as well as analysis of the peptide sequence obtained by LC-MS analysis (Figure A8 and A9).

2.5 Microbiological methods

2.5.1 Co-cultivation of bacteria and fungi

Different bacterial and fungal strains were similarly cultivated in liquid and on solid SXM and PDM. For both conditions bacteria were cultivated in LB medium (Bertani, 1951) at 30 °C overnight. The next day, bacteria were washed with sterile water. By photometry, the concentration was determined and calculated into colony-forming units (CFU; OD_{600}=1 or ~ 5 x10^8 CFU ml^{-1}) (Cui *et al.*, 2005). Bacterial cells were inoculated with OD_{600}=0.1 in liquid SXM and PDM and grown until OD_{600}=1. Fungal spores were adjusted to a concentration of 1x10^6 spores/ml.

On solid medium 1x10^5 fungal spores of *V. dahliae* JR2, *A. nidulans* A4 and *A. fumigatus* AfS35 were distributed using glass beads. A hole of 1 cm in diameter was cut into the center of the plate. Inside this hole, 60 µl of a bacterial suspension with OD_{600}=1 was inoculated. The plates were incubated at 25 °C at constant light for four days. Afterwards the diameter of the inhibition zone was measured.

Co-cultivation in liquid medium was conducted by inoculating 100 µl bacterial suspension (OD_{600}=1) together with 1x10^6 spores of *V. dahliae* JR2 in liquid SXM and PDM. The cultures were incubated under constant agitation at 25 °C. After 0, 12, 24, 48, 72 and 96 hours, three times 10 µl were taken from the cultures and inoculated on SXM or PDM plates supplemented with kanamycin (50 µg/ml), cefotaxime (300 µg/ml) and doxycycline (40 µg/ml). The plates were incubated for three days at 25 °C and fungal growth was observed. After co-cultivation of 96 hours, the bacterial survival was tested by inoculating 10 µl of the co-culture on LB plates. The plates were incubated for three days at 25 °C.

2.5.2 Phenotypic analysis

Ex planta phenotypical characterization was conducted on pectin-rich simulated xylem medium (SXM), glucose-rich potato dextrose medium (PDM) and minimal medium (Czapek-Dox-Medium, CDM). The minimal medium was modified according to Czapek (1902) and Dox (1910) [3 % (w/v) sucrose, 2 % (v/v) AspA (3.5 mM $NaNO_3$, 350 mM KCl, 550 mM KH_2PO_4, pH 5.5 with KOH), 2 mM $MgSO_4$ 1 % (w/v) $FeSO_4$, 2 % (w/v) agar]. On agar plates 5x10^4 freshly harvested fungal spores were spot inoculated and incubated either in constant light or constant darkness at 25 °C or during long day conditions (16 h, 25 °C: 8 h, 22 °C, light: dark; light: fluorescence: 60, GroLEDs: 100, illumination: 95 µmol) in a growth chamber for 10 to 14 days. Afterwards, plates were scanned and the colonies were examined by binocular (SZX12-ILLB2-200, Olympus Deutschland GmbH, Hamburg, Germany) and light microscopy (Axiolab

light microscope, Zeiss, Oberkochen, Germany). Pictures were taken with SC30 cameras (Olympus Deutschland GmbH, Hamburg, Germany) and processed with the cellSens Dimension software version 1.4 (Olympus Deutschland GmbH, Hamburg, Germany).

2.5.3 Quantification of conidiospores

For quantification of conidia production, $2x10^5$ freshly harvested spores were inoculated in exactly 50 ml SXM and incubated at 25 °C under constant agitation at 125 rpm for seven days. Each strain was inoculated in triplicates. After the incubation period, the spores were filtered with Miracloth filters (Calbiochem Merck, Darmstadt, Germany) and centrifuged at 3500 rpm for 10 min at 4 °C. The spore pellets were dissolved in equal amounts of sterile water. By using the Coulter Z2 Particle Counter (Beckman Coulter, Krefeld, Germany), the concentration of conidiospores was determined. The conidia formation was quantified relative to the wild type. Each experiment was performed with three technical replicates (n=1). Bars represent the mean values of all experiments and error bars correspond to standard deviations. Statistical significances were calculated by t-test with the Simple Interactive Statistical Analysis (SISA) online tool (Uitenbroek, 1997). Significances indicate: *,$p<0.05$; **,$p<0.01$; ***,$p<0.001$; ****,$p<0.0001$; ns, not significant.

2.5.4 Fluorescence microscopy and localization studies

In order to investigate the subcellular localization of the examined proteins, overexpression strains with C-terminal GFP fusions were constructed. The strains were furthermore transformed with a histone *H2B-RFP* overexpression construct to visualize the nuclei. In 15 µ-Slide 8 Well microscopy chambers (ibidi GmbH, Gräfelfing, Germany) filled with 300 µl PDM, $1x10^4$ freshly harvested fungal spores were inoculated and incubated at 25 °C for 16 hours either in light or darkness. Subcellular localization of the proteins was examined by fluorescence microscopy using a 100x/1.4 oil objective with the Zeiss Observer Z1 microscope (Zeiss, Oberkochen, Germany) with a CSU-X1 A1 confocal scanner unit (Yokogawa, Ratingen, Germany) and QuantEM:512SC digital camera (Photometrics, Tuscon, AZ, USA). Pictures were processed with the SlideBook 6.0 digital microscopy software (Intelligent Imaging Innovations, Göttingen, Germany). Exposure times were 500 ms and 800 ms for GFP and RFP, respectively.

2.5.5 Plant infection

2.5.5.1 *Arabidopsis thaliana* root infection

A. thaliana Col-0 seedlings were used for root infection studies with *V. dahliae* strains overexpressing free GFP to observe fungal colonization of the root. Surface sterilization of seeds was done by washing them for 5 min with 70 % (v/v) ethanol and 0.05 % (v/v) Tween80.

After removing the liquid, the seeds were washed for 5 min with 96 % ethanol and subsequently dried in a reaction tube at 35 °C. Seeds were grown on Murashige and Skoog medium (Murashige & Skoog, 1962) [0.22 % MS including vitamins (Duchefa Biochemie, Haarlem, Netherlands), 0.05 % MES (Carl Roth GmbH & Co. KG, Karlsruhe, Germany) 1 % sucrose, 1.5 % plant agar (Duchefa Biochemie, Haarlem, Netherlands) adjusted to pH 5.7 with KOH] overnight at 4 °C and afterwards for 21 days under long day conditions (16 hours light at 25 °C, 8 hours darkness at 22 °C; light: fluorescence: 60, GroLEDs: 100, illumination: 95 µmol) in a climate chamber. One day prior to infection with *V. dahliae* spores, the plants were transferred to 1 % water agarose plates. Infection was conducted by root dipping in a spore solution with $1x10^5$ spores/ml for 35 min. After infection, the plants were transferred back to the water agarose and the lower 2/3 of the plates were covered with aluminum foil to simulate the soil. The plants were further incubated for five days in a climate chamber. The roots were then stained with 0.0025 % (v/v) propidium iodide and 0.005 % (v/v) silwet for 5 min in darkness. Stained roots were fixated on object slides with 150 µl H_2O and 50 µl staining solution. Fungal colonization was monitored by fluorescence microscopy using a 20x objective for overview pictures and a 63x objective for close-up views (both Zeiss, Oberkochen, Germany). 3D volume views were generated from single picture stacks. Within each experiment different plants were investigated.

2.5.5.2 Tomato plant infection and stem assay

Tomatoes (*Solanum lycopersicum*, cultivar “Money-maker”) were used as host plant for *V. dahliae* and treated as described before (Harting *et al.*, 2020). Seedlings were surface sterilized while shaking them with 70 % (v/v) ethanol and 0.05 % (v/v) Tween80 for 5 min. The liquid was removed and the seeds were again washed with 96 % ethanol for 5 min. Dried seeds were grown for ten days in a 1:1 mixture of soil (Fruhstorfer Erde Typ T Struktur 1-fein-, Archut GmbH & Co. KG, Lauterbach, Germany) and sand (crystal silica sand 0.4-0.8 mm, Dorsilit, Hirschau, Germany). Before infection, roots were slightly wounded by rubbing and then incubated in a spore suspension of $1x10^7$ spores/ml for 40 min under constant agitation at ~30 rpm. Water served as mock control. Per strain 15 plants were infected. Infected plants were planted into planting pots (70x70x80 mm, Soparco GmbH, Saarbrücken, Germany) containing a 1:1 mixture of sand and soil. Afterwards, three times $1x10^7$ spores were pipetted to the soil. The plants were incubated for 21 days under long day conditions (16 hours light at 25 °C, 8 hours darkness at 22 °C; light: fluorescence: 60, GroLEDs: 100, illumination: 95 µmol) in a plant chamber.

After 21 days the height of the vegetation point, the size of the longest leaf and the fresh weight of the part above the soil were scored. Categories relative to mock plants were calculated (100-

80 % mean mock plants = 1, 79-60 % mean mock plants = 2, 59-40 % mean mock plants = 3, <40 % mean mock plants = 4). Thereby, a disease score was calculated for each plant (Harting *et al.*, 2020). Following the disease score, plants were categorized as healthy (1-1.99), weak symptoms (2-2.99), strong symptoms (3-3.99) and heavy symptoms (4). The scores for the tested plants relative to the total amount of plants were illustrated by a stack diagram. Independent experiments and transformants are summarized in the stack diagrams. Furthermore, the discoloration of the hypocotyl cross sections as sign for plant defense reaction was recorded with a binocular microscope (SZX12-ILLB2-200, Olympus Deutschland GmbH, Hamburg, Germany).

Fungal infections were confirmed by outgrowth tests from tomato stems. Stems of control as well as infected plants were harvested 21 days after infection. Stems were surface sterilized by washing them for 8 min with 70 % (v/v) ethanol and 8 min with 6 % (v/v) sodium hypochlorite. Afterwards, the stems were washed twice with sterile water. The ends of the stems were removed, the rest was cut in small pieces and transferred to PDM plates supplemented with 34 µg/ml chloramphenicol. The plates were incubated for seven days at 25 °C and fungal outgrowth was examined. PCR reactions were conducted to confirm fungal outgrowth of Δ*VEL1*. Therefore, genomic DNA of the outgrowing microorganism was isolated and tested with the primer pair AO24 and AO25. In the wild type a fragment with a size of 2130 bp was expected, in *VEL1* deletion strains the same primers would result in a fragment with a size of 4342 bp.

2.6 Protein methods

2.6.1 Protein extraction

Protein extracts were required for western hybridization and protein pull downs. For western analysis fungal strains were grown in 50 ml liquid PDM, liquid SXM or on 30 ml SXM plates covered with a sterile Amersham™ Hybond-N™ nylon membrane (GE Healthcare life sciences, München, Germany). For pull downs higher amounts of protein were required. Fungal spores were therefore inoculated in 500 ml liquid PDM. Fungal mycelium was harvested from liquid cultures through Miracloth filters (Calbiochem Merck, Darmstadt, Germany) and was washed with 0.96 % NaCl. Fungal material from plates was harvested by using a spatula to scrape it off from the membrane. All fungal material was dried and ground in liquid nitrogen to a fine powder. Small sample volumes were ground with a table mill (Retsch GmbH, Haan, Germany). Depending on the amount of fungal material, B* buffer [(300 mM NaCl, 100 mM Tris pH 7.5, 10 % glycerol, 2 mM EDTA, 0.02 % NP-40) freshly supplemented with 2 mM DTT, 10 µl/ml cOmplete™, EDTA-free Protease Inhibitor Cocktail (Roche, Penzberg, Germany; Stock: one tablet in 500 µl dH_2O) and for protein pull downs also with

1 mM PMSF)] was added to the powder to obtain a semi-fluid mixture. Buffer and ground material were vigorously mixed and centrifuged for 30 min at 13000 rpm at 4 °C (Centrifuge 5417 R Eppendorf AG, Hamburg, Germany). Samples for protein pull downs were centrifuged in SS34 centrifugation tubes (Thermo Fisher Scientific, Schwerte, Germany) for 1 h at 15000 rpm at 4 °C (Sorvall® RC-5B Plus Superspeed Centrifuge, Thermo Fisher Scientific, Schwerte, Germany). The supernatant was transferred into a new reaction tube and the protein concentration was determined according to Bradford. Protein samples were stored at -20 °C.

2.6.2 Determination of the protein concentration according to Bradford

The protein concentration was determined with the Bradford assay (Bradford, 1976). Diluted protein samples and a bovine serum albumin (BSA; Carl Roth GmbH & Co. KG, Karlsruhe, Germany) as protein standard were mixed with Roti®-Quant solution (Carl Roth GmbH & Co. KG, Karlsruhe, Germany). The absorbance of proteins and the standard were measured with an Infinite M200 microplate reader running with Magellan software (Tecan Trading AG, Männedorf, Schweiz).

2.6.3 SDS-PAGE

For separation of proteins according to their molecular weight, sodium dodecyl sulfate polyacrylamide gel electrophoresis (SDS-PAGE) as described by Smith (1984) was conducted. The extracted protein was mixed with sample buffer [250 mM Tris pH 6.8, 15 % (v/v) β-mercaptoethanol, 30 % glycerol, 7 % (w/v) SDS, 0.3 % bromophenol blue] and denatured at 95°C for 10 min. Gels with 12 % polyacrylamide were used within this study. The gels were composed of a stacking gel [666 µl polyacrylamide (stock: 30 %), 1.25 ml gel buffer (3 M Tris pH 8.45, 0.3 % SDS), 3 ml H_2O, 60 µl ammonium persulfate (APS, stock: 10 %), 10 µl N,N,N′,N′-tetramethylethan-1,2-diamine (TEMED), 10 µl Coomassie Brilliant Blue] and a running gel [2.1 ml H_2O, 3.75 ml 1 M Tris pH 8.8, 100 µl SDS (stock: 10 %), 4 ml polyacrylamide (stock: 30 %), 100 µl APS (stock: 10 %), 10 µl TEMED]. Loaded amounts of denatured protein are indicated. As size standard the PageRuler™ Prestained Protein Ladder 10-180 kDa (Thermo Fisher Scientific, Schwerte, Germany) was applied. Gels were run at 120-200 V in a Mini-Protean® Tetra Cell filled with running buffer [25 mM Tris Base, 250 mM glycine, 0.1 % SDS (w/v); (Laemmli, 1970)] with a Power Pac™ 3000 power supply (BIO-RAD Laboratories, Hercules, CA, USA).

2.6.4 Western hybridization

Proteins that were previously separated by SDS-PAGE were wet blotted to an Amersham™ Protran™ 0.45 µm NC nitrocellulose membrane (GE Healthcare life sciences, München, Germany) by using a Mini Trans-Blot® Electrophoretic Cell run with a Power Pac™ 3000 power

supply (BIO-RAD Laboratories ,Hercules, CA, USA). The blotting device was filled with transfer buffer [25 mM Tris Base, 192 mM glycine, 0.02 % (w/v) SDS, 20 % methanol]. Blotting was conducted at 100 V with a cool pack for at least 1 h. After blotting the membrane was stained under constant agitation with PonceauS [0.2 %(w/v) PonceauS, 3 % (v/v) trichloroacetic acid (TCA)] as loading control to visualize the transferred proteins (Romero-Calvo *et al.*, 2010). Afterwards the membrane was blocked for 1 h under constant agitation in 5 % (w/v) skimmed milk powder (Sucofin TSI GmbH & Co. KG, Zeven, Germany) diluted in TBST [10 mM Tris-HCl pH 8.0, 150 mM NaCl, 0.05 % (v/v) Tween20] to inhibit unspecific binding of the antibody. The membrane was incubated at 4 °C under constant agitation with the α-GFP antibody (sc-9996, Santa Cruz Biotechnology, Dallas, TX, USA) diluted as indicated in 5 % skimmed milk powder in TBST overnight. The next day, the membrane was washed three times for 10 min with TBST. Next, the secondary antibody coupled to a horseradish peroxidase was applied (mouse 115-035-003 antibody, Jackson ImmunoResearch, West Grove, PA, USA). The antibody was used diluted 1:2000 in TBST with 5 % skimmed milk powder. The membrane was incubated with the antibody for 1 h under constant agitation at room temperature. Later, the membrane was washed again three times for 10 min in TBST. In order to detect chemiluminescent signals, luminol was used as substrate of the horseradish peroxidase. Solution A (2.5 mM luminol, 400 µM paracoumarat, 100 mM Tris pH 8.5) and B (5.4 mM H_2O_2, 100 mM Tris pH 8.5) were mixed directly on the membrane. The membrane was incubated for 2 min under constant agitation in darkness with the solution. The signals were detected with Fusion SL chemiluminescence detector (PeqLab, Erlangen, Germany) operated with Fusion 15.18 (Vilber Lourmat Deutschland GmbH, Eberhardzell, Germany) and Amersham™ Hyperfilm™-ECL films (GE Healthcare life sciences, München, Germany). The films were developed using the Optimax® X-ray Film Processor (Protec GmbH & Co. KG, Oberstenfeld, Germany).

2.6.5 *In vitro* protein pull down with GFP-tagged proteins

Protein pull downs with strains labelled with GFP at the endogenous locus were conducted to identify interaction partners. Therefore, $5x10^7$ freshly harvested spores were inoculated in 500 ml PDM and grown for 72 h during constant agitation in light. Proteins were extracted as previously described in 2.6.1. The wild type ectopically expressing GFP and the wild type JR2 served as control and were mixed before protein extraction (1/3 with GFP, 2/3 without GFP) due to a higher amount of free GFP in VGB45 in comparison to the above mentioned velvet strains, which was observed with western hybridization experiments using a GFP-specific antibody. The protein concentration was measured according to Bradford as described in 2.6.2. Proteins were purified in Poly-Prep® Chromatography Columns (BIO-RAD Laboratories, Hercules, CA, USA) with 10 µl GFP-Trap® Agarose beads from ChromoTek GmbH (Planegg-Martinsried, Germany). Prior to protein loading, the beads were washed with B* buffer in the

column. For each sample, 12 mg of protein were mixed in Poly-Prep® Chromatography Columns with beads and adjusted to the same volume with B* buffer. GFP-Trap® Agarose beads were incubated for 2 h at 4 °C rotating. Afterwards, the beads were washed twice with 5 ml W300 buffer (300 mM NaCl, 10 mM Tris pH 7.5). To elute the proteins, 150 µl of 0.2 M glycine pH 2.5 was mixed with them by pipetting in the column for 30 sec. Immediately, 15 µl 1 M Tris pH 10.4 were added to neutralize the solution. The elution step was repeated twice leading to elution E1-E3. Samples were kept on ice and directly subjected to chloroform-methanol extraction.

2.6.6 Chloroform-Methanol extraction of proteins

The eluted proteins (E1-E3) were directly applied to chloroform-methanol extraction to remove detergents and salts and prepare them for in-solution enzyme digestion. The protocol was modified according to Wessel & Flügge (1984). Elution fractions were adjusted to 100 µl and vigorously mixed with 400 µl methanol. After a short centrifugation step for 10 sec at 10000 rpm, 100 µl chloroform were added, mixed and the centrifugation step was repeated. Next, 300 µl H_2O (HPLC grade) were added and vigorously mixed with the solution. To achieve two phases, the samples were centrifuged for 3 min at 10000 rpm at 4 °C. As the proteins are now at the interphase, the upper phase was discarded without destroying the interphase. After adding 300 µl methanol to the lower phase and vigorously mixing the solution, the samples were centrifuged for 10 min at 4 °C and 13000 rpm. The supernatant was removed, the protein sediments were dried in a Savant SPD 111V SpeedVac Concentrator (Thermo Fisher Scientific, Schwerte, Germany) at 50 °C and stored at -20 °C.

2.6.7 In solution digestion and peptide purification

For enhanced protein digestion, proteins were resuspended in *Rapi*GestSF Surfactant as indicated by the manufacturer (Waters Corporation, Milford, MA, USA). At this step, all elution fractions E1-E3 were mixed by dissolving the protein pellet of each strain in 40 µl 0.1 % *Rapi*Gest SF solution and transferring it to the next elution. DTT was added to a final concentration of 5 mM and the samples were incubated at 60 °C for 30 min. After cooling the samples down to room temperature, 15 mM iodoacetamide was added. The samples were incubated in darkness for 30 min at room temperature. Trypsin digestion was conducted overnight, final dilution 1:20 (Serva Electrophoresis GmbH, Heidelberg, Germany). The next day, 0.5 % (v/v) trifluoroacetic acid (TFA) was added to the digested peptides to precipitate the *Rapi*Gest SF solution. Within this step the pH value should be reduced to two. The samples were incubated at 37 °C for 45 min and centrifuged for 10 min at 13000 rpm at room temperature. The supernatant was transferred to a new LoBind reaction tube (Eppendorf AG,

Hamburg, Germany) and dried in a Savant SPD 111V SpeedVac Concentrator (Thermo Fisher Scientific Schwerte, Germany) at 50 °C.

2.6.8 C18 Stage tip purification

Before LC-MS analysis, salts and detergents were removed by Stop and Go Extraction (Stage) tip purification (Rappsilber *et al.*, 2003, 2007). Dried peptides were dissolved in 40 µl sample buffer [98 % (v/v) H_2O, 2 % (v/v) acetonitrile, 0.1 % (v/v) formic acid] by placing them in a shaker for 5 min and subsequently incubating them in an ultrasonic bath (Sonorex Super 10P, BANDELIN electronic GmbH & Co. KG, Berlin, Germany) for 3 min. C18 columns were prepared directly prior to use by putting two layers of C18 material (3M, Saint Paul, MN, USA) in a 200 µl pipette tip. The material was pushed as far as possible into the pipette tip to make sure that no space remained between the pipet tip wall and the material. The pipette tip was placed in a 2 ml reaction tube with an adaptor. The Stage tips were equilibrated by using 100 µl 0.1 % (v/v) formic acid in methanol (HPLC grade). The Stage tips were centrifuged for 2 min at 13000 rpm and the flow through was discarded. Next, 100 µl 70 % (v/v) acetonitrile with 0.1 % (v/v) formic acid were pipetted to the column, centrifuged and the flow through was discarded. Lastly, the column was washed twice with 100 µl 0.1 % (v/v) formic acid in H_2O, centrifuged and the flow through was discarded. The Stage tip was placed into a new 2 ml reaction tube. For loading, the samples were equally distributed on two Stage tip columns. To achieve contact of the liquid with the C18 material, the Stage tip was centrifuged for 5 sec at 1000 rpm and afterwards incubated for 5 min. Then the Stage tips were centrifuged for 5 min at 4000 rpm, the flow through was loaded onto the column again and the previous steps were repeated. After the second centrifugation step, all peptides should be attached to the C18 material and are washed twice with 200 µl 0.1 % (v/v) formic acid in H_2O to remove salts and contaminations. This time the Stage tips are centrifuged for 2 min at 10000 rpm. To elute the peptides, the Stage tips were placed into a new LoBind reaction tube (Eppendorf AG, Hamburg, Germany) and 60 µl 70 % (v/v) acetonitrile with 0.1 % (v/v) formic acid were pipetted to the column. Elution was achieved by centrifugation for 5 min at 4000 rpm. Separated samples were merged in one reaction tube and dried in a Savant SPD 111V SpeedVac Concentrator (Thermo Fisher Scientific Schwerte, Germany) at 50 °C. Dried samples were stored at -20 °C.

For LC-MS measurement, the peptides were dissolved in 20 µl fresh sample buffer [98 % (v/v) H_2O, 2 % (v/v) acetonitrile, 0.1 % (v/v) formic acid] by pipetting up and down and incubating them for 3 min in an ultrasonic bath (Sonorex Super 10P, BANDELIN electronic GmbH & Co. KG, Berlin, Germany) at maximum power. The solution was transferred to LC-MS vials (Agilent Technologies, Santa Clara, CA, USA).

2.6.9 Liquid chromatography-mass spectrometry (LC-MS) analysis of peptides

Dried peptide samples were dissolved in sample buffer as described in 2.6.8. From each sample 2 µl were subjected to reverse phase liquid chromatography for peptide separation using an RSLCnano Ultimate 3000 system (Thermo Fisher Scientific, Schwerte, Germany). Therefore, peptides were loaded on an Acclaim PepMap 100 pre-column (100 µm x 2 cm, C18, 5 µm, 100 Å; Thermo Fisher Scientific) with 0.07 % trifluoroacetic acid at a flow rate of 20 µL/min for 3 min. Analytical separation of peptides was done on an Acclaim PepMap RSLC column (75 µm x 50 cm, C18, 2 µm, 100 Å; Thermo Fisher Scientific) at a flow rate of 300 nL/min. The solvent composition was gradually changed within 94 min from 96 % solvent A (0.1 % formic acid) and 4 % solvent B (80 % acetonitrile, 0.1 % formic acid) to 10 % solvent B within 2 min, to 30 % solvent B within the next 58 min, to 45 % solvent B within the following 22 min, and to 90 % solvent B within the last 12 min of the gradient. All solvents and acids had Optima grade for LC-MS (Thermo Fisher Scientific). Eluting peptides were on-line ionized by nano-electrospray (nESI) using the Nanospray Flex Ion Source (Thermo Fisher Scientific) at 1.5 kV (liquid junction) and transferred into a Q Exactive HF mass spectrometer (Thermo Fisher Scientific). Full scans in a mass range of 300 to 1650 m/z were recorded at a resolution of 30000 followed by data-dependent top 10 HCD fragmentation at a resolution of 15000 (dynamic exclusion enabled). LC-MS method programming and data acquisition was performed with the XCalibur 4.0 software (Thermo Fisher Scientific). Measurements were conducted by Dr. Oliver Valerius and Dr. Kerstin Schmitt (Service Unit LCMS Protein Analytics of the Göttingen Center for Molecular Biosciences (GZMB) at the University of Göttingen, Germany; Grant DFG-GZ: INST 186/1230-1 FUGG to Stefanie Pöggeler).

LC-MS data was analysed with MaxQuant 1.6.0.16 (Cox & Mann, 2008) and Perseus 1.6.0.7 (Tyanova *et al.*, 2016). MaxQuant was used with default parameters and label free quantification (LFQ) to analyse the raw data. The protein database from Ensembl Fungi (Kersey *et al.*, 2018) was used in MaxQuant 1.6.0.16 but the entry of VDAG_JR2_Chr31209a was altered as indicated (Figure A8 and A9). Obtained data were evaluated with Perseus 1.6.0.7. Data were processed as indicated in Table 7.

Table 8: Perseus workflow for evaluation of the MaxQuant result files for the *in vitro* protein pull downs.

Step	Command	Description
1	Generic matrix upload	Upload proteingroups.txt Main: LFQ intensities Numerical: MS/MS counts, sequence coverage, unique peptides, razor + unique peptides
2	Filter rows based on categorical column	Remove rows with + for Only identified by site Remove rows with + for Reverse Remove rows with + for Potential contaminant
3	Rearrange	Remove empty columns
4	Transform	LFQ intensities = $\log_2(x)$
5	Categorical annotation rows	Groups: wild type control and examined velvet strain(s)
6	Analysis	Multi scatter plot Numeric Venn diagram
7	Filter rows based on valid values	Min. valids 3 in at least one group: examined velvet strain Values: valid Reduce matrix
8	Replace missing values from normal distribution	Mode: Total matrix
9	Analysis	Volcano Plot First group: Velvet strain Second group: wild type
10	Repeat step 8 and 9 at least 3 times	
11	Load significant interaction partners in Venny 2.1 (Oliveros, 2015) and generate a list of proteins found in all four repetitions of the statistical analysis as significant (step 8 and 9)	
12	Select rows with significant hits found in all four repetitions as co-enriched with the bait based on the result of step 11	Export selection (reduce matrix)
13	Select rows with significant hits found in all three repetitions as co-enriched with the bait	Export selection (reduce matrix)
14	Replace imputed values by NaN	Export Matrix, see Table A2, A4, A6, A8, A10
15	Select representative Volcano Blot	Label significant partners (found in all four repetitions)

2.7 Secondary metabolite extraction and LC-MS analysis

The extraction of secondary metabolites and LC-MS analysis was conducted as previously described (Köhler *et al.*, 2019). Per strain, two plates of 30 ml CDM with glucose as carbon source were inoculated with $1x10^6$ freshly harvested spores. The plates were incubated at 25 °C either in darkness or light for two weeks. A 50 ml falcon tube was used to cut a piece from each plate. The agar pieces were homogenized with a 20 ml syringe and mixed with 5 ml ethyl acetate (Carl Roth GmbH & Co. KG, Karlsruhe, Germany) and 5 ml H_2O (Merck KGaA (Darmstadt, Germany) (both LC-MS grade). The samples were incubated overnight during constant agitation at 220 rpm at 20 °C. The next day, the samples were centrifuged for 10 min at 2500 rpm at 4 °C. The upper phase was transferred into a vial and vaporized in a rotary evaporator Hei-VAP advantage (Heidolph Instruments GmbH & Co. KG, Schwabach, Germany) equipped with a LABOXACT® vacuum system (KNF Neuberger GmbH, Freiburg, Germany) and a cooling system (Lauda Dr. R. Wobser GmbH & Co. KG, Lauda-Königshofen, Germany). For measurement of metabolites, the samples were dissolved in 1:1 acetonitrile and H_2O (both LC-MS grade), centrifuged at 8 °C for 15 min at 13000 rpm to remove particles and transferred into LC-MS vials. Measurements were conducted by Dr. Jennifer Gerke (Department of Molecular Microbiology and Genetics, University of Göttingen, Germany; the LC-MS was founded by the DFG: INST 186/1287-1 FUGG).

Data was evaluated by using FreeStyle 1.6 (Thermo Fisher Scientific, Schwerte, Germany). Reproducible main peaks were analyzed in detail by comparing their sum formula and spectra to literature. Peaks, which could not be assigned to a mass were not further investigated.

2.8 Bioinformatic methods

Gene annotations were made according to the Ensembl Fungi database (Kersey *et al.*, 2018). BLAST searches were conducted using the Ensembl Fungi database (Kersey *et al.*, 2018). Accession numbers of genes investigated within this study were used according to the Ensembl Fungi database (Kersey *et al.*, 2018). Sequence analyses of proteins were carried out by using the InterPro website (Jones *et al.*, 2014; Mitchell *et al.*, 2019). Nuclear localization signals (NLS) were predicted by using cNLSmapper (Kosugi *et al.*, 2009) with default settings. Nuclear export signals (NES) were predicted using NetNES 1.1 Server with default settings (la Cour *et al.*, 2004). PEST motifs were predicted using epestfind (http://emboss.bioinformatics.nl/cgi-bin/emboss/epestfind) with default settings. The sequences of other fungi mentioned within this study were also obtained from the Ensembl Fungi database (Kersey *et al.*, 2018). Multiple sequence alignment of different fungi was performed by MegAlignPro (DNASTAR, version 12.1.0) using ClustalW sequence alignment.

Statistical analyses were carried out with the SISA online tool (Uitenbroek, 1997). Structural formulas were created using ChemDraw Professional 16.0 (PerkinElmer).

3 RESULTS

3.1 The velvet family of regulatory proteins is involved in diverse processes within the life cycle of *V. dahliae*

3.1.1 *V. dahliae* carries a similar set of four velvet domain protein encoding genes as *A. nidulans*

The first velvet family member, velvet A (VeA), was described in the filamentous ascomycete *A. nidulans*. A strain with a point mutation in the *veA* gene resulted in a truncated VeA protein and produced more conidia but fewer fruiting bodies (Käfer, 1965). In this study, homologs of velvet proteins were identified in *V. dahliae* JR2 by BLAST search with known identifiers from *A. nidulans*. The *V. dahliae* velvet domains vary between a length of 174 to 315 amino acids (aa) but the architecture of the velvet domain proteins is largely conserved between *V. dahliae* and *A. nidulans*.

The protein similar to *A. nidulans* VeA (ANIA_01052, full length VeA) was named Vel1 in *V. dahliae*. The genomic sequence of *VEL1* comprises three exons and two introns with a total size of 2877 base pairs (bp) (Figure 8a). The transcribed mRNA has a size of 2612 bp. The translated Vel1 protein consists of 552 aa yielding in a protein with a molecular mass of approximately 87 kDa, which means Vel1 has a similar size as *A. nidulans* VeA (Figure 5). Analysis of the Vel1 protein revealed one velvet domain at the N-terminus (amino acids 28-224) and predicted an NLS at the C-terminus at amino acid 489 with a score of eight suggesting that the protein is probably predominantly localized to the nucleus. The velvet domain of *A. nidulans* VeA is also localized at the N-terminus as well as the NLS. Furthermore, VeA contains an NES, which was not predicted for Vel1 of *V. dahliae*. Similar to VeA, Vel1 carries a PEST domain between amino acids 162-183, which might belong to a specific and conserved mechanism for controlling protein stability as described for *A. nidulans* VeA (Meister *et al.*, 2019). Alignment of Vel1 homologs from other fungi revealed similarities, especially in the region of the velvet domain (Figure A5). The highest sequence similarity for Vel1 was observed between *V. dahliae* and *Colletotrichum graminicola* (56.8 %). These two Sordariomycetes also cluster together in the phylogenetic tree (Figure 8b). *M. oryzae* and *N. crassa* have sequence similarities around 40 % to *V. dahliae* Vel1 and cluster together in the phylogenetic tree. *A. fumigatus*, *A. nidulans* and *B. cinerea* homologs possess sequence similarities around 35 % to *V. dahliae* Vel1.

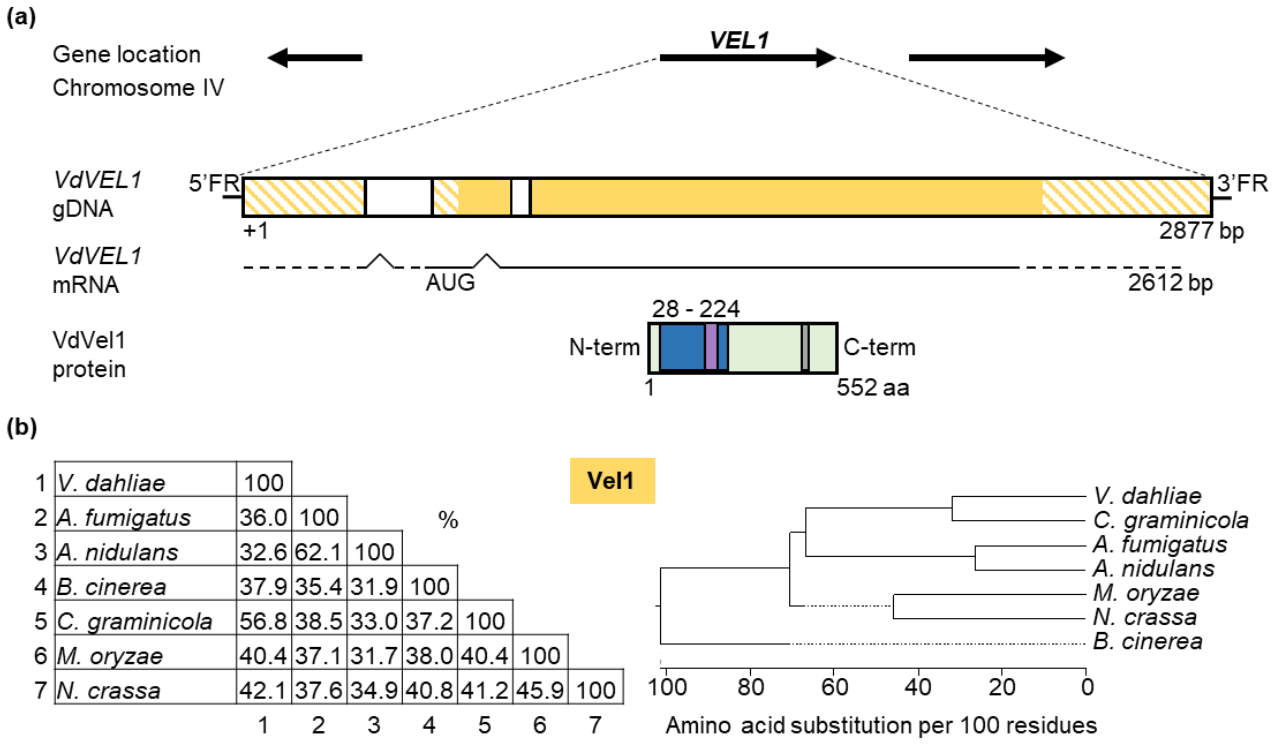

Figure 8: Structure of the *V. dahliae VEL1* gene and the deduced protein with comparison to Vel1-like proteins of other ascomycetes. (a) Genomic locus of the *VEL1* gene (VDAG_JR2_Chr7g04890a) and neighboring genes including transcription directions are shown. Introns are depicted in white, exons are depicted in yellow, hatched areas show the predicted untranslated region. Velvet domains (dark blue) were predicted by InterProScan according to entry IPR037525. Potential nuclear localization sequences (NLS, grey) and PEST motifs (purple) are shown. *VEL1* consists of three exons and two introns. The deduced Vel1 protein holds a velvet domain and a PEST motif at the N-terminus and an NLS at the C-terminus. **(b)** Protein sequences of *A. fumigatus* Af293, *A. nidulans* FGSC A4, *B. cinerea* BcDW1, *C. graminicola* M1.001, *M. oryzae* M68 and *N. crassa* OR74A similar to Vel1 of *V. dahliae* were aligned by multiple sequence alignment. Similarities of *V. dahliae* velvet proteins in different fungi are shown with a matrix of sequence identity in percent and a phylogenetic tree.

A homolog of *A. nidulans* VelB (ANIA_00363) was identified in *V. dahliae* and named Vel2. The gene consists of five exons and four introns leading to a total size of 2354 bp for the genomic DNA sequence and 2122 bp for the resulting mRNA (Figure 9a). Translation yields in a protein with a size of 460 aa leading to a molecular mass of 78 kDa. In comparison, *A. nidulans* VelB is smaller with a size of 369 aa (Figure 5). For the Vel2 protein one velvet domain was predicted (amino acids 130-445).

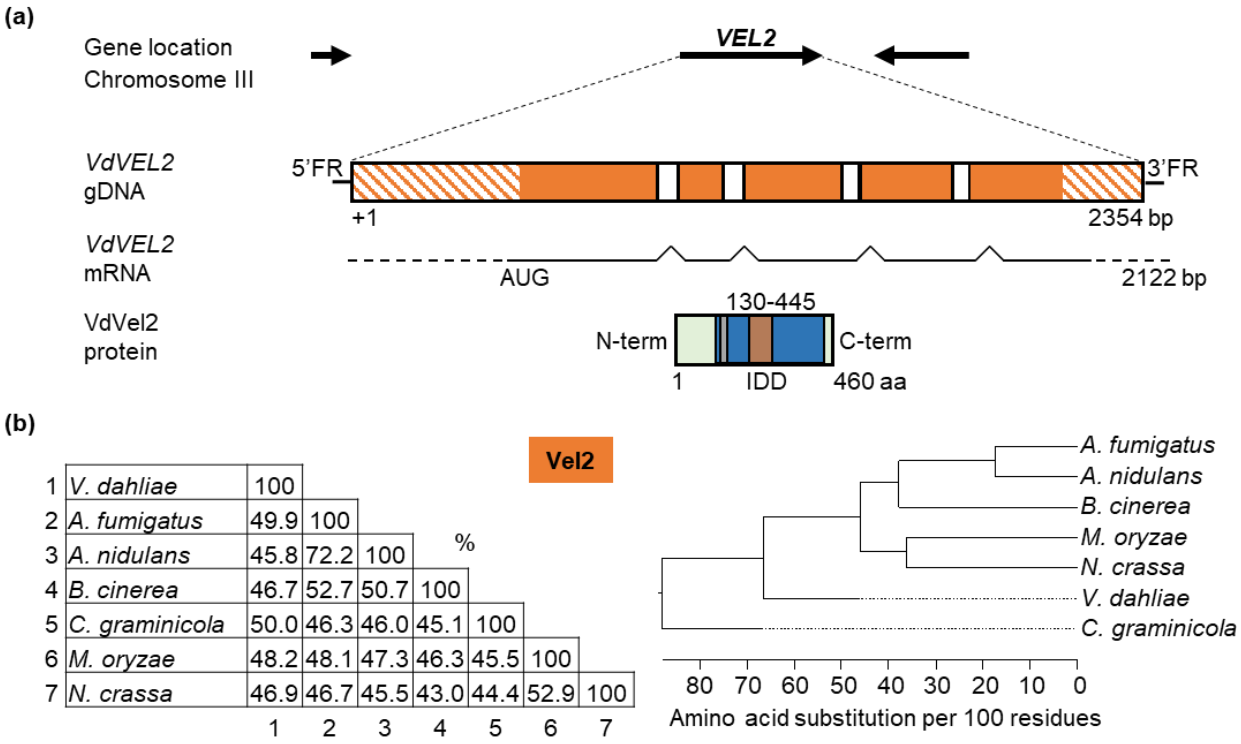

Figure 9: Structure of the *V. dahliae VEL2* gene and the deduced protein with comparison to Vel2-like proteins of other ascomycetes. (a) Genomic locus of the *VEL2* gene (VDAG_JR2_Chr3g06150a) and neighboring genes with transcription directions are shown. Introns are depicted in white, exons are depicted in orange, hatched areas show the predicted untranslated region. Velvet domains (dark blue) were predicted by InterProScan according to entry IPR037525. Potential nuclear localization sequences (NLS, grey) are indicated. *VEL2* consists of five exons and four introns. The Vel2 velvet domain includes an NLS and is interrupted by an intrinsically disordered domain (IDD) based on alignments. **(b)** Protein sequences of *A. fumigatus* Af293, *A. nidulans* FGSC A4, *B. cinerea* BcDW1, *C. graminicola* M1.001, *M. oryzae* M68 and *N. crassa* OR74A similar to Vel2 of *V. dahliae* were aligned by multiple sequence alignment. Similarities of *V. dahliae* velvet proteins in different fungi are shown with a matrix of sequence identity in percent and a phylogenetic tree.

Alignment of *V. dahliae* Vel2 with *A. nidulans* VelB revealed that both velvet domains are interrupted by an intrinsically disordered domain(IDD) (Thieme, 2018) (Figure A6). This domain does not interfere with the folding of the velvet domain in the X-ray structure (Ahmed *et al.*, 2013). Different to *A. nidulans* VelB were no NLS is predicted (Bayram & Braus, 2012), an NLS was predicted at amino acid 140 within the first part of the velvet domain of *V. dahliae* Vel2. The score of the NLS was 6.5, which means it might be localized to the nucleus and cytoplasm. Alignment of *V. dahliae* Vel2 with Vel2-like protein sequences of other related ascomycetes exhibited sequence similarities around 50 % aa identity (Figure 9b).

A protein similar to *A. nidulans* VelC (ANIA_02059) could be identified in *V. dahliae* and was named Vel3. The genomic DNA of *VEL3* consists of 1845 bp and has one exon (Figure 10a). Hence, the corresponding mRNA also has a size of 1845 bp. The resulting protein compromises 437 aa leading to a molecular mass of 76 kDa.

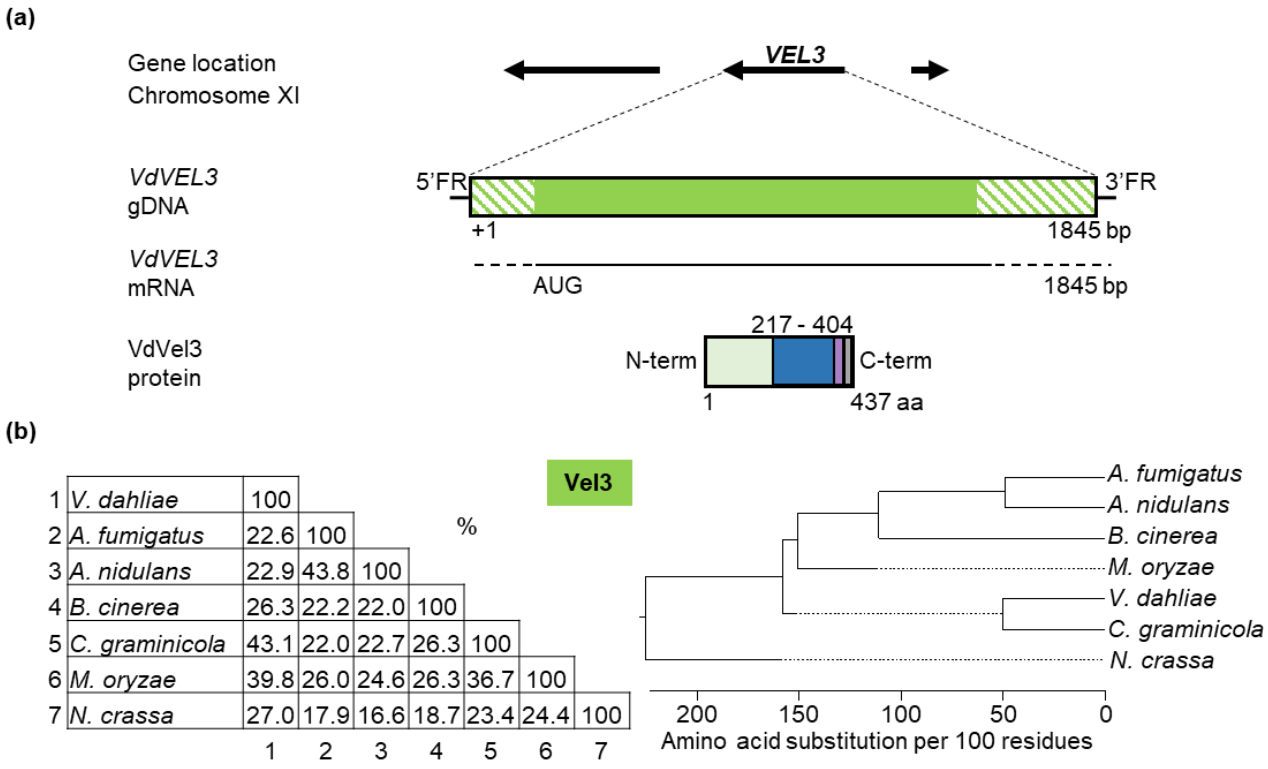

Figure 10: Structure of the *V. dahliae VEL3* gene and the deduced protein with comparison to Vel3-like proteins of other ascomycetes. (a) Genomic locus of the *VEL3* gene (VDAG_JR2_Chr6g00630a) and neighboring genes with transcription directions are shown. Introns are depicted in white, exons are depicted in green, hatched areas show the predicted untranslated region. Velvet domains (dark blue) were predicted by InterProScan according to entry IPR037525. Potential nuclear localization sequences (NLS, grey) and PEST motifs (purple) are shown. *VEL3* consists of a single exon. The Vel3 protein contains one velvet domain, an NLS and a PEST motif at the C-terminus. **(b)** Protein sequences of *A. fumigatus* Af293, *A. nidulans* FGSC A4, *B. cinerea* BcDW1, *C. graminicola* M1.001, *M. oryzae* M68 and *N. crassa* OR74A similar to Vel3 of *V. dahliae* were aligned by multiple sequence alignment. Similarities of *V. dahliae* velvet proteins in different fungi are shown with a matrix of sequence identity in percent and a phylogenetic tree.

A. nidulans VelC is with a size of 524 aa smaller than *V. dahliae* Vel3 (Figure 5). For Vel3 a velvet domain (amino acids 217-404) and an NLS (amino acid 429) were predicted at the C-terminus. The score of the NLS was 10, meaning it is localized to the nucleus. A PEST domain between amino acids 415-430 was predicted similar to *A. nidulans* VelC. *A. nidulans* VelC also possess a velvet domain at the C-terminus but no NLS is present (Figure A7). An alignment with Vel3-like proteins of other related ascomycetes showed that Vel3 has 43 % aa sequence identity with the corresponding protein in *C. graminicola* (Figure 10b). *V. dahliae* and *C. graminicola* also cluster together in the phylogenetic tree. With around 40 % aa sequence identity *M. oryzae* features a high similarity to *V. dahliae* and is in close proximity to *V. dahliae* and *C. graminicola* in the phylogenetic tree.

A protein with similarity to *A. nidulans* VosA (ANIA_01959) was identified in *V. dahliae* and named Vos1. The predicted size of the protein is 237 aa, which is quite small in comparison to

corresponding proteins in other fungi (425 aa – 501 aa) (Figure A8). Sequencing of *V. dahliae VOS1* cDNA revealed another start codon and a second intron in addition to the predicted one (Figure 11a), suggesting a different gene annotation which was used for following experiments. The sequencing result indicates three exons and two introns with a total size of 1242 bp for the gDNA. The deduced protein sequence was further verified by protein pull downs followed by mass spectrometry (Figure A9).

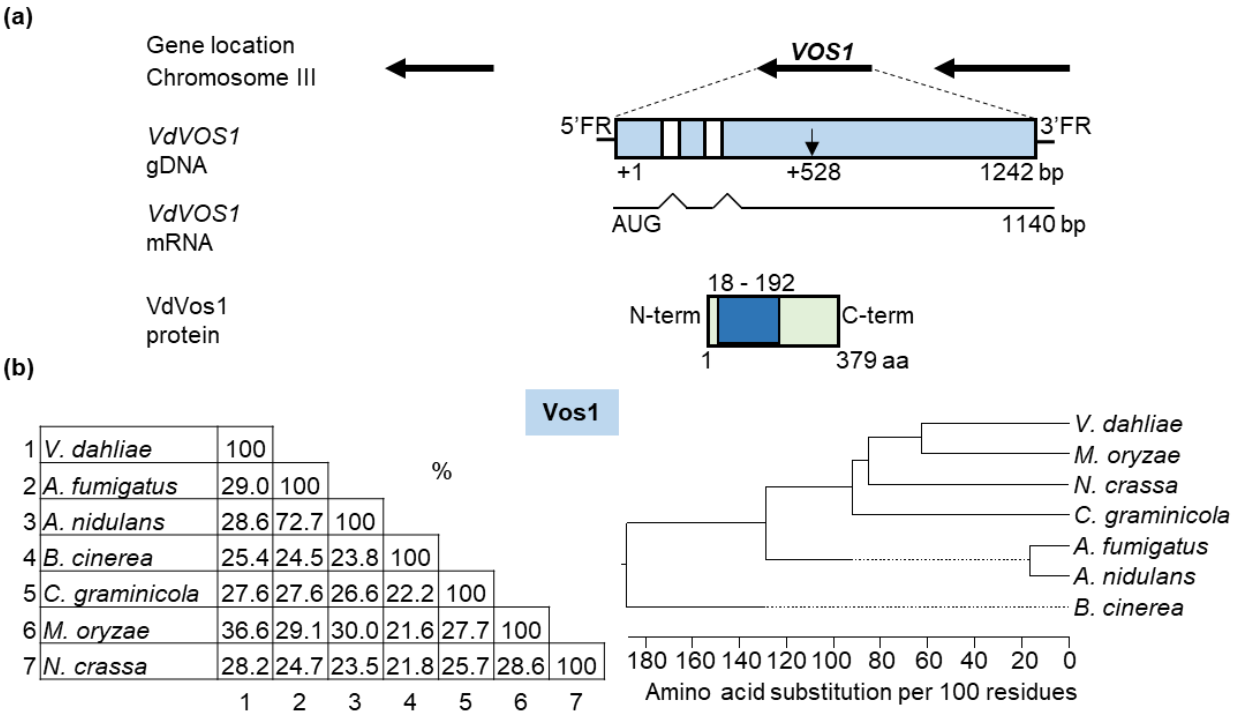

Figure 11: Structure of the *V. dahliae VOS1* gene and the deduced protein with comparison to Vos1-like proteins of other ascomycetes. (a) Genomic locus of the *VOS1* gene and neighboring genes including transcription directions are depicted. Introns are shown in white and exons are depicted in light blue. Velvet domains (dark blue) were predicted by InterProScan according to entry IPR037525. VDAG_JR2_Chr3g12090a encodes the *V. dahliae* Vos1 protein, although it is very small (starting point of coding sequence is indicated by a black arrow in the gDNA). *VOS1* cDNA was sequenced to verify the annotation. An earlier start codon and two introns were identified. The modified annotation was used for further studies and is depicted without potential untranslated regions. The corrected *VOS1* annotation results in three exons and two introns. The velvet domain of Vos1 is located at the N-terminus. **(b)** Protein sequences of *A. fumigatus* Af293, *A. nidulans* FGSC A4, *B. cinerea* BcDW1, *C. graminicola* M1.001, *M. oryzae* M68 and *N. crassa* OR74A similar to Vos1 of *V. dahliae* were aligned by multiple sequence alignment. Similarities of *V. dahliae* velvet proteins in different fungi are shown with a matrix of sequence identity in percent and a phylogenetic tree.

The transcribed mRNA of *VOS1* consists of 1140 bp and is translated into a protein with a size of 379 aa and a molecular mass of 68 kDa (Figure 11a). The *V. dahliae* Vos1 protein is slightly shorter than *A. nidulans* VosA (Figure 5). Similar to VosA, one potential velvet domain is located at the N-terminus of the protein (amino acids 18-192), but an NLS as in *A. nidulans* is not predicted in *V. dahliae* Vos1. Multiple sequence alignment revealed sequence similarities of *V. dahliae* Vos1 to corresponding proteins of other ascomycetes particularly in the region of

the velvet domain (Figure A8). The highest amino acid sequence similarity was observed for *M. oryzea* (36.6 %), which also clusters together with *V. dahliae* in the phylogenetic tree (Figure 11b). In comparison to the other velvet proteins, Vos1 is the one with the lowest similarity to other ascomycetes.

In summary, four velvet domain proteins were identified in *V. dahliae*. *Verticillium* spp. belong to the Sordariomycetes, which is the second-largest class of the Ascomycota, whereas *Aspergillus* spp. are assigned to the Eurotiomycetes class (Maharachchikumbura *et al.*, 2016; Spatafora *et al.*, 2017). The genera *Verticillium* as well as *Colletotrichum* are within their class in the same order of the Glomerellales (Maharachchikumbura *et al.*, 2016). Consistently, the highest overall amino acid sequence similarities for three deduced velvet domain proteins were observed between the corresponding *V dahliae* and *C. graminicola* counterparts. Only the primary amino acid sequence of *V. dahliae* Vos1 is more similar to the corresponding protein of the phytopathogenic *M. oryzae* as another representative of the Sordariomycetes.

3.1.2 Microsclerotia formation depends on Vel1, but requires Vel2 as additional positive and Vel3 as negative factors in light

3.1.2.1 Vel1 and Vel2 are positive regulators of microsclerotia formation

In *A. nidulans*, the formation of different velvet protein homo- and heterodimers is known to control fungal development and regulate secondary metabolism appropriate to the developmental stage (Bayram *et al.*, 2008b; Bayram & Braus, 2012). In the senescent host, *V. dahliae* forms melanized microsclerotia as long-term resting structures, which can remain in the soil for decades and germinate if a suitable host is present (Wilhelm, 1955; Depotter *et al.*, 2016). Due to their longevity in the soil, microsclerotia are potential antifungal targets (Deketelaere *et al.*, 2017). Deletion strains of *VEL1* and *VEL2* as well as double deletion strains were constructed by replacing the open reading frame (ORF) of the corresponding gene by homologous recombination with a hygromycin B or nourseothricin resistance cassette, respectively (Figure A1 and A2). In order to generate complementation strains, the ORF together with the 5' and 3' flanking region and a different resistance cassette were integrated into the deletion strain *in locus*. Vel2 was furthermore fused to GFP in the complementation strain.

All generated strains had a similar growth rate as the wild type on pectin-rich simulated xylem medium (SXM) and the minimal medium named Czapek-Dox-Medium (CDM) when grown for 10 days in constant light (Figure 12). On SXM the wild type produces melanized microsclerotia, which are visible on the overview pictures of a single colony, in cross sections and when colony material was investigated by microscopy (Figure 12a). Deletion of *VEL1* resulted in a strain that is unable to form microsclerotia as the wild type. The wild type phenotype could be

restored by reintegration of the gene in the complementation strain. A similar impairment in microsclerotia formation as shown for the *VEL1* deletion strain was observed for the *VEL2* deletion strain, which was as well restored in the respective complementation strain. In accordance, the double deletion strain of *VEL1* and *VEL2* is also hindered in forming microsclerotia, which was visible on the colony overview, the cross section and by microscopy. A similar phenotype as described for SXM was seen for fungal strains incubated in light for 10 days on CDM (Figure 12b). In comparison to SXM, the wild type produced less microsclerotia, but they are still visible on the colony overview. In contrast, no microsclerotia were visible for the single and double deletion strains of *VEL1* and *VEL2*.

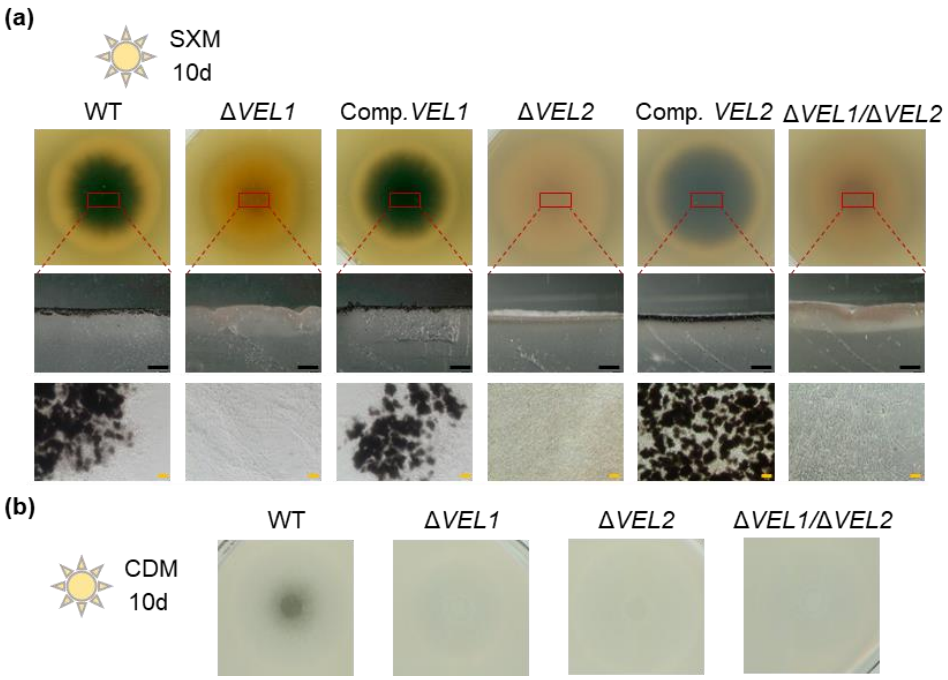

Figure 12: *V. dahliae* microsclerotia formation in light depends on Vel1 and Vel2. 5x10^4 spores of the indicated strains were spotted on indicated plates (SXM: simulated xylem medium; CDM: minimal Czapek-Dox-Medium) and incubated for 10 days at 25 °C in constant light. **(a)** Vel1 and Vel2 are required for microsclerotia development in the presence of light during growth on SXM. Microsclerotia formation of the Δ*VEL1* or Δ*VEL2* strains was compared to wild type (WT) and respective complementation strains (Comp. *VEL1*, Comp. *VEL2*) in overviews of a single colony, cross sections and microscopy of colony material. Deletion and double deletion strains of *VEL1* and *VEL2* were impaired in microsclerotia formation on SXM in light. The wild type phenotype could be restored in the complementation strain. Black scale bar = 1 mm, yellow scale bar = 20 µm. **(b)** Microsclerotia formation on CDM in light requires Vel1 and Vel2. The ability to produce microsclerotia was compared between the wild type (WT) and Δ*VEL1* or Δ*VEL2* strains in overviews of a single colony. Deletion and double deletion strains of *VEL1* and *VEL2* were unable to form microsclerotia on CDM in light.

Consequently, Vel1 and Vel2 are required for the formation of microsclerotia as long-term resting structure in *V. dahliae* in light on pectin-rich medium as well as on minimal medium.

3.1.2.2 Vel2-induced microsclerotia production is light-dependent

The soil-borne fungus *V. dahliae* has mainly limited access to light. Growth of the constructed *VEL1* and *VEL2* single and double deletion strains was hence also investigated in constant darkness. In darkness, the wild type strain formed more microsclerotia on SXM and CDM in comparison to cultivation in light (Figure 13). The *VEL1* single deletion strain as well as the *VEL1* and *VEL2* double deletion strain were impaired in microsclerotia formation in darkness on both media. Their phenotypes were similar to the one observed in constant light (Figure 12). In contrast, the *VEL2* deletion strain was able to produce microsclerotia, but in a reduced manner in comparison to the wild type when incubated in constant darkness on SXM (Figure 13). This effect was not observed on CDM, which might be due to the general reduction in microsclerotia formation on this medium.

These results suggest a light-dependent function of Vel2 in microsclerotia formation, whereas Vel1 induces microsclerotia production independently of light.

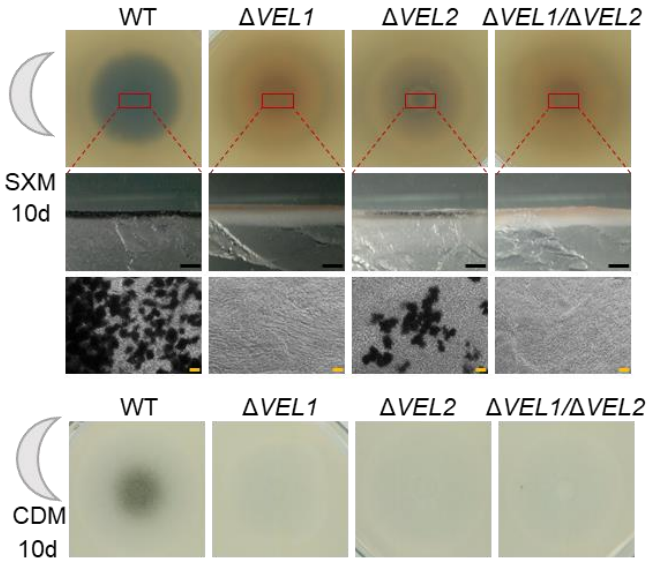

Figure 13: Vel1 is primarily required for microsclerotia formation in darkness with a smaller contribution of Vel2 in *V. dahliae*. From the indicated strains $5x10^4$ spores were spotted on plates (SXM: simulated xylem medium; CDM: minimal Czapek-Dox-Medium) and incubated for 10 days at 25 °C in constant darkness. Shown are overview pictures of a single colony, cross section and microscopy picture of material from a colony. Wild type (WT) as well as the *VEL2* deletion strain produce microsclerotia in darkness, but absence of *VEL2* leads to a colony with only reduced amounts of microsclerotia. The *VEL1* deletion strain as well as the *VEL1* and *VEL2* double deletion strain are impaired in microsclerotia formation in darkness. Black scale bar = 1 mm, yellow scale bar = 20 µm.

In fungi, light response can be interconnected to temperature and the circadian system (Franco *et al.*, 2017; Yu & Fischer, 2019). The *V. dahliae* wild type forms microsclerotia and aerial hyphae on SXM in response to light (16 h in light, 25 °C) and dark (8 h in darkness, 22 °C) cycles. According to the changes between light and darkness a characteristic ring-like structure can be observed in the colony morphology of *V. dahliae* (Figure 14).

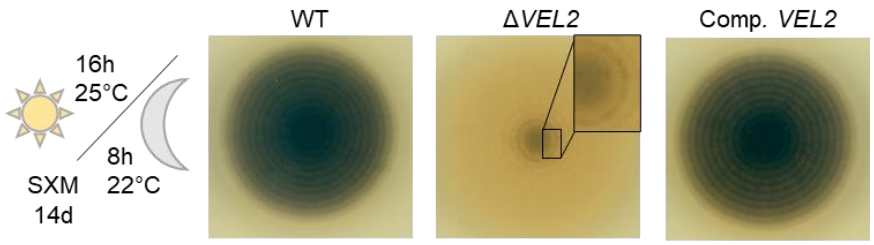

Figure 14: Vel2 function is independent of the fungal light/dark control in *V. dahliae*. 5x10^4 spores of the wild type, *VEL2* deletion and complementation strain were spotted on simulated xylem medium (SXM) and incubated during long day/night cycling conditions (16 h, 25 °C: 8 h, 22 °C, light : dark) for 14 days. The wild type (WT) and the complementation strain display a ring-like structure around the point of inoculation with melanized microsclerotia and reduced color of the microsclerotia towards the margins of the colony. The *VEL2* deletion strain is also capable to form the ring-like structure but with hardly any melanization (black box).

A similar ring-like structure was visible when the deletion strain of *VEL2* was incubated during the above mentioned long-day conditions. In contrast to the wild type, only initial melanization in the center and in the first rings, which was abolishing in the outer part of the colony, was seen for the Δ*VEL2* strain (black box in Figure 14). The complementation exhibited a wild type-like phenotype.

These results indicate that the light-dependent function of Vel2 in microsclerotia production is independent of the fungal light/dark cycle control.

3.1.2.3 Formation of microsclerotia is negatively influenced by Vel3

The velvet proteins are tightly connected to each other by forming homo- and heterodimers (Bayram & Braus, 2012; Sarikaya-Bayram *et al.*, 2015). For a comprehensive study, a deletion strain of *VEL3* was constructed by replacing the ORF of the gene with a nourseothricin resistance cassette by homologous recombination (Figure A3). A complementation strain of Δ*VEL3* was constructed by integrating the ORF of the gene with its 5' and 3' flanking regions and a hygromycin B resistance cassette at the native locus in the deletion strain. The wild type, deletion strain of *VEL3* and the complementation strain were examined on SXM and CDM in constant light and darkness (Figure 15). Incubation of the indicated strains on SXM as well as on CDM in darkness had no phenotypical effect. During incubation on minimal medium (CDM) in light, the Δ*VEL3* strain produced more microsclerotia than the wild type, which can especially be seen in the colony cross sections.

Deletion strains of *VEL1* and *VEL3* have oppositional phenotypes on plate. A double deletion strain was constructed to better understand the interplay of these two genes by replacing the ORF of the appropriate gene with a hygromycin B or nourseothricin resistance cassette by homologous recombination (Figure A1 and A3). On CDM incubated in light the double deletion strain of *VEL1* and *VEL3* resembled the phenotype of the *VEL1* single deletion strain assuming that Vel3 requires the presence of Vel1 for its light-dependent inhibitory function.

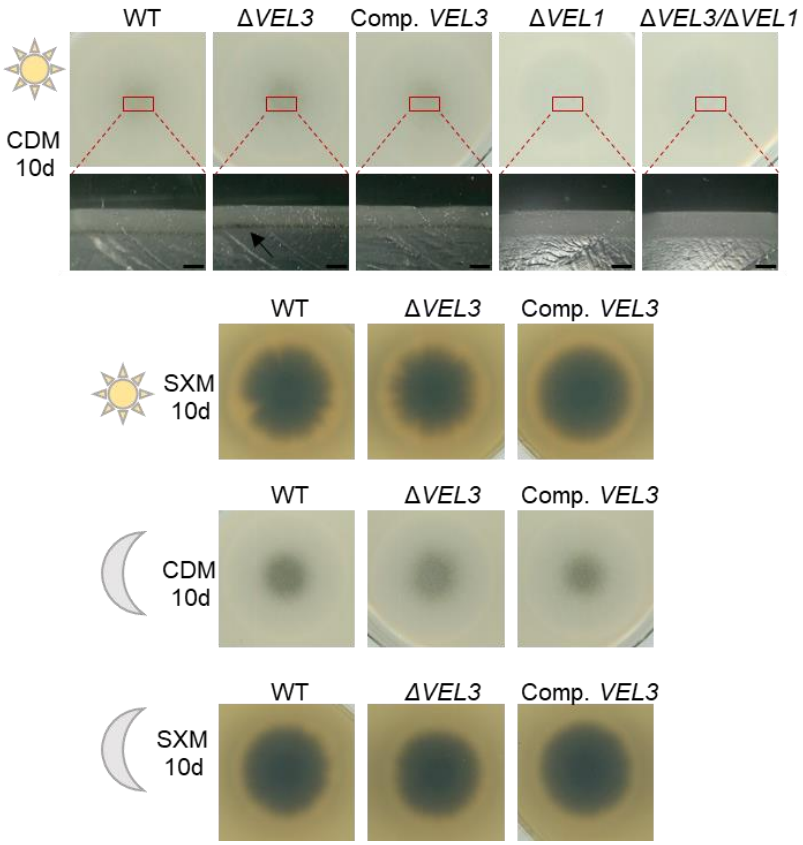

Figure 15: Vel3 inhibits *V. dahliae* microsclerotia formation in light without strong impact in dark on minimal medium. Of the indicated strains 5x10^4 spores were spotted on simulated xylem medium (SXM) or minimal Czapek-Dox-Medium (CDM), respectively. The phenotype was examined after incubation for 10 days at 25 °C in constant light or darkness. The *VEL3* deletion strain forms more microsclerotia compared to the wild type (WT) or complementation strain on minimal medium in light. A double deletion strain of *VEL3* and *VEL1* resembled the *VEL1* deletion strain phenotype. Black scale bar = 1 mm.

Summing up the previous results, Vel3 acts as negative regulator of microsclerotia formation in light. In contrast, Vel1 and Vel2 promote the production of microsclerotia. The role of Vel2 in microsclerotia formation is light-dependent but not connected to the fungal light/dark cycle.

3.1.2.4 Vos1 is dispensable for microsclerotia production

A. nidulans VosA can bind to many promoter sequences and possesses a transcription activation domain (Ahmed *et al.*, 2013). For a more detailed investigation about the function of *V. dahliae* Vos1, two different deletion strains were constructed by replacing the ORF of the gene with a nourseothricin or a hygromycin B resistance cassette by homologous recombination (Figure A4). Phenotypical analysis of colony overviews and cross sections of the *VOS1* deletion strain incubated on SXM or CDM in constant light or darkness revealed no visible differences of the colony morphology in comparison to the wild type (Figure 16). Hence, microsclerotia production in *V. dahliae* functions independently of Vos1.

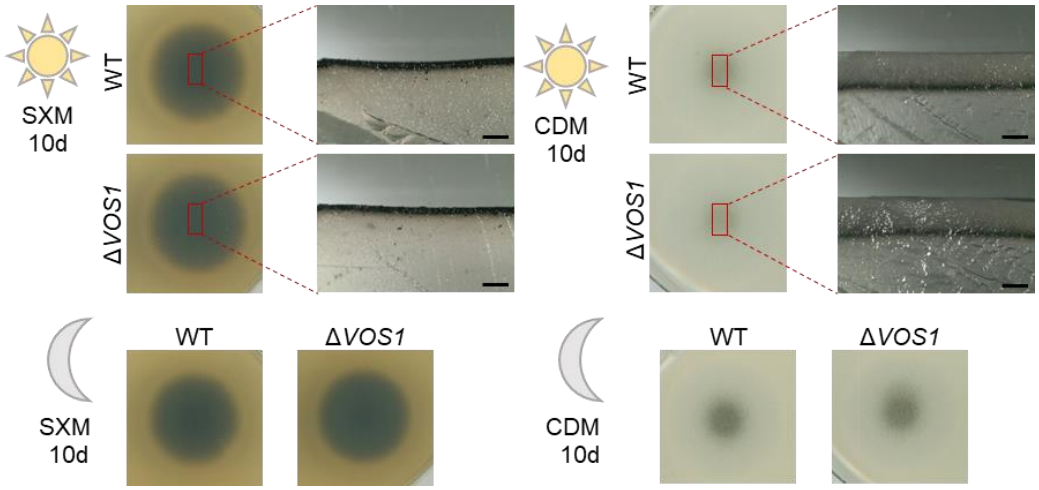

Figure 16: *V. dahliae* microsclerotia development functions independently of Vos1. Images give an overview of fungal colonies after spotting 5x10^4 spores of the wild type (WT) and *VOS1* deletion strain on plates with either simulated xylem medium (SXM) or Czapek-Dox-Medium (CDM) and subsequent incubation for 10 days at 25 °C during constant light or darkness. Shown are colony overviews and cross sections. Growth and development of the *VOS1* deletion strain and the wild type are similar. Black scale bar = 1 mm.

In *A. nidulans* VosA and VelC are forming a heterodimer and may influence genes for sexual development and spore viability (Park *et al.*, 2014; Sarikaya-Bayram *et al.*, 2015). The construction of a double deletion strain of these two genes in *A. nidulans* produced fewer cleistothecia and had similar effects as the *vosA* single deletion strain indicating an epistatic role for VosA in sexual development (Park *et al.*, 2014). To elucidate if the homologs in *V. dahliae* also have a genetic regulation, a *VOS1*/*VEL3* double deletion strain was constructed. For the construction of the double deletion strain the ORF of *VOS1* was replaced by the hygromycin B resistance cassette by homologous recombination and transformed with the deletion construct of *VEL3* containing a nourseothricin resistance cassette (Figure A3 and Figure A4). Spores of the constructed deletion and double deletion strains were spotted on minimal CDM and incubated in constant light (Figure 17). As previously observed, the deletion strain of *VOS1* had a wild type-like phenotype and the deletion strain of *VEL3* produced more microsclerotia in comparison to the wild type. The double deletion strain of *VOS1* and *VEL3* resembled the phenotype of the *VEL3* single deletion strain. In contrast to *A. nidulans, V. dahliae VOS1* seems not to be epistatic to *VEL3*.

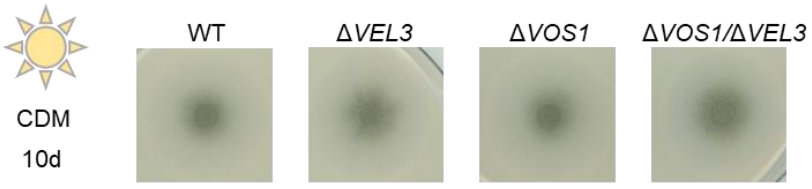

Figure 17: The phenotype of a *V. dahliae VEL3* and *VOS1* double deletion strain resembles the phenotype of the *VEL3* single deletion strain. The pictures show colony overviews after spotting 5x10^4 spores of indicated *V. dahliae* strains on plates with Czapek-Dox-Medium (CDM) and subsequent incubation for 10 days at 25 °C during constant light. The phenotype of the *VEL3* and *VOS1* double deletion strain is similar to the phenotype of the *VEL3* single deletion strain.

3.1.3 Formation of specific *V. dahliae* secondary metabolites is promoted by Vel1 and Vel2 but reduced by Vel3

3.1.3.1 Vel1 and Vel2 induce the formation of melanin-associated secondary metabolites

Secondary metabolite production, including the production of toxic substances for pathogenic interactions or signaling molecules for communication with other microorganisms, and fungal development as for instance the formation of fungal resting structures are coordinated by velvet domain protein complexes (Bayram & Braus, 2012; Gerke & Braus, 2014; Macheleidt *et al.*, 2016).

The constructed *V. dahliae* strains with deletions in genes encoding *VEL1* and *VEL2* were compared to the wild type and the corresponding complementation strains for their ability to produce secondary metabolites. Metabolite extracts of the indicated strains were applied to liquid chromatography (LC-MS) combined with photodiode array detection analysis. All samples were ionized positively and negatively to observe all changes in the metabolite profile. Comparison of chromatograms of the wild type, the Δ*VEL1* strain and the corresponding complementation strain revealed at least five substances (indicated as I-V), which were reduced in the deletion strain (Figure 18a). Furthermore, at least four substances (indicated as VI-IX) were more abundant in the *VEL1* deletion strain in comparison to the wild type and the complementation strain. Chromatograms of the wild type, the Δ*VEL2* strain and the corresponding complementation strain exhibited that the same five substances (I-V), which were reduced in the Δ*VEL1* strain seem to be also decreased in the Δ*VEL2* strain (Figure 18b). An exact mass and a predicted sum formula could be assigned to these substances (Table 8). By using single ion monitoring, the relative amount of the exact mass in the different samples was determined. Hereby, the reduction of substance I-V in the Δ*VEL1* and Δ*VEL2* strains was confirmed (Table 9, Figure A10-A14). Moreover, the substances were investigated in more detail by comparing their MS2 spectra (Figure A10-A14) with data deposited in databases. Only two substances resembled deposited compounds (Table 8). Substance I was most likely identified as the DHN melanin precursor scytalone (Wang *et al.*, 2018), which is in line with the reduced melanization of the deletion strains (Figure 12). Substance III is similar to Saccharonol A and might be a precursor of 6-methoxymellein, which was found in endophytic and plant pathogenic species as well as in fungi-infected carrot roots (Nishi & Kurosaki, 1993; Shao *et al.*, 2009). Moreover, 6-methoxymellein is a precursor of terrein, which is produced by *A. terreus* and harms the surface of fruits (Marinelli *et al.*, 1996; Zaehle *et al.*, 2014).

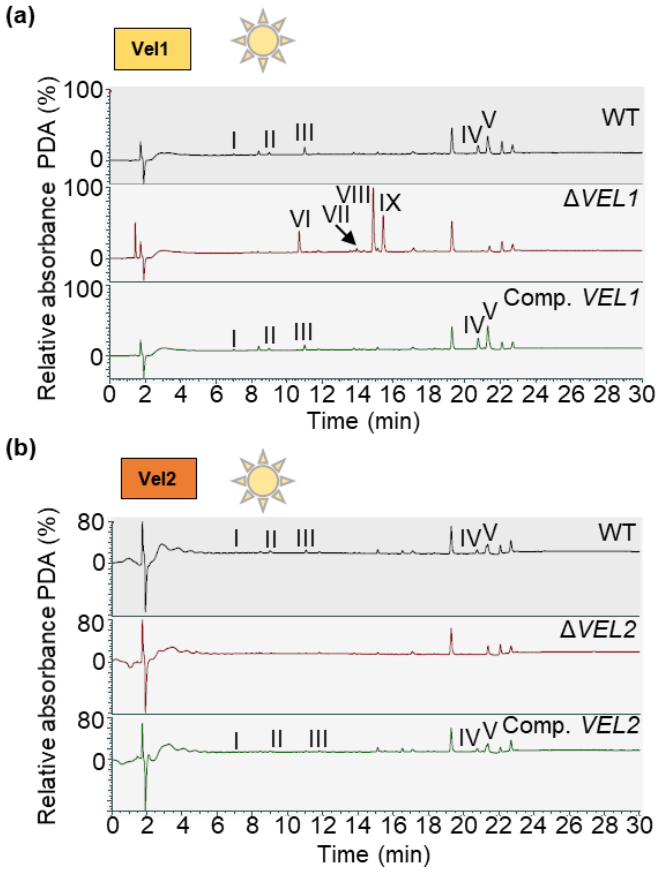

Figure 18: *V. dahliae* Vel1 and Vel2 control secondary metabolite production. Displayed are chromatograms of metabolites extracted from Δ*VEL1* **(a)** and Δ*VEL2* **(b).** LC-MS combined with photodiode array detection (PDA) analysis is shown. Secondary metabolites were extracted from two-week-old fungal mycelium grown in light on minimal Czapek-Dox-Medium (CDM) supplemented with glucose. Deletion of *VEL1* (Δ*VEL1*) leads to reduced formation of five substances (I-V) and increased production of four substances (VI-IX) in comparison to the wild type (WT) or complementation (Comp. *VEL1*) control strains. The same five substances (I-V), which were absent in the *VEL1* deletion strain, are also missing in extracts of the *VEL2* deletion strain.

Although an exact mass could be assigned to the substances produced by the Δ*VEL1* strain and respective MS2 spectra were available, no deposited spectra in databases resembled the compounds produced in the deletion strain (Table 8, Figure A15-A18).

Taking the results into account, a partial overlap in the function of Vel1 and Vel2 is likely, because the substances I-V were reduced in both deletion strains.

Table 9: Differentially expressed metabolites of *V. dahliae* detected by LC-MS.

ID	Metabolite marker	Retention time (min)	Detected as	Predicted sum formula	Exact mass measured	Exact mass calculated [M]	Confirmed by	Reference
I	Scytalone	7.00	$[M-H]^-$	$C_{10}H_{10}O_4$	193.0493	194.0579	MS2 spec-trum	(Bell *et al.*, 1976; Dictionary of Natural Products, 2020)
II	UN	8.98	$[M-H]^-$	$C_{12}H_{12}O_5$	235.0603	236.0685		-
III	6,8-Dihydroxy-3-methyl-1H-2-benzopyran-1-one (Saccharonol A or 3,4-Dehydro-6-hydroxymellein)	10.98	$[M+H]^+$	$C_{10}H_8O_4$	193.0499	192.0423	MS2 spec-trum	(MoNA database, 2007)
IV	UN	20.76	$[M+H]^+$	$C_{29}H_{48}N_6O_6$	577.3732	576.3635		-
V	UN	21.30	$[M+H]^+$	$C_{30}H_{50}N_6O_6$	591.3887	590.3792		-
VI	UN	10.68	$[M-H]^-$	$C_{15}H_{20}O_4$	263.1284	264.1362		-
VII	UN	13.92	$[M-H]^-$	$C_{18}H_{24}O_5S$	351.1264	352.1344		-
VIII	UN	14.85	$[M+H]^+$	$C_{15}H_{20}O_2$	233.1544	232.1463		-
IX	UN	15.41	$[M+H]^+$	$C_{15}H_{20}O_3$	249.1483	248.1412		-
X	UN	15.99	$[M-H]^-$	$C_{20}H_{12}O_5$	331.0606	332.0685		-
XI	UN	16.52	$[M-H]^-$	$C_{20}H_{14}O_4$	317.0811	318.0892		-

UN = unknown

Since the deletion strain of *VEL1* is impaired in microsclerotia formation, an overexpression might produce more resting structures. The wild type was transformed with a strain ectopically overexpressing Vel1, which was C-terminally fused to GFP. To exclude side effects of the GFP-tag, the wild type was also transformed with Vel1-GFP under the native promoter. Phenotypic analysis of colony overviews and cross sections on CDM revealed that the wild type and the *VEL1-GFP* strain with the native promoter produced similar amounts of microsclerotia (Figure 19a). As previously shown, the Δ*VEL1* strain was hindered in microsclerotia formation. In contrast, more microsclerotia were produced by the overexpression strain. Expression of the fusion protein in the strains with native and increased Vel1-GFP expression was visualized by western analysis using a GFP antibody (Figure 19b). Full length fusion protein was detectable for both strains but was more abundant in the overexpression strain.

Table 10: Metabolites detected by LC-MS in different *V. dahliae* strains. x indicates presence of the metabolite. (x) indicates that the exact mass of the substance is detectable, but no clear peak in the chromatograms, or a small peak in some replicates is present.

ID	Retention time (min)	Exact mass measured	Predicted sum formula	Found in									
				WT	Δ*VEL1*	comp. *VEL1*	OE-*VEL1*	Δ*VEL2*	comp. *VEL2*	Δ*VEL3*	comp. *VEL3*	Δ*VOS1*	Δ*LAE1*
I	7.00	193.0493	$C_{10}H_{10}O_4$	x		x	x		x	x	x	x	x
II	8.98	235.0603	$C_{12}H_{12}O_5$	x		x	x		x	x	x	x	x
III	10.98	193.0499	$C_{10}H_8O_4$	x		x	x		x	x	x	x	x
IV	20.76	577.3732	$C_{29}H_{48}N_6O_6$	x		x	x		x	x	x	x	x
V	21.30	591.3887	$C_{30}H_{50}N_6O_6$	x		x	x		x	x	x	x	x
VI	10.68	263.1284	$C_{15}H_{20}O_4$		x								
VII	13.92	351.1264	$C_{18}H_{24}O_5S$		x								
VIII	14.85	233.1544	$C_{15}H_{20}O_2$		x								
IX	15.41	249.1483	$C_{15}H_{20}O_3$		x								
X	15.99	331.0606	$C_{20}H_{12}O_5$				x			(x)			
XI	16.52	317.0811	$C_{20}H_{14}O_4$	(x)	(x)	(x)	x	(x)	(x)	x	(x)	(x)	(x)

The metabolite extracts of the wild type and the *VEL1* overexpression strain were subjected to liquid chromatography (LC-MS) combined with photodiode array detection analysis. Overexpression of *VEL1* resulted in increased production of the substances I-V (Figure 19c). Additionally, the formation of two other compounds (indicated as X and XI) accelerated. The two substances could be assigned to a mass and a sum formula was predicted (Table 8). Even though MS2 spectra of both substances were available (Figure A19 and A20), the substance could not be connected to already described compounds. Substance X was not detected in chromatograms of the wild type. Substance XI was detectable in the wild type, but no clear peak in the chromatograms, or just a small peak in some replicates was present (Table 9). However, single ion monitoring suggested decreased amounts of both substances in the wild type compared to the *VEL1* overexpression strain.

Summarizing, the overexpression strain of *VEL1* shows an increased melanization and production of the substances I-V, which are reduced in the non-melanizing Δ*VEL1* strain.

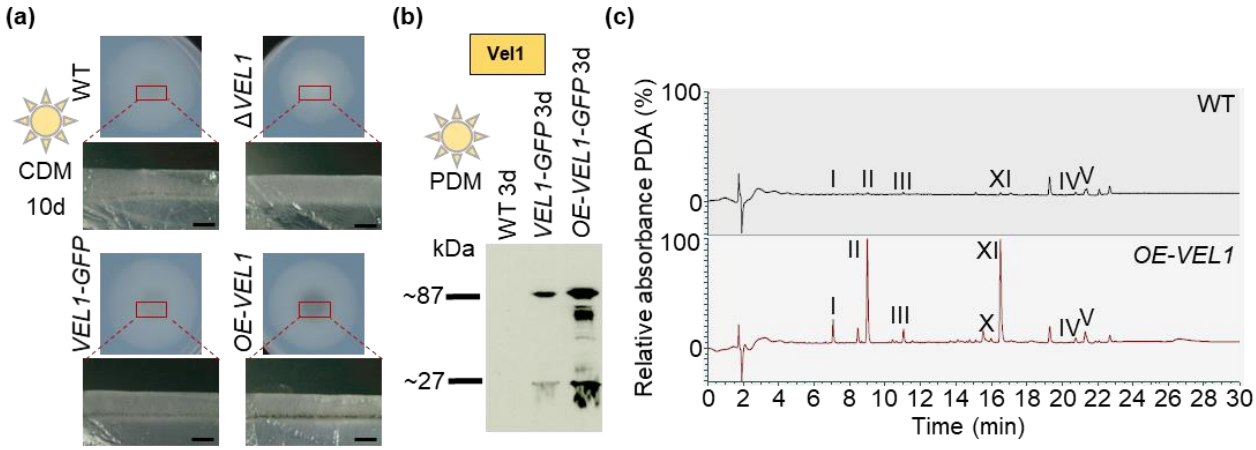

Figure 19: *VEL1* overexpression increases melanization and alters the expression of secondary metabolites. (a) Phenotypical analysis of wild type, *VEL1* deletion strain and *VEL1-GFP* strains harboring *VEL1* fused to *GFP* under control of the native and overexpression promoter. $5x10^4$ spores of the indicated strains were spotted on minimal Czapek-Dox-Medium (CDM) and incubated for 10 days at 25 °C in light. An overview of a single colony and a cross section are displayed. The *VEL1* deletion strain (Δ*VEL1*) was hindered in formation of melanized microsclerotia. In contrast, the overexpression strain of *VEL1* fused to *GFP* (*OE-VEL1*) melanized more than the wild type (WT) or a strain with *VEL1-GFP* integrated at the locus as controls. Black scale bar = 1 mm. **(b)** Western analysis of wild type, *VEL1* fused to *GFP* and overexpression strain of *VEL1* fused to *GFP*. Liquid potato dextrose medium (PDM) cultures inoculated with $1x10^6$ freshly harvested spores were grown for three days at 25 °C in light. Free GFP (27 kDa), Vel1-GFP (87 kDa) or increased amounts of Vel1-GFP in the overexpression strain were detected with a GFP antibody (dilution 1:500) using 80 µg of crude extracts. **(c)** Chromatogram of secondary metabolites of wild type and *VEL1-GFP* overexpression (*OE-VEL1*) strain extracts from two-week-old fungal mycelium grown on Czapek-Dox-Medium (CDM) supplemented with glucose. Depicted is a chromatogram from LC-MS analysis with photodiode array detection (PDA) analysis. Seven substances (I-V, X and XI) are more abundant in *OE-VEL1* than in wild type.

3.1.3.2 Production of specific secondary metabolites is negatively affected by Vel3

During phenotypical analysis of the *VEL3* deletion strain an increase in microsclerotia production was observed (Figure 15). In contrast, *VEL1* and *VEL2* deletion strains are impaired in microsclerotia formation (Figure 12) and are altered in secondary metabolite production (Figure 18). The *VEL3* deletion strain was also examined regarding its ability to produce secondary metabolites in comparison to the wild type and the complementation strain. The metabolite extracts of the mentioned strains were analyzed as described before.

The chromatograms of the wild type, the *VEL3* deletion strain and the corresponding complementation strain are similar, but relative absorbance of the substances I-V was higher in the *VEL3* deletion strain (Figure 20). However, the increase in relative absorbance of samples from the *VEL3* deletion strain was not as obvious as for the overexpression strain of *VEL1* (Figure 19c).

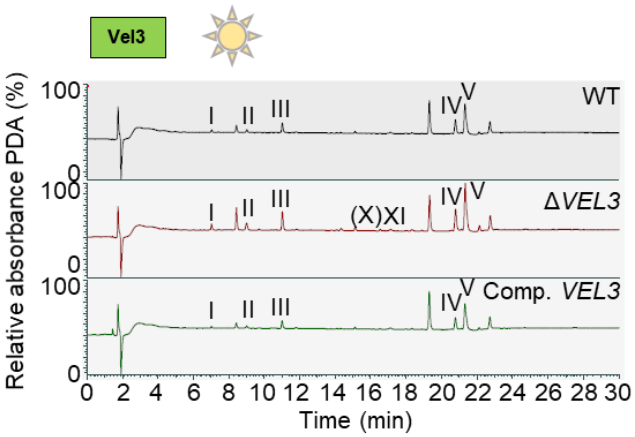

Figure 20: Vel3 of *V. dahliae* reduces specific secondary metabolite production. Displayed are chromatograms of metabolites extracted from wild type, Δ*VEL3* strain and *VEL3* complementation strain from LC-MS combined with photodiode array detection (PDA) analysis. Secondary metabolites were extracted from two-week-old fungal mycelium grown in light on minimal Czapek-Dox-Medium (CDM) supplemented with glucose. Depicted are the wild type (WT), *VEL3* deletion strain (Δ*VEL3*) and a *VEL3* complementation strain (Comp. *VEL3*). All peaks can be detected in the three chromatograms with an increase in abundance for the substances I-V in the *VEL3* deletion strain. In the Δ*VEL3* strain substance X and XI could also be detected.

Single ion monitoring analysis of the substances I-V was used for a better illustration of the increased substance amounts in the Δ*VEL3* strain in comparison to the wild type and the complementation strain (Figure 21). Substances X and XI were more abundant in the *VEL1* overexpression strain (Figure 19c, A19 and A20). Hence, single ion monitoring was also conducted for both in the *VEL3* deletion strain. All substances (I-V, X and XI) were increased in the Δ*VEL3* strain in comparison to the wild type and the complementation strain (Figure 21). The secondary metabolite profiles of the *VEL1* overexpression and the Δ*VEL3* strain as well as their melanization phenotype, which was increased compared to the wild type are similar. Taking the altered metabolite pattern and the phenotype of both strains into account, one can conclude that Vel1 is required to form melanized microsclerotia and Vel3 negatively affects this process. This coincides with the fact that substance I most likely is the DHN melanin precursor scytalone, as this substance is increased in the deletion strain of *VEL3* and also in the overexpression strain of *VEL1*, but not in the *VEL1* deletion strain (Table 9). These data support that primarily Vel1, but also Vel2, specifically control secondary metabolite formation and are counteracted by Vel3. Secondary metabolites affected by the velvet proteins have possible functions in fungal protection by pigmentation and interactions with plants.

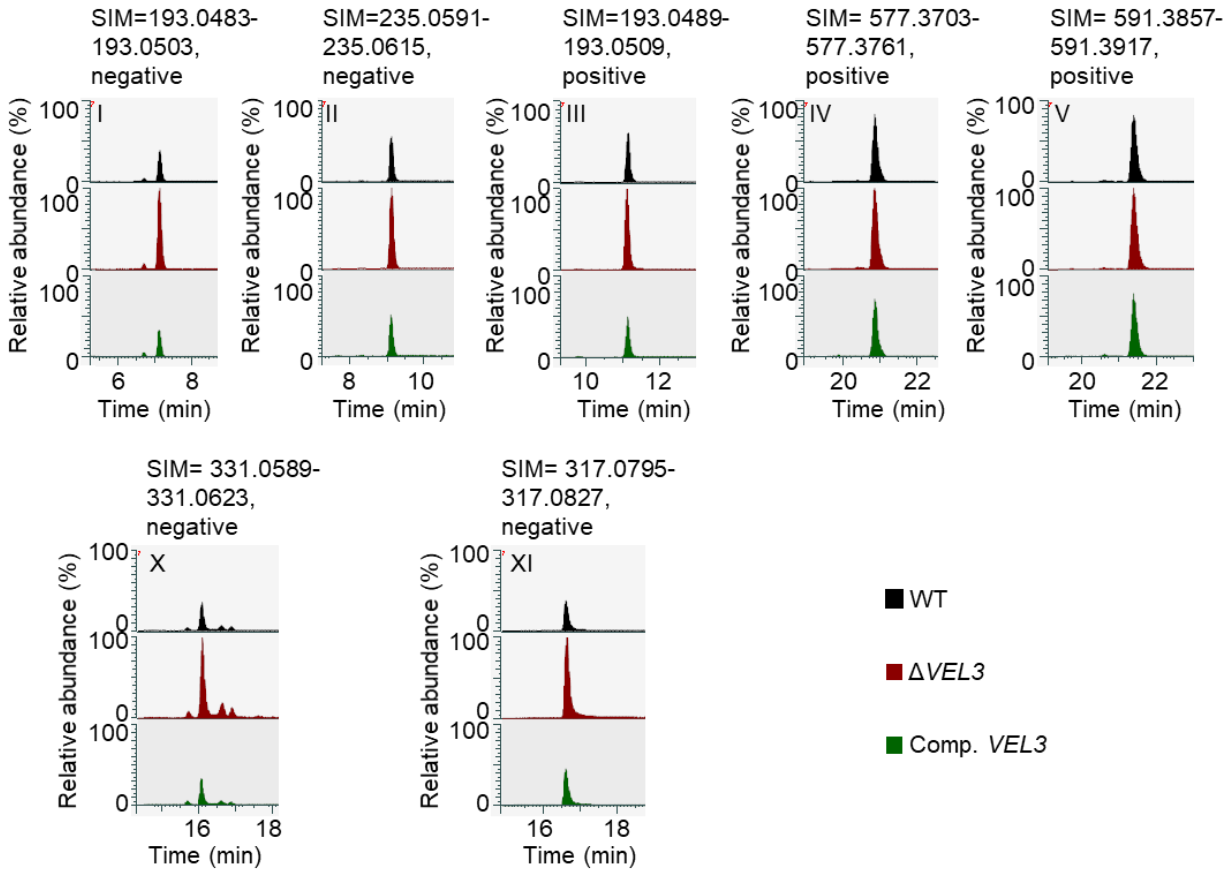

Figure 21: Single ion monitoring for selected substances more abundant in the Δ*VEL3* strain. Single ion monitoring (SIM) for substances increased in the *VEL3* deletion strain in comparison to the wild type and *VEL3* complementation strain (black: wild type, red: Δ*VEL3*, green: Comp. *VEL3*). Substance I: m/z 193.0493, mass tolerance 5.00 ppm; substance II: m/z 235.0603, mass tolerance 5.00 ppm; substance III: m/z 193.0499, mass tolerance 5.00 ppm; substance IV: m/z 577.3722, mass tolerance 5.00 ppm; substance V: m/z 591.3887, mass tolerance 5.00 ppm; substance X: m/z 331.0606, mass tolerance 5.00 ppm; substance XI: m/z 317.0811, mass tolerance 5.00 ppm.

3.1.3.3 Secondary metabolite regulation by Vel1 and Vel2 is independent of light

Previous experiments revealed that the effect of Vel2 on microsclerotia production is light-dependent (Figure 12 and 13). Vel2 is moreover required for the production of the same secondary metabolites that are affected by Vel1. Hence, both deletion strains were incubated in darkness and metabolites were extracted. Subsequently, the extracts were analyzed as mentioned before.

Chromatograms of extracts obtained from dark or light grown cultures of a Δ*VEL1* strain revealed a similar metabolite pattern: during both conditions the substances I-V were reduced and the substances VI-IX displayed increased abundance (Figure 22). Comparison of extracts of the Δ*VEL2* strain from cultures grown in dark or light also showed that in both conditions the substances I-V were reduced in the deletion strain (Figure 22).

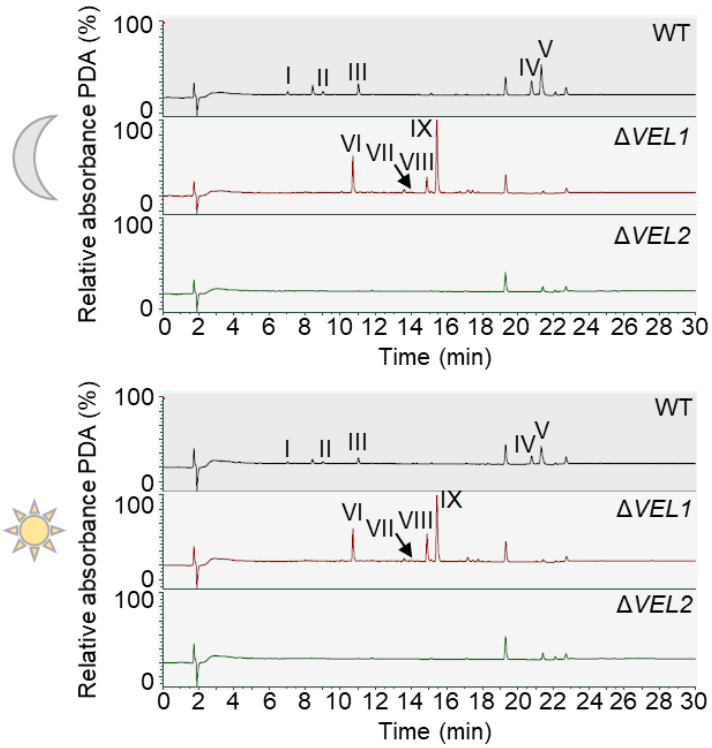

Figure 22: Chromatograms of metabolites extracted from *V. dahliae* wild type, Δ*VEL1* and Δ*VEL2* strains during incubation in darkness or light. LC-MS combined with photodiode array detection (PDA) analysis of secondary metabolites. Secondary metabolites were extracted from two-week-old fungal mycelium grown either in darkness or light on minimal Czapek-Dox-Medium (CDM) supplemented with glucose. Chromatograms of the wild type and both deletion strains exhibit the same presence and absence of secondary metabolites in darkness or light.

Although the phenotype of the *VEL2* deletion strain is light-dependent, these results suggest that secondary metabolite production regulated by Vel2 functions independently of light. In addition, the role of Vel1 in secondary metabolite formation is light independent as well.

3.1.3.4 *V. dahliae* Vos1 and Lae1 are dispensable for secondary metabolite production

Besides Vel1, Vel2 and Vel3, also a protein similar to *A. nidulans* VosA is present in *V. dahliae*, which was named Vos1. Metabolites were extracted from the *V. dahliae VOS1* deletion strain and analyzed as previously mentioned. Comparison of the wild type and the *VOS1* deletion strain revealed that Vos1 has no major impact on secondary metabolism in *V. dahliae* (Figure 23a).

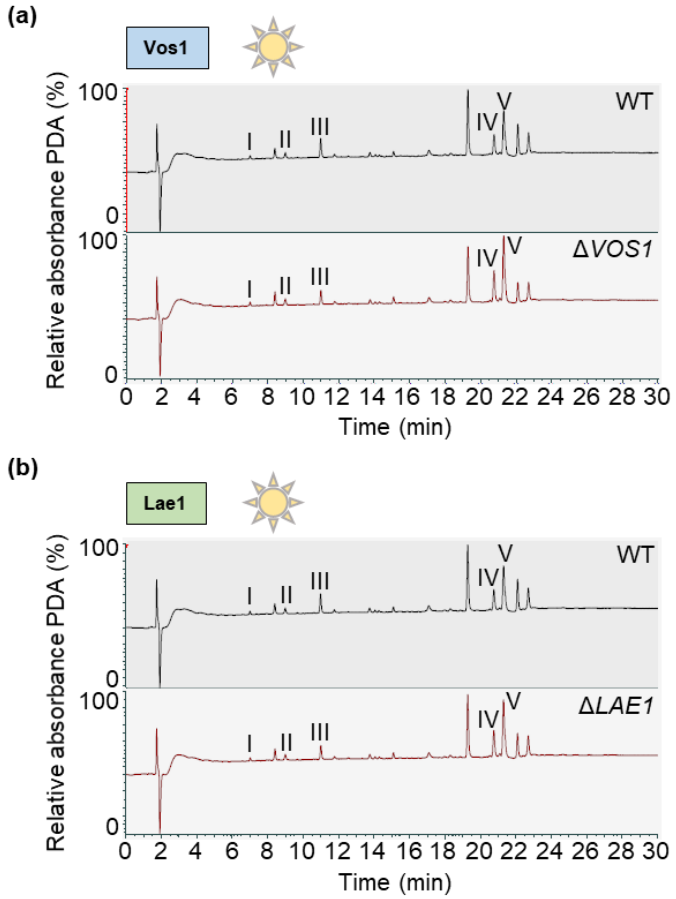

Figure 23: Chromatograms of metabolites extracted from *V. dahliae VOS1* and *LAE1* deletion strains. LC-MS combined with photodiode array detection (PDA) analysis of secondary metabolites. Secondary metabolites were extracted from two-week-old fungal mycelium grown in light on Czapek-Dox-Medium (CDM) supplemented with glucose. Chromatograms of both deletion strains resemble the wild type pattern.

LaeA is a major epigenetic secondary metabolite regulator that interacts with velvet domain proteins in *A. nidulans* (Bok & Keller, 2004; Bayram *et al.*, 2008b). Secondary metabolites were extracted from a deletion strain of the homologous gene *LAE1* in *V. dahliae* and analyzed as mentioned afore. Deletion of *V. dahliae LAE1* did not alter the metabolite pattern in comparison to the wild type (Figure 23b).

These results suggest that neither Vos1 nor Lae1 are required for secondary metabolite production in *V. dahliae* under the tested conditions. In contrast, Vel1 and Vel2 promote secondary metabolism whereas Vel3 reduces the formation of these substances. Taking these results into account, Vel1 and Vel2 might be possible targets for antifungal drugs.

3.1.4 Vel1 and Vel3 are required for efficient *V. dahliae* conidiospore formation whereas Vel2 and Vos1 are dispensable

In planta, *V. dahliae* propagates by the formation of conidia (Berlanger & Powelson, 2000; Fradin & Thomma, 2006). Hence, asexual spore formation represents another major developmental program besides the production of microsclerotia. In contrast to *A. nidulans* and

numerous other fungi, the resulting *V. dahliae* conidia are not produced for dispersal through the air, but for distribution inside the plant by the xylem sap (Fradin & Thomma, 2006; Bayram & Braus, 2012). Conidia formation is therefore an important step during host invasion (Depotter *et al.*, 2016). The abilities of the Δ*VEL1-3* or Δ*VOS1* strains to produce spores in liquid simulated xylem medium (SXM) were compared to wild type (Figure 24).

The spore numbers produced by the Δ*VEL1* strain declined by more than 80 % in comparison to wild type and could be restored by reintroduction of the *VEL1* gene at the genomic locus. The *VEL3* gene also contributes substantially to conidia formation with an approximately 60 % reduction in numbers for the Δ*VEL3* strain compared to wild type. This effect could also be restored by the *VEL3* complementation strain.

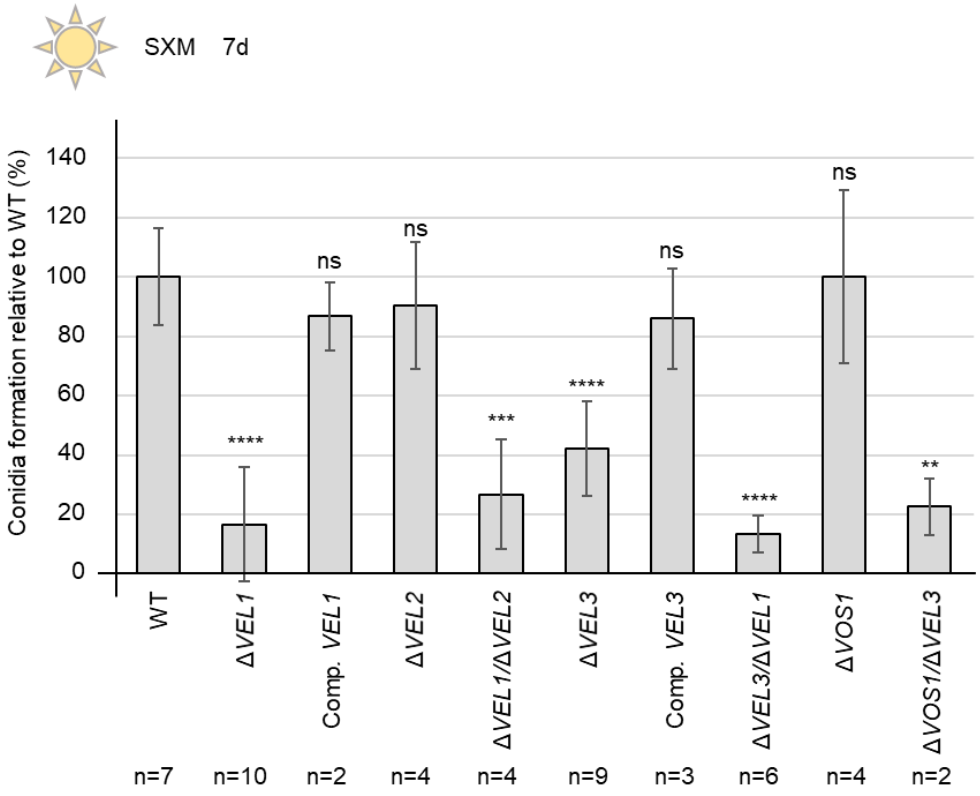

Figure 24: *V. dahliae* conidiospore formation requires the *VEL1* and *VEL3* genes. 2x10^5 freshly harvested spores were inoculated in liquid simulated xylem medium (SXM) and incubated at 25 °C for seven days under constant agitation and light. The conidia production was quantified relative to the wild type (WT). Each experiment was performed with three technical replicates (n=1). Two individual transformants were used for the following strains: Δ*VEL1*, Δ*VEL2*, Δ*VEL1*/Δ*VEL2*, Δ*VEL3*, Δ*VEL3*/Δ*VEL1* and Δ*VOS1*. Bars represent the mean values of all experiments and error bars correspond to standard deviations. *VEL1* and *VEL3* single and double deletion strains are impaired in conidia formation. *VEL2* and *VOS1* are dispensable for conidiation. Wild type-like conidia production was observed for the corresponding complementation strains. Significant differences to the wild type were calculated by t-test and are indicated: **,p<0.01; ***,p<0.001; ****,p<0.0001; ns: not significant.

For a comprehensive picture, all velvet domain proteins were analyzed regarding their impact on conidia production. Quantification revealed similar amounts of spores for the Δ*VEL2* and Δ*VOS1* strains in comparison to the wild type (Figure 24), which suggests that the corresponding velvet domain proteins are dispensable for *V. dahliae* conidia formation.
These data show that Vel1 and Vel3 both support the formation of *V. dahliae* asexual conidia. This is in contrast to their antagonistic function in the control of microsclerotia formation in light and during secondary metabolite formation. In addition, conidiation in *V. dahliae* functions independently of Vel2 and Vos1.

3.1.4.1 *VEL1* is epistatic to *VEL2* and *VEL3* whereas *VEL3* is epistatic to *VOS1* in *V. dahliae* regulation of conidiation

This study revealed involvement of Vel1 and Vel3 in the formation of conidia in *V. dahliae*. Both proteins also regulate microsclerotia formation and secondary metabolite production but have opposing roles in these processes. Vel2 is involved in microsclerotia formation and secondary metabolism but dispensable for conidiation. So far, the function of Vos1 is uncertain. From *A. nidulans* and other fungi the formation of different dimers and trimers is known (Bayram *et al.*, 2008b; Park *et al.*, 2012a; Chang *et al.*, 2013; Schumacher *et al.*, 2015; Sarikaya-Bayram *et al.*, 2019). To further understand the regulation of conidiation in *V. dahliae* and elucidate a possible connection between the four velvet domain proteins, different double deletion strains were constructed and examined regarding their ability to produce conidia.
The *VEL1* single deletion strain and the *VEL1* and *VEL2* double deletion strain are both similarly impaired in conidia production, whereas the *VEL2* single deletion strain showed wild type-like spore production (Figure 24) indicating an epistatic function of *VEL1* to *VEL2* in conidiation. The phenotype of the single and double deletion strains on plate were similar for *VEL1* and *VEL2* (Figure 12). One can assume that both, Vel1 and Vel2, are required in the important process of microsclerotia formation but during conidiation solely Vel1 is needed.
Both, Vel1 and Vel3, are involved in spore formation. The analysis of a *V. dahliae* double deletion strain revealed that conidia formation is also reduced in the Δ*VEL1*/Δ*VEL3* double deletion strain (Figure 24). Taking a closer look at the number of produced spores of both single deletion strains one can see that the Δ*VEL1* strain produces significantly less conidia than the Δ*VEL3* strain (p-value: 0.0028). The double deletion strain of *VEL1* and *VEL3* also produces significantly less spores than the Δ*VEL3* strain (p-value: 0.0003) but exhibits a similar spore production phenotype as the Δ*VEL1* strain (p-value: 0.3153). This phenotype coincidences with the developmental phenotype on plate as the Δ*VEL1*/Δ*VEL3* double mutant strain resembled the *VEL1* single deletion strain in terms of the decline in microsclerotia production (Figure 15). Hence *VEL1* might be epistatic to *VEL3*.

In *A. nidulans* VosA and VelC are forming a heterodimer that affects genes for sexual development and spore viability (Park *et al.*, 2014; Sarikaya-Bayram *et al.*, 2015). The *V. dahliae VEL3* and *VOS1* double deletion strain was examined for its ability to produce conidia. The double deletion strain produced significantly less spores than the wild type (Figure 24), but the difference to the deletion strain of *VEL3* was not significant (p-value: 0.0888), indicating that solely *VEL3* is responsible for the reduced number of conidia and functions epistatic to *VOS1* in this regulation.

These results show that there is a genetic regulation between the genes encoding for the velvet proteins regarding conidiation. Here, we evaluated that *VEL1* is epistatic to *VEL2* and *VEL3* whereas *VEL3* is epistatic to *VOS1* in the regulation of conidiation.

3.1.5 All velvet domain proteins are present in the nucleus during *V. dahliae* vegetative filamentous growth and can form three heterodimers

3.1.5.1 Velvet domain proteins are detectable during hyphal growth of *V. dahliae*

Hyphal growth is required for the fungus to grow into the direction of a host plant and subsequently colonize the root (Klosterman *et al.*, 2009). The presence of velvet domain proteins in *V. dahliae* was analyzed in liquid glucose-rich potato dextrose medium (PDM), which favors filamentous growth. Strains with functional *GFP* fusions at the 3' end of the respective gene integrated at the endogenous *VEL1-3* and *VOS1* loci driven by their respective natural promoters were analyzed by western experiments. The four GFP-tagged velvet domain proteins Vel1-3 and Vos1 were present after three as well as six days of growth in PDM during constant light (Figure 25).

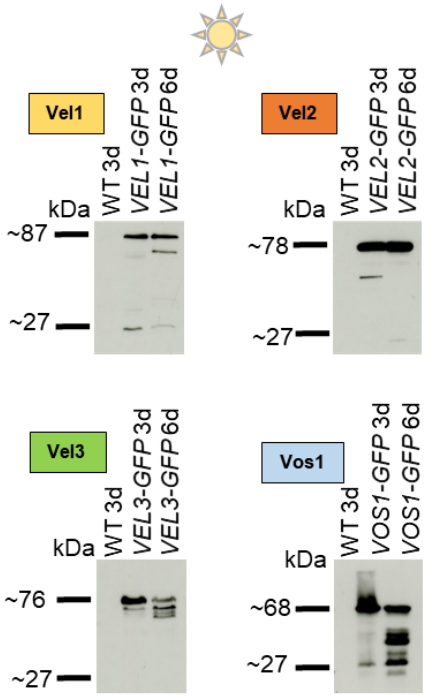

Protein \ Condition	Hyphal growth	
	3d	6d
Vel1	+	+
Vel2	+	+
Vel3	+	+
Vos1	+	+

Figure 25: Steady state levels of velvet domain proteins during vegetative growth of *V. dahliae*. Western analysis with a GFP antibody (dilution 1:500) for velvet domain proteins fused to the green fluorescent protein (GFP) in extracts from *V. dahliae* strains of *VEL1-GFP*, *VEL2-GFP*, *VEL3-GFP* and *VOS1-GFP* grown during conditions stimulating filamentous growth (PDM: liquid potato dextrose medium). $1x10^6$ freshly harvested spores were inoculated and extracts were prepared after growth for three and six days at 25 °C in light (free GFP: 27 kDa; Vel1-GFP: 87 kDa; Vel2-GFP: 78 kDa; Vel3-GFP 76 kDa; Vos1-GFP: 68 kDa). From the protein extracts 50 µg were used for western hybridization. Presence of full-length velvet proteins during hyphal growth is indicated in the table (+).

3.1.5.2 *V. dahliae* velvet proteins are mainly localized to the nucleus independently of light during filamentous growth

In *A. nidulans* VeA exhibits an enrichment in the nucleus in the dark whereas VelB localization to the cytoplasm and nucleus is hardly altered by light or darkness (Bayram *et al.*, 2008b). The subcellular localization of the velvet proteins was investigated by construction of ectopic overexpression strains of *VEL1-3* and *VOS1*, respectively, fused to *GFP* and transformation into a strain with histone *H2B-RFP* overexpression. As controls, the wild type strain, a strain overexpressing *GFP* and a strain with histone *H2B-RFP* overexpression were used. Incubation of the four velvet strains in constant light revealed a predominant nuclear localization of Vel1, Vel3 and Vos1. Vel2 is also mainly localized to the nucleus but additional subpopulations are present in the cytoplasm (Figure 26a).

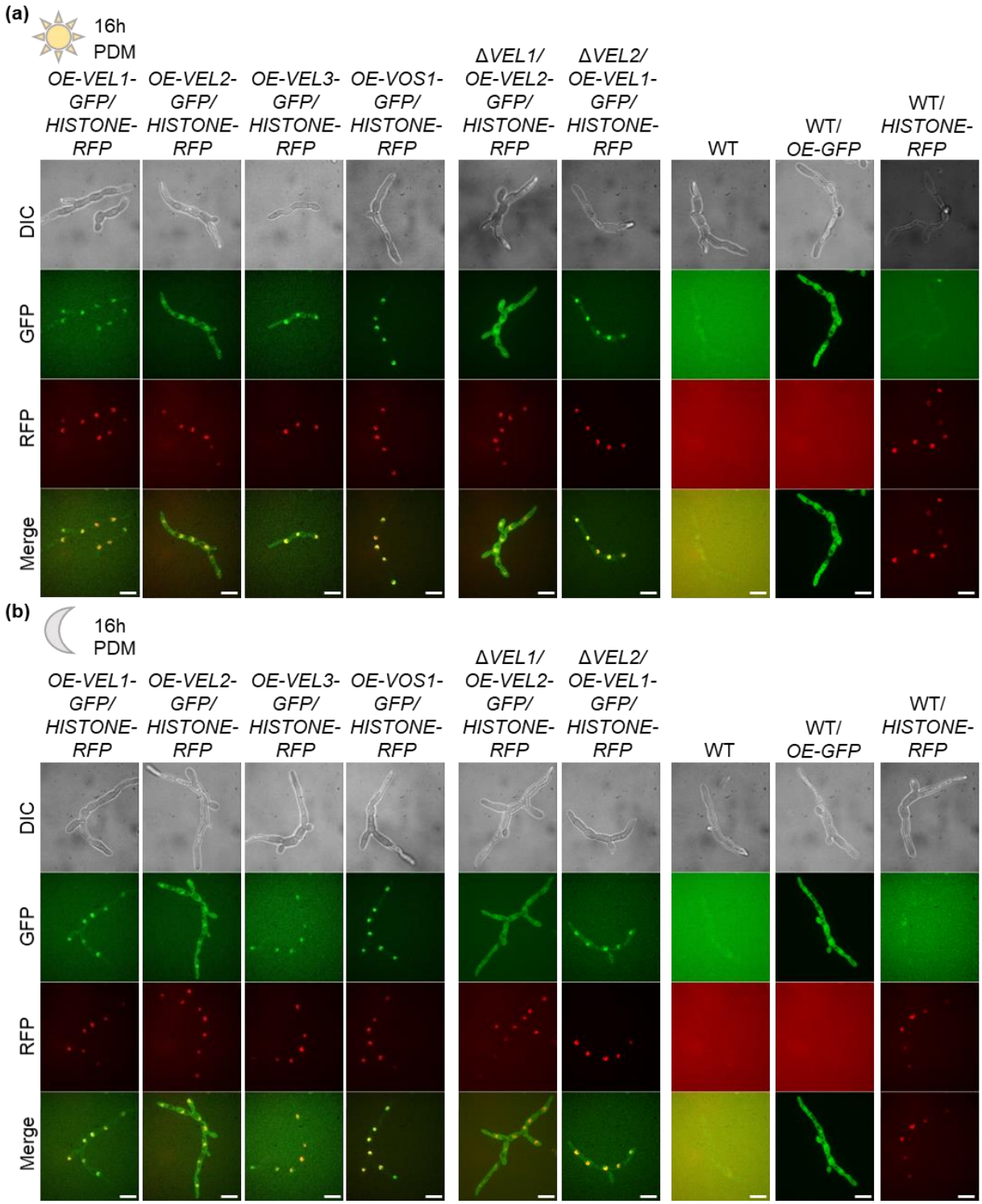

Figure 26: Light-independent nuclear localization of *V. dahliae* velvet domain proteins. Subcellular localization analysis of Vel1, Vel2, Vel3 and Vos1 fusions with GFP by fluorescence microscopy. 1x10^4 freshly harvested spores were incubated in PDM for 16 h at 25 °C in light **(a)** or darkness **(b)**, respectively. Differential interference contrast (DIC), green fluorescent filter view (GFP), red fluorescent filter view (RFP) and a merge of GFP and RFP channel are shown. Scale bar = 10 µm. Velvet protein subpopulations are primarily localized to the nucleus in light as well as darkness. Small subpopulations of Vel2 are present in the cytoplasm. Nuclei are visualized in red by histone H2B-RFP. High levels of Vel1 or Vel2 can enter the nucleus independently of each other in light as well as in darkness in a Δ*VEL1* and a Δ*VEL2* strain, respectively. The wild type (WT) was used as negative control, a strain with overexpressed *GFP* (WT/*OE-GFP*) as positive control and a strain in which histone *H2B-RFP* is overexpressed (WT/*HISTONE-RFP*) as positive control.

Incubation of the same strains in constant darkness did not change the localization pattern (Figure 26b). Concluding, the subcellular localization of all four velvet domain proteins is light independent.

Research in *A. nidulans* presented VeA as supporter of nuclear entry for VelB (Bayram *et al.*, 2008b). A *V. dahliae* strain overexpressing *VEL2-GFP* in a *VEL1* deletion background with histone *H2B-RFP* overexpression still showed nuclear localization of the Vel2-GFP fusion protein and subpopulations in the cytoplasm during incubation in constant light and constant darkness (Figure 26), which is similar to the strain with Vel1 present. A strain with *VEL1-GFP* overexpression in the *VEL2* deletion background with histone *H2B-RFP* overexpression also revealed predominantly nuclear localization of Vel1-GFP in light and darkness (Figure 26) as did the strain with intact Vel2. These results suggest that, different to *A. nidulans*, *V. dahliae* Vel1 and Vel2 can enter the nucleus independently of each other and of light.

3.1.5.3 The *V. dahliae* velvet domain proteins can form three heterodimers during filamentous growth

Velvet proteins form various homo- and heterodimer combinations in *A. nidulans* (Sarikaya-Bayram *et al.*, 2015). Within this study protein pull downs were conducted to examine interaction partners of *V. dahliae* velvet proteins by mass spectrometry. Velvet genes were fused to *GFP* under control of the native promoters and the respective fusion proteins were enriched from cell lysates through affinity purification. Protein samples from the enrichment were digested into peptides and analyzed with LC-MS for protein identification and label-free relative quantification. Several significant interaction partners were identified for Vel1 (eight proteins), Vel2 (42 proteins) and Vos1 (23 proteins), whereas Vos1 was the only significant interactor found for Vel3 (Table A1-A8). Within the velvet domain proteins three heterodimers were identified under the tested conditions: Vel1-Vel2, Vel2-Vos1 and Vos1-Vel3 (Figure 27). Vel1 interaction partners included proteins involved in redox and protein metabolism. Except for one protein involved in proteolysis (VDAG_JR2_Chr1g15440a) all other proteins interacting with Vel1 were also significantly enriched in Vel2. One protein interacting with both, Vel1 and Vel2, is encoded by VDAG_JR2_Chr5g09190a. The deduced protein corresponds to *N. crassa* HAM-13, which is involved in fungal communication (Dettmann *et al.*, 2014).

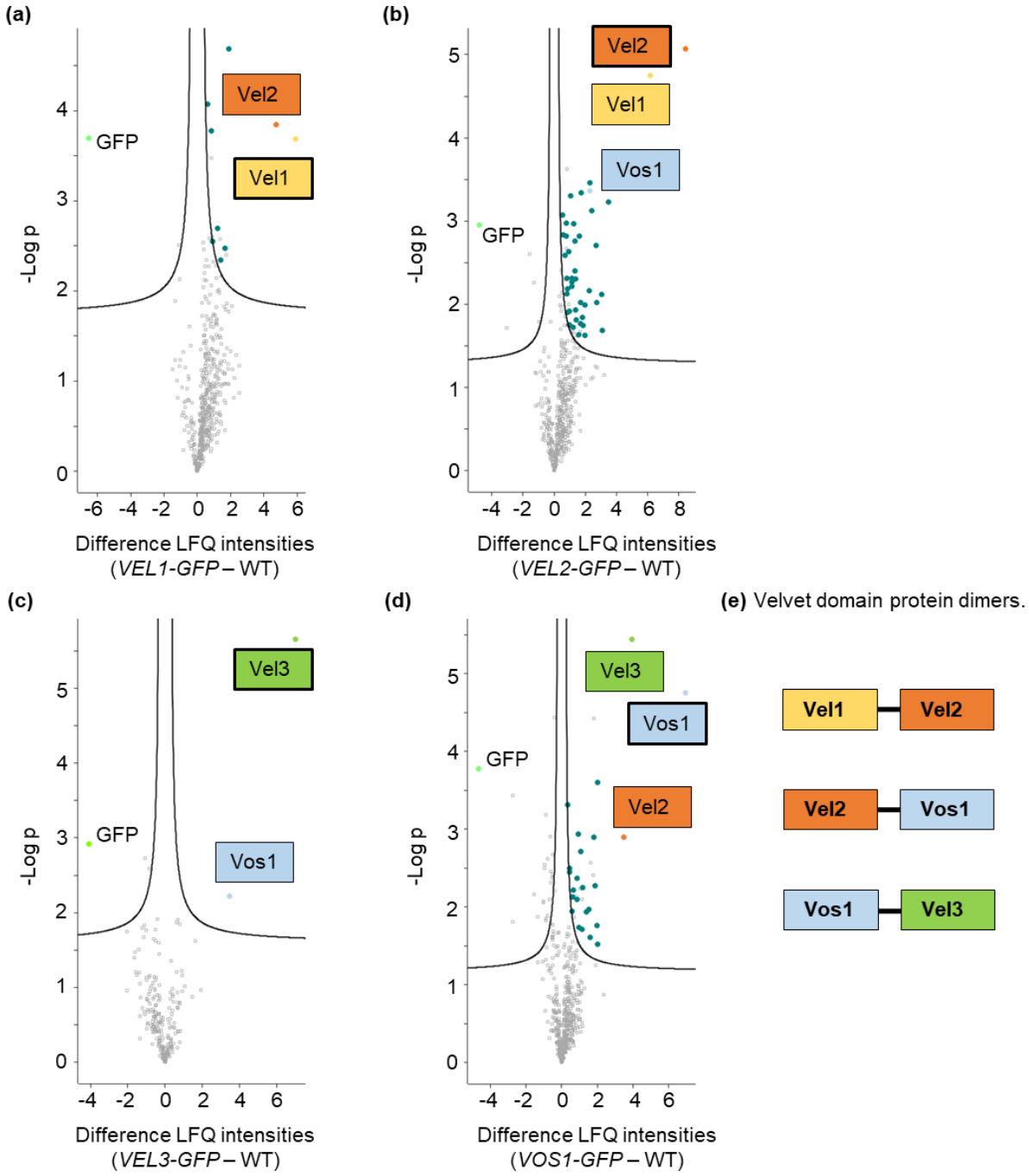

Figure 27: Vel1-3-GFP and Vos1-GFP interacting proteins during filamentous vegetative *V. dahliae* growth. 5x10^7 freshly harvested spores were inoculated in 500 ml PDM and grown for 72 h during constant agitation in light at 25 °C. Protein extracts of the strains were subjected to GFP-trap-pull down, trypsin digested and resulting peptides were analyzed by LC-MS. Volcano plots show differences of examined *VELVET-GFP* strains in comparison to the wild type (WT) on the x-axis and -Log p-values on the y-axis. Displayed is the mean of three independent experiments. Significant hits of the protein interaction study are visible in the upper right part. Missing values were replaced four times with imputed values to obtain reliable interaction candidates. Proteins that were significant in all four repetitions are colored (Vel1: yellow, Vel2: orange, Vel3: green, Vos1: light blue, other proteins: dark blue). GFP is indicated in lime and the bait is framed by a black line. **(a)** Vel1 interacts with eight other proteins including Vel2. **(b)** Vel2 interacts with Vel1, Vos1 and 40 other proteins. **(c)** Vel3 interacts with Vos1. **(d)** Vos1 interacts with Vel2 and Vel3 as well as 21 other proteins. **(e)** Summary of the velvet protein dimer complexes identified during *V. dahliae* vegetative growth.

Many Vel2 interaction partners are connected to different metabolic processes such as carbohydrate and redox metabolism. A few proteins are also connected to fatty acid and amino acid metabolism. Vos1 interacting proteins are mainly involved in energy metabolism and transport. For Vos1 no NLS was predicted with the program used, which might explain the association of Vos1 to proteins involved in transport. Vos1, which is required for viability of spores in *A. nidulans* (Ni & Yu, 2007), is part of the two *V. dahliae* heterodimers Vel3-Vos1 and Vel2-Vos1. Their function in the plant pathogen *V. dahliae* is yet elusive, because the Δ*VOS1* strain did not reveal any obvious differences in comparison to wild type under the tested conditions.

In our experimental setup, no significant interaction could be identified between the velvet proteins with any epigenetic methyltransferase as Lae1, which is described as VelA-VelB interacting protein in other fungi such as *A. nidulans*, *N. crassa*, or *B. cinerea* (Bayram *et al.*, 2008b; Schumacher *et al.*, 2015; Sarikaya-Bayram *et al.*, 2019). Some proteins were significantly enriched in samples of *VEL1-GFP* and *VEL2-GFP* strains. It is possible that Vel1 and Vel2 form another complex with one of these proteins.

The protein pull downs in *V. dahliae* revealed the presence of the three heterodimers Vel1-Vel2, Vel2-Vos1 and Vos1-Vel3. Furthermore, other significantly interacting proteins were identified for Vel1, Vel2 and Vos1.

3.1.5.4 The intrinsically disordered domain of Vel2 alters the interaction profile of the protein

Vel2 is the only velvet protein with an interrupted velvet domain (Figure 9a). The intrinsically disordered domain (IDD) of VelB in *A. nidulans* is needed to form homo- and heterodimers (Thieme, 2018). As the velvet domain is known to be a protein-protein interaction domain, a *V. dahliae* strain expressing *VEL2* without *IDD* (*VEL2*$^{\Delta IDD}$) fused to *GFP* was constructed for protein interaction studies. Protein pull downs were conducted in the same way as for the other velvet strains. For the *VEL2-GFP* strain, 42 proteins were significantly enriched (Figure 27b). Deletion of the *IDD* reduced the number of significant interactions in comparison to the wild type by more than 80 % to only six proteins (Figure 28a, Table A9-A10).

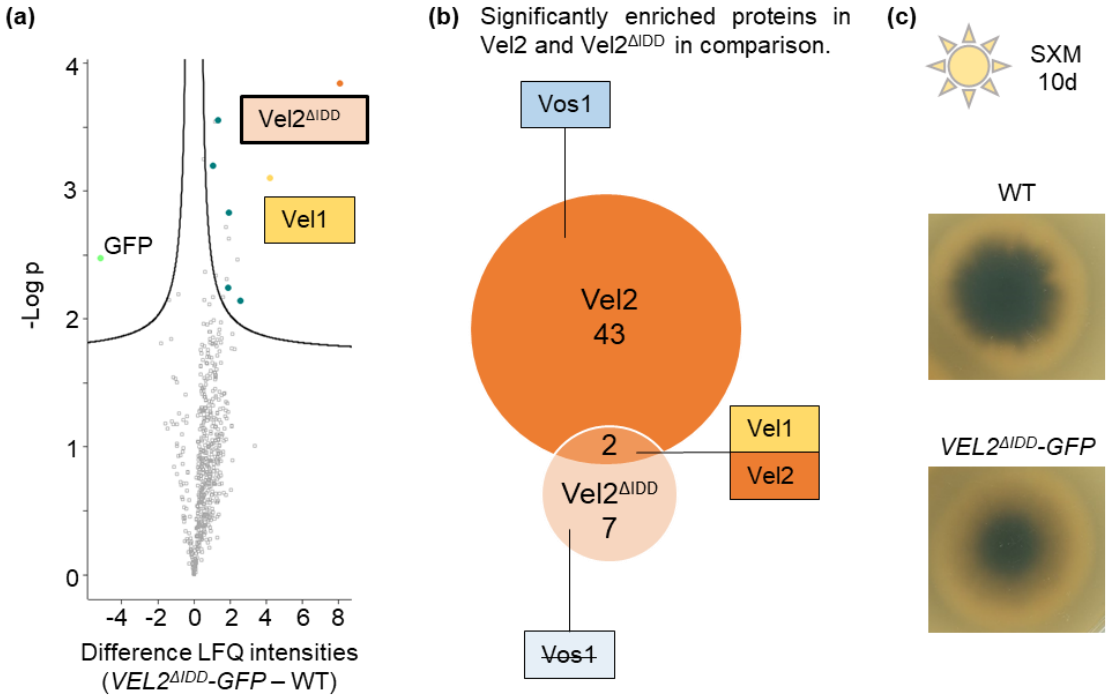

Figure 28: The IDD of Vel2 is required for protein interactions and wild type-like microsclerotia production. (a) Fungal strains were incubated in liquid PDM at 25 °C with constant light and agitation for 72 h. After protein extraction, the samples were subjected to GFP-trap-pull down and digested with trypsin. Subsequently, the peptides were analyzed by LC-MS. The *VEL2$^{\Delta IDD}$-GFP* strain was used as bait. The *VEL2$^{\Delta IDD}$-GFP* strain and the wild type (WT) are displayed on the x-axis in the volcano plot. The y-axis shows the -Log p value. The plot exhibits the mean of three independent experiments. The significant hits are displayed in the upper right part of the plot. Missing values were replaced four times with imputed values to obtain reliable interaction candidates. Proteins that were significant in all four repetitions are colored (Vel1: yellow, Vel2 respectively Vel2$^{\Delta IDD}$: orange, other proteins: dark blue. GFP is indicated in lime. Vel2$^{\Delta IDD}$ significantly interacts with Vel1 and five other proteins. **(b)** Comparison of significantly enriched proteins in Vel2 and Vel2$^{\Delta IDD}$ pull downs by Venny 2.1. Among the 43 significantly enriched proteins in the *VEL2-GFP* strain and seven enriched proteins in the *VEL2$^{\Delta IDD}$-GFP* strain are two overlaps, Vel1 and Vel2. Within the proteins co-purified with Vel2-GFP is also Vos1. Vos1 is no more enriched in the *VEL2$^{\Delta IDD}$-GFP* strain. **(c)** Phenotypical analysis of the wild type and the *VEL2$^{\Delta IDD}$-GFP* strain. 5x10^4 spores of the indicated strains were spotted on simulated xylem medium (SXM) and incubated for 10 days at 25 °C in light. An overview of a single colony is displayed. The *VEL2$^{\Delta IDD}$-GFP* strain produces less microsclerotia than the wild type.

The significantly enriched proteins in the *VEL2-GFP* and the *VEL2$^{\Delta IDD}$-GFP* strain were compared in a Venn diagram (Figure 28b). Solely Vel2 itself and Vel1 were enriched in both strains. Vos1 was detected among the proteins exclusively co-purified with Vel2. Phenotypical characterization of the *VEL2$^{\Delta IDD}$-GFP* strain incubated in light on SXM revealed that this strain forms less microsclerotia in comparison to the wild type (Figure 28c).

Taking these results into account, the IDD seems to be required for the interaction to other proteins such as Vos1 but is dispensable for the interaction of Vel2 with Vel1. Deletion of the *IDD* seems to strongly alter the interaction profile as merely Vel1 and Vel2 were enriched in both, the *VEL2-GFP* and *VEL2$^{\Delta IDD}$-GFP* strain.

3.1.6 All velvet domain proteins are present during early *V. dahliae* conidia production whereas only Vel2 and Vel3 are present during early microsclerotia formation in light

Germination of fungal spores on appropriate substrates leads to vegetative hyphae, which are initially incompetent to react to environmental triggers in several filamentous ascomycetes (Etxebeste *et al.*, 2010; Noble & Andrianopoulos, 2013). Only when developmental competence is established, the fungus can receive and respond to environmental signals as light with substantial shifts in differential gene expression (Bayram *et al.*, 2016).

V. dahliae velvet domain proteins were detected during filamentous growth (Figure 25). Presence of the fusion proteins was further monitored in growth conditions, which induce different developmental programs. Cultivation in liquid pectin-rich simulated xylem medium (SXM) favors the development of conidiospores, whereas incubation on SXM plates induces microsclerotia development. For both conditions early (three days) and later (six days) developmental stages in constant illumination were tested (Figure 29).

In liquid cultures, during conidiation, velvet proteins were destabilized after six days and the amount of free GFP increased. Phenotypical analysis revealed that microsclerotia formation in light is promoted by Vel1 and Vel2 but inhibited by Vel3. Western analyses with extracts from mycelia grown on SXM plates showed that Vel2-GFP and Vel3-GFP are the only velvet domain proteins, which were identified after three days, but are destabilized after six days of cultivation (Figure 29).

Taken together, all velvet proteins are present in the early phase of conidia production in light. Only Vel2 and Vel3 are detectable in the early phases of microsclerotia formation during constant illumination.

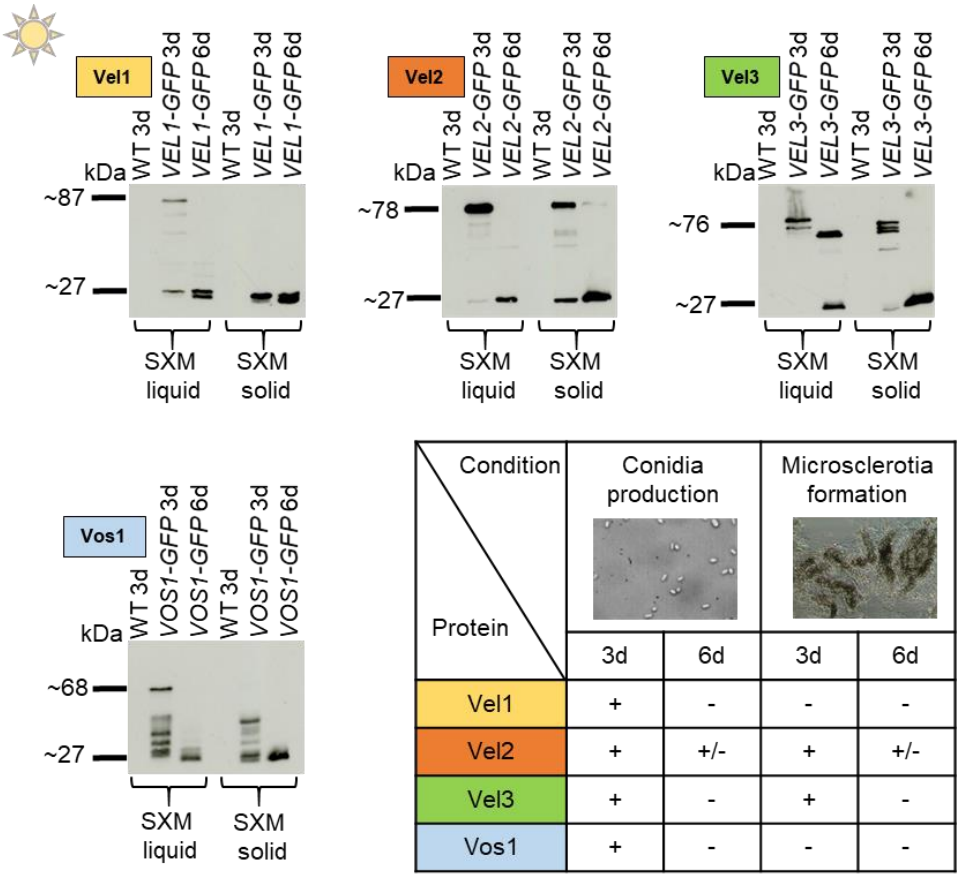

Condition / Protein	Conidia production		Microsclerotia formation	
	3d	6d	3d	6d
Vel1	+	-	-	-
Vel2	+	+/-	+	+/-
Vel3	+	-	+	-
Vos1	+	-	-	-

Figure 29: Steady state levels of velvet domain proteins during conidia and microsclerotia formation of *V. dahliae*. Western analysis with a GFP antibody (dilution 1:500) for velvet domain proteins fused to the green fluorescent protein (GFP) in extracts from *V. dahliae* strains of *VEL1-GFP*, *VEL2-GFP*, *VEL3-GFP* and *VOS1-GFP* grown during conditions stimulating conidia (SXM: pectin-rich simulated xylem medium) or microsclerotia (SXM plates covered by a nylon membrane) formation. $1x10^6$ freshly harvested spores were inoculated and extracts were prepared after growth for three and six days at 25 °C in light (free GFP: 27 kDa; Vel1-GFP: 87 kDa; Vel2-GFP: 78 kDa; Vel3-GFP 76 kDa; Vos1-GFP: 68 kDa). From the protein extracts 50 µg were used for western hybridization. Presence of full-length velvet proteins under the different conditions is indicated in the table. Presence (+) or absence (-) of full-length velvet domain proteins during conidia production and microsclerotia formation. +/- means that in some replicates a weak signal was detected.

3.1.6.1 Stability of the Vel2 protein depends on light

Vel2 positively regulates microsclerotia production specifically in light (Figure 12 and 13). The stability pattern of Vel2-GFP was examined during different developmental stages in light (Figure 29) but protein abundances in darkness were also investigated. For this reason, the *VEL2-GFP* strain was incubated in darkness during conditions favoring hyphal growth, conidiation or microsclerotia formation. Incubation in light or darkness did not change the Vel2-GFP protein amount in liquid PDM (Figure 30a). Asexual spore formation is independent of Vel2 and resulted in a different stability pattern. Vel2-GFP was detectable in liquid SXM for both time points during incubation in darkness with slightly increased amounts after six days in comparison to the same condition in light (Figure 30b). On solid SXM after three days only little full-length Vel2-GFP was detectable but strong degradation signals were present in

comparison to the same time point in light where a strong full-length band was visible (Figure 30c). Consistent with the phenotype on plate incubated in light or darkness, Vel2-GFP is more stable in light than in darkness during microsclerotia formation.

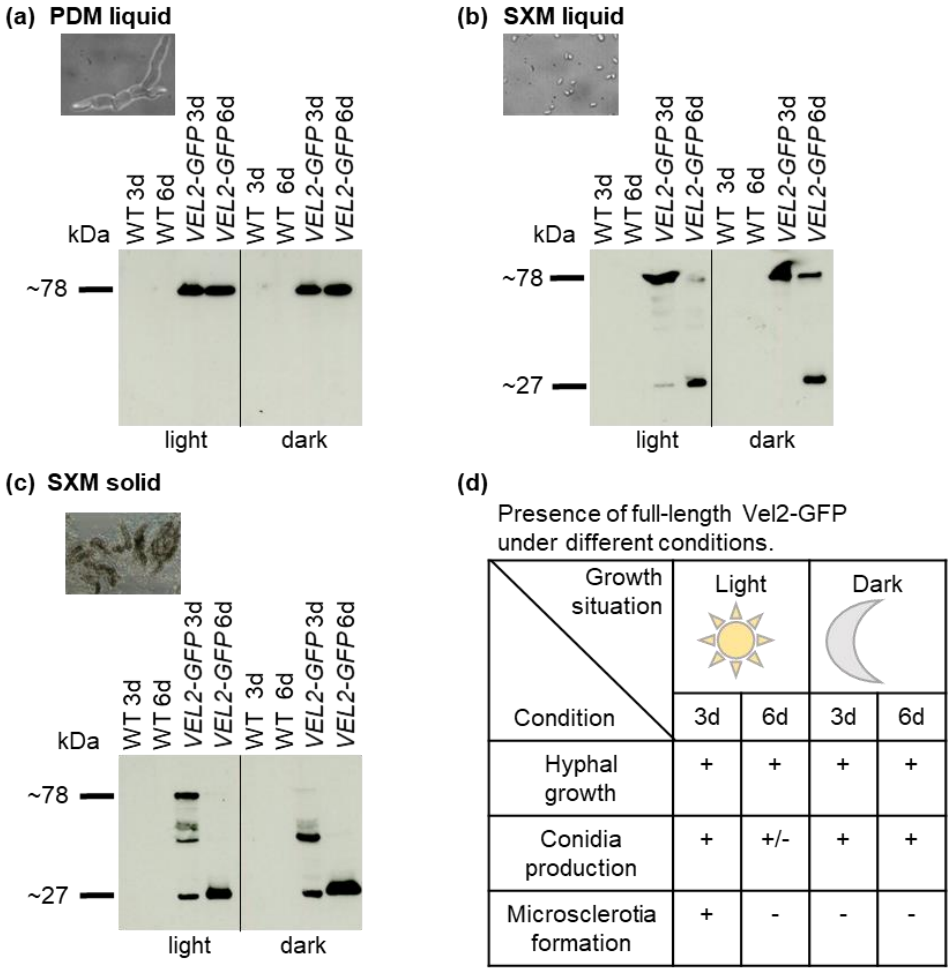

(d)

Presence of full-length Vel2-GFP under different conditions.

Growth situation / Condition	Light 3d	Light 6d	Dark 3d	Dark 6d
Hyphal growth	+	+	+	+
Conidia production	+	+/-	+	+
Microsclerotia formation	+	-	-	-

Figure 30: *V. dahliae* Vel2 is stable during filamentous growth, stabilized during conidiation in darkness and initially more stable in light than in darkness during microsclerotia formation. $1x10^6$ freshly harvested spores were inoculated for analysis of protein abundances **(a)** in liquid potato dextrose medium (PDM) for filamentous growth, **(b)** liquid pectin-rich simulated xylem medium (SXM) for conidia formation and **(c)** on SXM plates covered with a nylon membrane for microsclerotia development. The fungus was grown for three and six days at 25 °C in light or darkness. Western hybridization with a GFP antibody (dilution 1:500) was performed with 50 µg crude extracts of the indicated strains (free GFP: 27 kDa; Vel2-GFP: 78 kDa). **(d)** Presence (+) or absence (-) of full-length protein during growth in light or darkness during different developmental conditions (hyphal growth in PDM, spore production in liquid SXM, microsclerotia formation on SXM plates) after three and six days. +/- means that in some replicates a weak signal was detected.

In summary, during filamentous growth (liquid PDM) Vel2-GFP is stable in light as well as in darkness (Figure 30d). During conidiation (liquid SXM), Vel2-GFP is destabilized in light, but more stable in darkness. In microsclerotia formation conditions (solid SXM) Vel2-GFP is more stable in light than in darkness.

3.1.7 The Vel1 protein induces disease symptoms in *V. dahliae* infected tomato plants

V. dahliae Vel1 and Vel3 are required for efficient conidiospore formation suggesting a potential impact of the velvet domain proteins on causing Verticillium wilt of a host plant. Moreover, both proteins are present during hyphal growth and early conidia formation, which are required for fungal transport within the plant vascular system. Velvet proteins of different fungal pathogens have been connected to plant virulence in general (López-Berges *et al.*, 2013; Schumacher *et al.*, 2015; Wu *et al.*, 2018).

To gain further information about the involvement of the velvet domain proteins and especially Vel1 and Vel3 in plant infection and symptom development in *V. dahliae*, roots of 10-day-old tomato seedlings were wounded and inoculated with the same number of fungal spores by root dipping. After 21 days disease symptoms caused by wild type and corresponding mutant strains were compared and calculated into a disease score. This disease score classified the plants as healthy plant or plants with weak symptoms, strong symptoms and heavy symptoms (Harting *et al.*, 2020).

Water treated plants served as control and resulted in a majority of healthy and less than 10 % plants with weak symptoms (Mock). When treated with the wild type, less than 10 % of the plants were classified as healthy and additional approximately 25 % showed only weak symptoms. In contrast, the majority of plants (approximately 65 %) suffered from strong or heavy symptoms induced by the fungal pathogen (Figure 31a). Δ*VOS1* or Δ*VEL3* strains resulted in even more plants with strong or heavy symptoms. The corresponding Vos1 and Vel3 proteins are therefore not required to induce disease under the tested conditions, although Vel3 contributes to conidia formation as important transport vehicle of the fungus within the xylem of the host. Infection with the Δ*VEL2* strain also led to more than 50 % plants with strong or heavy symptoms, which does not support an essential function of Vel2 for fungal virulence in *V. dahliae* either.

In contrast, infection of tomato plants with the Δ*VEL1* strain resulted in almost 80 % plants, which are either healthy (more than 50 %) or show only weak symptoms, and hardly any plants with heavy symptoms. This effect could be restored in a complementation strain where the *VEL1* gene was reintroduced. Plant treatment with double deletion strains as Δ*VEL1*/Δ*VEL2* or Δ*VEL1*/Δ*VEL3* resulted in reduced disease severity compared to wildtype infected plants with approximately 30 % of plants displaying strong or heavy symptoms. This suggests that the *VEL1* gene plays a significant role in the *V. dahliae* caused disease in tomato.

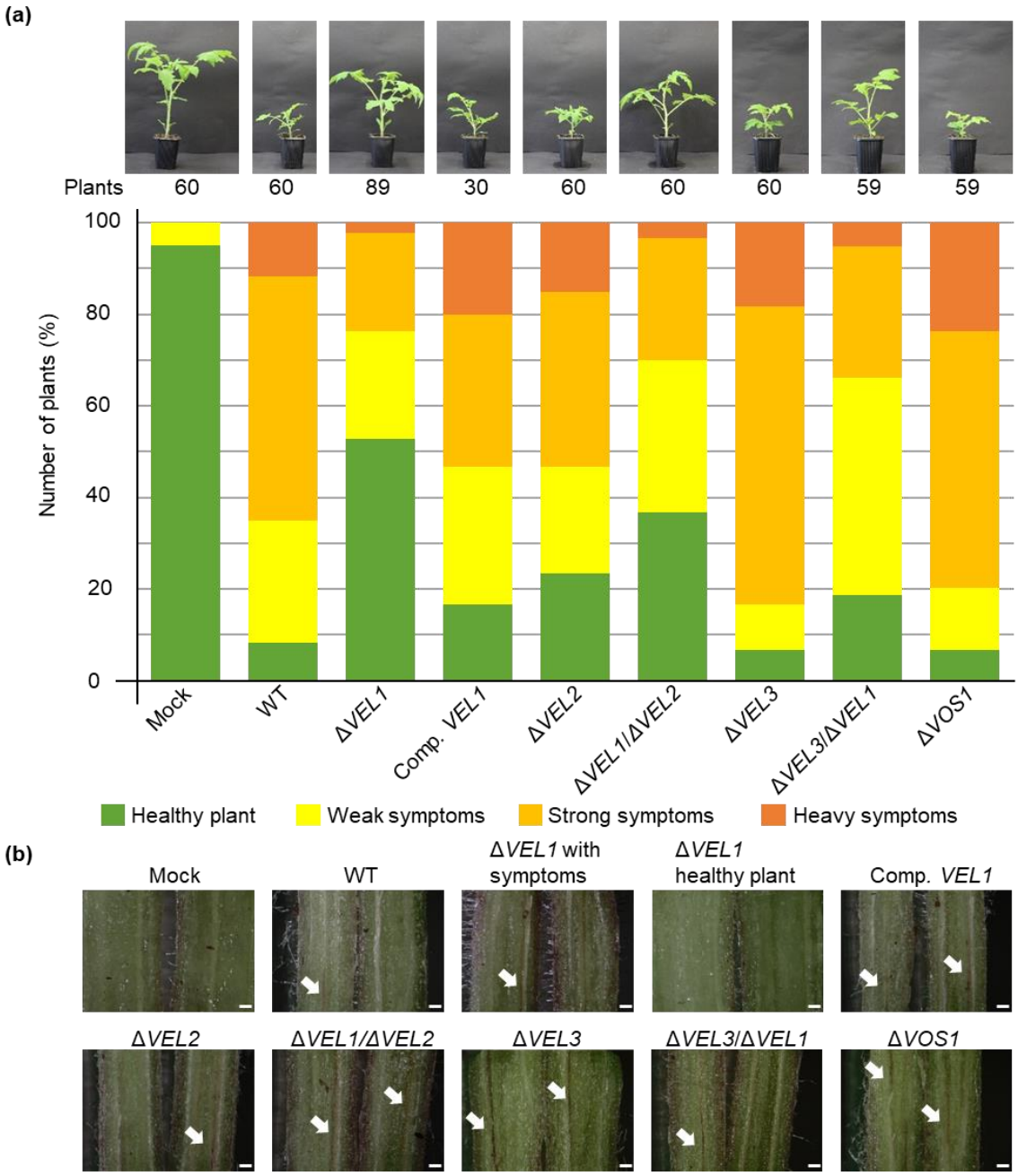

Figure 31: *V. dahliae* requires Vel1 to induce disease symptoms in tomato plants. Tomato plants were grown for 10 days and inoculated by root dipping with fungal spores of *V. dahliae* wild type and indicated mutant strains defective in genes encoding for velvet domain proteins. The mock control was treated with demineralized water. Single experiments included at least 14 plants and two different transformants for each deletion and double deletion strain were used. Each strain was analyzed in at least two independent experiments. **(a)** Disease symptoms were scored after 21 days of incubation under long day conditions (16 h, 25 °C: 8 h, 22 °C, light: dark). Measurements included height of plants until the vegetation point, length of the longest leaf and fresh weight of aerial plant parts. Parameters were calculated into a disease score leading to the categories healthy plant, weak symptoms, strong symptoms and heavy symptoms. The diagram shows the relative number of plants of each category and a representative plant for each strain. Mock treated plants were mostly healthy with some plants with weak symptoms. More than 60 % of plants inoculated with the wild type developed heavy or strong disease symptoms. **(b)** Images of hypocotyl cross sections show discolorations (marked with arrows), which are not found in uninfected plants and in approximately 40 % of plants treated with the Δ*VEL1* strain. Scale bar = 500 µm.

As additional indicator of disease or plant immune response, hypocotyl cross sections of the plants were investigated for discoloration caused by fungal infection (Figure 31b). In hypocotyl cross sections from healthy plants no discoloration was observed. Plants with symptoms infected by the wild type or complementation strains exhibited brownish discoloration indicated by white arrows. The same was found when the Δ*VEL2*, Δ*VEL3* or Δ*VOS1* strains were applied. Whereas 97 % of wild type treated plants showed strong discolorations of the hypocotyl only approximately 60 % of plants inoculated with *VEL1* deletion strains had changes in hypocotyl color, which mostly seemed to be less severe. These results indicate that Vel1 is required for the circumvention of the plant's defense reaction and corroborate a potential role of Vel1 in *V. dahliae* pathogenicity on tomatoes.

3.1.7.1 Successful plant infection by *V. dahliae* relies on intact Vel1

Previous results showed that Vel1 is required for efficient asexual spore formation in *V. dahliae* (Figure 24). To evaluate whether there are differences in the infection potential on plants after inoculation with the same number of conidia, the infection rate between the wild type, the Δ*VEL1* strain and the complementation strain was compared. The amount of plants without disease symptoms relative to Mock was determined (Figure 32).

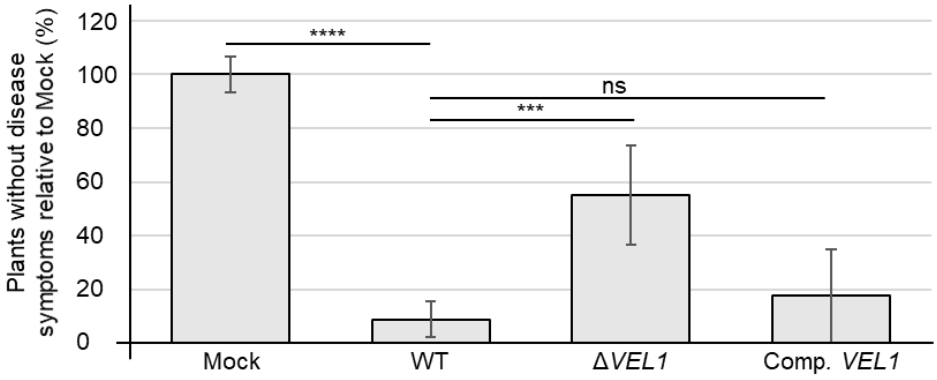

Figure 32: Quantification of plants without disease symptoms. Means and error bars represent the standard deviation and mean of two independent experiments including at least 14 plants and at least two deletion strains. Significant differences calculated by t-test are indicated: ***,p<0.001; ****,p<0.0001; ns: not significant.

The wild type strain of *V. dahliae* caused disease symptoms in significantly more than 80 % of all plants. In contrast, only about half of the plants developed disease symptoms when infected with spores of the *VEL1* deletion strain.

These results lead to the suggestion that the *VEL1* deletion strain does not only produce less conidia than wild type but also spores with a lower potential to infect a host.

3.1.7.2 *VEL1* can be re-isolated from stems of infected plants

In order to confirm that induced symptoms were caused by *V. dahliae*, the presence of the fungus in the plant was analyzed. Therefore, intersections of tomato stems were surface sterilized and incubated on PDM plates supplemented with chloramphenicol to remove bacteria and to re-isolate fungal material. Hyphae could grow from intersections of plants inoculated with spores of the wild type, the complementation strain of Δ*VEL1* or from plants inoculated with the Δ*VEL1* strain showing symptoms (Figure 33a). No fungal material grew from uninfected plants (Mock) or symptomless plants treated with the Δ*VEL1* strain. The presence of the wild type or the Δ*VEL1* strain was verified by PCR using DNA from the isolated fungal material as template. Wild type spores were inoculated in PDM as positive control. Thereby, the presence of the wild type and the *VEL1* deletion strain in the plant could be confirmed (Figure 33b).

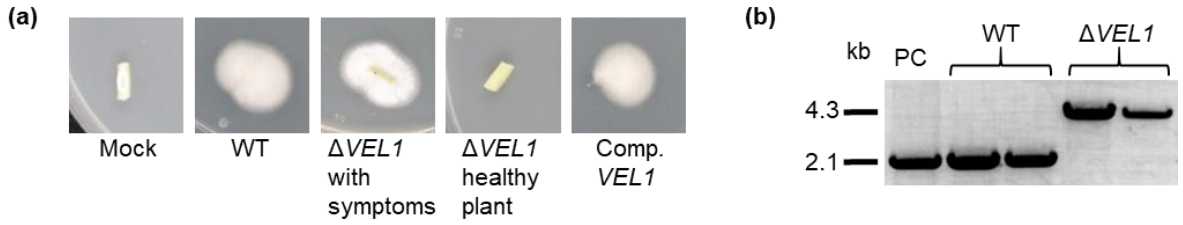

Figure 33: Fungal growth from stem sections of tomato plants. (a) Stems of tomato plants treated with indicated *V. dahliae* strains were surface sterilized and incubated for seven days at 25 °C on PDM plates supplemented with chloramphenicol. Wild type as well as *VEL1* complementation strain could be re-isolated from the stem. The *VEL1* deletion strain could only be re-isolated from plants displaying disease symptoms. **(b)** Verification of isolated fungal strains by PCR. Fungal material isolated from plate was inoculated in PDM for mycelia production. Spores of the wild type were inoculated in PDM as positive control (PC). Genomic DNA was extracted and PCR was conducted to verify the wild type (WT: 2130 bp) or *VEL1* deletion (Δ*VEL1*: 4342 bp) genotype by using the primers AO24 and AO25, which bind in the 5' or 3' flanking region of the gene, respectively.

These data suggest that the *VEL1* regulatory gene of *V. dahliae*, which is required for microsclerotia and conidia formation and the control of secondary metabolism, encodes a velvet domain protein with a substantial role in fungal virulence in a plant host. Fungal strains deficient in *VEL1* had difficulties to establish a successful infection. Hence, the first contact between plant root and pathogen was investigated in detail hereinafter.

3.1.8 Vel1 is required for initial steps in plant root colonization by *V. dahliae*

Initial steps of *V. dahliae* infection of plants include the colonization of the host root by the fungus and subsequent penetration at suitable sites with the help of hyphopodia, which are swollen hyphal tips (Reusche *et al.*, 2014; Zhao *et al.*, 2014). The Vel1 protein is present during hyphal growth of *V. dahliae* (Figure 25) and involved in disease symptom induction in tomato plants (Figure 31). In order to elucidate the exact role of Vel1 in the vascular plant pathogen *V. dahliae* regarding root colonization, *A. thaliana* roots were examined for initial fungal colonization and entry.

Plant roots were transferred into a spore solution either with the wild type strain ectopically overexpressing *GFP* or the *VEL1* deletion strain carrying the same construct. After incubation under long day conditions for five days, the roots were examined by fluorescence microscopy. The wildtype was able to colonize the root surface (Fig. 34a). A more detailed view exhibited penetration points with swollen hyphae indicating hyphopodia formation (Fig. 34b, white arrow). Generation of 3D volume views from 2D pictures showed the entry into the root for the wildtype (Fig. 34c, white arrow).

Roots infected with the *VEL1* deletion strain showed less fungal colonization than the wild type (Figure 34a). In addition, propidium iodide staining indicated substantial amounts of dead hyphae, which are not present in the wild type (Figure 34b). Penetration points as seen for the wild type were not visible. In the 3D view, hyphae were detected which are vacuolized and swollen suggesting fitness problems of the fungus (Figure 34c).

These data suggest that *V. dahliae* Vel1 is not only required for spore dependent transport of the fungus in the plant xylem system, but already necessary for the first phases of plant colonization including the potential to form hyphae, which are viable during fungal-root interaction. Vel1 functions include the fungal potential to penetrate plant barriers with the help of hyphopodia as prerequisite for successful entry into the vascular xylem system and the induction of disease symptoms.

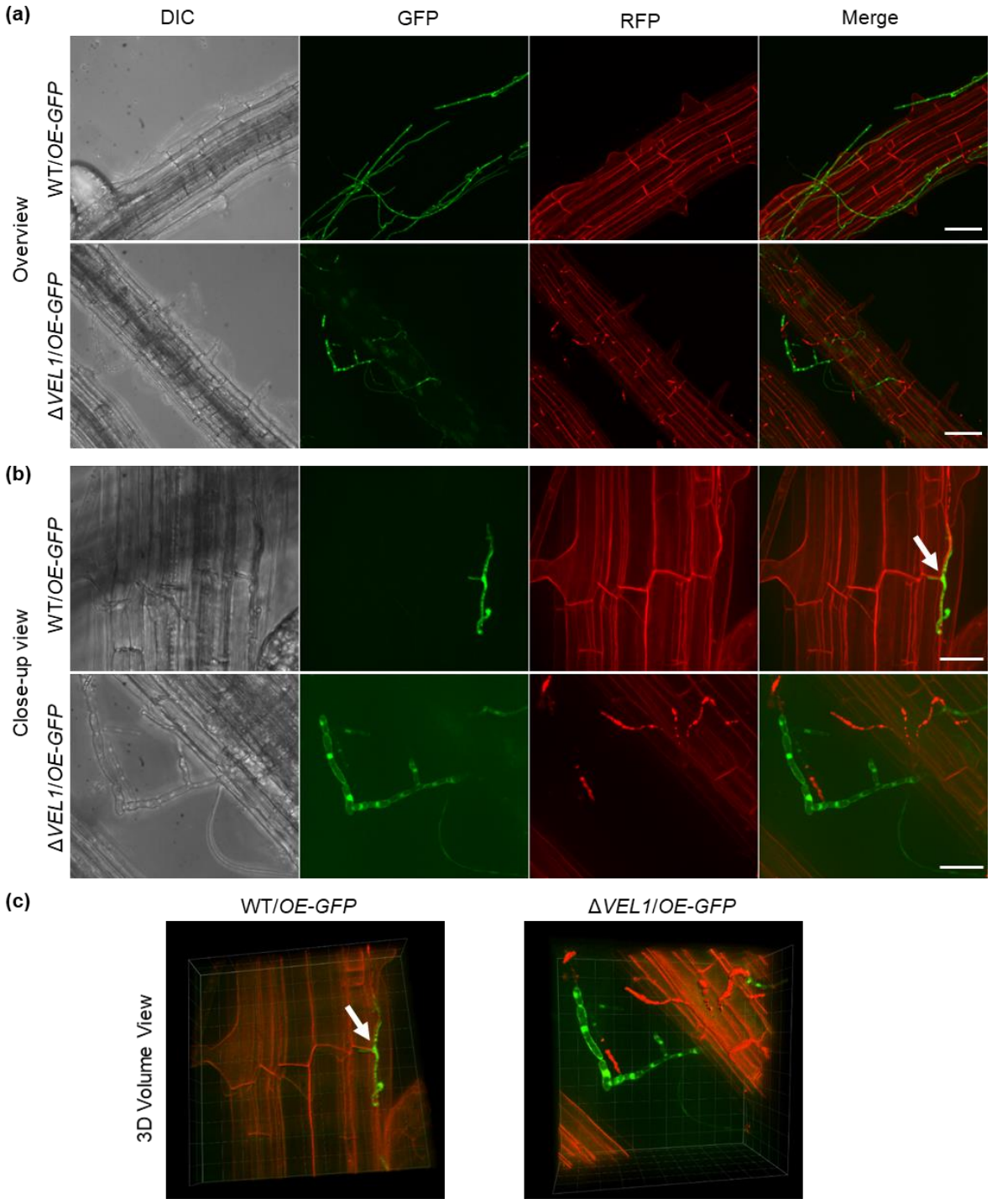

Figure 34: Vel1 is required for colonization and penetration of *A. thaliana* roots. Fluorescence microscopy images of wild type ectopically overexpressing green fluorescent protein (GFP, WT/*OE-GFP*) and the Δ*VEL1* strain ectopically overexpressing *GFP* (Δ*VEL1*/*OE-GFP*). Surface sterilized *A. thaliana* seeds were grown for three weeks during long-day conditions (16 h, 25 °C: 8 h, 22 °C, light: dark) on Murashige and Skoog Medium. One day prior to the infection the plants were transferred to 1 % agarose. After inoculation with fungal spores by root dipping, the plants were further incubated for five days. *A. thaliana* roots were stained with propidium iodide solution for microscopy (0.0025 % propidium iodide, 0.005 % silwet). Differential interference contrast (DIC), green fluorescent filter view (GFP), red fluorescent filter view (RFP) and a merge of GFP and RFP channels are presented. White arrows indicate potential fungal penetration points on the root surface, which are absent in the Δ*VEL1* strain. **(a)** Overview projections of stacks of single images of wild type and Δ*VEL1* strains, both overexpressing *GFP*; scale bar = 50 µm. **(b)** Close-up view of the same strains as in (a); scale bar = 20 µm. **(c)** 3D volume view of single picture stacks displaying the same position as in (b).

3.2 Fluorescent pseudomonads inhibit fungal growth and conidia germination

3.2.1 Pseudomonads reduce growth of *V. dahliae* and to a smaller extent of *Aspergillus* spp.

V. dahliae Vel1 is required to colonize and penetrate the root and later needed for fungal distribution in the plant. In the rhizosphere the pathogen encounters different bacteria such as fluorescent pseudomonads, which might interfere with the fungus during root colonization and penetration.

In a recent publication we could show that *P. fluorescens* DSM8569 (P_rhizo), which was isolated from the rhizosphere of *Brassica napus* is able to inhibit growth of the rapeseed pathogen *V. longisporum* as well as growth of *V. dahliae*. Similar observations were made for *P. synxantha* (formerly *P. fluorescens* 2-79; P_phen) and *P. protegens* CHA0 (P_DAPG). (Nesemann *et al.*, 2018). Besides *Verticillium* spp., the soil comprises a huge number of different microorganisms including different *Aspergillus* spp. Therefore, the interaction of this saprophytic fungus with different pseudomonads was investigated to examine how specific the inhibitory effects of the bacteria are.

A comparison of the bacterial genomes regarding their potential metabolite clusters revealed differences and similarities between the three strains (Table 10).

Table 11: Presence of gene clusters for the production of bioactive compounds in different Pseudomonads. Investigated were the gene clusters for the production of phenazines, DAPG, HCN, pyoluteorin and the GacS/GacA control system in *P. synxantha* (formerly *P. fluorescens* 2-79, P_phen), *P. protegens* CHA0 (P_DAPG) and *P. fluorescens* DSM8569 (P_rhizo). The table was modified from Nesemann *et al.* (2018).

Organism	Phenazine cluster	DAPG cluster	HCN cluster	Pyoluteorin cluster	GacS/GacA system	GacS/GacA regulation
P_phen	+	-	o	-	+	o
P_DAPG	-	+	+	+	+	+
P_rhizo	-	o	+	-	+	o

gene cluster completely present: +, partial gene cluster: o, gene cluster absent: -;
DAPG: 2,4-diacetylphloroglucinol, HCN: hydrogen cyanide

P_phen is the only one of the examined strains with a gene cluster that might enable the bacterium to produce phenazines. In contrast, P_DAPG is the only assumed producer of 2,4-diacetylphloroglucinol (DAPG) because the cluster is just partially present in P_rhizo. Hydrogen cyanide (HCN) is supposed to be synthesized by P_rhizo and P_DAPG, but pyoluteorin seems to be solely produced by P_DAPG. According to the predicted gene clusters, all examined strains contain the GacS/GacA two-component system whereas only P_DAPG possesses the regulatory components of this system (Nesemann *et al.*, 2018).

In a previous study we could show that the fungal inhibition potential of the bacterium on plate depends on the medium and the bacterium's repertoire of metabolites. On glucose-rich agar P_phen seems to require metabolites like phenazines for inhibition, but P_rhizo induced the

strongest inhibitory effect although it does not have a phenazine cluster. In contrast, the GacS/GacA system of P_DAPG is essential for inhibition on pectin-rich agar, but strong inhibition effects for P_phen were observed on agar surfaces (Nesemann *et al.*, 2018).

In the course of this thesis, co-cultivation experiments were conducted with the well-studied model fungus *A. nidulans* and *A. fumigatus*, which is an opportunistic pathogen for immunocompromised humans. For the purpose of comparison, the *V. dahliae* wild type was included in the experiment. When comparing the inhibition potential of *P. synxantha* (formerly *P. fluorescens* 2-79, P_phen), *P. protegens* CHA0 (P_DAPG) and *P. fluorescens* DSM8569 (P_rhizo) against the different fungi, it was visible that the inhibitory potential of the bacteria is reduced towards the *Aspergillus* spp. in comparison to *V. dahliae* (Figure 35).

Taking a closer look at the size of the inhibition zone on glucose-rich PDM, revealed that growth of *A. nidulans* on this medium is not inhibited by any of the bacterial strains used. Co-cultivation of the different bacteria together with *A. fumigatus* led to a slight inhibition (approximately 1 mm inhibition zone) of fungal growth during cultivation with P_DAPG. For the other two bacterial strains no inhibition was visible. Growth of *V. dahliae* was inhibited by all bacterial strains.

In contrast to results on PDM, the inhibition towards the *Aspergillus* spp. was stronger on pectin-rich SXM. For co-cultivations with *V. dahliae* an inhibition zone without or just minimal fungal growth was observed. During co-cultivation with *Aspergillus* spp. two different zones were detected: zones without fungal growth and zones with less hyphae and conidiophores. On this medium P_phen induced the strongest inhibition on *V. dahliae* (approximately 15 mm) compared to smaller inhibition zones for *Aspergillus* spp. Here, a zone without fungal growth was not observed but in close proximity to the bacterial application site a zone with less hyphae and conidiophores was detected, which had a size of 3 mm ± 0.5 for *A. nidulans* and 7 mm ±0.5 for *A*. *fumigatus*. For the co-cultivation of P_DAPG with *V. dahliae* the inhibition zone had a size of around 8 mm. The zone of inhibition for *A. nidulans* was approximately 3 mm ± 0.4 wide. For *A. fumigatus* two different zones of inhibition were detected: a zone with complete inhibition (approximately 3.6 mm ± 0.6) and a zone with less hyphae and conidiophores (approximately 9 mm ± 1.5). A measurable inhibitory effect of P_rhizo against *A. nidulans* and *A. fumigatus* was not observed on pectin-rich medium.

Taking these results into account, fluorescent pseudomonads seem to be more specific and effective against plant pathogens such as *V. dahliae*, but have also a smaller inhibitory potential on other soil-borne fungi as *Aspergillus* spp., which is stronger on pectin-rich medium in comparison to glucose medium.

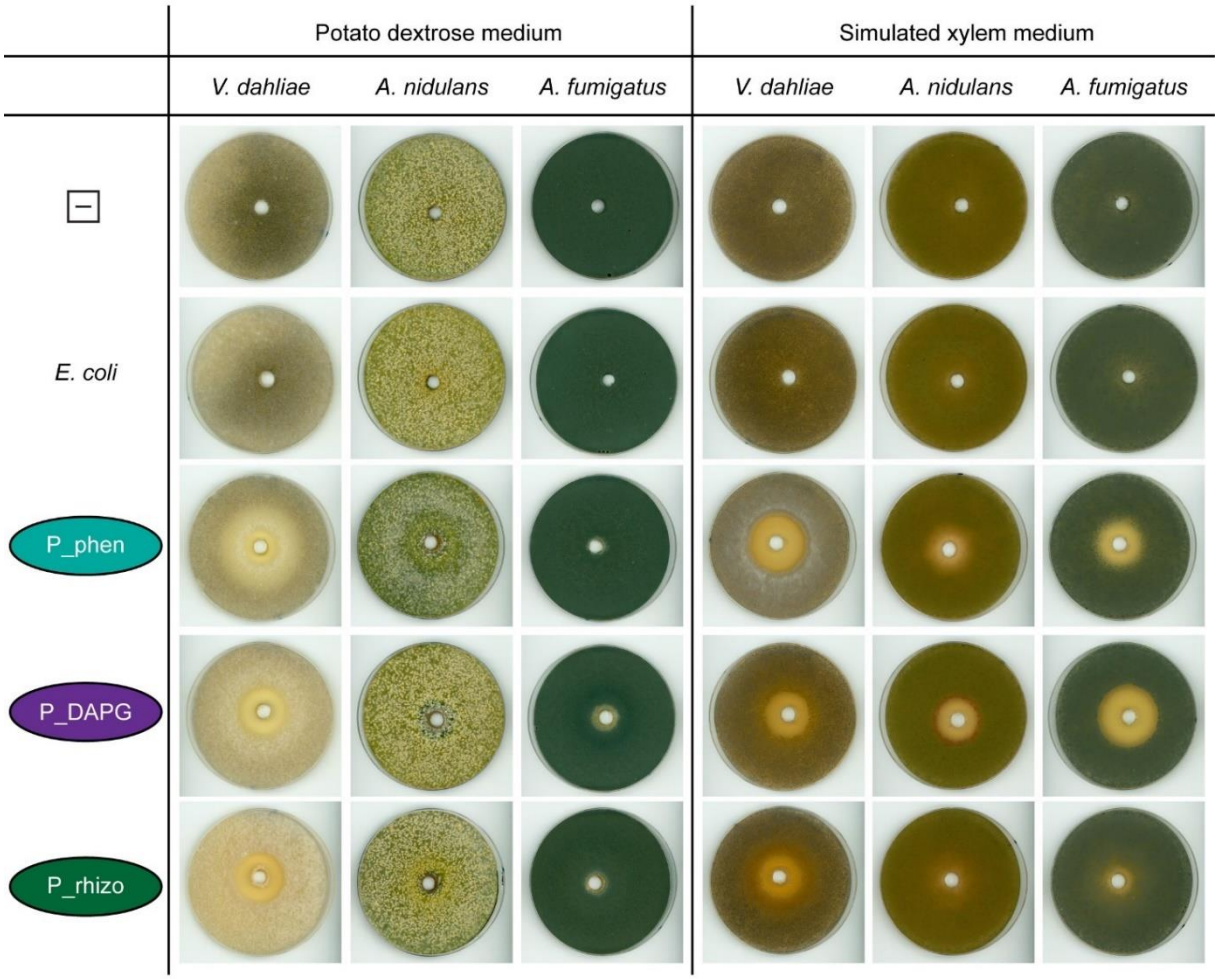

Figure 35: Co-cultivation of *P. synxantha* (formerly *P. fluorescens* 2-79, P_phen), *P. protegens* CHA0 (P_DAPG) and *P. fluorescens* DSM8569 (P_rhizo) with *V. dahliae* wild type JR2, *A. nidulans* wild type A4 and *A. fumigatus* wild type AfS35. Co-cultivation was done on plates of glucose-rich potato dextrose medium (PDM) and pectin-rich simulated xylem medium (SXM). For cultivation $1x10^5$ conidia and $7x10^7$ colony forming units of the respective bacterial culture were used. Incubation of the plates was conducted at 25 °C for four days. As control untreated fungi and *E. coli* were used. The experiment was performed with two biological replicates and three technical replicates each.

3.2.2 *Pseudomonas* strains are able to inhibit fungal spore germination dependent on the culture medium

Verticillium spp. propagate *in planta* by the formation of conidia in the xylem sap. In previous co-cultivation experiments on plate P_phen, P_DAPG and P_rhizo had similar inhibitory effects on *V. dahliae* and *V. longisporum* (Nesemann *et al.*, 2018). Hence, in the following solely *V. dahliae* was examined. In order to investigate if the bacterial strains inhibit fungal growth of *V. dahliae* in liquid medium, bacteria and fungi were co-cultivated in liquid glucose-rich PDM and pectin-rich SXM. Therefore, freshly harvested conidia of *V. dahliae* were co-cultivated with P_phen, P_DAPG and P_rhizo, respectively. After 0, 12, 24, 48, 72 and 96 h, aliquots of the cultures were distributed on plates containing antibiotics to prevent bacterial growth and to examine if the fungus is able to regain growth after co-cultivation with bacteria. As controls

fungus without bacteria and the non-inhibiting bacterium *E. coli* in co-culture with the fungus were used. In glucose-rich medium (PDM) the strongest effect on fungal growth was observed for P_rhizo as the fungus was unable to grow after co-cultivation with the bacterium for 48 h (Table 11). On the contrary, when co-cultivated with P_phen and P_DAPG, the fungus was able to regain growth in some but not all cultivations after co-cultivation of 72 h or 96 h, respectively. These results suggest that P_rhizo is the most efficient bacterium for persistent inhibition of fungal growth on glucose-rich agar. P_phen and P_DAPG are able to inhibit fungal growth but need more time to suppress expansion of the fungus. Cultivation with *E. coli* did not affect fungal growth.

Table 12: Bacterial influence on *V. dahliae* growth in liquid co-cultivation. *P. synxantha* (formerly *P. fluorescens* 2-79, P_phen), *P. fluorescens* DSM8569 (P_rhizo) and *P. protegens* CHA0 (P_DAPG) were co-cultivated with *V. dahliae* either in liquid PDM or SXM for 0, 12, 24, 48, 72 and 96 h, respectively. Aliquots were distributed on PDM and SXM plates containing antibiotics. After incubation for three days at 25 °C fungal growth was observed. Cultures without bacteria (w/o) and with *E. coli* were used as control. Data derived from two independent experiments with three replicates each.

Potato dextrose medium (PDM)					
	w/o bacteria	*E. coli*	P_phen	P_DAPG	P_rhizo
0 h	+	+	+	+	+
12 h	+	+	+	+	+
24 h	+	+	+	+	+
48 h	+	+	+	+	-
72 h	+	+	+/-	+	-
96 h	+	+	+/-	+/-	-
Simulated xylem medium (SXM)					
0 h	+	+	+	+	+
12 h	+	+	+	+	+
24 h	+	+	+/-	+	+
48 h	+	+	-	+	+
72 h	+	+	-	+	+
96 h	+	+	-	+	+

+ = growth in all replicates; - = no growth in all replicates; +/- = growth in some replicates but not all

During co-cultivation in pectin-rich SXM, P_phen, in some cases was able to inhibit fungal growth after as early as 24 h co-cultivation (Table 11). This inhibitory effect was constant after 48 h of co-cultivation. P_DAPG and P_rhizo did not alter fungal growth after co-cultivation in SXM. Cultivation without bacteria or with *E. coli* resulted in normal fungal growth. Bacteria could be re-isolated from aliquots of both media, PDM and SXM. Hence, the fungus did not hinder bacterial growth.The experiments in liquid medium revealed that the bacterium is able to harm the fungus persistently under certain conditions with regard to the medium and the co-cultivation time. Even after removal of the bacterium, the fungus was unable to grow on solid medium. Similarly to the experiments conducted on solid medium (Nesemann *et al.*, 2018), P_rhizo had a strong potential to reduce fungal growth on glucose-rich medium and P_phen was efficient in fungal growth reduction on pectin-rich medium.

4 DISCUSSION

The main novel finding of this thesis is that Vel1 as one of four *V. dahliae* velvet domain proteins is required to colonize and penetrate plant roots, to propagate the fungus in the xylem system and therefore to cause disease symptoms. Another finding is that pseudomonads isolated from the rhizosphere can inhibit germination of *V. dahliae* conidia in a medium dependent manner.

The velvet domain proteins combine the regulation of secondary metabolite production, which is needed when living together with different microorganisms in the soil, and developmental processes, that have to be adjusted due to changing environmental conditions. The role of the *V. dahliae* velvet proteins is diverse and requires for most processes a regulatory interplay of several velvet proteins. The formation of melanized resting structures relies on the presence of Vel1 and light dependent Vel2 as positive regulators and Vel3 as negative modulator. In line with this, the synthesis of melanin precursors and other secondary metabolites is promoted by Vel1 and Vel2 but hindered by Vel3. Conidia formation requires the presence of Vel1 and Vel3. In contrast, only Vel1 seems to have remarkable impact on plant colonization and disease symptom induction *in planta* (Figure 36). The other velvet proteins are not as omnipresent as Vel1, which makes Vel1 a possible target to combat Verticillium wilt.

Pseudomonads and *V. dahliae* are present in the microbiome of the plant rhizosphere. Interactions between bacterium and fungus are likely. Inhibition of vegetative fungal growth on plate was already shown for pseudomonads (Nesemann *et al.*, 2018), however *in planta Verticillium* spp. propagate by the formation of conidia in the xylem sap. In order to elucidate if conidia are also impaired by bacterial metabolites, co-cultivation of fungus and bacterium was conducted in liquid medium, which resulted in a persistent inhibitory effect on conidia germination or even destruction of the conidia (Figure 36). In the rhizosphere the bacteria encounter besides plant pathogenic fungi, such as *V. dahliae*, also saprophytic fungi as for instance *Aspergillus* spp. Growth of *A. nidulans* and *A. fumigatus* was also reduced by the fluorescent bacteria but to a lesser extent than for *V. dahliae*.

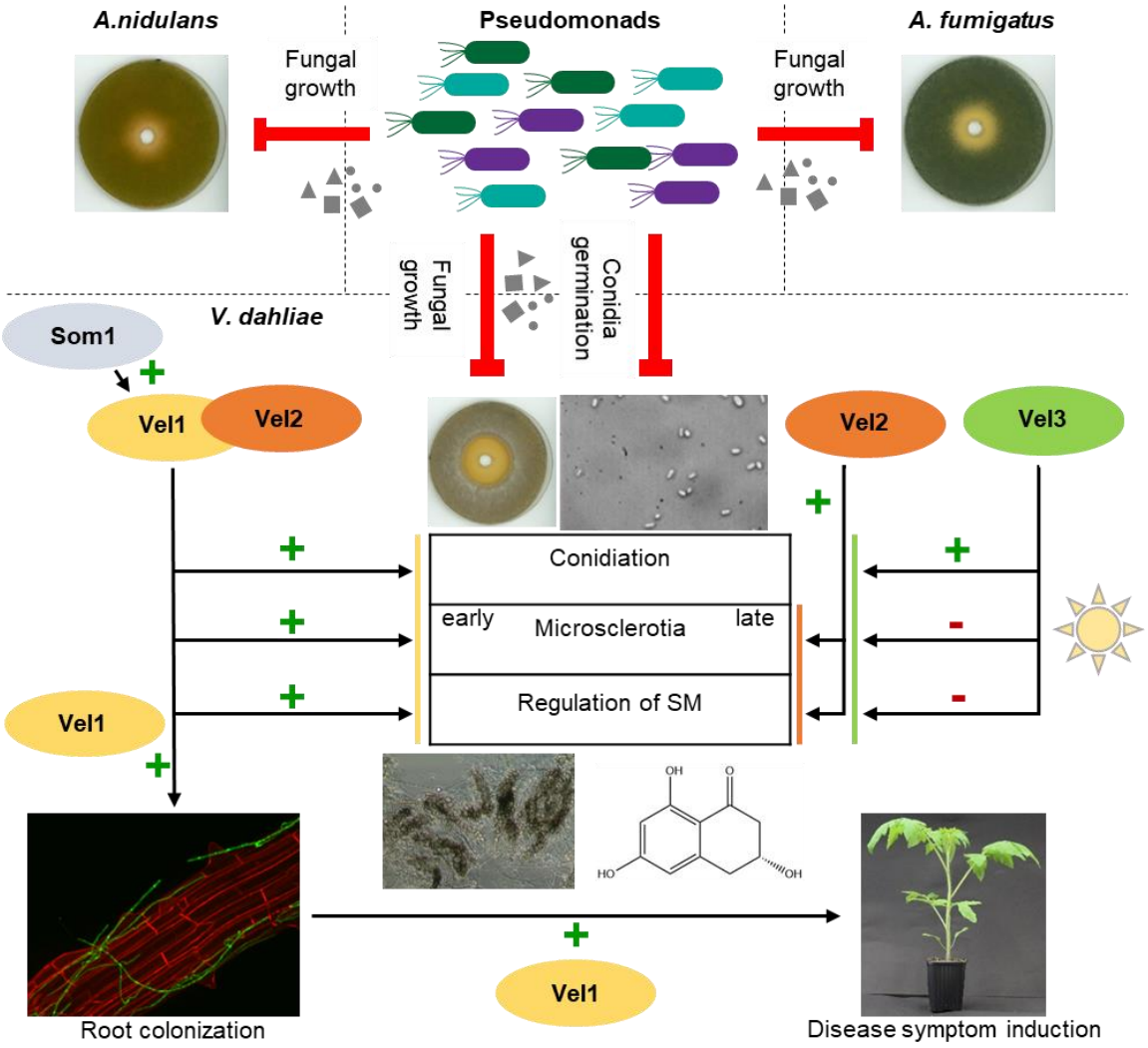

Figure 36: Regulation of *V. dahliae* growth and development by the velvet family of regulatory proteins and fluorescent pseudomonads. Developmental process such as conidiation to propagate within the plant and microsclerotia resting structure formation of *V. dahliae* require velvet domain proteins. Vel1 (yellow) forms a heterodimer with Vel2 during vegetative growth and activates *V. dahliae* conidiation, microsclerotia formation and a specific secondary metabolism (SM). Vel1 is required for initial root colonization, penetration and propagation within the host, which includes conidia formation, resulting in the induction of disease symptoms. Vel1 is positively regulated by Som1 (light grey) (Bui *et al.*, 2019). Vel2 (orange) contributes to a specific SM and is also present during microsclerotia formation when Vel1 is absent and supports resting structure formation in light. Vel3 (green) reduces Vel1 activated SM as well as microsclerotia formation in light, but promotes conidiation. The *Pseudomonas* isolates P_phen, P_DAPG and P_rhizo (indicated in green, purple and blue) secrete different secondary metabolites such as phenazines, DAPG or pyoluteorin (dark grey triangles, circles and squares) that inhibit fungal growth of the plant pathogen *V. dahliae* but also reduce growth of saprophytes as *A. nidulans* and *A. fumigatus*. The bacteria are also able to inhibit germination of *V. dahliae* conidia in liquid medium (red arrow: inhibition, + indicates supportive functions, - reducing functions).

4.1 Velvet domain proteins control different developmental steps of *V. dahliae ex planta* as well as *in planta*

4.1.1 Velvet proteins regulate different developmental steps in *V. dahliae*

The velvet domain proteins are well-studied in *A. nidulans* (Bayram & Braus, 2012). Spores of the fungus germinate and form a mycelium. After reaching developmental competence, this mycelium can either grow or undergo an asexual or sexual developmental program (Bayram & Braus, 2012; Noble & Andrianopoulos, 2013). Environmental conditions, including nutrition, presence of pheromones, light and oxygen supply can trigger asexual conidiation or the formation of closed sexual fruiting bodies named cleistothecia (Bayram & Braus, 2012; Bayram *et al.*, 2016). *A. nidulans* cleistothecia and microsclerotia of *V. dahliae* are both overwintering structures. However, they differ strongly in their appearance and cleistothecia are connected to meiosis and a sexual program, which is not known for *V. dahliae* (Milgroom *et al.*, 2014; Bayram *et al.*, 2016). *A. nidulans* velvet proteins are involved in both developmental programs. In darkness, VeA and VelB activate sexual development and secondary metabolite production (Bayram *et al.*, 2008b). VelC positively influences sexual development, but also controls genes for asexual development (Park *et al.*, 2014). VosA regulates spore viability, trehalose biosynthesis and controls genes for secondary metabolism (Ni & Yu, 2007; Kim *et al.*, 2020). Light is not just a regulator of developmental processes and metabolic pathways but also influences the localization of proteins within the fungal cell (Tisch & Schmoll, 2010; Bayram & Braus, 2012; Kopke *et al.*, 2013). In *V. dahliae* all velvet proteins are predominantly localized to the nucleus and just subpopulations of Vel2 are present in the cytoplasm independently of light (Figure 26). In *A. nidulans* VelB is shuttled to the nucleus in the dark together with VeA and the help of the importin KapA (Bayram *et al.*, 2008b). In contrast, *V. dahliae* Vel2 and Vel1 can enter the nucleus in light as well as in darkness independently from each other.

A. nidulans VelB is a light-dependent regulator of fungal development and secondary metabolism (Bayram *et al.*, 2008b). In general, fungi sense light by photoreceptors, which induce adaptive reactions to environmental conditions (Yu & Fischer, 2019). Processes as for instance conidia germination, vegetative growth, secondary metabolism, pathogenicity and circadian rhythms are controlled by light and are often also affected by changing temperatures (Yu & Fischer, 2019). The circadian system of *N. crassa* is well-studied. Central components of the system are the transcription factors WC-1 and WC-2, which form the White Collar Complex and regulate the expression of the light-regulated *frq* gene (Chen *et al.*, 2010; Dunlap & Loros, 2017; Yu & Fischer, 2019). FRQ induces together with the white collar complex a negative feedback loop to control its own activity (Chen *et al.*, 2010; Dunlap & Loros, 2017).

As *Verticillium* spp. are soil-borne fungi that start infection at the roots, grow into the xylem and colonize the rest of the host, light perception instead of circadian rhythms might be more

important and may be a way to ascertain a position in the soil or *in planta*. However, in *V. dahliae* circadian components as for instance WC-1, WC-2 and Frq are also present (Salichos & Rokas, 2010). Frq was recently investigated in *V. dahliae* (Leonard, 2019; Cascant-Lopez *et al.*, 2020). A deletion strain of *FRQ* induced microsclerotia formation in constant light indicating that Frq acts light-dependently. Incubation of the *V. dahliae* wild type strain in light/dark cycles resulted in a ring-like structure with alternating zones of microsclerotia density suggesting the fungus is able to sense light or darkness (Leonard, 2019). However, this ring-like structure was not visible when the *FRQ* deletion strain was incubated in light/dark cycles due to the enhanced production of microsclerotia (Leonard, 2019). Other studies on Frq indicate that a circadian system in *V. dahliae* is absent as no free-running rhythm was found for developmental processes as conidia and microsclerotia formation and clock genes were not expressed in a circadian rhythm (Cascant-Lopez *et al.*, 2020). Incubation of the *VEL2* deletion strain in changing light conditions revealed differences in microsclerotia production. Therefore, the *V. dahliae* Vel2 function is presumably light-dependent (Figure 12 and 13) and independent from fungal light/dark cycle control as the *VEL2* deletion strain still formed ring-like structures similar to the wild type when incubated in changing light conditions (Figure 14). This suggests that the fungus is still able to distinguish between light and dark when Vel2 is absent.

The Vel2 protein is stabilized during microsclerotia formation in light, which is in accordance with phenotypical observations that it is required for this process (Figure 29 and 30c). This suggests that *V. dahliae* possesses a control system, which increases cellular Vel2 steady state levels during microsclerotia formation in light but decreases them in darkness. Such a control system might regulate the increased protein stability in light in combination with gene expression. In contrast, Vel1 seems to be less stable and might be involved in earlier developmental processes (Figure 29). Protein stability might be controlled by the PEST sequence in Vel1. Formation of a Vel1-Vel2 heterodimer might occur only during early development. Later Vel1 might be degraded but Vel2 is still present and might form a complex with another protein or functions on its own. Previous work in *A. nidulans* shows that the deubiquitinase UspA affects VeA protein amounts (Meister *et al.*, 2019). In line with the early developmental function of *V. dahliae* Vel1*, A. nidulans* VeA degradation occurs within 24 h of development corroborating an initiation function of VeA (Meister *et al.*, 2019).

Similar to Vel1, Vel3 also degrades in the course of time, suggesting it functions in early steps of development. Vel3 also carries a PEST instability region and is destabilized during further development. The Vel3 function in microsclerotia formation is reminiscent to the *A. nidulans* counterpart VelC, which is required during the early phase of fruiting body formation (Park *et al.*, 2014). VelC interacts with VosA, which is epistatic to VelC (Park *et al.*, 2014). For *V. dahliae* no sexual reproduction is known (Milgroom *et al.*, 2014), but our phenotypical analyses showed

that Vel3 functions in conidiation and microsclerotia formation. Although protein interaction studies revealed a connection of *V. dahliae* Vos1 to many proteins, including Vel2 and Vel3, the cellular functions of Vos1 remain elusive. *A. nidulans* VosA is interwoven with many processes (Ni & Yu, 2007; Ahmed *et al.*, 2013; Kim *et al.*, 2020), but VosA of the plant pathogenic fungus *M. oryzae*, seems to be dispensable for development and pathogenicity (Kim *et al.*, 2014), similar to what we observed for *V. dahliae* Vos1.

All velvet domain proteins are present during the early phase of conidiation. Only Vel1 and Vel3 are directly involved in the production of conidia. It might be possible that the fungus initially induces the expression of several proteins after reaching developmental competence in order to be prepared for different developmental processes. The proteins not involved in conidiation might be required for other processes happening at the same time. One of these processes could be the regulation of secondary metabolites for conidia of *V. dahliae*. Vel1, Vel2 and Vel3 are involved in secondary metabolism, presumably also during conidiation. So far, research regarding secondary metabolites in *V. dahliae* conidia is scarce. *A. fumigatus* produces five main secondary metabolites in spores: tryptoquivaline F, fumiquinazole C, and the toxic substances questin, monomethylsulochrin and trypacidin (Gauthier *et al.*, 2012). The fungus also produces different secondary metabolites as for instance melanin to protect its conidia from the environment (Chai *et al.*, 2010; Kyrmizi *et al.*, 2018; Blachowicz *et al.*, 2020). Germinating conidia of the opportunistic pathogenic fungus *A. terreus* also contain proteins connected to secondary metabolite production and synthesis of mycotoxins, suggesting the presence of different metabolites during spore germination (Thakur & Shankar, 2017). Spores of *Aspergillus* spp. are distributed by air or water and are therefore exposed to the environment, which makes protective secondary metabolites helpful (Bayram & Braus, 2012; Bayram *et al.*, 2016). The conidia of *V. dahliae* have a different function and are mainly produced in the plant where they are distributed by the xylem and are not able to live in the soil for a long time (Fradin & Thomma, 2006; Klosterman *et al.*, 2009). Distribution of conidia by air requires other properties of the spore and its cell wall than distribution by the xylem sap and might therefore lead to the presence of other secondary metabolites remaining to be identified. *V. dahliae* Vos1 could not be connected to secondary metabolism so far. If there is a specific function in secondary metabolism associated with development has to be investigated as well.

4.1.2 *V. dahliae* velvet proteins coordinate resting structure formation with melanin biosynthesis

The fungus remains in the plant after a successful infection until the host dies. Microsclerotia as long-term resting structures are formed. This developmental program allows that the fungus can survive in the soil until the next growing season of appropriate host plants. Vel1 and Vel2

are positive regulators of microsclerotia formation, whereas Vel3 is a negative regulator of resting structure production. Microsclerotia contain the pigment melanin, a secondary metabolite, which enables the fungus to overcome difficult environmental conditions (Eisenman & Casadevall, 2012; Wang *et al.*, 2018; Fan *et al.*, 2020). Secondary metabolite analyses of different velvet strains revealed that Vel1 and Vel2 positively influence the formation of the melanin precursor scytalone whereas Vel3 negatively effects scytalone production. This result corroborates the phenotype on plate as *VEL1* and *VEL2* deletion strains are hindered in microsclerotia production and Δ*VEL3* shows stronger melanization than wild type. The regulatory connection between the velvet proteins and other modulators of the melanin synthesis remains elusive. Several regulators have been described to control melanin production in *V. dahliae*. A transcription factor, which coordinates secondary metabolism in *V. dahliae* is the MADS-box transcription factor Mcm1. Moreover Mcm1 is involved in diverse processes including conidiation, microsclerotia formation and required for virulence (Xiong *et al.*, 2016). The transmembrane protein Sho1 is needed for melanin biosynthesis and plant penetration (Li *et al.*, 2019). The response regulator Ssk1, which responds to external signals, is required for the regulation of genes for melanin biosynthesis. In addition, this protein is involved in stress response and virulence (Zheng *et al.*, 2019). In the plant pathogenic fungus *B. cinerea* VEL1 differentially regulates expression of secondary metabolite related genes as *pks12*, which is involved in melanogenesis and less expressed if *VEL1* is absent (Schumacher *et al.*, 2014, 2015). This indicates that the Vel1 function in melanogenesis is conserved.

The *VEL2* deletion strain is hindered in microsclerotia formation but dispensable for conidiation and induces similar disease symptoms in the plant as observed for the wild type, suggesting that microsclerotia production and virulence are independent from each other in *V. dahliae*. Deletion strains of *VEL1* and *VEL2* are both impaired in formation of the melanized resting structure. Melanin contributes significantly to the long-time survival of the fungus (Fan *et al.*, 2020), assuming that both strains would be unable to survive as inoculum in nature. However, it has to be considered that plant infection studies were conducted with spore suspensions and not with microsclerotia, which are the natural inoculum. Though, the role of melanin in *V. dahliae* pathogenicity is controversial as some studies in pigment mutants revealed less virulence, but others observed no effect. *V. dahliae* Vayg1 is required for melanin biosynthesis, but also needed to produce microsclerotia and induce virulence (Fan *et al.*, 2017). An effect on virulence of *V. dahliae* in lettuce and tobacco for the melanin deficient *PKS1* deletion strain could not be detected (Wang *et al.*, 2018). Another study using cotton as host described that Pks1 is required for virulence (Zhang *et al.*, 2017b). The hydrophobin gene *VDH1* in *V. dahliae* is involved in microsclerotia production but dispensable for virulence in tomatoes (Klimes & Dobinson, 2006). For *VTA1* and *CMR1 V. dahliae* deletion strains, which are deficient in

melanin but not in microsclerotia production, no impact on virulence was found (Wang *et al.*, 2018; Harting *et al.*, 2020).

Often strains with defects in melanin formation and pathogenicity had additional phenotypical alterations. *V. dahliae VAYG1* deletion strains are additionally impaired in root attachment, penetration as well as colonization (Fan *et al.*, 2017). Vta3 and Som1 are needed for microsclerotia formation and are involved in pathogenicity of *V. dahliae* but they are also required for root colonization, conidiation and involved in oxidative stress response (Bui *et al.*, 2019). In contrast to that, the rice blast disease inducing fungus *M. oryzae* requires melanin in its appressoria to induce pathogenicity. The mutants *AP1* and *MET13* in *M. oryzae* are impaired in pigmentation and pathogenicity (Guo *et al.*, 2011; Yan *et al.*, 2013). Deletion of velvet genes in *M. oryzae* did not alter melanin production but deletion of *VEA* led to reduced virulence and defects in appressorium formation indicating that not just melanin contributes to virulence of this fungus (Kim *et al.*, 2014). A similar connection between pathogenicity and appressorium development was not just stated for *Magnaporthe* spp., but also for *C. graminicola* and *Venturia inaequalis*, which require melanin in their appressoria for successful penetration and infection (Howard & Ferrari, 1989; Steiner & Oerke, 2007; Ryder & Talbot, 2015). Appressoria of *M. oryzae* seem to require melanin for structural reasons and turgor generation as melanin represses leakage of solutions such as glycerol during the infection process (Scharf *et al.*, 2014; Ryder & Talbot, 2015). In contrast, for *B. cinerea* a connection between pathogenicity and melanin was not found as melanin is dispensable for virulence (Schumacher, 2016). However, melanin is not just involved in virulence of plant pathogenic fungi but also connected to pathogenicity of the human opportunistic pathogen *A. fumigatus* where melanin protects fungal spores from the immune system of the host (Scharf *et al.*, 2014).

V. dahliae does not form appressoria, which are simplified germ tubes of spores, but hyphopodia, which are the swollen tips of hyphae (Reusche *et al.*, 2014; Zhao *et al.*, 2014; Ryder & Talbot, 2015). Melanin is most likely not required for hyphopodia formation of *V. dahliae*, which might be the reason why strains deficient in melanogenesis or microsclerotia formation are still able to induce wild type-like disease symptoms as observed for the deletion strain of *VEL2*.

4.1.2.1 Regulation of other *V. dahliae* secondary metabolites is coordinated by velvet proteins independently of light

Besides the putative melanin precursor, another metabolite regulated by Vel1 and Vel2 was likely identified as an intermediate in the production of 6-methoxymellein, which might harm plant cells similar to terrein of *A. terrreus* (Marinelli *et al.*, 1996; Zaehle *et al.*, 2014). Not much is known about the biosynthetic pathway of terrein, but the presence of a gene cluster is

described (Zaehle *et al.*, 2014). BLAST search of the deduced protein sequences identified proteins in *V. dahliae* with similar predicted functions as for *A. terreus* and an amino acid identity between 26 and 69 % (Table 12). This leaves the possibility, that *V. dahliae* can produce a similar substance. It is also possible that this substance contributes to *V. dahliae* virulence. However, this contribution might be minor as the Δ*VEL2* strain is impaired in the production of this metabolite but induces strong disease symptoms.

Table 13: Comparison of deduced protein sequences from the terrein gene cluster of *A. terreus* with best hits in *V. dahliae*. Indicated are the accession numbers, the names and putative function of the proteins associated with terrein synthesis in *A. terreus* (Zaehle *et al.*, 2014). Best hits from *V. dahliae*, their predicted domains and protein identity to *A. terreus* are shown.

A. terreus			***V. dahliae***		**Protein identity (%)**
Accession number	**Name**	**Putative function**	**Best hit**	**Predicted domain**	
ATEG_00135	*terJ*	Major facility transporter (MFS)	VDAG_JR2_Chr3g12960a	MFS transporter superfamily	26.3
ATEG_00136	*terI*	Protein of superfamily of bleomycin resistance protein, glyoxalase I, and type I ring-cleaving dioxygenases	VDAG_JR2_Chr3g10270a	Glyoxalase/Bleomycin resistance protein/ Dihydroxybiphenyl dioxygenase	36.1
ATEG_00137	*terH*	NAD dependent epimerase/dehydratase	VDAG_JR2_Chr5g08010a	NAD-dependent epimerase/dehydratase	44.4
ATEG_00138	*terG*	Major facility transporter (MFS)	VDAG_JR2_Chr8g03000a	MFS transporter superfamily	27.7
ATEG_00139	*terR*	Zn_2Cys_6 transcriptional regulator	VDAG_JR2_Chr4g03300a	Zn(2)-C6 fungal-type DNA-binding domain	40.0
ATEG_00140	*terF*	Protein with kelch motif	VDAG_JR2_Chr1g13270a	Kelch-type beta propeller	33.3
ATEG_00141	*terE*	Multicopper oxidase	VDAG_JR2_Chr1g15860a	Multicopper oxidase	30.6
ATEG_00142	*terD*	FAD dependent monooxygenase	VDAG_JR2_Chr5g05570a	FAD-binding domain	48.3
ATEG_00143	*terC*	FAD dependent monooxygenase	VDAG_JR2_Chr5g08080a	P-loop containing nucleoside triphosphate hydrolase	30.2
ATEG_00144	*terB*	DH-KR, multidomain protein with dehydratase and ketoreductase function	VDAG_JR2_Chr8g10310a	Alcohol dehydrogenase, Beta-ketoacyl synthase	30.3
ATEG_00145	*terA*	Non-reducing polyketide synthase	VDAG_JR2_Chr1g15880a	Polyketide synthase	69.3

Subcellular localization and complex formation of velvet domain proteins in *A. nidulans* is regulated by light. Conclusively, the formation of secondary metabolites is also influenced by illumination (Bayram *et al.*, 2008b). In *V. dahliae* the ability to form secondary metabolites was not altered when the wild type or *VEL1* and *VEL2* deletion strains were incubated either in light or in darkness. Moreover, the subcellular localization of velvet proteins was not affected by illumination. Hence, velvet protein associated secondary metabolism and localization of the

velvet domain proteins are independent from light in *V. dahliae*. This is in accordance with the microsclerotia production of the wild type strain during incubation in light and darkness. However, the *VEL2* deletion strain also produces small amounts of microsclerotia in darkness especially on SXM, but still less than wild type. Secondary metabolites were isolated from minimal medium supplemented with glucose, where microsclerotia production in general is decreased compared to SXM. This might explain the similar metabolite pattern of the *VEL2* deletion strain during incubation in light and darkness.

The methyltransferase LaeA regulates secondary metabolism in *Aspergillus* spp. as deletion of *A. nidulans laeA* reduces the production of the aflatoxin precursor sterigmatocystin and deletion of *laeA* in *A. fumigatus* decreases the production of the immunotoxin gliotoxin (Bok & Keller, 2004; Bayram *et al.*, 2008b). Homologs of the LaeA encoding gene are also connected to secondary metabolism in plant pathogens as for example *B. cinerea* LAE1 influences secondary metabolite connected gene expression and *F. oxysporum* LaeA promotes production of the mycotoxin beauvericin (López-Berges *et al.*, 2013; Schumacher *et al.*, 2015). In contrast, *V. dahliae* Lae1 is dispensable for secondary metabolite production under the tested conditions. Silencing of *LAE1* in *V. longisporum* reduced the pathogenicity towards its host plant *B. napus*. In contrast, deletion of *LAE1* in *V. dahliae* was dispensable for virulence on tomato plants (Timpner, 2013). In *Verticillium* spp. several methyltransferase domain containing proteins are present. These might have been co-silenced in *V. longisporum*, which could explain the reduced pathogenicity of the *LAE1* silencing strain (Timpner, 2013).

The other Lae1-like methyltransferases might have redundant functions. Deletion of the *LAE1* gene was therefore negligible for pathogenicity of *V. dahliae*. However, analysis of secondary metabolite core genes is different *in vitro* and *in planta* assuming that the secondary metabolite pattern might change during plant infection as other metabolites could be required during this step (Shi-Kunne *et al.*, 2019). Consequently, *V. dahliae* Lae1 might be required under different conditions than the tested ones.

4.1.2.2 *V. dahliae* velvet proteins are involved in repression of secondary metabolite forming genes

The connection between developmental processes and production of secondary metabolites was found in numerous fungal species with velvet domain proteins identified as central regulators (Calvo *et al.*, 2004; Duran *et al.*, 2007; Bayram *et al.*, 2008b; Dhingra *et al.*, 2012; Kopke *et al.*, 2013; López-Berges *et al.*, 2013; Schumacher *et al.*, 2015; Wu *et al.*, 2018; Sarikaya-Bayram *et al.*, 2019). The influence on secondary metabolite production makes the velvet domain proteins possible switches for genetic manipulation in order to find new metabolites with antibiotic activity, which is an urgent need due to increasing resistances arising from the frequent and irrational use of antibiotics (Frieri *et al.*, 2017; Machowska &

Stålsby Lundborg, 2019). Deletion of *VEL1* results in the production of so far unidentified secondary metabolites (Figure 18a, Table 8 and 9). Purification of these substances and investigation of their bioactivity towards different fungi and bacteria might hint to their applicability as new antibiotic or antimycotic.

In *Aspergillus* spp. co-cultivation with bacteria induces the expression of silent gene clusters associated with secondary metabolite production (Schroeckh *et al.*, 2009; König *et al.*, 2013; Netzker *et al.*, 2015). *V. dahliae* is also able to produce secondary metabolites. However, there were no hints that co-cultivation of *V. dahliae* with different fluorescent pseudomonads did alter bacterial growth. This suggests that either no compounds were produced, metabolites that were produced did not harm the bacteria or concentrations were too low to have an effect. Other studies showed that co-cultivation of fungi and bacteria alters the metabolism of both interaction partners (Benoit *et al.*, 2015). The fluorescent pseudomonads used in this study are assumed to produce different metabolites with antagonistic activity (Nesemann *et al.*, 2018) and absence of Vel1 results in formation of secondary metabolites that are not produced in the *V. dahliae* wild type strain. Taking this into account, a combination of both, namely co-cultivation of bacteria with velvet deletion strains, might result in the production of even different metabolites being a possible source for new antibiotics.

4.1.3 *V. dahliae* velvet proteins interact with velvet and non-velvet proteins during filamentous growth

4.1.3.1 The formation of velvet heterodimers is conserved between *A. nidulans* and *V. dahliae*

Hyphae grow vegetatively into the direction of the host plant after germination of a *V. dahliae* microsclerotium. In this filamentous growth phase, all velvet proteins are present. The velvet domain functions in protein-protein homo- and heterodimer formation allowing distinct specific roles in the regulation of developmental processes and secondary metabolite production (Bayram & Braus, 2012; Sarikaya-Bayram *et al.*, 2015). *A. nidulans* VosA is required for spore viability and survival as well as correct secondary metabolism of ascospores (Ni & Yu, 2007; Ahmed *et al.*, 2013; Kim *et al.*, 2020). Our interaction studies showed that Vos1 is associated with Vel2, Vel3 and 23 other proteins. However, the processes *V. dahliae* Vos1 might be involved in, remain elusive. Proteins enriched using Vos1 as bait were often associated with transport processes and energy metabolism, which does not allow concrete conclusion on Vos1 function.

VeA-VelB, VelB-VosA and VelC-VosA interactions are known from *A. nidulans* (Bayram *et al.*, 2008b; Sarikaya-Bayram *et al.*, 2010; Park *et al.*, 2012b, 2014). Additional non-velvet domain interactions include epigenetic methyltransferases such as LaeA or VapB-VipC (Bayram *et al.*,

2008b; Sarikaya-Bayram *et al.*, 2014, 2015). Heterodimers of Vel1-Vel2, Vel2-Vos1 and Vel3-Vos1 were also found in this study in *V. dahliae* but interactions with putative epigenetic methyltransferase are yet missing and it is currently unclear whether they exist during specific environmental growth conditions or after induction of specific developmental programs. The interaction between VeA, VelB and LaeA is not only described for *A. nidulans*. Yeast-two hybrid experiments in *A. flavus* revealed that both, VelB and LaeA, are connected to VeA suggesting that these interactions are conserved in *Aspergillus* spp. (Chang *et al.*, 2013). In the model fungus *N. crassa* the presence of a trimeric VE-1/VE-2/ LAE-1 complex was verified (Sarikaya-Bayram *et al.*, 2019) and the formation of a complex consisting of VEL1, VEL2 and LAE1 is also suggested for the plant pathogenic fungus *B. cinerea* (Schumacher *et al.*, 2015). Taking these results into account, one could have expected to find this complex to be conserved also in *V. dahliae*. The protein interactions in *V. dahliae* were examined in cultures incubated in constant light, but in *A. nidulans* the formation of the trimeric velvet complex happens mainly in darkness (Bayram *et al.*, 2008b). The velvet domain proteins of *V. dahliae* revealed a light-independent predominantly nuclear localization, suggesting that velvet complex formation might be possible in light as well as in darkness. Moreover, all velvet domain proteins were expressed in glucose-rich medium under the examined point of time. Subcellular localization and protein expression of Lae1 were not investigated during this study. Hence, it might be possible that absence of Lae1 under the tested conditions might be the reason for the missing complex in *V. dahliae*. The trimeric velvet complex regulates developmental processes in other fungi (Bayram *et al.*, 2008b; Sarikaya-Bayram *et al.*, 2019). During this study, solely vegetative growth was investigated leaving the possibility that the complex might be present under different growth conditions.

VEL1 and *VEL2* deletion strains exhibit the same phenotype regarding microsclerotia formation and show similarities in secondary metabolism, which further supports a common function of a Vel1-Vel2 heterodimer. Potential interaction partners of Vel1 were in most cases also interacting with Vel2. Vel1 and Vel2 are both interacting with VDAG_JR2_Chr5g09190a. The corresponding gene is a homolog of the *N. crassa* gene encoding HAM-13, which is phosphorylated by MAK-2 as part of a mitogen-activated protein kinase signaling pathway and important for fungal communication (Dettmann *et al.*, 2014). It remains to be shown if a corresponding complex consisting of this protein together with Vel1 and Vel2 coordinates developmental processes, interaction with host cells and signaling in *V. dahliae*. Furthermore, Vel1 as well as Vel2 interact with a haem peroxidase (VDAG_JR2_Chr6g10140a). During the infection process of a plant host, plant pathogens have to cope with an increased production of ROS induced by the plant as defense mechanism (Camejo *et al.*, 2016). Incubation of *V. lonigsporum* in the xylem sap of its host plant *B. napus* induced the expression of genes encoding oxidative stress response proteins including a catalase peroxidase. The initial phase

of plant infection was unaffected in deletion strains of the catalase peroxidase but not the late phase. The protein is presumably required to protect the fungus against oxidative stress during this stage (Singh *et al.*, 2012). V*. nonalfalfae* also secretes increased amounts of a peroxidase during infection of hop. Deletion of the peroxidase resulted in decreased virulence indicating that it has a role in fungal virulence (Flajsman *et al.*, 2016). A connection of Vel1 and Vel2 to a haem peroxidase under non-stress conditions was identified. This connection might be useful as Vel1 is involved in the early phase of plant root colonization. Together the Vel1-Vel2 heterodimer might be only present in the early stages of developmental programs. The interaction of Vel1 and the haem peroxidase might be more important for pathogenicity as absence of Vel2 still allows wild type-like disease symptom induction in the plant.

Vel2 co-purified most putative interaction partners among the examined velvet proteins indicating that it is connected to many processes, which are often associated with metabolism (Table A3). Vel2 as bait enriched a protein involved in thiamine metabolism (VDAG_JR2_Chr4g11880a). Thiamine biosynthesis is related to stress response in *V. dahliae* and involved in disease induction in tomato plants (Hoppenau *et al.*, 2014). Plant infection experiments with the *VEL2* deletion strain led to a similar disease severity as observed for the wild type indicating that Vel2 interactions might be dispensable for the plant infection.

These results revealed that most developmental processes of *V. dahliae* require a regulatory interplay of several velvet domain proteins. The possible interaction of the velvet domain regulators with proteins linked to metabolism was a novel finding as velvet proteins are mainly suggested to function as transcription factors (Ahmed *et al.*, 2013; Sarikaya-Bayram *et al.*, 2015). Interactions have to be further verified and the function has to be elucidated. In addition, interactions that might occur during different developmental processes should be analyzed in the future.

4.1.3.2 The intrinsically disordered domain of Vel2 is needed for protein interactions

Intrinsically disordered proteins are highly dynamic in their structure and therefore considered as central point for different interactions leading to various outcomes (Wright & Dyson, 2015). *V. dahliae* Vel2 is a protein containing an intrinsically disordered domain (Thieme, 2018) (Figure 9a). In this study, we could show that it interacts with several proteins involved in diverse metabolic processes. Deletion of the *VEL2 IDD* alters the interaction pattern with other proteins and reduces the overall number of significant interactions drastically by approximately 80 %. Vel1 is still co-purified with Vel2$^{\Delta IDD}$-GFP but the significant interaction with Vos1 gets lost when using Vel2$^{\Delta IDD}$ as bait. These results lead to the suggestion that protein interactions do not only take place at the velvet domain but also require the IDD.

It might be possible that Vel2 with an intact IDD accurately fits to the binding site of a partner. In contrast, Vel2 without IDD might have an altered structure, which does not bind properly to other proteins maybe due to reduced flexibility of a different spatial arrangement. The interaction between Vel1 and Vel2 is still present when the IDD is deleted suggesting it might be an important connection because both proteins are involved in microsclerotia formation and secondary metabolite production. The IDD of Vel2 is also involved in microsclerotia production, however the strain without IDD is still able to produce smaller amounts of the resting structures. This leads to the suggestion that the Vel1-Vel2 heterodimer formation is not as strong as in the wild type or requires the presence of another interaction partner.

In contrast, the function of the Vel2-Vos1 heterodimer in *V. dahliae* is unknown leading to the assumption that minor relevant interactions require the presence of the IDD. However, the VelB-VosA heterodimer in *A. nidulans* is known to be important during spore viability, trehalose biosynthesis and repression of asexual sporulation during unfavorable conditions (Park *et al.*, 2012b; Sarikaya-Bayram *et al.*, 2015) but the heterodimer is also absent if the IDD of VelB is deleted (Thieme, 2018). Hence, one could speculate if other dimers might fulfil the function of the VelB-VosA interaction as the viability of spores in *A. nidulans* was not altered when the heterodimer was absent (Thieme, 2018). There were no hints that viability of spores was impaired in the *V. dahliae VOS1* deletion strain. When comparing the significant interaction partners of Vel2 and Vel2$^{\Delta IDD}$, the proteins specifically enriched with the mutated version of the protein were not only fewer but also five new potential interactors were identified. These proteins have putative functions in transport, proteolysis, and metabolism. In *A. nidulans* deletion of the VelB IDD resulted in 32 putative interaction partners, which were not found when VelB was used as bait. In contrast, only three putative interaction partners were identified when VelB was used as bait (Thieme, 2018). Comparison of the proteins enriched in *A. nidulans* and *V. dahliae* revealed no homologous proteins but in both fungi proteins with functions in metabolic processes were enriched. Summarizing, the IDD in both fungi alters the putative interaction profile.

Intrinsically disordered proteins are also present in tardigrades, which are microscopic animals and able to survive extreme conditions as for instance desiccation, freezing and external salinity (Møbjerg *et al.*, 2011; Boothby *et al.*, 2017). During stress induced by dehydration, the expression of intrinsically disordered proteins is constitutively increased indicating these proteins are required during desiccation and enable tardigrades to survive harsh conditions (Boothby *et al.*, 2017). Intrinsically disordered proteins are often posttranslationally modified for example by phosphorylation or alternatively spliced, which alters the protein confirmation, function and interactions to other proteins (Flock *et al.*, 2014; Wright & Dyson, 2015; Thieme, 2018). It might be possible that specific environmental conditions such as stress or a different developmental program lead to the modification of the IDD in *V. dahliae* as for instance by

phosphorylation (Figure 37). As consequence, the protein structure might be changed leading to altered accessibility of the velvet domain and/or IDD for interaction partners. Hence, the interaction profile of Vel2 might also change in connection to environmental requirements.

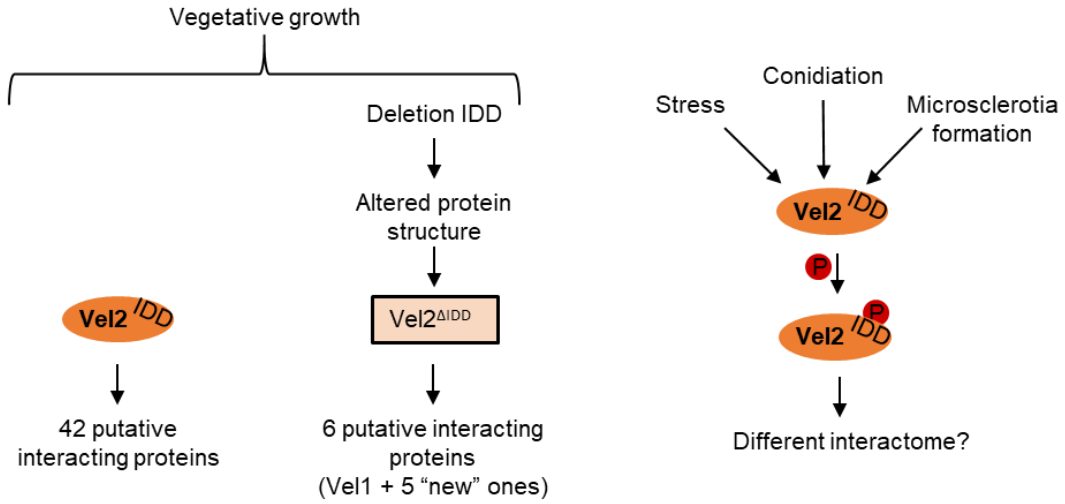

Figure 37: Environmental condition induced changes in the interactome of *V. dahliae* Vel2. During vegetative growth 42 proteins were enriched in interaction studies with Vel2 as bait. Deletion of the *VEL2 IDD* leads to a different interaction pattern. Vel1 was still identified as putative interacting protein of Vel2$^{\Delta IDD}$ and five proteins that were not found in the Vel2 strain were enriched as well. Considering this it might be possible that stress or different developmental programs as for instance conidiation or formation of microsclerotia induce posttranslational modifications of the IDD as for instance by phosphorylation (indicated by red circle), which alters the protein structure and accessibility to the velvet domain and maybe also to the IDD leading to changes in the interactome.

4.1.4 *V. dahliae* Vel1 is a central regulator of pathogenicity related processes

The vascular fungal pathogen *Verticillium* enters its host via the roots and later colonizes the whole plant (Fradin & Thomma, 2006; Klosterman *et al.*, 2009). Prerequisites are host sensing and microsclerotia germination in the soil followed by directed fungal hyphal growth to reach the rhizosphere of a susceptible plant root. During vegetative growth, all velvet proteins are detectable in the cell and the formation of different velvet protein dimers occurs. In the plant rhizosphere, root colonization by the fungus is the first step for a successful infection. At this stage, Vel1 is needed to form hyphopodia and to enter the vascular tissue. Hyphae of the *VEL1* deletion strain were often dead or looked vacuolized indicating fitness problems. Previous studies showed, that root colonization depends on fungal adhesion (Tran *et al.*, 2014; Bui *et al.*, 2019).

A screen with a non-adhesive yeast revealed the presence of six genes required for adhesion, which were named *Verticillium* transcription activator of adhesion (Vta) (Tran *et al.*, 2014). Root infection studies with deletion strains of *VTA2* and *VTA3* showed that both genes are needed for a successful colonization (Tran *et al.*, 2014; Bui *et al.*, 2019). In contrast, Vta1 is dispensable for plant infection and root colonization but needed to produce melanized

microsclerotia (Harting *et al.*, 2020). Another gene involved in regulation of adhesion in *V. dahliae* and the human opportunistic pathogen *A. fumigatus* is *SOM1* (Lin *et al.*, 2015; Bui *et al.*, 2019). *V. dahliae* Som1 is required for plant root penetration, proliferation and controls expression of *VEL1* (Bui *et al.*, 2019). A regulatory connection between adhesion regulators and velvet proteins, especially Vel1, is probably required for plant penetration and colonization. The *VEL1* deletion strain is unable to form hyphopodia and colonize the plant root. Fungal entry into the host can be facilitated if the root is damaged. Parasitic nematodes often feed on roots and thereby make an infection with *V. dahliae* easier (Fradin & Thomma, 2006). The *VEL1* deletion strain is able to enter wounded tomato roots in some cases. If the plant roots are already harmed by nematodes, the disease is often more severe (Back *et al.*, 2002). Reasons for this are the increase of easily accessible fungal penetration sites, leakage of root exudates that attract fungi as well as stimulate germination of microsclerotia and changes in xylem sap composition that enhance germination of conidia (Back *et al.*, 2002; Katsantonis *et al.*, 2005; Fradin & Thomma, 2006).

Pathogens, such as *Verticillium* spp., which colonize the plants xylem vessels and thereby inducing wilting, have to cope with the composition of the xylem sap, which is unfavorable. It contains mineral nutrients, peptides, proteins and hormones but can vary during stress and non-stress conditions (Singh *et al.*, 2010; Carella *et al.*, 2016). In *V. longisporum* silencing of the chorismate synthase Aro2 that catalyzes the last common step of the biosynthesis of the three aromatic amino acids, leads to reduced plant infection efficiency. This suggests that secondary metabolites, which are derivatives of aromatic amino acids, are decreased (Singh *et al.*, 2010). Deletion of *VEL1* leads to reduced plant infection capacity and changes in the secondary metabolite pattern of the fungus supporting the idea that secondary metabolites might enhance fungal infection success.

A set of genes is involved in colonization of the xylem sap in wilt inducing pathogens (Klosterman *et al.*, 2011). Among them is a glucan glucosyltransferase (GT, VDAG_02071), which might be used to maintain the osmotic stability in the xylem vessels. Pathogenicity tests in *Nicotiana benthamiana* revealed a slower disease induction in plants inoculated with the deletion strain. The gene is likely a virulence factor important for the aggressiveness of *V. dahliae* (Klosterman *et al.*, 2011). *V. longisporum* is well-prepared to live in the nutrient-poor xylem sap. The chorismate synthase Aro2 is needed to produce the three aromatic amino acids phenylalanine, tyrosine, tryptophan and their derivatives. Silencing of this gene in *V. longisporum* led to induction of the cross-pathway transcriptional activator Cpc1. The expression of this bZIP transcription factor is translationally controlled and is low during non-starvation conditions and induced during growth *in planta*, where amino acids are scarce (Singh *et al.*, 2010). The Cpc1 protein allows *V. longisporum* to assemble all required amino acids during unbalanced amino acid conditions. Further research confirmed the importance of

Cpc1 for *V. longisporum* as well as *V. dahliae* in amino acid production and pathogenicity (Timpner *et al.*, 2013). Vel1 is involved in many developmental processes, secondary metabolite production and pathogenicity. A connection to other cellular regulators in order to control these processes is likely even though the exact target genes are not identified so far.
V. dahliae Vel1 is required for root colonization and disease induction *in planta* (Figure 31 and 34). The expression of pathogenesis-related genes has to be well-organized as a high number of genes is involved in the infection process. One example in this network is the transcription factor FTF1, which contains a Fungal_trans domain known to regulate cellular and metabolic processes in other fungal transcription factors (Zhang *et al.*, 2018). FTF1 had no impact on fungal growth or conidiation but RNA-seq analysis and qRT-PCR exhibited a role in expression of pathogenesis-related genes and several plant cell wall degrading enzymes. Consequently, FTF1 is required for virulence in cotton (Zhang *et al.*, 2018). Another regulator for cell wall degrading enzymes is the sucrose nonfermenting 1 gene *(SNF1*). Deletion of the encoding gene also led to reduced virulence of *V. dahliae* as well as defects in root colonization (Tzima *et al.*, 2011). The secreted effector SnodProt1-like protein CP1 of *V. dahliae* is a member of the cerato-platanin protein (CPP) family (Zhang *et al.*, 2017a). The filamentous fungal specific CPPs are small and secreted proteins that interact with other organisms and thereby often function as elicitors or virulence factors (Gaderer *et al.*, 2014). CP1 deletion strains were less pathogenic than the wild type strain in cotton and CP1 was even able to induce resistance towards *B. cinerea*, *Pseudomonas syringae* pv. tabaci and *V. dahliae* in plants treated with the purified protein. Due to the fact that the deletion strain was more sensitive to chitinase treatment this effector may guard the fungal cell wall from degradation (Zhang *et al.*, 2017a).
In several fungal species, velvet proteins have been described to influence pathogenicity. In the apple pathogen *V. mali* VeA and VelB negatively regulate conidiation; VeA and to a smaller extent also VelB reduce virulence (Wu *et al.*, 2018). In *F. oxysporum* f. sp. *lycopersici* VeA is crucial for virulence in mammals and plants whereas VelB is only involved in plant virulence (López-Berges *et al.*, 2013). In *F. oxysporum* f. sp. *cucumerinum Vel1* is also associated with reduced conidiation and virulence (Li *et al.*, 2015). *B. cinerea* VEL1 is required for full virulence as it is needed during the phase of plant tissue colonization but not required in the early infection during penetration of host cells (Schumacher *et al.*, 2012). *Ustilago maydis* induces corn smut, which is not a crucial disease for plants, but in Mexico infection is carried out on purpose to gain a traditional dish from inoculated maize. The fungus is rather a model for a biotrophic basidiomycete and hence object of intense research (Dean *et al.*, 2012). The two velvet domain proteins *umv1* and *umv2* are involved in teliospore development and disease induction in maize (Karakkat *et al.*, 2013). The connection of Vel1 homologs to pathogenicity in different plant pathogens might make this protein a promising candidate to diminish fungal diseases.

In some other fungi such as *M. oryzae*, *F. oxysporum*, *V. mali* and *U. maydis* homologs of the genes for Vel2 or Vel3, respectively, are often connected to virulence in addition to the homologs encoding Vel1 (Karakkat *et al.*, 2013; López-Berges *et al.*, 2013; Kim *et al.*, 2014; Wu *et al.*, 2018). No significant contribution of Vel2 or Vel3 to virulence of *V. dahliae* was observed. The total number of velvet genes in fungi differs. *V. dahliae* and *A. nidulans* possess four velvet genes, whereas *A. flavus* contains five velvet genes (Bayram & Braus, 2012; Eom *et al.*, 2018). *F. oxysporum* lacks a *VOS1* ortholog and hence solely contains three velvet genes (López-Berges *et al.*, 2013). As velvet genes are paralogs it might be possible that in some fungi genes with redundant functions were eliminated but in other fungi the genes gained distinct functions without redundancy or even overlap in some but not all functions (Kuzmin *et al.*, 2020). Hence, the velvet genes, which are still present in fungi, have likely divergent roles but also overlapping functions.

4.1.4.1 Successful plant colonization requires the production of enough conidia

V. dahliae Vel1 and Vel3 share a function in the promotion of fungal conidiation, which facilitates the colonization of the upper parts of the host plants after successful invasion (Figure 24). VeA of different *Aspergillus* spp. is also involved in conidiation (Calvo *et al.*, 2004; Amaike & Keller, 2009; Duran *et al.*, 2009; Wang *et al.*, 2015; Eom *et al.*, 2018). Our experiments using wounded tomato plants allowed the Δ*VEL1* strain, which was not able to colonize roots to the same extend as the wild type, to enter the host as shown by the re-isolation of fungal material from infected plants. However, symptom induction in plants treated with this strain was decreased in comparison to the wild type, which might be due to the reduction of conidia production of the deletion strain and as a consequence decreased propagation within the plant vascular system. Vel3 influences conidiation but not to the same extend as Vel1. Symptom induction in tomato plants was comparable to the wild type when the Δ*VEL3* strain was used for inoculation.

The *V. dahliae* transcription factors Som1, Vta2 and Vta3 are similar to Vel1 positive regulators of conidiation and required for pathogenicity (Tran *et al.*, 2014; Bui *et al.*, 2019). The suppression of flocculation-related gene (*SFL1*) promotes conidiation and is required for virulence in tomato plants but dispensable for root colonization (Leonard, 2019). *SFL1* expression is controlled by Vta3 (Bui *et al.*, 2019). Conidiation and virulence are connected by the circadian clock component Frq in *V. dahliae* (Leonard, 2019). Conidiation and disease symptom induction in fungi are often linked as strains with defects in spore formation frequently are less virulent. The velvet proteins in *V. dahliae* exhibit a high sequence similarity to other plant pathogenic fungi as for instance *M. oryzae*, where *VEA*, *VELB* and *VELC* contribute to conidiation and *VEA* and *VELC* induce disease development and are involved in plant cell penetration (Kim *et al.*, 2014). The O-mannosyltransferase protein Pmt2 of *M. oryzae*, which

is involved in glycosylation, is associated with appressorium formation and pathogenicity but also connected to conidiation, which is delayed in the deletion strain (Guo *et al.*, 2016). The phytopathogenic fungus *Alternaria alternata* causes crop losses worldwide. Also the protein kinase SNF1, which enables utilization of non-fermentable carbon sources, is required for conidiation and pathogenicity (Tang *et al.*, 2020).

The adequate production of conidia seems to determine the infection success of the fungus. The *VEL3* deletion strain is impaired in conidiation, but spore numbers seem to be sufficient to efficiently colonize plants. The *VEL1* deletion strain is severely impaired in conidiation and hyphopodia formation but in rare cases able to enter wounded plant roots. Formation of penetration structures like appressoria or hyphopodia are important factors for host invasion but once the fungus is in the plant, conidiation seems to be a limiting factor for pathogenicity.

4.1.5 Velvet domain proteins from a complex network coordinating developmental process, secondary metabolite production and pathogenicity

A major finding of this study is the broad contribution of velvet domain proteins in diverse processes in the life cycle of *V. dahliae in* as well as *ex planta*. Physical and regulatory connections between the velvet proteins result in a complex control network of velvet domain proteins interacting with other proteins (Figure 38). Vel1 has an omnipresent role within this network. Solely, Vel1 promotes root colonization and disease symptom induction. The expression of *VEL1* is positively regulated by Som1, which also promotes plant root penetration, colonization, disease induction and conidiation (Bui *et al.*, 2019). Vel2 forms a heterodimer together with Vel1, which promotes the formation of microsclerotia and secondary metabolites. However, *VEL1* seems to have an epistatic effect on *VEL2*. Both, Vel1 and Vel3, promote the formation of conidia but Vel1 has a more pronounced effect suggesting *VEL1* is acting epistatically to *VEL3*. At the moment, the function of Vos1 is uncertain, but *VEL3* seems to be epistatic to *VOS1*. In contrast to Vel1 and Vel2, Vel3 has a negative impact on microsclerotia formation and secondary metabolite production leading to an antagonistic role of Vel3. Heterodimer functions of Vel2-Vos1 and Vel3-Vos1 remain still elusive and have to be dissected in future studies.

Summing up, a novel Vel1 function as a key factor for initial plant root colonization and disease induction could be discovered in the vascular plant pathogen *V. dahliae*. Vel1 also controls fungal development as conidiation and microsclerotia formation. This is coordinated with secondary metabolite formation, which is reminiscent to findings in other fungi. Except of Vos1, the other velvet proteins contribute to the developmental processes and secondary metabolism. None of the other velvet domain proteins is as omnipresent as Vel1 making this protein a possible target to decrease Verticillium wilt.

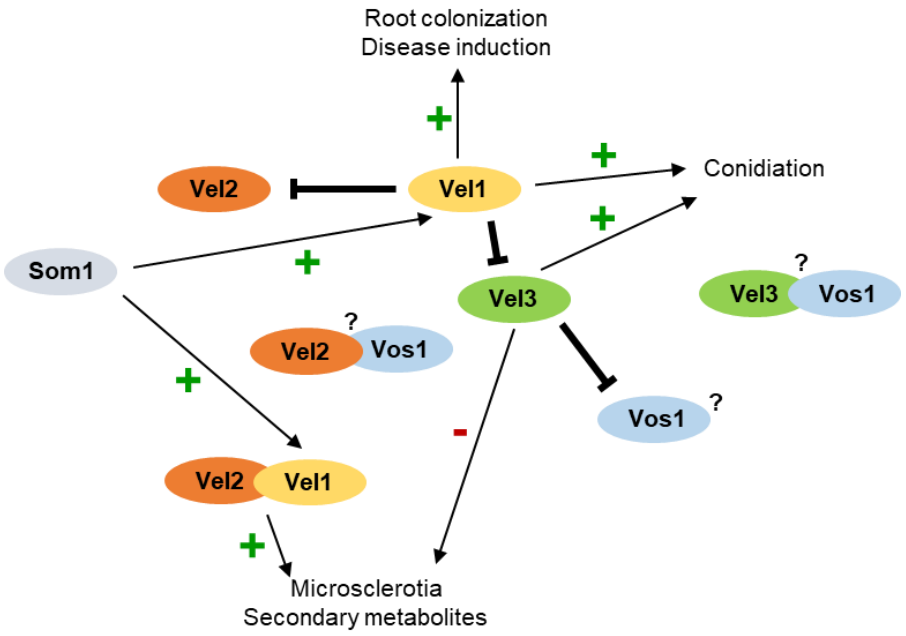

Figure 38: Interplay of velvet domain proteins in *V. dahliae*. Som1 positively regulates the expression of *VEL1* (Bui *et al.*, 2019). Vel1 can form a heterodimer with Vel2. This heterodimer might have positive effects on microsclerotia formation and secondary metabolite production. Only Vel1 induces conidiation, root colonization and disease symptoms. *VEL1* might have an epistatic effect on *VEL2* and *VEL3*. Vel3 inhibits the formation of resting structures and secondary metabolites and thus acts antagonistically to Vel1 and Vel2. In contrast, Vel3 is required for conidiation and seems to have an epistatic effect on *VOS1*, which function remains elusive. The formation of a Vel2-Vos1 as well as a Vel3-Vos1 heterodimer was observed but the exact role of the dimers are unknown so far.

4.2 Fluorescent pseudomonads are efficient fungal antagonists

4.2.1 A combination of different pseudomonads might inhibit growth of *V. dahliae* effectively

Several organisms such as bacteria, fungi, oomycetes, nematodes, algae, archaea or viruses are present in the plants rhizosphere (Mendes *et al.*, 2013; Fierer, 2017). Microsclerotia of *V. dahliae* germinate if root exudates are present and hyphae grow towards the host plant where they colonize the root, enter the xylem sap and distribute by conidia, which germinate in trapping sites and colonize nearby vessels (Fradin & Thomma, 2006; Klosterman *et al.*, 2009). In a previous study *V. longisporum* and *V. dahliae* were co-cultivated with three different *Pseudomonas* spp. named P_phen, P_DAPG and P_rhizo on solid pectin-rich simulated xylem medium (SXM) and glucose-rich potato dextrose medium (PDM) to investigate their ability to inhibit fungal growth. Fungal growth inhibition was media-dependent as on glucose-rich medium phenazines are able to inhibit growth whereas on pectin-rich simulated xylem medium the GacS/GacA two-component system was most important for the antagonistic function (Nesemann *et al.*, 2018).

As already mentioned, the fungal plant pathogen *V. dahliae* propagates *in planta* by conidiation but spores on the root surface can also function as a secondary inoculum (Klosterman *et al.*,

2009). Bacteria in the soil secrete different metabolites, which might be useful to curb the infection on a field. It might be difficult to target conidia inside the plant by the bacterium, but possibly the metabolites that inhibit spore germination can be isolated and applied to the plant directly. However, this requires an efficient production of the metabolite, an application strategy and negative side effects on the plant need to be excluded.

The impact of *Pseudomonas* spp. on fungal conidia germination and the persistence of this effect after removal of bacteria was tested. In glucose-rich medium P_rhizo had the strongest effect on the fungus. In contrast, only P_phen inhibited fungal growth persistently when co-cultivated in pectin-rich SXM (Table 11). Depending on the combination of medium and bacteria, the fungus was not able to regain growth when the bacterium was removed. It might be possible that the bacterium destroyed the conidia, but it is also feasible that germination of the conidia is inhibited permanently. Conidia are not considered as long-term survival structures (Klosterman *et al.*, 2009) and might therefore not be sheltered in the same way as for instance microsclerotia by melanin (Fan *et al.*, 2020). Substances produced by the bacteria might thus harm conidia persistently. On solid as well as in liquid co-cultivations the strongest inhibition potential on glucose-rich medium was observed for P_rhizo, which does not contain a phenazine cluster. Similarly in or on pectin-rich medium, P_phen induced the strongest inhibition, which does not possess the GacS/GacA regulatory system (Nesemann *et al.*, 2018). Conclusively, the bacteria are able to harm the conidia in liquid culture and germinating hyphae on solid medium.

According to genome predictions the bacteria might be able to produce different metabolites (Nesemann *et al.*, 2018). Taking the genomic potential of the bacteria into account one can assume that on solid PDM phenazines were required to reduce fungal growth and on solid SXM the GacS/GacA system contributed to growth inhibition (Nesemann *et al.*, 2018), suggesting that a mixture of genes for different metabolites is responsible for the bacterial growth inhibition on solid medium. For an efficient and persistent inhibition of conidia germination in liquid medium also a combination of different metabolites seems to be useful as the inhibitory effect of the bacteria was media-dependent (Figure 39).

Certain metabolites are presumably only produced under specific cultivation conditions. Besides, the distribution of bacterial metabolites differs on solid and liquid medium. On solid medium the bacterium was inoculated in the middle of the petri dish and hence induced a decrease in metabolite concentration to the margins of the petri dish. This gradient in secreted bacterial metabolites is perceived by the fungus, which might lead to negative chemotaxis and fungal branching in order to avoid the bacterium. In accordance with this, confrontation experiments in microfluidic devices showed that single hyphae try to avoid the bacterium by growing into another direction (unpublished data, Kai Nesemann).

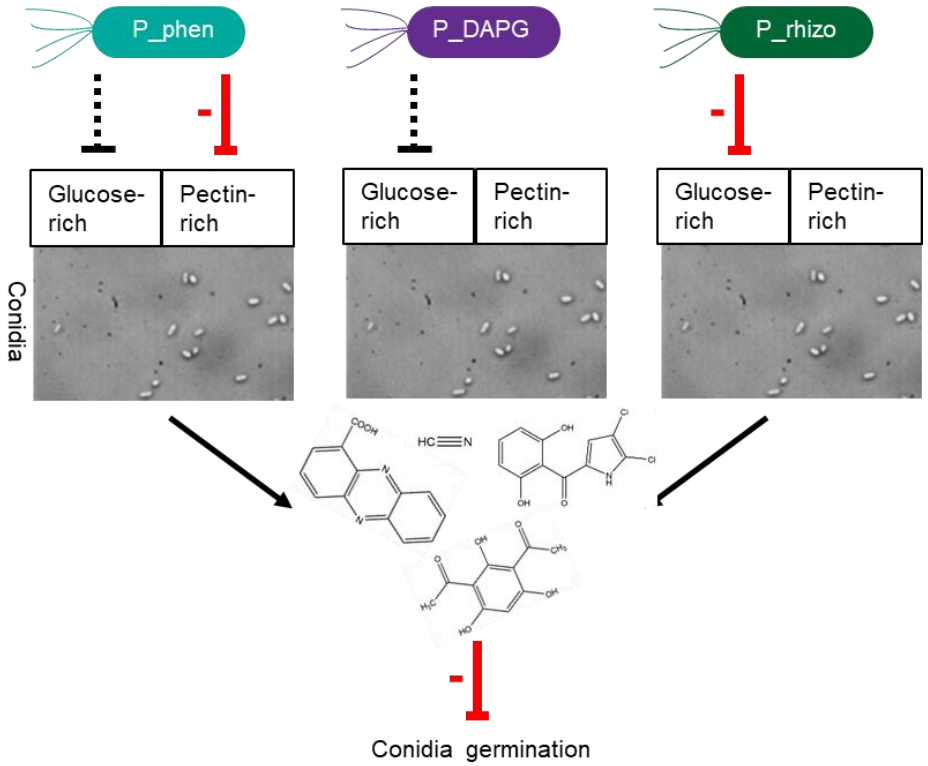

Figure 39: Different fluorescent pseudomonads inhibit *V. dahliae* conidia germination. P_phen, P_DAPG and P_rhizo were tested in co-cultivation experiments with *V. dahliae* conidia in glucose-rich potato dextrose medium (PDM) and pectin-rich simulated xylem medium (SXM). The potential to inhibit conidia germination depends on the bacterial strain and the medium. P_phen had the strongest inhibitory effect on SXM (red arrow) but also reduced fungal ability to regain growth on PDM (dashed line). P_DAPG did not inhibit conidia germination on SXM but to a small extend on PDM. P_rhizo induced a strong inhibitory effect in PDM but had no effect when cultivated with conidia in SXM. P_phen and P_rhizo produce secondary metabolites, which are able to hinder the germination of conidia in different media persistently. A combination of both bacterial strains might result in a mixture that inhibits conidia germination media-independently and durably.

In contrast, fungus and bacterium are equally distributed in liquid medium. Bacterial metabolites are evenly spread and the fungus is unable to avoid these substances. For the application of *Pseudomonas* spp. as biocontrol agent against emerging plant pathogens such as *V. dahliae* or also *V. longisporum*, a combination of bacteria with antagonistic potential might be useful in order to have the possibility for efficient antagonism under diverse nutrient conditions.

Whether fluorescent pseudomonads are useful as biocontrol agents against Verticillium wilt is so far ambiguous as experiments *in planta* or on the field need to be conducted. Several bacteria with antagonistic capacity have been described, especially *Pseudomonas* spp. and *Bacillus* spp. (Weller *et al.*, 2002; Fravel, 2005; Haas & Défago, 2005; Deketelaere *et al.*, 2017; Syed Ab Rahman *et al.*, 2018). Different Ascomycota as *Trichoderma* spp., *Fusarium* spp., *Verticillium* spp. and *Penicilium* spp. are also known as antagonistic fungal agents (Woo *et al.*, 2014; Zachow *et al.*, 2016; Deketelaere *et al.*, 2017; Keswani *et al.*, 2019; de Lamo & Takken, 2020; Toghueo, 2020; Toghueo & Boyom, 2020). Although some of the afore-mentioned

species include plant pathogens, individual non- or less-virulent isolates might be beneficial for plants.

One fungus, which is useful against Verticillium wilt is the antagonistic ascomycete *Talaromyces flavus*, that protects different crop plants as cotton, cucumber, potato and tomato against the pathogen and additionally enhances growth of cotton and potato (Naraghi *et al.*, 2007, 2010a,b,c, 2012). Another fungus with known biocontrol activity is the rhizofungus *Coniothyrium minitans*, which is commercially produced by Bayer CropScience Deutschland GmbH and used against the plant pathogen *Sclerotinia sclerotiorum* (Zeng *et al.*, 2012). Furthermore, also yeasts as *Aureobasidium pullulans*, *Metschnikowia fructicola*, *Cryptococcus albidus, Candida oleophila* and *Saccharomyces cerevisiae* provide antifungal activity, are well-studied and easily applicable (Freimoser *et al.*, 2019). This broad spectrum of microorganisms with antagonistic activity against fungi offers a load of possibilities to combat fungal disease without using substances that are harmful to the environment or to humans.

Bacteria as well as fungi are able to induce the production of various secondary metabolites with antimicrobial activity (Gerke & Braus, 2014; Macheleidt *et al.*, 2016; Keswani *et al.*, 2019, 2020). Whole-genome sequencing and bioinformatic methods revealed the presence of several gene clusters in fungi and bacteria, that are not induced under laboratory conditions or are just expressed at low levels (Keller *et al.*, 2005; Bergmann *et al.*, 2007; Scherlach & Hertweck, 2009; Sanchez *et al.*, 2012). The function of these clusters often remained speculative but they might encode virulence factors, toxins or new drugs (Keller *et al.*, 2005; Bergmann *et al.*, 2007).

Co-cultivation of fungi and bacteria might alter the expression of secondary metabolites. The influence of different bacteria on secondary metabolite synthesis in *Aspergillus* spp. has been investigated in numerous studies as they are producers of mycotoxins and induce agricultural pests (Pfliegler *et al.*, 2020). Several studies showed that these so-called silent or cryptic gene clusters can be induced during co-cultivation of bacteria and fungi as for instance described for interactions between *Aspergillus* spp. and *Streptomyces* spp. (Schroeckh *et al.*, 2009; König *et al.*, 2013; Netzker *et al.*, 2015). Co-cultivation experiments with *B. subtilis* and *A. niger* revealed that both, the bacterium and the fungus, alter their metabolism (Benoit *et al.*, 2015). *Pseudomonas* spp. might produce another set of secondary metabolites during the co-cultivation with *Verticillium* spp., which would explain the differences in the inhibitory potential of different wild type isolates and deletion strains for phenazines or the GacS/GacA system (Nesemann *et al.*, 2018). Regarding secondary metabolite production not much is known about *V. dahliae*, but *in silico* predictions revealed the presence of 25 potential gene clusters for synthesis of different compounds leading to the assumption that the fungus might be able to produce siderophores and fujikurin besides the already described melanin (Shi-Kunne *et al.*, 2019).

Modifications of the chromatin structure regulate the expression of secondary metabolite gene clusters (Keller *et al.*, 2005; Bok *et al.*, 2009; Scherlach & Hertweck, 2009; Gacek & Strauss, 2012). Chromosomes contain euchromatin and heterochromatin. In general, euchromatic chromosomal regions include transcribed genes and heterochromatic chromosomal regions are genetically inert (Keller *et al.*, 2005). Often bacteria induce chromatin remodeling in fungi, which leads to the production of new metabolites (Netzker *et al.*, 2015). Co-cultivation of *A. nidulans* with *S. rapamycinicus* activates silent genes for the production of orsellinic acid and its derivatives in the fungus dependent on the histone acetyltransferase complex Saga/Ada, which increases histone 3 acetylation (Nützmann *et al.*, 2011). Research in *A. nidulans* revealed that acetylated histones were not just associated with genes involved in secondary metabolism but also in metabolic pathways for amino acid or nitrogen metabolism, signaling and encoded transcription factors such as BasR, which in the fungus is involved in transducing bacterial signals (Fischer *et al.*, 2018). In fungi the expression of many secondary metabolites is coordinated by the global regulator LaeA, which is present in many *Aspergillus* spp. and other fungi such as *V. dahliae* (Bok & Keller, 2004; Sanchez *et al.*, 2012; Timpner, 2013). LaeA might also influence the chromatin structure, which may result in a changed metabolic profile (Reyes-Dominguez *et al.*, 2010; Sanchez *et al.*, 2012; Sarikaya-Bayram *et al.*, 2015).

Co-cultivation experiments with a *V. dahliae LAE1* deletion strain and pseudomonads did not alter the inhibitory potential of the bacterium suggesting that the fungus can not use metabolites regulated by Lae1 to harm the bacterium (Nesemann *et al.*, 2018). In addition, *V. dahliae* Lae1 is dispensable for secondary metabolite production (Figure 23b) and was not identified as interaction partner of Vel1 in protein interaction experiments (Table A1). *V. dahliae* Lae1 seems to be dispensable for the interaction with bacteria under the tested conditions. Another possibility is, that the fungus has proteins with redundant functions. The function of Lae1 potentially in a complex with the velvet proteins, remains to be elucidated.

4.2.2 Plant-associated pseudomonads exhibit antifungal activity against plant pathogens and saprophytes

The *Pseudomonas* strains used in this study were isolated from the rhizosphere of different plants. P_phen derived from wheat roots, which were grown in soil suppressive to the plant disease “take-all”, which is induced by the fungal plant pathogen *Gaeumannomyces graminis* (Weller & Cook, 1983). P_DAPG was obtained from tobacco roots, which were grown in soil suppressive to black root rot (Stutz *et al.*, 1986). P_rhizo was isolated from the rhizosphere of rape seed in northern Germany (Berg & Ballin, 1994). A comparison of the genome potentials of the different *Pseudomonas* spp. revealed that they contain different gene clusters for the production of mycotoxins (Nesemann *et al.*, 2018). Co-cultivation experiments revealed that

P_rhizo is not just able to inhibit growth of the *B. napus* pathogen *V. longisporum* but is also repressive towards the fungal pathogen *V. dahliae* suggesting its inhibitory potential is not restricted to fungal pathogens of its natural habitat (Nesemann *et al.*, 2018). Similar effects were observed for P_phen and P_DAPG, which were able to inhibit growth of both *Verticillium* spp. (Nesemann *et al.*, 2018).

Bacteria in the rhizosphere do not only encounter plant-pathogenic fungi but also saprophytic fungi such as *Aspergillus* spp. The bacteria were able to reduce growth of both, *A. nidulans* and *A. fumigatus,* but the inhibitory influence was decreased in comparison to the effect on *V. dahliae* (Figure 35). These data support that the inhibitory effect of pseudomonads is not limited to fungi living in the natural rhizosphere where the bacterium had been isolated from. The differences in the inhibition potential might be explained by the different lifestyles of the examined fungi. Saprophytic fungi such as *A. nidulans* and *A. fumigatus* always compete with other microorganism for nutrients and space in the soil (Crowther *et al.*, 2012). It might be possible that their hyphal growth has adapted to these conditions and they might have a constitutive self-defense mechanism. In contrast, plant pathogenic fungi such as *V. dahliae* mainly enter a hostile environment when colonizing a plant as they have to deal with the plant immune response (Song *et al.*, 2020). One could speculate that during vegetative growth on a solid medium *V. dahliae* is not prepared to encounter another organism, which results in a bigger inhibition of fungal growth for the plant pathogen than for saprophytes, which are always aware of enemies. In addition, it is possible, that the inhibition zone on plate is a sign for avoidance of competitive regions in the soil. *V. dahliae* might specifically infect roots in less competitive regions to maximize the infection success.

Fungal growth reduction for *V. dahliae* as well as *A. nidulans* and *A. fumigatus* was media-dependent with a general stronger inhibition on pectin-rich simulated xylem medium (SXM) (Figure 35). Depending on the nutrient source and the bacterium, the fungus might adapt its growth strategy. The presence of the phenazine-producer P_phen induced the strongest inhibition on pectin-rich SXM for *V. dahliae* and similar inhibitory effects as P_DAPG for *A. nidulans* and *A. fumigatus*. It is possible that the fungus on this medium tries to escape from the antagonist by directly growing into another direction. In comparison to pectin, glucose is more easily degradable (Mohnen, 2008). On the glucose-rich medium the fungus reduces the growth rate of vegetative hyphae to react to changing conditions. A similar effect was reported for *A. fumigatus* in the human blood, which is a hostile but nutrient-rich environment. In the blood, the fungus down-regulates energy-consuming metabolic pathways and uptake mechanisms and instead establishes a resting mycelium stage to overcome the harsh conditions and adapt to the environment (Irmer *et al.*, 2015).

In summary, interactions between different bacteria and fungi provide a wide field to combat fungal diseases of plants and maybe also in humans. Experiments were so far solely

conducted *in vitro* and an inhibitory effect on the fungal burden *in planta* is uncertain. Due to their media-dependent inhibition potential and differences in the presence of clusters for metabolite synthesis, the combination of different *Pseudomonas* strains might be useful to combat Verticillium wilt in the field, which should be tested in co-cultivation experiments of bacteria, fungi and plants. Furthermore, bacterial-fungal interactions often induce the expression of cryptic metabolite clusters, which might lead to the identification of new metabolites with antibiotic effects.

References

Aguirre J, Ríos-Momberg M, Hewitt D, Hansberg W. **2005**. Reactive oxygen species and development in microbial eukaryotes. *Trends in Microbiology* **13**: 111–118.

Ahmed YL, Gerke J, Park HS, Bayram Ö, Neumann P, Ni M, Dickmanns A, Kim SC, Yu JH, Braus GH, *et al.* 2013. The velvet family of fungal regulators contains a DNA-binding domain structurally similar to NF-κB. *PLoS Biology* **11**: e1001750.

Ajwa HA, Trout T, Mueller J, Wilhelm S, Nelson SD, Soppe R, Shatley D. **2002**. Application of alternative fumigants through drip irrigation systems. *Phytopathology* **92**: 1349–1355.

Alexandratos N, Bruinsma J. **2012**. World agriculture towards 2030/2050: the 2012 revision. ESA Working paper No. 12-03. Rome, FAO.

Amaike S, Keller NP. **2009**. Distinct roles for VeA and LaeA in development and pathogenesis of *Aspergillus flavus*. *Eukaryotic Cell* **8**: 1051–1060.

Amaike S, Keller NP. **2011**. *Aspergillus flavus*. *Annual Review of Phytopathology* **49**: 107–133.

Back MA, Haydock PPJ, Jenkinson P. **2002**. Disease complexes involving plant parasitic nematodes and soilborne pathogens. *Plant Pathology* **51**: 683–697.

Bardwell L. **2005**. A walk-through of the yeast mating pheromone response pathway. *Peptides* **26**: 339–350.

Bayram Ö, Biesemann C, Krappmann S, Galland P, Braus GH. **2008a**. More than a repair enzyme: *Aspergillus nidulans* photolyase-like CryA is a regulator of sexual development. *Molecular Biology of the Cell* **19**: 3254–3262.

Bayram Ö, Braus GH. **2012**. Coordination of secondary metabolism and development in fungi: the velvet family of regulatory proteins. *FEMS Microbiology Reviews* **36**: 1–24.

Bayram Ö, Braus GH, Fischer R, Rodriguez-Romero J. **2010**. Spotlight on *Aspergillus nidulans* photosensory systems. *Fungal Genetics and Biology* **47**: 900–908.

Bayram Ö, Feussner K, Dumkow M, Herrfurth C, Feussner I, Braus GH. **2016**. Changes of global gene expression and secondary metabolite accumulation during light-dependent *Aspergillus nidulans* development. *Fungal Genetics and Biology* **87**: 30–53.

Bayram Ö, Krappmann S, Ni M, Bok JW, Helmstaedt K, Valerius O, Braus-Stromeyer S, Kwon NJ, Keller NP, Yu JH, *et al.* 2008b. VelB/VeA/LaeA complex coordinates light signal with fungal development and secondary metabolism. *Science* **320**: 1504–1506.

Bayram Ö, Krappmann S, Seiler S, Vogt N, Braus GH. **2008c**. *Neurospora crassa ve*-1 affects asexual conidiation. *Fungal Genetics and Biology* **45**: 127–138.

Bayram Ö, Sarikaya-Bayram Ö, Ahmed YL, Maruyama J, Valerius O, Rizzoli SO, Ficner R, Irniger S, Braus GH. **2012**. The Aspergillus nidulans MAPK module AnSte11-Ste50-Ste7-Fus3 controls development and secondary metabolism. *PLoS Genetics* **8**: e1002816.

Bell AA, Stipanovic RD, Puhalla JE. **1976**. Pentaketide metabolites of *Verticillium dahliae*: identification of (+)-scytalone as a natural precursor of melanin. *Tetrahedron* **32**: 1353–1356.

Bell AA, Wheeler MH. **1986**. Biosynthesis and functions of fungal melanins. *Annual Review of Phytopathology* **24**: 411–451.

Belozerskaya TA, Gessler NN, Aver`yanov AA. **2017**. Melanin pigments of fungi. In: Merillon JM, Ramawat K, eds. Fungal Metabolites. Springer, Cham: Springer International Publishing, 263–291.

Benoit I, van den Esker MH, Patyshakuliyeva A, Mattern DJ, Blei F, Zhou M, Dijksterhuis J, Brakhage AA, Kuipers OP, de Vries RP, *et al.* 2015. *Bacillus subtilis* attachment to *Aspergillus niger* hyphae results in mutually altered metabolism. *Environmental Microbiology* **17**: 2099–2113.

Berg G, Ballin G. **1994**. Bacterial antagonists to *Verticillium dahliae* Kleb. *Journal of Phytopathology* **141**: 99–110.

Bergkessel M, Guthrie C. **2013**. Colony PCR. In: Lorsch J, ed. Laboratory Methods in Enzymology. San Diego, United States: Elsevier, 299–309.

Bergmann S, Schümann J, Scherlach K, Lange C, Brakhage AA, Hertweck C. **2007**. Genomics-driven discovery of PKS-NRPS hybrid metabolites from *Aspergillus nidulans*. *Nature Chemical Biology* **3**: 213–217.

Berlanger I, Powelson ML. **2000**. Verticillium wilt. *The Plant Health Instructor*: DOI: 10.1094/PHI-I-2000-0801-01. Updated 2005.

Bertani G. **1951**. Studies on lysogenesis. I. The mode of phage liberation by lysogenic *Escherichia coli*. *Journal of bacteriology* **62**: 293–300.

Biessy A, Filion M. **2018**. Phenazines in plant-beneficial *Pseudomonas* spp.: biosynthesis, regulation, function and genomics. *Environmental Microbiology* **20**: 3905–3917.

Blachowicz A, Raffa N, Bok JW, Choera T, Knox B, Lim FY, Huttenlocher A, Wang CCC, Venkateswaran K, Keller NP. **2020**. Contributions of spore secondary metabolites to UV-C protection and virulence vary in different *Aspergillus fumigatus* strains. *mBio* **11**: e03415-19.

Bok JW, Chiang Y-M, Szewczyk E, Reyes-Domingez Y, Davidson AD, Sanchez JF, Lo H-C, Watanabe K, Strauss J, Oakley BR, *et al.* 2009. Chromatin-level regulation of biosynthetic gene clusters. *Nature Chemical Biology* **5**: 462–464.

Bok JW, Keller NP. **2004**. LaeA, a regulator of secondary metabolism in *Aspergillus* spp. *Eukaryotic Cell* **3**: 527–535.

Bolton MD, van Esse HP, Vossen JH, de Jonge R, Stergiopoulos I, Stulemeijer IJE, van den Berg GCM, Borrás-Hidalgo O, Dekker HL, de Koster CG, *et al.* 2008. The novel *Cladosporium fulvum* lysin motif effector Ecp6 is a virulence factor with orthologues in other fungal species. *Molecular Microbiology* **69**: 119–136.

Boothby TC, Tapia H, Brozena AH, Piszkiewicz S, Smith AE, Giovannini I, Rebecchi L, Pielak GJ, Koshland D, Goldstein B. **2017**. Tardigrades use intrinsically disordered proteins to survive desiccation. *Molecular Cell* **65**: 975–984.

Bradford MM. **1976**. A rapid and sensitive method for the quantitation of microgram quantities of protein utilizing the principle of protein-dye binding. *Analytical Biochemistry* **72**: 248–254.

Brakhage AA. **2013**. Regulation of fungal secondary metabolism. *Nature Reviews Microbiology* **11**: 21–32.

Braun EJ, Howard RJ. **1994**. Adhesion of fungal spores and germlings to host plant surfaces. *Protoplasma* **181**: 202–212.

Brückner S, Mösch HU. **2012**. Choosing the right lifestyle: adhesion and development in *Saccharomyces cerevisiae*. *FEMS Microbiology Reviews* **36**: 25–58.

Bui T. **2017**. *Verticillium dahliae* transcription factors Som1 and Vta3 control microsclerotia formation and sequential steps of plant root penetration and colonisation to induce disease. *Dissertation at the Georg-August-Universität Göttingen*.

Bui T, Harting R, Braus-Stromeyer SA, Tran V, Leonard M, Höfer A, Abelmann A, Bakti F, Valerius O, Schlüter R, *et al.* 2019. *Verticillium dahliae* transcription factors Som1 and Vta3 control microsclerotia formation and sequential steps of plant root penetration and colonisation to induce disease. *New Phytologist* **221**: 2138–2159.

Calvo AM, Bok J, Brooks W, Keller NP. **2004**. *veA* is required for toxin and sclerotial production in *Aspergillus parasiticus*. *Applied and Environmental Microbiology* **70**: 4733–4739.

Calvo AM, Wilson RA, Bok JW, Keller NP. **2002**. Relationship between secondary metabolism and fungal development. *Microbiology and Molecular Biology Reviews* **66**: 447–459.

Camejo D, Guzmán-Cedeño Á, Moreno A. **2016**. Reactive oxygen species, essential molecules, during plant-pathogen interactions. *Plant Physiology and Biochemistry* **103**: 10–23.

Carella P, Wilson DC, Kempthorne CJ, Cameron RK. **2016**. Vascular sap proteomics: providing insight into long-distance signaling during stress. *Frontiers in Plant Science* **7**: 651.

Carroll CL, Carter CA, Goodhue RE, Lawell C-YCL, Subbarao K V. 2018. A review of control options and externalities for Verticillium wilts. *Phytopathology* **108**: 160–171.

Casadevall A, Cordero RJB, Bryan R, Nosanchuk J, Dadachova E. **2017**. Melanin, radiation, and energy transduction in fungi. *Microbiology Spectrum* **5**: FUNK-0037-2016.

Cascant-Lopez E, Crosthwaite S, Johnson LJ, Harrison RJ. **2020**. No evidence that homologues of key circadian clock genes direct circadian programmes of development or mRNA abundance in *Verticillium dahliae*. *Frontiers in Microbiology* **11**: 1977.

Chai LYA, Netea MG, Sugui J, Vonk AG, van de Sande WWJ, Warris A, Kwon-Chung KJ, Kullberg BJ. **2010**. *Aspergillus fumigatus* conidial melanin modulates host cytokine response. *Immunobiology* **215**: 915–920.

Chang P-K, Scharfenstein LL, Li P, Ehrlich KC. **2013**. *Aspergillus flavus* VelB acts distinctly from VeA in conidiation and may coordinate with FluG to modulate sclerotial production. *Fungal Genetics and Biology* **58**–**59**: 71–79.

Chatterjee P, Davis E, Yu F, James S, Wildschutte JH, Wiegmann DD, Sherman DH, McKay RM, LiPuma JJ, Wildschutte H. **2017**. Environmental Pseudomonads inhibit cystic fibrosis patient-derived *Pseudomonas aeruginosa*. *Applied and Environmental Microbiology* **83**: e02701-16.

Chen C-H, Dunlap JC, Loros JJ. **2010**. Neurospora illuminates fungal photoreception. *Fungal Genetics and Biology* **47**: 922–929.

Collins A, Okoli CAN, Morton A, Parry D, Edwards SG, Barbara DJ. **2003**. Isolates of *Verticillium dahliae* pathogenic to crucifers are of at least three distinct molecular types. *Phytopathology* **93**: 364–376.

la Cour T, Kiemer L, Mølgaard A, Gupta R, Skriver K, Brunak S. **2004**. Analysis and prediction of leucine-rich nuclear export signals. *Protein Engineering, Design and Selection* **17**: 527–536.

Covert SF, Kapoor P, Lee M, Briley A, Nairn CJ. **2001**. *Agrobacterium tumefaciens*-mediated transformation of *Fusarium circinatum*. *Mycological Research* **105**: 259–264.

Cox J, Mann M. **2008**. MaxQuant enables high peptide identification rates, individualized p.p.b.-range mass accuracies and proteome-wide protein quantification. *Nature Biotechnology* **26**: 1367–1372.

Crowther TW, Boddy L, Hefin Jones T. **2012**. Functional and ecological consequences of saprotrophic fungus-grazer interactions. *ISME Journal* **6**: 1992–2001.

Cui J, Bahrami AK, Pringle EG, Hernandez-Guzman G, Bender CL, Pierce NE, Ausubel FM. **2005**. *Pseudomonas syringae* manipulates systemic plant defenses against pathogens and herbivores. *Proceedings of the National Academy of Sciences of the United States of America* **102**: 1791–1796.

Czapek F. **1902**. Untersuchung über die Stickstoffbindung und Eiweiß-bildung der Pflanzen. *Beitr. Chem. Physiol. u. Pahtol.* **1**: 540–560.

David H, Özçelik IS, Hofmann G, Nielsen J. **2008**. Analysis of *Aspergillus nidulans* metabolism at the genome-scale. *BMC Genomics* **9**: 163.

Dean R, van Kan JAL, Pretorius ZA, Hammond-Kosack KE, Di Pietro A, Spanu PD, Rudd JJ, Dickman M, Kahmann R, Ellis J, *et al.* 2012. The top 10 fungal pathogens in molecular plant pathology. *Molecular Plant Pathology* **13**: 414–430.

Deketelaere S, Tyvaert L, França SC, Höfte M. **2017**. Desirable traits of a good biocontrol agent against Verticillium wilt. *Frontiers in Microbiology* **8**: 1186.

Depotter JRL, Deketelaere S, Inderbitzin P, von Tiedemann A, Höfte M, Subbarao K V, Wood TA, Thomma BP. **2016**. *Verticillium longisporum*, the invisible threat to oilseed rape and other brassicaceous plant hosts. *Molecular Plant Pathology* **17**: 1004–1016.

Depotter JRL, Shi-Kunne X, Missonnier H, Liu T, Faino L, van den Berg GCM, Wood TA, Zhang B, Jacques A, Seidl MF, *et al.* 2019. Dynamic virulence-related regions of the plant pathogenic fungus *Verticillium dahliae* display enhanced sequence conservation. *Molecular Ecology* **28**: 3482–3495.

Dettmann A, Heilig Y, Valerius O, Ludwig S, Seiler S. **2014**. Fungal communication requires the MAK-2 pathway elements STE-20 and RAS-2, the NRC-1 adapter STE-50 and the MAP kinase scaffold HAM-5. *PLoS Genetics* **10**: e1004762.

Dhingra S, Andes D, Calvo AM. **2012**. VeA regulates conidiation, gliotoxin production, and protease activity in the opportunistic human pathogen *Aspergillus fumigatus*. *Eukaryotic Cell* **11**: 1531–1543.

Dictionary of Natural Products. **2020**. Dictionary of Natural Products 29.1. [WWW document] URL http://dnp.chemnetbase.com/faces/chemical/ChemicalSearch.xhtml. [accessed July 2020].

Dox AW. **1910**. The intracellular enzymes of *Penicillium* and *Aspergillus* with special references to those of *P. camenberti*. *U.S. Dept. of Agriculture, Bureau of Animal Industry* **120**: 170.

Duniway JM. **2002**. Status of chemical alternatives to methyl bromide for pre-plant fumigation of soil. *Phytopathology* **92**: 1337–1343.

Dunlap JAYC, Loros JJ. **2017**. Making time: conservation of biological clocks from fungi to animals. *Microbiology Spectrum* **5**: FUNK-0039-2016.

Duran RM, Cary JW, Calvo AM. **2007**. Production of cyclopiazonic acid, aflatrem, and aflatoxin by *Aspergillus flavus* is regulated by *veA*, a gene necessary for sclerotial formation. *Applied Microbiology and Biotechnology* **73**: 1158–1168.

Duran RM, Cary JW, Calvo AM. **2009**. The role of *veA* in *Aspergillus flavus* infection of peanut, corn and cotton. *The Open Mycology Journal* **3**: 27–36.

Duressa D, Anchieta A, Chen D, Klimes A, Garcia-Pedrajas MD, Dobinson KF, Klosterman SJ. **2013**. RNA-seq analyses of gene expression in the microsclerotia of *Verticillium dahliae*. *BMC Genomics* **14**: 607.

EFSA PLH Panel (EFSA Panel on Plant Health). **2014**. Scientific opinion on the pest categorisation of *Verticillium dahliae* Kleb. *EFSA Journal* **12**: 3928.

Egamberdieva D, Wirth SJ, Alqarawi AA, Abd-Allah EF, Hashem A. **2017**. Phytohormones and beneficial microbes: essential components for plants to balance stress and fitness. *Frontiers in Microbiology* **8**: 2104.

Eisenman HC, Casadevall A. **2012**. Synthesis and assembly of fungal melanin. *Applied Microbiology and Biotechnology* **93**: 931–940.

Eom T-J, Moon H, Yu J-H, Park H-S. **2018**. Characterization of the velvet regulators in *Aspergillus flavus*. *Journal of Microbiology* **56**: 893–901.

Etxebeste O, Garzia A, Espeso EA, Ugalde U. **2010**. *Aspergillus nidulans* asexual development: making the most of cellular modules. *Trends in Microbiology* **18**: 569–576.

Eynck C, Koopmann B, Grunewaldt-Stoecker G, Karlovsky P, von Tiedemann A. **2007**. Differential interactions of *Verticillium longisporum* and *V. dahliae* with *Brassica napus* detected with molecular and histological techniques. *European Journal of Plant Pathology* **118**: 259–274.

Fan R, Gong X, Gao L, Shang W, Hu X, Xu X. **2020**. Temporal dynamics of the survival of *Verticillium dahliae* microsclerotia with or without melanin in soils amended with biocontrol agents. *European Journal of Plant Pathology* **157**: 521–531.

Fan R, Klosterman SJ, Wang C, Subbarao K V., Xu X, Shang W, Hu X. **2017**. Vayg1 is required for microsclerotium formation and melanin production in *Verticillium dahliae*. *Fungal Genetics and Biology* **98**: 1–11.

Fierer N. **2017**. Embracing the unknown: disentangling the complexities of the soil microbiome. *Nature Reviews Microbiology* **15**: 579–590.

Fischer J, Müller SY, Netzker T, Jäger N, Gacek-Matthews A, Scherlach K, Stroe MC, García-Altares M, Pezzini F, Schoeler H, *et al.* 2018. Chromatin mapping identifies BasR, a key regulator of bacteria-triggered production of fungal secondary metabolites. *eLife* **7**: e40969.

Flajsman M, Mandelc S, Radisek S, Stajner N, Jakse J, Kosmelj K, Javornik B. **2016**. Identification of novel virulence-associated proteins secreted to xylem by *Verticillium nonalfalfae* during colonization of hop plants. *Molecular Plant-Microbe Interactions* **29**: 362–373.

Flock T, Weatheritt RJ, Latysheva NS, Babu MM. **2014**. Controlling entropy to tune the functions of intrinsically disordered regions. *Current Opinion in Structural Biology* **26**: 62–72.

Fradin EF, Thomma BPHJ. **2006**. Physiology and molecular aspects of Verticillium wilt diseases caused by *V. dahliae* and *V. albo-atrum*. *Molecular Plant Pathology* **7**: 71–86.

Fradin EF, Zhang Z, Juarez Ayala JC, Castroverde CDM, Nazar RN, Robb J, Liu C-M, Thomma BPHJ. **2009**. Genetic dissection of Verticillium wilt resistance mediated by tomato Ve1. *Plant physiology* **150**: 320–332.

Franco DL, Canessa P, Bellora N, Risau-Gusman S, Olivares-Yañez C, Pérez-Lara R, Libkind D, Larrondo LF, Marpegan L. **2017**. Spontaneous circadian rhythms in a cold-adapted natural isolate of *Aureobasidium pullulans*. *Scientific Reports* **7**: 13837.

Fravel DR. **2005**. Commercialization and implementation of biocontrol. *Annual Review of Microbiology* **43**: 337–359.

Freimoser FM, Rueda-Mejia MP, Tilocca B, Migheli Q. **2019**. Biocontrol yeasts: mechanisms and applications. *World Journal of Microbiology and Biotechnology* **35**: 154.

Frieri M, Kumar K, Boutin A. **2017**. Antibiotic resistance. *Journal of Infection and Public Health* **10**: 369–378.

Gacek A, Strauss J. **2012**. The chromatin code of fungal secondary metabolite gene clusters. *Applied Microbiology and Biotechnology* **95**: 1389–1404.

Gaderer R, Bonazza K, Seidl-Seiboth V. **2014**. Cerato-platanins: a fungal protein family with intriguing properties and application potential. *Applied Microbiology and Biotechnology* **98**: 4795–4803.

Gauthier T, Wang X, Dos Santos J, Fysikopoulos A, Tadrist S, Canlet C, Artigot MP, Loiseau N, Oswald IP, Puel O. **2012**. Trypacidin, a spore-borne toxin from *Aspergillus fumigatus*, is cytotoxic to lung cells. *PLoS ONE* **7**: e29906.

Gerke J, Braus GH. **2014**. Manipulation of fungal development as source of novel secondary metabolites for biotechnology. *Applied Microbiology and Biotechnology* **98**: 8443–8455.

Gessler NN, Aver'yanov AA, Belozerskaya T. **2007**. Reactive oxygen species in regulation of fungal development. *Biochemistry (Mosc)* **72**: 1091–1109.

Gijzen M, Nürnberger T. **2006**. Nep1-like proteins from plant pathogens: recruitment and diversification of the NPP1 domain across taxa. *Phytochemistry* **67**: 1800–1807.

Gouda S, Kelly RG, Das G, Paramithiotis S, Shin HS, Patra JK. **2018**. Revitalization of plant growth promoting rhizobacteria for sustainable development in agriculture. *Microbiological Research* **206**: 131–140.

Griffiths DA. **1970**. The fine structure of developing microsclerotia of *Verticillium dahliae* Kleb. *Archiv für Mikrobiologie* **74**: 207–212.

Guo M, Chen Y, Du Y, Dong Y, Guo W, Zhai S, Zhang H, Dong S, Zhang Z, Wang Y, *et al.* 2011. The bZIP transcription factor MoAP1 mediates the oxidative stress response and is critical for pathogenicity of the rice blast fungus *Magnaporthe oryzae*. *PLoS pathogens* **7**: e1001302.

Guo M, Tan L, Nie X, Zhu X, Pan Y, Gao Z. **2016**. The Pmt2p-mediated protein O-mannosylation is required for morphogenesis, adhesive properties, cell wall integrity and full virulence of *Magnaporthe oryzae*. *Frontiers in Microbiology* **7**: 630.

Haas D, Défago G. **2005**. Biological control of soil-borne pathogens by fluorescent pseudomonads. *Nature Reviews Microbiology* **3**: 307–319.

Hanahan D, Jessee J, Bloom FR. **1991**. Plasmid transformation of *Escherichia coli* and other bacteria. *Methods in Enzymology* **204**: 63–113.

Harting R, Höfer A, Tran V-T, Weinhold LM, Barghahn S, Schlüter R, Braus G. **2020**. The Vta1 transcriptional regulator is required for microsclerotia melanization in *Verticillium dahliae*. *Fungal Biology* **124**: 490–500.

Heeb S, Haas D. **2001**. Regulatory roles of the GacS/GacA two-component system in plant-associated and other gram-negative bacteria. *Molecular Plant-Microbe Interactions* **14**: 1351–1363.

Hill TW, Käfer E. **2001**. Improved protocols for *Aspergillus* minimal medium: trace element and minimal medium salt stock solutions. *Fungal Genetics Reports* **48**: 20–21.

Hoffmann B, Valerius O, Andermann M, Braus GH. **2001**. Transcriptional autoregulation and inhibition of mRNA translation of amino acid regulator gene *cpcA* of filamentous fungus *Aspergillus nidulans*. *Molecular Biology of the Cell* **12**: 2846–2857.

Hoffmann B, Wanke C, LaPaglia SK, Braus GH. **2000**. c-Jun and RACK1 homologues regulate a control point for sexual development in *Aspergillus nidulans*. *Molecular Microbiology* **37**: 28–41.

Hollensteiner J, Wemheuer F, Harting R, Kolarzyk AM, Diaz Valerio SM, Poehlein A, Brzuszkiewicz EB, Nesemann K, Braus-Stromeyer SA, Braus GH, *et al.* 2017. *Bacillus thuringiensis* and *Bacillus weihenstephanensis* inhibit the growth of phytopathogenic *Verticillium* species. *Frontiers in Microbiology* **7**: 2171.

Hoppenau CE, Tran VT, Kusch H, Aßhauer KP, Landesfeind M, Meinicke P, Popova B, Braus-Stromeyer SA, Braus GH. **2014**. *Verticillium dahliae* VdTHI4, involved in thiazole biosynthesis, stress response and DNA repair functions, is required for vascular disease induction in tomato. *Environmental and Experimental Botany* **108**: 14–22.

Howard RJ, Ferrari MA. **1989**. Role of melanin in appressorium function. *Experimental Mycology* **13**: 403–418.

Husaini AM, Sakina A, Cambay SR. **2018**. Host–pathogen interaction in *Fusarium oxysporum* infections: where do we stand? *Molecular Plant-Microbe Interactions* **31**: 889–898.

Inderbitzin P, Bostock RM, Davis RM, Usami T, Platt HW, Subbarao K V. 2011a. Phylogenetics and taxonomy of the fungal vascular wilt pathogen *Verticillium*, with the descriptions of five new species. *PLoS ONE* **6**: e28341.

Inderbitzin P, Davis RM, Bostock RM, Subbarao K V. 2011b. The ascomycete *Verticillium longisporum* is a hybrid and a plant pathogen with an expanded host range. *PLoS ONE* **6**: e18260.

Inderbitzin P, Subbarao K V. **2014**. *Verticillium* systematics and evolution: how confusion impedes Verticillium wilt management and how to resolve it. *Phytopathology* **104**: 564–574.

Ingram R. **1968**. *Verticillium dahliae* var. *longisporum*, a stable diploid. *Transactions of the British Mycological Society* **51**: 339–341.

Inoue H, Nojima H, Okayama H. **1990**. High efficiency transformation of *Escherichia coli* with plasmids. *Gene* **96**: 23–28.

Irmer H, Tarazona S, Sasse C, Olbermann P, Loeffler J, Krappmann S, Conesa A, Braus GH. **2015**. RNAseq analysis of *Aspergillus fumigatus* in blood reveals a just wait and see resting stage behavior. *BMC Genomics* **16**: 640.

Jones P, Binns D, Chang HY, Fraser M, Li W, McAnulla C, McWilliam H, Maslen J, Mitchell A, Nuka G, *et al.* 2014. InterProScan 5: genome-scale protein function classification. *Bioinformatics* **30**: 1236–1240.

de Jonge R, van Esse HP, Kombrink A, Shinya T, Desaki Y, Bours R, van der Krol S, Shibuya N, Joosten MHAJ, Thomma BPHJ. **2010**. Conserved fungal LysM effector Ecp6 prevents chitin-triggered immunity in plants. *Science* **329**: 953–955.

de Jonge R, Thomma BPHJ. **2009**. Fungal LysM effectors: extinguishers of host immunity? *Trends in Microbiology* **17**: 151–157.

Jyothishwaran G, Kotresha D, Selvaraj T, Srideshikan SM, Rajvanshi PK, Jayabaskaran C. **2007**. A modified freeze-thaw method for efficient transformation of *Agrobacterium tumefaciens*. *Current Science* **93**: 770–772.

Käfer E. **1965**. Origins of translocations in *Aspergillus nidulans*. *Genetics* **52**: 217–232.

Käfer E. **1977**. The anthranilate synthetase enzyme complex and the trifunctional *trpC* gene of *Aspergillus*. *Canadian Journal of Genetics and Cytology* **19**: 723–738.

Kamble A, Koopmann B, von Tiedemann A. **2013**. Induced resistance to *Verticillium longisporum* in *Brassica napus* by β-aminobutyric acid. *Plant Pathology* **62**: 552–561.

Karakkat BB, Gold SE, Covert SF. **2013**. Two members of the *Ustilago maydis* velvet family influence teliospore development and virulence on maize seedlings. *Fungal Genetics and Biology* **61**: 111–119.

Karapapa VK, Bainbridge BW, Heale JB. **1997**. Morphological and molecular characterization of *Verticillium longisporum* comb. nov., pathogenic to oilseed rape. *Mycological Research* **101**: 1281–1294.

Kato N, Brooks W, Calvo AM. **2003**. The expression of sterigmatocystin and penicillin genes in *Aspergillus nidulans* is controlled by *veA*, a gene required for sexual development. *Eukaryotic Cell* **2**: 1178–1186.

Katsantonis D, Hillocks RJ, Gowen S. **2005**. Enhancement of germination of spores of *Verticillium dahliae* and *Fusarium oxysporum* f.sp. *vasinfectum* in vascular fluid from cotton plants infected with the root-knot nematode. *Phytoparasitica* **33**: 215–224.

Keller NP. **2019**. Fungal secondary metabolism: regulation, function and drug discovery. *Nature Reviews Microbiology* **17**: 167–180.

Keller NP, Turner G, Bennett JW. **2005**. Fungal secondary metabolism — from biochemistry to genomics. *Nature Reviews Microbiology* **3**: 937–947.

Kersey PJ, Allen JE, Allot A, Barba M, Boddu S, Bolt BJ, Carvalho-Silva D, Christensen M, Davis P, Grabmueller C, *et al.* 2018. Ensembl Genomes 2018: an integrated omics infrastructure for non-vertebrate species. *Nucleic Acids Research* **46**: D802-D808.

Keswani C, Singh HB, García-Estrada C, Caradus J, He YW, Mezaache-Aichour S, Glare TR, Borriss R, Sansinenea E. **2020**. Antimicrobial secondary metabolites from agriculturally important bacteria as next-generation pesticides. *Applied Microbiology and Biotechnology* **104**: 1013–1034.

Keswani C, Singh HB, Hermosa R, García-Estrada C, Caradus J, He Y-W, Mezaache-Achiour S, Glare TR, Borriss R, Vinale F, *et al.* 2019. Antimicrobial secondary metabolites from agriculturally important fungi as next biocontrol agents. *Applied Microbiology and Biotechnology* **103**: 9287–9303.

Kim HS, Han KY, Kim KJ, Han DM, Jahng KY, Chae KS. **2002**. The *veA* gene activates sexual development in *Aspergillus nidulans*. *Fungal Genetics and Biology* **37**: 72–80.

Kim HJ, Han JH, Kim KS, Lee YH. **2014**. Comparative functional analysis of the velvet gene family reveals unique roles in fungal development and pathogenicity in *Magnaporthe oryzae*. *Fungal Genetics and Biology* **66**: 33–43.

Kim MJ, Lee MK, Pham HQ, Gu MJ, Zhu B, Son SH, Hahn D, Shin JH, Yu JH, Park HS, *et al.* 2020. The velvet regulator VosA governs survival and secondary metabolism of sexual spores in *Aspergillus nidulans*. *Genes* **11**: 103.

Kipreos ET, Pagano M. **2000**. The F-box protein family. *Genome Biology* **1**: reviews3002.1.

Klebahn H. **1913**. Beiträge zur Kenntnis der Fungi imperfecti. I. Eine *Verticillium*-Krankheit auf Dahlien. *Mycologisches Centralblatt* **3**: 49–66.

Klimes A, Dobinson KF. **2006**. A hydrophobin gene, *VDH1*, is involved in microsclerotial development and spore viability in the plant pathogen *Verticillium dahliae*. *Fungal Genetics and Biology* **43**: 283–294.

Klosterman SJ, Atallah ZK, Vallad GE, Subbarao K V. 2009. Diversity, pathogenicity, and management of *Verticillium* species. *Annual Review of Phytopathology* **47**: 39–62.

Klosterman SJ, Subbarao K V., Kang S, Veronese P, Gold SE, Thomma BPHJ, Chen Z, Henrissat B, Lee YH, Park J, *et al.* 2011. Comparative genomics yields insights into niche adaptation of plant vascular wilt pathogens. *PLoS Pathogens* **7**: e1002137.

Köhl J, Kolnaar R, Ravensberg WJ. **2019**. Mode of action of microbial biological control agents against plant diseases: relevance beyond efficacy. *Frontiers in Plant Science* **10**: 845.

Köhler AM, Harting R, Langeneckert AE, Valerius O, Gerke J, Meister C, Strohdiek A, Braus GH. **2019**. Integration of fungus-specific CandA-C1 into a trimeric CandA complex allowed splitting of the gene for the conserved receptor exchange factor of CullinA E3 ubiquitin ligases in Aspergilli. *mBio* **10**: e01094-19.

Kolar M, Punt PJ, van den Hondel CAMJJ, Schwab H. **1988**. Transformation of *Penicillium chrysogenum* using dominant selection markers and expression of an *Escherichia coli lacZ* fusion gene. *Gene* **62**: 127–134.

König CC, Scherlach K, Schroeckh V, Horn F, Nietzsche S, Brakhage AA, Hertweck C. **2013**. Bacterium induces cryptic meroterpenoid pathway in the pathogenic fungus *Aspergillus fumigatus*. *ChemBioChem* **14**: 938–942.

Kopke K, Hoff B, Bloemendal S, Katschorowski A, Kamerewerd J, Kück U. **2013**. Members of the *Penicillium chrysogenum* velvet complex play functionally opposing roles in the regulation of penicillin biosynthesis and conidiation. *Eukaryotic Cell* **12**: 299–310.

Kosugi S, Hasebe M, Tomita M, Yanagawa H. **2009**. Systematic identification of cell cycle-dependent yeast nucleocytoplasmic shuttling proteins by prediction of composite motifs. *Proceedings of the National Academy of Sciences of the United States of America* **106**: 10171–10176.

Krappmann S, Sasse C, Braus GH. **2006**. Gene targeting in *Aspergillus fumigatus* by homologous recombination is facilitated in a nonhomologous end- joining-deficient genetic background. *Eukaryotic Cell* **5**: 212–215.

Kroken S, Glass NL, Taylor JW, Yoder OC, Turgeon BG. **2003**. Phylogenomic analysis of type I polyketide synthase genes in pathogenic and saprobic ascomycetes. *Proceedings of the National Academy of Sciences* **100**: 15670–15675.

Kuzmin E, VanderSluis B, Nguyen Ba AN, Wang W, Koch EN, Usaj M, Khmelinskii A, Usaj MM, van Leeuwen J, Kraus O, *et al.* 2020. Exploring whole-genome duplicate gene retention with complex genetic interaction analysis. *Science* **368**: eaaz5667.

Kyrmizi I, Ferreira H, Carvalho A, Figueroa JAL, Zarmpas P, Cunha C, Akoumianaki T, Stylianou K, Deepe GSJ, Samonis G, *et al.* 2018. Calcium sequestration by fungal melanin inhibits calcium–calmodulin signalling to prevent LC3-associated phagocytosis. *Nature Microbiology* **3**: 791–803.

Laemmli UK. **1970**. Cleavage of structural proteins during the assembly of the head of bacteriophage T4. *Nature* **227**: 680–685.

de Lamo FJ, Takken FLW. **2020**. Biocontrol by *Fusarium oxysporum* using endophyte-mediated resistance. *Frontiers in Plant Science* **11**: 37.

Latgé J-P, Chamilos G. **2019**. *Aspergillus fumigatus* and aspergillosis in 2019. *Clinical Microbiology Reviews* **33**: e00140-18.

Lazo GR, Stein PA, Ludwig RA. **1991**. A DNA transformation-competent *Arabidopsis* genomic library in *Agrobacterium*. *Biotechnology (N Y)* **9**: 963–967.

van der Lee R, Buljan M, Lang B, Weatheritt RJ, Daughdrill GW, Dunker AK, Fuxreiter M, Gough J, Gsponer J, Jones DT, *et al.* 2014. Classification of intrinsically disordered regions and proteins. *Chemical Reviews* **114**: 6589–6631.

Leonard M. **2019**. Developmental regulators and secreted effector molecules of the fungal pathogen *Verticillium* spp . *Dissertation at the Georg-August-Universität Göttingen*.

Leonard M, Kühn A, Harting R, Maurus I, Nagel A, Starke J, Kusch H, Valerius O, Feussner K, Feussner I, *et al.* 2020. *Verticillium longisporum* elicits media-dependent secretome responses with capacity to distinguish between plant-related environments. *Frontiers in Microbiology* **11**: 1876.

Li P, Pu X, Feng B, Yang Q, Shen H, Zhang J, Lin B. **2015**. *FocVel1* influences asexual production, filamentous growth, biofilm formation, and virulence in *Fusarium oxysporum* f. sp. *cucumerinum*. *Frontiers in Plant Science* **6**: 312.

Li J-J, Zhou L, Yin C-M, Zhang D-D, Klosterman SJ, Wang B-L, Song J, Wang D, Hu X-P, Subbarao K V., *et al.* 2019. The *Verticillium dahliae* Sho1-MAPK pathway regulates melanin biosynthesis and is required for cotton infection. *Environmental Microbiology* **21**: 4852–4874.

Lin CJ, Sasse C, Gerke J, Valerius O, Irmer H, Frauendorf H, Heinekamp T, Straßburger M, Tran VT, Herzog B, *et al.* 2015. Transcription factor SomA is required for adhesion, development and virulence of the human pathogen *Aspergillus fumigatus*. *PLoS Pathogens* **11**: e1005205.

López-Berges MS, Hera C, Sulyok M, Schäfer K, Capilla J, Guarro J, Di Pietro A. **2013**. The velvet complex governs mycotoxin production and virulence of *Fusarium oxysporum* on plant and mammalian hosts. *Molecular Microbiology* **87**: 49–65.

López-Berges MS, Di Pietro A, Daboussi MJ, Wahab HA, Vasnier C, Roncero MIG, Dufresne M, Hera C. **2009**. Identification of virulence genes in *Fusarium oxysporum* f. sp. *lycopersici* by large-scale transposon tagging. *Molecular Plant Pathology* **10**: 95–107.

Macheleidt J, Mattern DJ, Fischer J, Netzker T, Weber J, Schroeckh V, Valiante V, Brakhage AA. **2016**. Regulation and role of fungal secondary metabolites. *Annual Review of Genetics* **50**: 371–392.

Machowska A, Stålsby Lundborg C. **2019**. Drivers of irrational use of antibiotics in Europe. *International Journal of Environmental Research and Public Health* **16**: 27.

Maharachchikumbura SSN, Hyde KD, Jones EBG, McKenzie EHC, Bhat JD, Dayarathne MC, Huang SK, Norphanphoun C, Senanayake IC, Perera RH, *et al.* 2016. Families of Sordariomycetes. *Fungal Diversity* **79**: 1–317.

Marinelli F, Zanelli U, Nuti Ronchi V. **1996**. Toxicity of 6-methoxymellein and 6-hydroxymellein to the producing carrot cells. *Phytochemistry* **42**: 641–643.

Martin FN. **2003**. Development of a alternative strategies for management of soilborne pathogens currently controlled with methyl bromide. *Annual Review of Phytopathology* **41**: 325–350.

Mavrodi D V., Blankenfeldt W, Thomashow LS. **2006**. Phenazine compounds in fluorescent *Pseudomonas* spp. biosynthesis and regulation. *Annual Review of Phytopathology* **44**: 417–445.

McCluskey K, Wiest A, Plamann M. **2010**. The Fungal Genetics Stock Center: a repository for 50 years of fungal genetics research. *Journal of Biosciences* **35**: 119–126.

Meister C, Thieme KG, Thieme S, Köhler AM, Schmitt K, Valerius O, Braus GH. **2019**. COP9 signalosome interaction with UspA/Usp15 deubiquitinase controls VeA-mediated fungal multicellular development. *Biomolecules* **9**: 238.

Mendes R, Garbeva P, Raaijmakers JM. **2013**. The rhizosphere microbiome: significance of plant beneficial, plant pathogenic, and human pathogenic microorganisms. *FEMS Microbiology Reviews* **37**: 634–663.

Milgroom MG, Jimenez-Gasco M d M, Olivares-Garcia C, Drott MT, Jimenez-Diaz RM. **2014**. Recombination between clonal lineages of the asexual fungus *Verticillium dahliae* detected by genotyping by sequencing. *PLoS ONE* **9**: e106740.

Mitchell AL, Attwood TK, Babbitt PC, Blum M, Bork P, Bridge A, Brown SD, Chang HY, El-Gebali S, Fraser MI, *et al.* 2019. InterPro in 2019: improving coverage, classification and access to protein sequence annotations. *Nucleic Acids Research* **47**: D351–D360.

Møbjerg N, Halberg KA, Jørgensen A, Persson D, Bjørn M, Ramløv H, Kristensen RM. **2011**. Survival in extreme environments - on the current knowledge of adaptations in tardigrades. *Acta Physiologica* **202**: 409–420.

Mohnen D. **2008**. Pectin structure and biosynthesis. *Current Opinion in Plant Biology* **11**: 266–277.

MoNA database. **2007**. MoNA - MassBank of North America. [WWW document] URL https://mona.fiehnlab.ucdavis.edu/. [accessed July 2020].

Mooney JL, Hassett DE, Yager LN. **1990**. Genetic analysis of suppressors of the *veA1* mutation in *Aspergillus nidulans*. *Genetics* **126**: 869–874.

Mooney JL, Yager LN. **1990**. Light is required for conidiation in *Aspergillus nidulans*. *Genes and Development* **4**: 1473–1482.

Mousa WK, Raizada MN. **2015**. Biodiversity of genes encoding anti-microbial traits within plant associated microbes. *Frontiers in Plant Science* **6**: 231.

Mullins ED, Chen X, Romaine P, Raina R, Geiser DM, Kang S. **2001**. *Agrobacterium*-mediated transformation of *Fusarium oxysporum*: an efficient tool for insertional mutagenesis and gene transfer. *Phytopathology* **91**: 173–180.

Murashige T, Skoog F. **1962**. A revised medium for rapid growth and bio assays with tobacco tissue cultures. *Physiologia Plantarum* **15**: 474–497.

Naraghi L, Heydari A, Rezaee S. **2012**. Biocontrol agent *Talaromyces flavus* stimulates the growth of cotton and potato. *Journal of Plant Growth Regulation* **31**: 471–477.

Naraghi L, Heydari A, Rezaee S, Razavi M, Afshari-Azad H. **2010a**. Biological control of Verticillium wilt of greenhouse cucumber by *Talaromyces flavus*. *Phytopathologia Mediterranea* **49**: 321–329.

Naraghi L, Heydari A, Rezaee S, Razavi M, Jahanifar H. **2010b**. Study on antagonistic effects of *Talaromyces flavus* on *Verticillium albo-atrum*, the causal agent of potato wilt disease. *Crop Protection* **29**: 658–662.

Naraghi L, Heydari A, Rezaee S, Razavi M, Jahanifar H, Khaledi EM. **2010c**. Biological control of tomato Verticillium wilt disease by *Talaromyces flavus*. *Journal of Plant Protection Research* **50**: 360–365.

Naraghi L, Zareh-Maivan H, Heydari A, Afshari-Azad H. **2007**. Investigation of the effect of heating, vesicular arbuscular mycorrhiza and thermophilic fungus on cotton wilt disease. *Pakistan Journal of Biological Sciences* **10**: 1596–1603.

Naranjo-Ortiz MA, Gabaldón T. **2019**. Fungal evolution: diversity, taxonomy and phylogeny of the fungi. *Biological Reviews* **94**: 2101–2137.

Nesemann K, Braus-Stromeyer SA, Harting R, Höfer A, Kusch H, Batista Ambrosio A, Timpner C, Braus GH. **2018**. Fluorescent pseudomonads pursue media-dependent strategies to inhibit growth of pathogenic *Verticillium* fungi. *Applied Microbiology and Biotechnology* **102**: 817–831.

Netzker T, Fischer J, Weber J, Mattern DJ, König CC, Valiante V, Schroeckh V, Brakhage AA. **2015**. Microbial communication leading to the activation of silent fungal secondary metabolite gene clusters. *Frontiers in Microbiology* **6**: 299.

Neumann MJ, Dobinson KF. **2003**. Sequence tag analysis of gene expression during pathogenic growth and microsclerotia development in the vascular wilt pathogen *Verticillium dahliae*. *Fungal Genetics and Biology* **38**: 54–62.

Ni M, Yu J. **2007**. A novel regulator couples sporogenesis and trehalose biogenesis in *Aspergillus nidulans*. *PLoS ONE* **2**: e970.

Nishi A, Kurosaki F. **1993**. XIII Daucus carota L. (Carrot): *in vitro* production of carotenoids and phytoalexins. In: Bajaj YPS, ed. Biotechnology in agriculture and Forestry 24. Springer Science & Business Media.

Njoroge SMC, Kabir Z, Martin FN, Koike ST, Subbarao K V. 2009. Comparison of crop rotation for Verticillium wilt management and effect on *Pythium* species in conventional and organic strawberry production. *Plant Disease* **93**: 519–527.

Noble LM, Andrianopoulos A. **2013**. Reproductive competence: a recurrent logic module in eukaryotic development. *Proceedings of the Royal Society B: Biological Sciences* **280**: 20130819.

Nützmann H-W, Reyes-Dominguez Y, Scherlach K, Schroeckh V, Horn F, Gacek A, Schümann J, Hertweck C, Strauss J, Brakhage AA. **2011**. Bacteria-induced natural product formation in the fungus *Aspergillus nidulans* requires Saga/Ada-mediated histone acetylation. *Proceedings of the National Academy of Sciences* **108**: 14282–14287.

O'Dea E, Hoffmann A. **2010**. The regulatory logic of the NF-κB signaling system. *Cold Spring Harbor Perspectives in Biology* **2**: a000216.

Oeckinghaus A, Hayden MS, Ghosh S. **2011**. Crosstalk in NF-κB signaling pathways. *Nature Immunology* **12**: 695–708.

Oliveros JC. **2015**. Venny. An interactive tool for comparing lists with Venn`s diagrams. [WWW document] URL https://bioinfogp.cnb.csic.es/t. [accessed June 2020].

Palmer JM, Theisen JM, Duran RM, Grayburn WS, Calvo AM, Keller NP. **2013**. Secondary metabolism and development is mediated by LlmF control of VeA subcellular localization in *Aspergillus nidulans*. *PLoS Genetics* **9**: e1003193.

Park HS, Bayram Ö, Braus GH, Kim SC, Yu J-H. **2012a**. Characterization of the velvet regulators in Aspergillus fumigatus. *Molecular Microbiology* **86**: 937–953.

Park HS, Nam TY, Han KH, Kim SC, Yu JH. **2014**. VelC positively controls sexual development in *Aspergillus nidulans*. *PLoS ONE* **9**: e89883.

Park HS, Ni M, Jeong KC, Kim YH, Yu JH. **2012b**. The role, interaction and regulation of the velvet regulator VelB in *Aspergillus nidulans*. *PLoS ONE* **7**: e45935.

Pegg GF, Brady BL. **2002**. *Verticillium Wilts* (GF Pegg and BL Brady, Eds.). Wallingford: CABI Publishing.

Pemberton CL, Salmond GP. **2004**. The Nep1-like proteins — a growing family of microbial elicitors of plant necrosis. *Molecular Plant Pathology* **5**: 353–359.

Perfect JR, Tenor JL, Miao Y, Brennan RG. **2017**. Trehalose pathway as an antifungal target. *Virulence* **8**: 143–149.

Petrasch S, Knapp SJ, van Kan JAL, Blanco-Ulate B. **2019**. Grey mould of strawberry, a devastating disease caused by the ubiquitous necrotrophic fungal pathogen *Botrytis cinerea*. *Molecular Plant Pathology* **20**: 877–892.

Pfliegler WP, Pócsi I, Győri Z, Pusztahelyi T. **2020**. The *Aspergilli* and their mycotoxins: metabolic interactions with plants and the soil biota. *Frontiers in Microbiology* **10**: 2921.

Pieterse CMJ, Zamioudis C, Berendsen RL, Weller DM, Van Wees SCM, Bakker PAHM. **2014**. Induced systemic resistance by beneficial microbes. *Annual Review of Phytopathology* **52**: 347–375.

Punt PJ, Dingemanse MA, Jacobs-Meijsing BJM, Pouwels PH, van den Hondel CAMJJ. **1988**. Isolation and characterization of the glyceraldehyde-3-phosphate dehydrogenase gene of *Aspergillus nidulans*. *Gene* **69**: 49–57.

Purschwitz J, Müller S, Kastner C, Schösser M, Haas H, Espeso EA, Atoui A, Calvo AM, Fischer R. **2008**. Functional and physical interaction of blue- and red-light sensors in *Aspergillus nidulans*. *Current Biology* **18**: 255–259.

Qutob D, Kemmerling B, Brunner F, Küfner I, Engelhardt S, Gust AA, Luberacki B, Seitz HU, Stahl D, Rauhut T, *et al.* 2006. Phytotoxicity and innate immune responses induced by Nep1-like proteins. *The Plant Cell* **18**: 3721–3744.

Raaijmakers JM, Mazzola M. **2012**. Diversity and natural functions of antibiotics produced by beneficial and plant pathogenic bacteria. *Annual Review of Phytopathology* **50**: 403–424.

Rappsilber J, Ishihama Y, Mann M. **2003**. Stop And Go Extraction tips for matrix-assisted laser desorption/ionization, nanoelectrospray, and LC/MS sample pretreatment in proteomics. *Analytical Chemistry* **75**: 663–670.

Rappsilber J, Mann M, Ishihama Y. **2007**. Protocol for micro-purification, enrichment, pre-fractionation and storage of peptides for proteomics using StageTips. *Nature Protocols* **2**: 1896–1906.

Rauscher S, Pacher S, Hedtke M, Kniemeyer O, Fischer R. **2016**. A phosphorylation code of the *Aspergillus nidulans* global regulator VelvetA (VeA) determines specific functions. *Molecular Microbiology* **99**: 909–924.

Rechsteiner M, Rogers SW. **1996**. PEST sequences and regulation by proteolysis. *Trends in Biochemical Sciences* **21**: 267–271.

Reusche M, Thole K, Janz D, Truskina J, Rindfleisch S, Drübert C, Polle A, Lipka V, Teichmann T. **2012**. *Verticillium* infection triggers VASCULAR-RELATED NAC DOMAIN7 – dependent de novo xylem formation and enhances drought tolerance in *Arabidopsis*. *The Plant Cell* **24**: 3823–3837.

Reusche M, Truskina J, Thole K, Nagel L, Rindfleisch S, Tran VT, Braus-Stromeyer SA, Braus GH, Teichmann T, Lipka V. **2014**. Infections with the vascular pathogens *Verticillium longisporum* and *Verticillium dahliae* induce distinct disease symptoms and differentially affect drought stress tolerance of *Arabidopsis thaliana*. *Environmental and Experimental Botany* **108**: 23–37.

Reyes-Dominguez Y, Bok JW, Berger H, Shwab EK, Basheer A, Gallmetzer A, Scazzocchio C, Keller N, Strauss J. **2010**. Heterochromatic marks are associated with the repression of secondary metabolism clusters in *Aspergillus nidulans*. *Molecular Microbiology* **76**: 1376–1386.

Romero-Calvo I, Ocón B, Martínez-Moya P, Suárez MD, Zarzuelo A, Martínez-Augustin O, de Medina FS. **2010**. Reversible Ponceau staining as a loading control alternative to actin in Western blots. *Analytical Biochemistry* **401**: 318–320.

Ryder LS, Talbot NJ. **2015**. Regulation of appressorium development in pathogenic fungi. *Current Opinion in Plant Biology* **26**: 8–13.

Saiki RK, Gelfand DH, Stoffel S, Scharf SJ, Higuchi R, Horn GT, Mullis KB, Erlich HA. **1988**. Primer-directed enzymatic amplification of DNA with a thermostable DNA polymerase. *Science* **239**: 487–491.

Saito H. **2010**. Regulation of cross-talk in yeast MAPK signaling pathways. *Current Opinion in Microbiology* **13**: 677–683.

Salichos L, Rokas A. **2010**. The diversity and evolution of circadian clock proteins in fungi. *Mycologia* **102**: 269–278.

Sanchez JF, Somoza AD, Keller NP, Wang CCC. **2012**. Advances in *Aspergillus* secondary metabolite research in the post-genomic era. *Natural Product Reports* **29**: 351–371.

Santhanam P, van Esse HP, Albert I, Faino L, Nürnberger T, Thomma BPHJ. **2013**. Evidence for functional diversification within a fungal NEP1-like protein family. *Molecular Plant-Microbe Interactions* **26**: 278–286.

Sarikaya-Bayram Ö, Bayram Ö, Feussner K, Kim J-H, Kim H-S, Kaever A, Feussner I, Chae KS, Han DM, Han KH, *et al.* 2014. Membrane-bound methyltransferase complex VapA-VipC-VapB guides epigenetic control of fungal development. *Developmental Cell* **29**: 406–420.

Sarikaya-Bayram Ö, Bayram Ö, Valerius O, Park HS, Irniger S, Gerke J, Ni M, Han K-H, Yu J-H, Braus GH. **2010**. LaeA control of velvet family regulatory proteins for light-dependent development and fungal cell-type specificity. *PLoS genetics* **6**: e1001226.

Sarikaya-Bayram Ö, Dettmann A, Karahoda B, Moloney NM, Ormsby T, McGowan J, Cea-Sánchez S, Miralles-Durán A, Brancini GTP, Luque EM, *et al.* 2019. Control of development, secondary metabolism and light-dependent carotenoid biosynthesis by the velvet complex of *Neurospora crassa*. *Genetics* **212**: 691–710.

Sarikaya-Bayram Ö, Palmer JM, Keller N, Braus GH, Bayram Ö. **2015**. One Juliet and four Romeos: VeA and its methyltransferases. *Frontiers in Microbiology* **6**: 1.

Scharf DH, Heinekamp T, Brakhage AA. **2014**. Human and plant fungal pathogens: the role of secondary metabolites. *PLoS Pathogens* **10**: e1003859.

Scherlach K, Hertweck C. **2009**. Triggering cryptic natural product biosynthesis in microorganisms. *Organic and Biomolecular Chemistry* **7**: 1753–1760.

Schnathorst WC. **1963**. Theoretical relationships between inoculum potential and disease severity based on a study of the variation in virulence among isolates of *V. albo-atrum*. *Phytopathology* **53**: 888–894.

Schroeckh V, Scherlach K, Nützmann H-W, Shelest E, Schmidt-Heck W, Schuemann J, Martin K, Hertweck C, Brakhage AA. **2009**. Intimate bacterial-fungal interaction triggers biosynthesis of archetypal polyketides in *Aspergillus nidulans*. *Proceedings of the National Academy of Sciences of the United States of America* **106**: 14558–14563.

Schumacher J. **2016**. DHN melanin biosynthesis in the plant pathogenic fungus *Botrytis cinerea* is based on two developmentally regulated key enzyme (PKS)-encoding genes. *Molecular Microbiology* **99**: 729–748.

Schumacher J, Pradier JM, Simon A, Traeger S, Moraga J, Collado IG, Viaud M, Tudzynski B. **2012**. Natural variation in the *VELVET* gene *bcvel1* affects virulence and light-dependent differentiation in *Botrytis cinerea*. *PLoS ONE* **7**: e47840.

Schumacher J, Simon A, Cohrs KC, Traeger S, Porquier A, Dalmais B, Viaud M, Tudzynski B. **2015**. The VELVET complex in the gray mold fungus *Botrytis cinerea*: impact of BcLAE1 on differentiation, secondary metabolism, and virulence. *Molecular Plant-Microbe Interactions* **28**: 659–674.

Schumacher J, Simon A, Cohrs KC, Viaud M, Tudzynski P. **2014**. The transcription factor BcLTF1 regulates virulence and light responses in the necrotrophic plant pathogen *Botrytis cinerea*. *PLoS Genetics* **10**: e1004040.

Shao CL, Han L, Li CY, Liu Z, Wang CY. **2009**. 6,8-Dihydroxy-3-methyl-isocoumarin. *Acta Crystallographica Section E: Structure Reports Online* **65**: o736.

Shi-Kunne X, Jové R de P, Depotter JRL, Ebert MK, Seidl MF, Thomma BPHJ. **2019**. *In silico* prediction and characterisation of secondary metabolite clusters in the plant pathogenic fungus *Verticillium dahliae*. *FEMS Microbiology Letters* **366**: fnz081.

Short DPG, Gurung S, Hu X, Inderbitzin P, Subbarao K V. **2014**. Maintenance of sex-related genes and the co-occurrence of both mating types in *Verticillium dahliae*. *PLoS ONE* **9**: e112145.

Singh S, Braus-Stromeyer SA, Timpner C, Tran VT, Lohaus G, Reusche M, Knüfer J, Teichmann T, von Tiedemann A, Braus GH. **2010**. Silencing of Vlaro2 for chorismate synthase revealed that the phytopathogen *Verticillium longisporum* induces the cross-pathway control in the xylem. *Applied Microbiology and Biotechnology* **85**: 1961–1976.

Singh S, Braus-Stromeyer SA, Timpner C, Valerius O, von Tiedemann A, Karlovsky P, Druebert C, Polle A, Braus GH. **2012**. The plant host *Brassica napus* induces in the pathogen *Verticillium longisporum* the expression of functional catalase peroxidase which is required for the late phase of disease. *Molecular Plant-Microbe Interactions* **25**: 569–581.

Smith BJ. **1984**. SDS polyacrylamide gel electrophoresis of proteins. In: Walker JM, ed. Methods in Molecular Biology. 41–55.

Song R, Li J, Xie C, Jian W, Yang X. **2020**. An overview of the molecular genetics of plant resistance to the Verticillium wilt pathogen *Verticillium dahliae*. *International Journal of Molecular Sciences* **21**: 1120.

Southern EM. **1975**. Detection of specific sequences among DNA fragments separated by gel electrophoresis. *Journal of Molecular Biology* **98**: 503–508.

Spatafora JW, Aime MC, Grigoriev IV, Martin F, Stajich JE, Blackwell M. **2017**. The fungal tree of life: from molecular systematics to genome-scale phylogenies. In: Heitman J, Howlett B, Crous P, Stukenbrock E, James T, Gow N, eds. *The Fungal Kingdom*. Washington, D.C.: ASM Press, 3–34.

Stadler M, von Tiedemann A. **2014**. Biocontrol potential of *Microsphaeropsis ochracea* on microsclerotia of *Verticillium longisporum* in environments differing in microbial complexity. *BioControl* **59**: 449–460.

Starke J. **2019**. Interplay of *Verticillium* signaling genes favoring benefical or detrimental outcomes in interactions with plant hosts. *Dissertation at the Georg-August-Universität Göttingen*.

Starke J, Harting R, Maurus I, Bremenkamp R, Kronstad JW, Braus GH. **2020**. Unfolded protein response and scaffold independent pheromone MAP kinase signalling control *Verticillium dahliae* growth, development and plant pathogenesis. *bioRxiv*: doi: 10.1101/2020.02.10.941450.

Steiner U, Oerke EC. **2007**. Localized melanization of appressoria is required for pathogenicity of *Venturia inaequalis*. *Phytopathology* **97**: 1222–1230.

Stinnett SM, Espeso EA, Cobeño L, Araújo-Bazán L, Calvo AM. **2007**. *Aspergillus nidulans* VeA subcellular localization is dependent on the importin α carrier and on light. *Molecular Microbiology* **63**: 242–255.

Stutz EW, Defago G, Kern H. **1986**. Naturally occuring fluorescent pseudomonads involved in suppression of black root rot of tobacco. *Phytopathology* **76**: 181–185.

Syed Ab Rahman SF, Singh E, Pieterse CMJ, Schenk PM. **2018**. Emerging microbial biocontrol strategies for plant pathogens. *Plant Science* **267**: 102–111.

Szewczyk E, Nayak T, Oakley CE, Edgerton H, Xiong Y, Taheri-Talesh N, Osmani SA, Oakley BR. **2006**. Fusion PCR and gene targeting in *Aspergillus nidulans*. *Nature Protocols* **1**: 3111–3120.

Tang K, Lv W, Zhang Q, Zhou C. **2020**. Coding the α-subunit of SNF1 kinase, *Snf1* is required for the conidiogenesis and pathogenicity of the *Alternaria alternata* tangerine pathotype. *Fungal Biology* **124**: 562–570.

Thakur R, Shankar J. **2017**. Proteome profile of *Aspergillus terreus* conidia at germinating stage: identification of probable virulent factors and enzymes from mycotoxin pathways. *Mycopathologia* **182**: 771–784.

Thieme S. **2018**. Insertion of an intrinsically disordered domain in VelB supports selective heterodimer formation of fungal velvet domain regulatory proteins in *Aspergillus nidulans*. *Dissertation at the Georg-August-Universität Göttingen*.

Thieme KG, Gerke J, Sasse C, Valerius O, Thieme S, Karimi R, Heinrich AK, Finkernagel F, Smith K, Bode HB, *et al.* 2018. Velvet domain protein VosA represses the zinc cluster transcription factor SclB regulatory network for *Aspergillus nidulans* asexual development, oxidative stress response and secondary metabolism. *PLoS Genetics* **14**: e1007511.

Tian L, Wang Y, Yu J, Xiong D, Zhao H, Tian C. **2016**. The mitogen-activated protein kinase kinase VdPbs2 of *Verticillium dahliae* regulates microsclerotia formation, stress response, and plant infection. *Frontiers in Microbiology* **7**: 1532.

Timpner C. **2013**. Roles of the Cpc1 regulator of the cross-pathway control in the *Verticillium* plant pathogens. *Dissertation at the Georg-August-Universität Göttingen*.

Timpner C, Braus-Stromeyer SA, Tran VT, Braus GH. **2013**. The Cpc1 regulator of the cross-pathway control of amino acid biosynthesis is required for pathogenicity of the vascular pathogen Verticillium longisporum. *Molecular Plant-Microbe Interactions* **26**: 1312–1324.

Tisch D, Schmoll M. **2010**. Light regulation of metabolic pathways in fungi. *Applied Microbiology and Biotechnology* **85**: 1259–1277.

Toghueo RMK. **2020**. Bioprospecting endophytic fungi from *Fusarium* genus as sources of bioactive metabolites. *Mycology* **11**: 1–21.

Toghueo RMK, Boyom FF. **2020**. Endophytic *Penicillium* species and their agricultural, biotechnological, and pharmaceutical applications. *3 Biotech* **10**: 107.

Tran VT, Braus-Stromeyer SA, Kusch H, Reusche M, Kaever A, Kühn A, Valerius O, Landesfeind M, Aßhauer K, Tech M, *et al.* 2014. Verticillium transcription activator of adhesion Vta2 suppresses microsclerotia formation and is required for systemic infection of plant roots. *New Phytologist* **202**: 565–581.

Tran VT, Braus-Stromeyer SA, Timpner C, Braus GH. **2013**. Molecular diagnosis to discriminate pathogen and apathogen species of the hybrid *Verticillium longisporum* on the oilseed crop *Brassica* napus. *Applied Microbiology and Biotechnology* **97**: 4467–4483.

Troppens DM, Köhler AM, Schlüter R, Hoppert M, Gerke J, Braus GH. **2020**. Hülle cells of *Aspergillus nidulans* with nuclear storage and developmental backup functions are reminiscent of multipotent stem cells. *mBio* **11**: e01673-20.

Tyanova S, Temu T, Sinitcyn P, Carlson A, Hein MY, Geiger T, Mann M, Cox J. **2016**. The Perseus computational platform for comprehensive analysis of (prote)omics data. *Nature Methods* **13**: 731–740.

Tzima AK, Paplomatas EJ, Rauyaree P, Ospina-Giraldo MD, Kang S. **2011**. *VdSNF1*, the sucrose nonfermenting protein kinase gene of *Verticillium dahliae*, is required for virulence and expression of genes involved in cell-wall degradation. *Molecular Plant-Microbe Interactions* **24**: 129–142.

Uitenbroek DG. **1997**. *SISA Binomial* [WWW document] URL http://www.quantitativeskills.com/sisa/tableprocs/meanst.htm. [accessed February 2020].

Vallad GE, Subbarao KV. 2008. Colonization of resistant and susceptible lettuce cultivars by a green fluorescent protein-tagged isolate of *Verticillium dahliae*. *Phytopathology* **98**: 871–885.

de Vries RP, Riley R, Wiebenga A, Aguilar-Osorio G, Amillis S, Uchima CA, Anderluh G, Asadollahi M, Askin M, Barry K, *et al.* 2017. Comparative genomics reveals high biological diversity and specific adaptations in the industrially and medically important fungal genus *Aspergillus*. *Genome Biology* **18**: 28.

Waldron KW, Parker ML, Smith AC. **2003**. Plant cell wall and food quality. *Comprehensive Reviews In Food Science And Food Safety* **2**: 101–119.

Wang F, Dijksterhuis J, Wyatt T, Wösten HAB, Bleichrodt RJ. **2015**. VeA of *Aspergillus niger* increases spore dispersing capacity by impacting conidiophore architecture. *Antonie van Leeuwenhoek* **107**: 187–199.

Wang Y, Hu X, Fang Y, Anchieta A, Goldman PH, Hernandez G, Klosterman SJ. **2018**. Transcription factor VdCmr1 is required for pigment production, protection from UV irradiation, and regulates expression of melanin biosynthetic genes in *Verticillium dahliae*. *Microbiology* **164**: 685–696.

Wang Y, Tian L, Xiong D, Klosterman SJ, Xiao S, Tian C. **2016**. The mitogen-activated protein kinase gene, *VdHog1*, regulates osmotic stress response, microsclerotia formation and virulence in *Verticillium dahliae*. *Fungal Genetics and Biology* **88**: 13–23.

Weller DM, Cook RJ. **1983**. Suppression of take-all of wheat by seed treatments with fluorescent pseudomonads. *Phytopathology* **73**: 463–469.

Weller DM, Landa BB, Mavrodi O V., Schroeder KL, De La Fuente L, Blouin Bankhead S, Allende Molar R, Bonsall RF, Mavrodi D V., Thomashow LS. **2007**. Role of 2,4-diacetylphloroglucinol-producing fluorescent *Pseudomonas* spp. in the defense of plant roots. *Plant Biology* **9**: 4–20.

Weller DM, Raaijmakers JM, McSpadden Gardener BB, Thomashow LS. **2002**. Microbial populations responsible for specific soil suppressiveness to plant pathogens. *Annual Review of Microbiology* **40**: 309–348.

Wessel D, Flügge UI. **1984**. A method for the quantitative recovery of protein in dilute solution in the presence of detergents and lipids. *Analytical Biochemistry* **138**: 141–143.

Wheeler TA, Bordovsky JP, Keeling JW. **2019**. The effectiveness of crop rotation on management of Verticillium wilt over time. *Crop Protection* **121**: 157–162.

Widmann C, Gibson S, Jarpe MB, Johnson GL. **1999**. Mitogen-activated protein kinase: conservation of a three-kinase module from yeast to human. *Physiological Reviews* **79**: 143–180.

Wilhelm S. **1955**. Longevity of the Verticillium wilt fungus in the laboratory and field. *Phytopathology* **45**: 180–181.

Wilson RA, Talbot NJ. **2009**. Under pressure: investigating the biology of plant infection by *Magnaporthe oryzae*. *Nature Reviews Microbiology* **7**: 185–195.

Woo SL, Ruocco M, Vinale F, Nigro M, Marra R, Lombardi N, Pascale A, Lanzuise S, Manganiello G, Lorito M. **2014**. *Trichoderma*-based products and their widespread use in agriculture. *The Open Mycology Journal* **8**: 71–126.

Wright PE, Dyson HJ. **2015**. Intrinsically disordered proteins in cellular signaling and regulation. *Nature Reviews Molecular Cell Biology* **16**: 18–29.

Wu Y, Xu L, Yin Z, Dai Q, Gao X, Feng H, Voegele RT, Huang L. **2018**. Two members of the velvet family, VmVeA and VmVelB, affect conidiation, virulence and pectinase expression in *Valsa mali*. *Molecular Plant Pathology* **19**: 1639–1651.

Xiong D, Wang Y, Tian L, Tian C. **2016**. MADS-box transcription factor *VdMcm1* regulates conidiation, microsclerotia formation, pathogenicity, and secondary metabolism of *Verticillium dahliae*. *Frontiers in Microbiologyicrobiology* **7**: 1192.

Yan X, Que Y, Wang H, Wang C, Li Y, Yue X, Ma Z, Talbot NJ, Wang Z. **2013**. The MET13 methylenetetrahydrofolate reductase gene is essential for infection-related morphogenesis in the rice blast fungus *Magnaporthe oryzae*. *PLOS ONE* **8**: e76914.

Yan L, Zhu J, Zhao X, Shi J, Jiang C, Shao D. **2019**. Beneficial effects of endophytic fungi colonization on plants. *Applied Microbiology and Biotechnology* **103**: 3327–3340.

Yu Z, Fischer R. **2019**. Light sensing and responses in fungi. *Nature Reviews Microbiology* **17**: 25–36.

Yu J-H, Keller N. **2005**. Regulation of secondary metabolism in filamentous fungi. *Annual Review of Phytopathology* **43**: 437–458.

Zachow C, Berg C, Müller H, Monk J, Berg G. **2016**. Endemic plants harbour specific *Trichoderma* communities with an exceptional potential for biocontrol of phytopathogens. *Journal of Biotechnology* **235**: 162–170.

Zaehle C, Gressler M, Shelest E, Geib E, Hertweck C, Brock M. **2014**. Terrein biosynthesis in *Aspergillus terreus* and its impact on phytotoxicity. *Chemistry & Biology* **21**: 719–731.

Zare R, Gams W, Starink-Willemse M, Summerbell RC. **2007**. *Gibellulopsis*, a suitable genus for *Verticillium nigrescens*, and *Musicillium*, a new genus for *V. theobromae*. *Nova Hedwigia* **85**: 463–489.

Zeise K, von Tiedemann A. **2002**. Application of RAPD-PCR for virulence type analysis within *Verticillium dahliae* and *V. longisporum*. *Journal of Phytopathology* **150**: 557–563.

Zeng W, Wang D, Kirk W, Hao J. **2012**. Use of *Coniothyrium minitans* and other microorganisms for reducing *Sclerotinia sclerotiorum*. *Biological Control* **60**: 225–232.

Zhang Y, Gao Y, Liang Y, Dong Y, Yang X, Yuan J, Qiu D. **2017a**. The *Verticillium dahliae* SnodProt1-like protein VdCP1 contributes to virulence and triggers the plant immune system. *Frontiers in Plant Science* **8**: 1880.

Zhang WQ, Gui YJ, Short DPG, Li TG, Zhang DD, Zhou L, Liu C, Bao YM, Subbarao KV., Chen JY, *et al.* 2018. *Verticillium dahliae* transcription factor VdFTF1 regulates the expression of multiple secreted virulence factors and is required for full virulence in cotton. *Molecular Plant Pathology* **19**: 841–857.

Zhang T, Zhang B, Hua C, Meng P, Wang S, Chen Z, Du Y, Gao F, Huang J. **2017b**. VdPKS1 is required for melanin formation and virulence in a cotton wilt pathogen *Verticillium dahliae*. *Science China Life Sciences* **60**: 868–879.

Zhao P, Zhao Y-L, Jin Y, Zhang T, Guo H-S. **2014**. Colonization process of *Arabidopsis thaliana* roots by a green fluorescent protein-tagged isolate of *Verticillium dahliae*. *Protein and Cell* **5**: 94–98.

Zhao YL, Zhou TT, Guo HS. **2016**. Hyphopodium-specific VdNoxB/VdPls1- dependent ROS-Ca^{2+} signaling is required for plant infection by *Verticillium dahliae*. *PLoS Pathogens* **12**: e1005793.

Zheng J, Tang C, Deng C, Wang Y. **2019**. Involvement of a response regulator VdSsk1 in stress response, melanin biosynthesis and full virulence in *Verticillium dahliae*. *Frontiers in Microbiology* **10**: 606.

Appendix

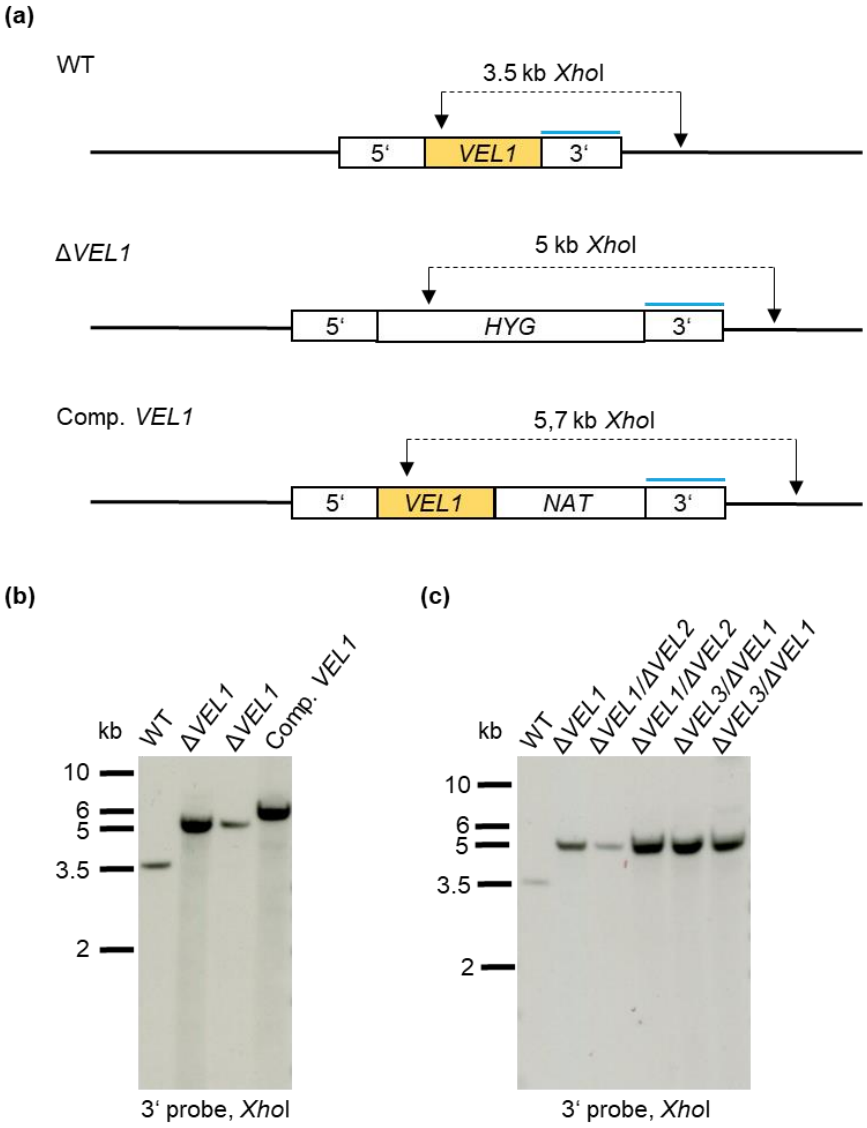

Figure A1: Southern hybridization of the *V. dahliae VEL1* deletion (Δ*VEL1*), double deletion with *VEL2* and *VEL3* and *VEL1* complementation strains. Genomic DNA (gDNA) was extracted from the wild type (WT), two independent transformants of the *VEL1* deletion strain (Δ*VEL1*) with hygromycin resistance cassette (*HYG*), the complementation strain of *VEL1* (Comp. *VEL1*) with nourseothricin resistance cassette (*NAT*) and two independent transformants of *VEL1* and *VEL2* (Δ*VEL1*/Δ*VEL2*) or *VEL3* (Δ*VEL3*/Δ*VEL1*) double deletion strains, each. gDNA was restricted with *Xho*I and used for Southern hybridization with the 3’ region labeled as a probe. **(a)** Restriction sites of *Xho*I in the wildtype, deletion and complementation strains and binding site of the 3’ probe (marked in blue). For each strain the expected fragment size is depicted. **(b)** Southern hybridization of the *VEL1* deletion and complementation strains with wild type control. For the wild type a fragment of 3.5 kb was obtained. Both tested *VEL1* deletion strains resulted in a fragment with a size of 5 kb. The complementation strain shows a fragment with a size of 5.7 kb. **(c)** Southern hybridization of the *VEL1* single, *VEL1*/*VEL2* as well as *VEL3*/*VEL1* double deletion strains and wild type control. The wild type exhibits a fragment with a size of 3.5 kb. All strains containing the deletion cassette of *VEL1* result in a fragment with a size of 5 kb.

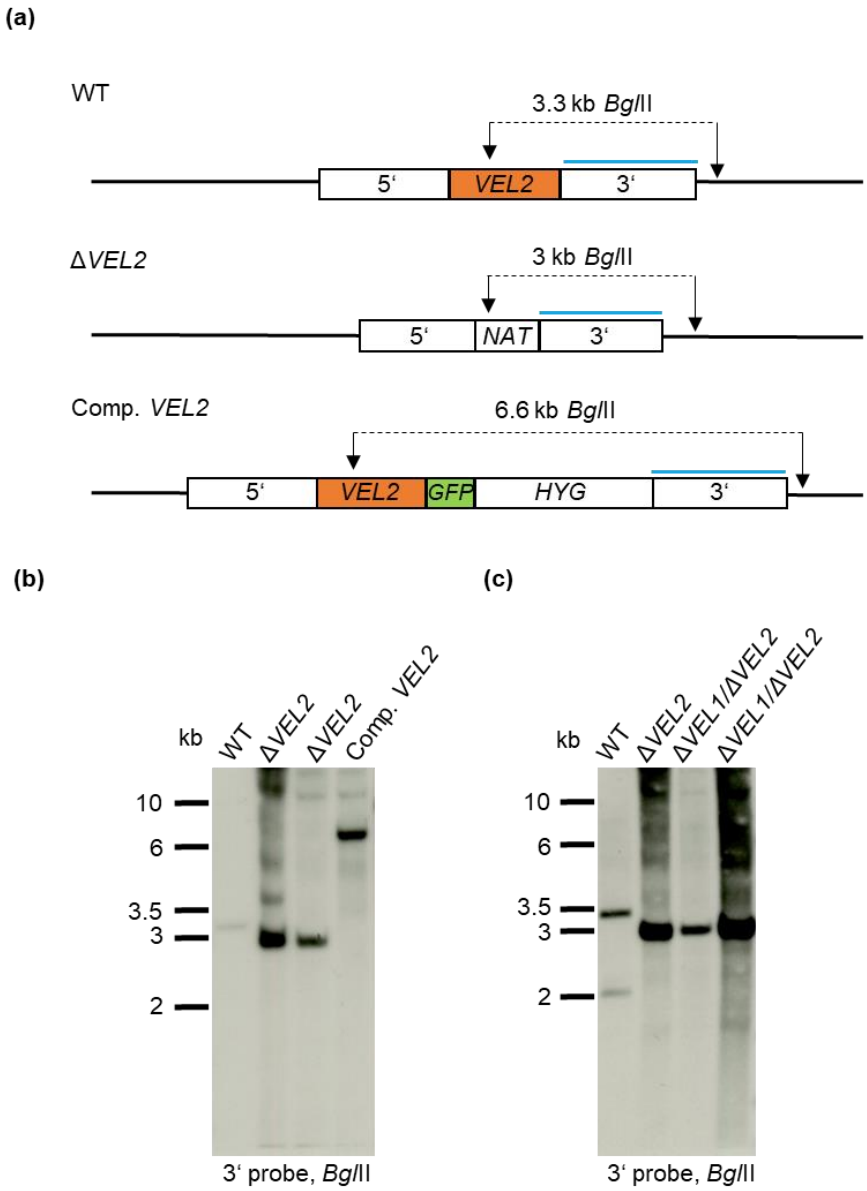

Figure A2: Southern hybridization of the *V. dahliae VEL2* deletion (Δ*VEL2*), double deletion with *VEL1* and *VEL2* and complementation strains. Extracted genomic DNA (gDNA) of the wild type (WT), two independent transformants of the *VEL2* deletion strain (Δ*VEL2*) with nourseothricin resistance cassette (*NAT*), the complementation strain of *VEL2* (Comp. *VEL2*) with hygromycin resistance cassette (*HYG*) and two independent transformants of the double deletion strains of *VEL1* and *VEL2* (Δ*VEL1*/Δ*VEL2*) was restricted with *Bgl*II. The restricted gDNA was used for Southern hybridization with the 3' region as probe. **(a)** Restriction sites of *Bgl*II in the wild type, deletion and complementation strains. The binding site of the 3'region, which was used as probe, is marked in blue. The expected fragment size for each strain is shown. **(b)** Southern hybridization of the *VEL2* deletion and the complementation strains with wild type control. The wild type exhibits a fragment with the size of 3.3 kb. The tested deletion strains show fragments with a size of 3 kb. The complementation strain results in a fragment with a size of approximately 6.6 kb. **(c)** Southern hybridization of the wild type, *VEL2* deletion and *VEL1* and *VEL2* double deletion strains restricted with *Bgl*II and incubated with the 3' probe. The wild type exhibits a fragment size of 3.3 kb. Strains containing the *VEL2* deletion cassette show a fragment with a size of 3 kb.

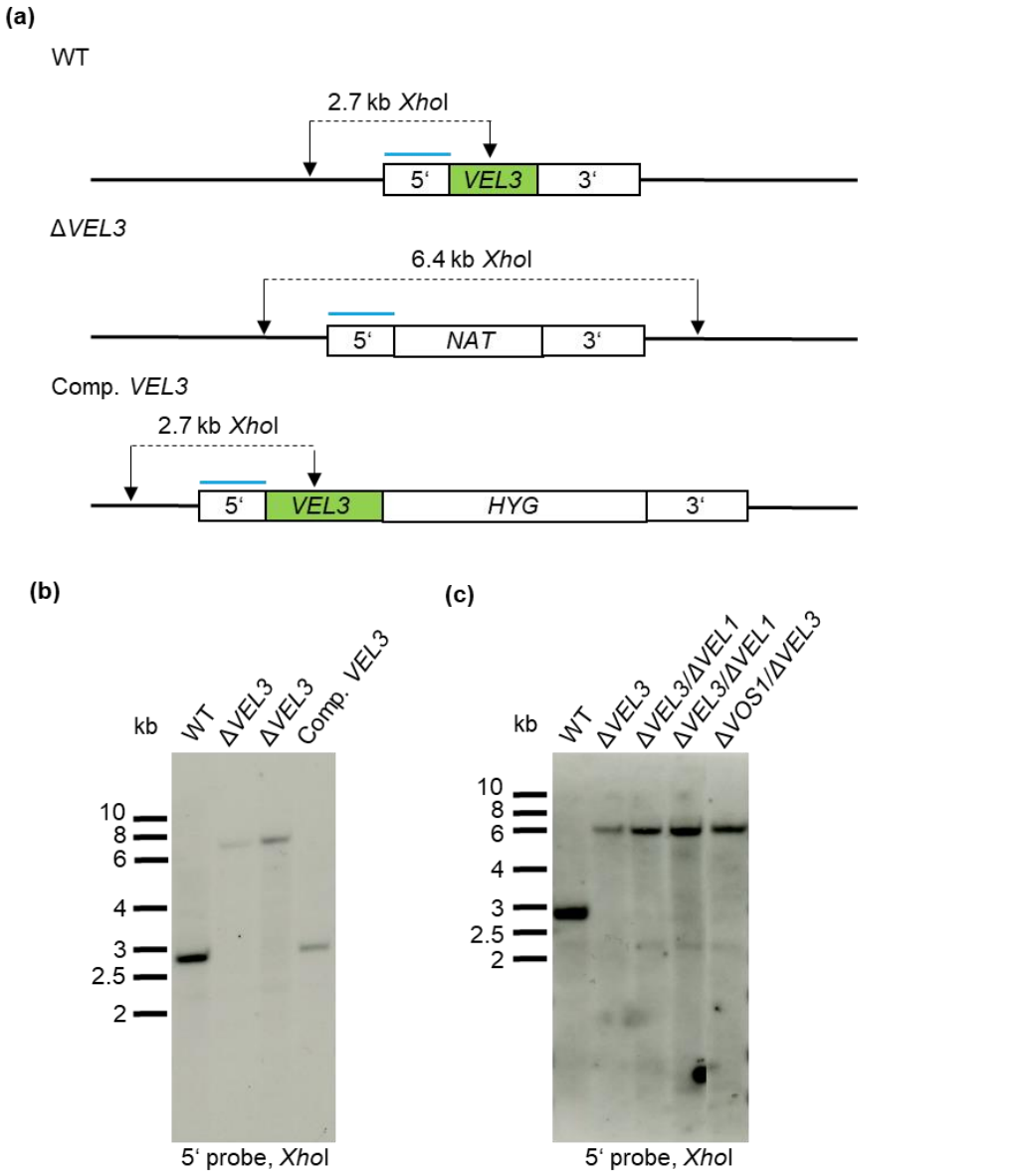

Figure A3: Southern hybridization of the *V. dahliae VEL3* deletion (Δ*VEL3*), double deletion with *VEL1* or *VOS1* and complementation strains. Genomic DNA (gDNA) of the wild type (WT), two independent transformants of the *VEL3* deletion strain (Δ*VEL3*) with nourseothricin resistance cassette (*NAT*), the *VEL3* complementation strain (Comp. *VEL3*) with hygromycin resistance cassette (*HYG*) and two independent transformants of the *VEL3* and *VEL1* (Δ*VEL3*/Δ*VEL1*) as well as a single transformant of *VOS1* and *VEL3* (Δ*VOS1*/Δ*VEL3*) double deletion strains was restricted with *Xho*I. The restricted gDNA was used for Southern hybridization. **(a)** Restriction sites of *Xho*I in the wild type, deletion and complementation strains. The binding site of the 5’ region, which was used as probe, is marked in blue. **(b)** Southern hybridization of the *VEL3* deletion and the complementation strains with wild type control. The wild type results in a fragment with a size of approximately 2.7 kb. The two tested deletion transformants exhibit fragments with a size of 6.4 kb. The complementation shows a fragment with a size of 2.7 kb. **(c)** Southern hybridization of the *VEL3* deletion and *VEL3* and *VEL1* as well as *VOS1* and *VEL3* double deletion strains with wild type control. The wild type results in a fragment of 2.7 kb. Strains containing the *VEL3* deletion cassette exhibit a fragment with a size of 6.4 kb.

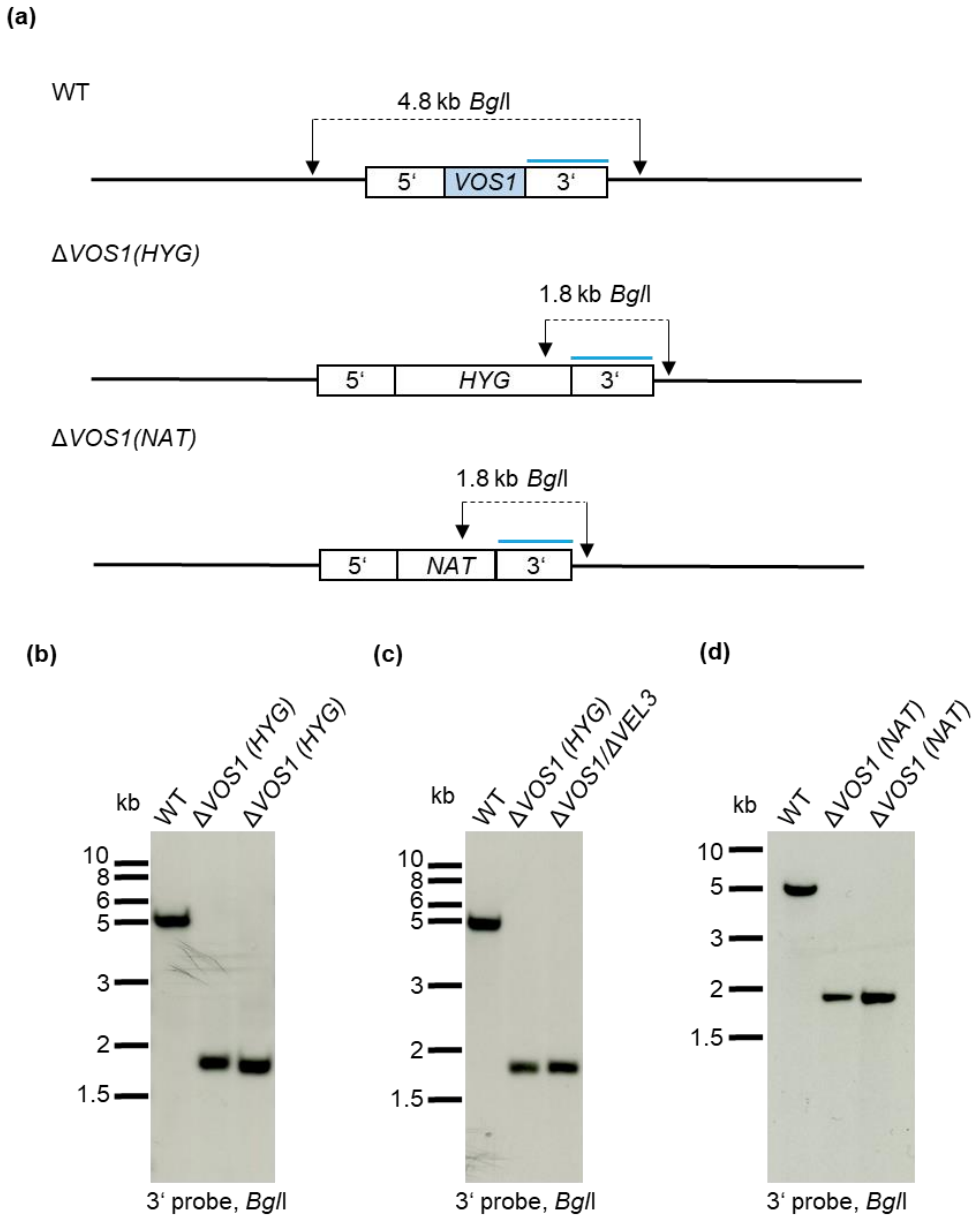

Figure A4: Southern hybridization of the *V. dahliae VOS1* deletion (Δ*VOS1*) and double deletion strains with *VEL3*. Extracted genomic DNA (gDNA) of the wild type (WT), two independent transformants of the *VOS1* deletion strain (Δ*VOS1*) with hygromycin resistance cassette (*HYG*) and the double deletion strain of *VOS1* and *VEL3* (Δ*VOS1*/Δ*VEL3*) as well as two independent transformants of the *VOS1* deletion strain (Δ*VOS1*) with nourseothricin resistance cassette (*NAT*) was restricted with *Bgl*I and incubated with the 3’ region as probe. **(a)** Restriction sites of *Bgl*I in the wild type and deletion strains. The 3’ flanking region was used as probe (marked by a blue line). **(b)** Southern hybridization of *VOS1* deletion strains with hygromycin resistance cassette (*HYG*) with wild type control. The wild type exhibits a fragment with a size of 4.8 kb. The two tested *VOS1* deletion transformants show fragments with a size of 1.8 kb. **(c)** Southern hybridization of the *VOS1* deletion with hygromycin resistance cassette (*HYG*), double deletion strains with *VEL3* and wild type control. The wild type results in a fragment with a size of 4.8 kb. *VOS1* deletion strains show fragments with a size of 1.8 kb. **(d)** Southern hybridization of the *VOS1* deletion strains with nourseothricin resistance cassette with wild type control. The labeled fragment of the wild type has a size of 4.8 kb. The two tested deletion transformants exhibit a fragment with a size of 1.8 kb.

.

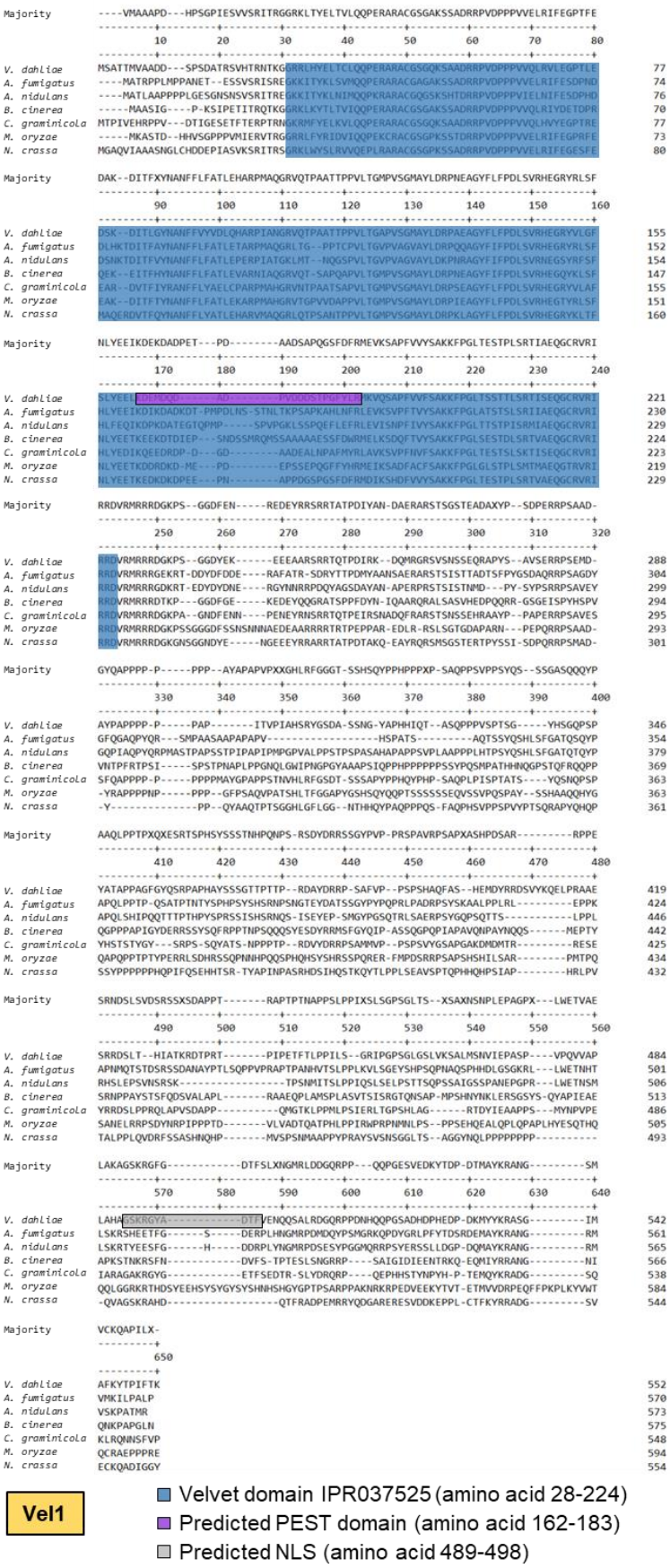

Figure A5: Comparison of Vel1-like proteins of *V. dahliae* and different fungi. Deduced proteins of *Aspergillus fumigatus* Af293, *Aspergillus nidulans* FGSC A4, *Botrytis cinerea* BcDW1, *Colletotrichum graminicola* M1.001, *Magnaporthe oryzae* M68 and *Neurospora crassa* OR74A similar to Vel1 of *V. dahliae* JR2 were aligned by MegAlignPro (DNASTAR) using ClustalW multiple sequence alignment. The velvet domain predicted by InterProScan for the Vel1 protein (VDAG_JR2_Chr7g04890a) is depicted in dark blue according to IPR037525. The predicted NLS is shown in grey and the PEST motif in purple.

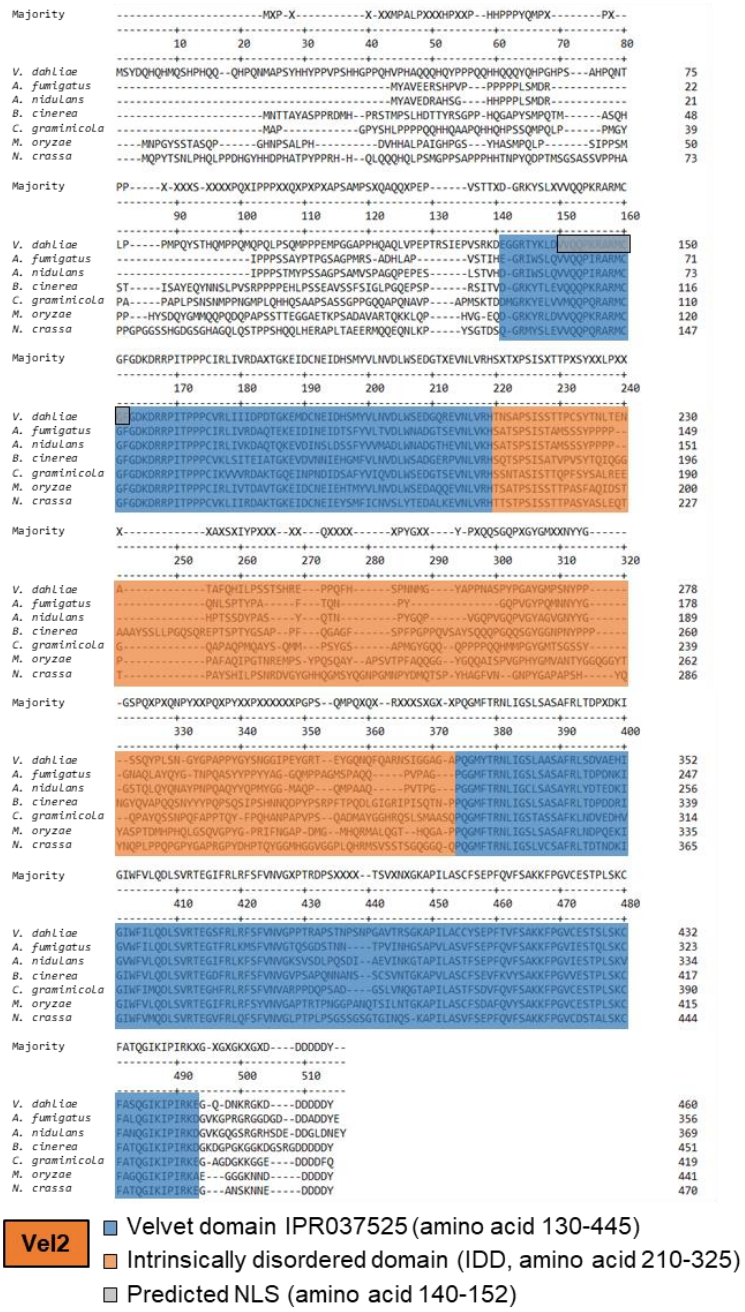

Figure A6: Comparison of Vel2-like proteins of *V. dahliae* and different fungi. Deduced proteins of *A. fumigatus* Af293, *A. nidulans* FGSC A4, *B. cinerea* BcDW1, *C. graminicola* M1.001, *M. oryzae* M68 and *N. crassa* OR74A similar to Vel2 of *V. dahliae* JR2 were aligned by MegAlignPro (DNASTAR) using ClustalW multiple sequence alignment. The velvet domain predicted by InterProScan according to IPR037525 for the Vel2 protein (VDAG_JR2_Chr3g06150a) is depicted in dark blue. Homologies to other ascomycetes indicate that all Vel2-like velvet domains are interrupted by an intrinsically disordered domain (IDD), which is indicated by an orange color. The predicted NLS is shown in grey.

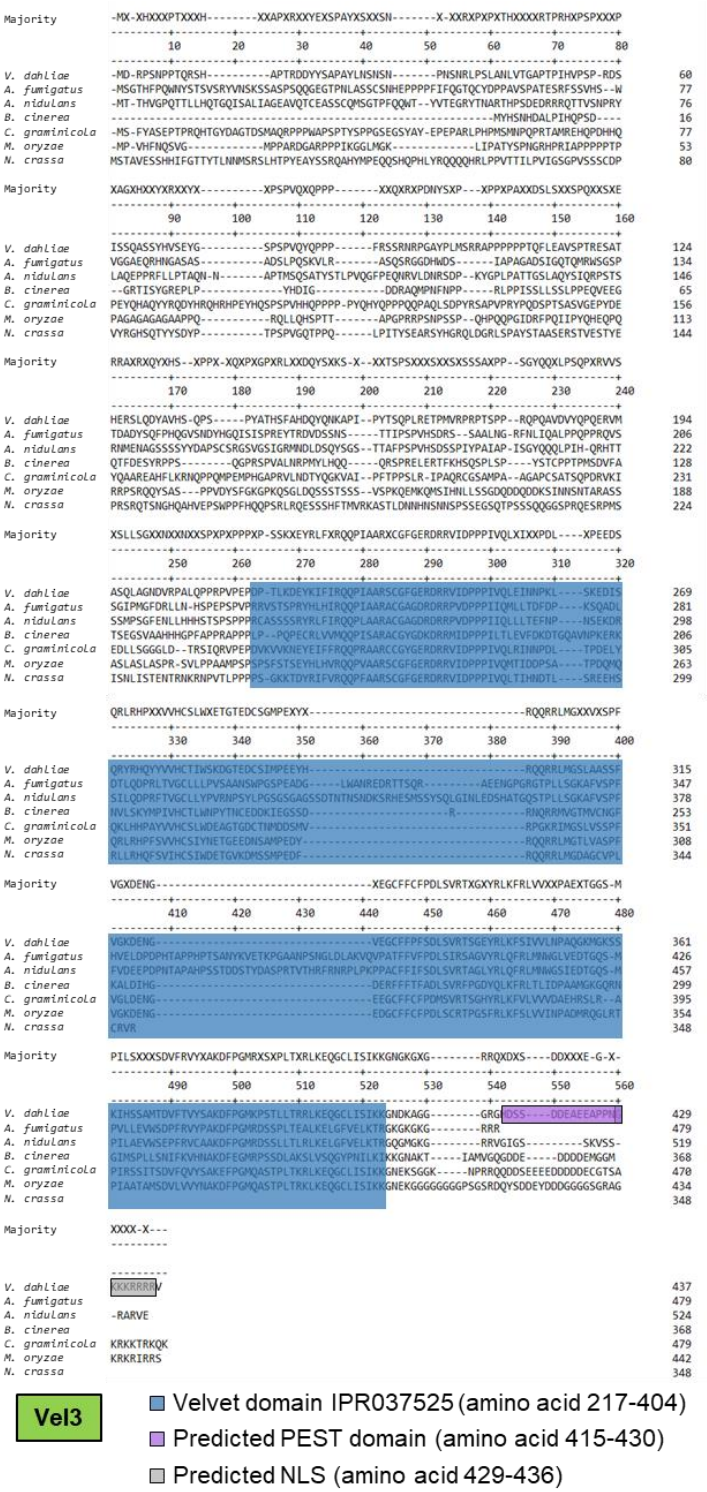

Figure A7: Comparison of Vel3-like proteins of *V. dahliae* and different fungi. Deduced proteins of *A. fumigatus* Af293, *A. nidulans* FGSC A4, *B. cinerea* BcDW1, *C. graminicola* M1.001, *M. oryzae* M68 and *N. crassa* OR74A similar to Vel3 of *V. dahliae* JR2 were aligned by MegAlignPro (DNASTAR) using ClustalW multiple sequence alignment. The velvet domain predicted by InterProScan for the Vel3 protein (VDAG_JR2_Chr6g00630a) is depicted in dark blue. The domain is predicted according to IPR037525. The predicted NLS is shown in grey and the PEST motif in purple.

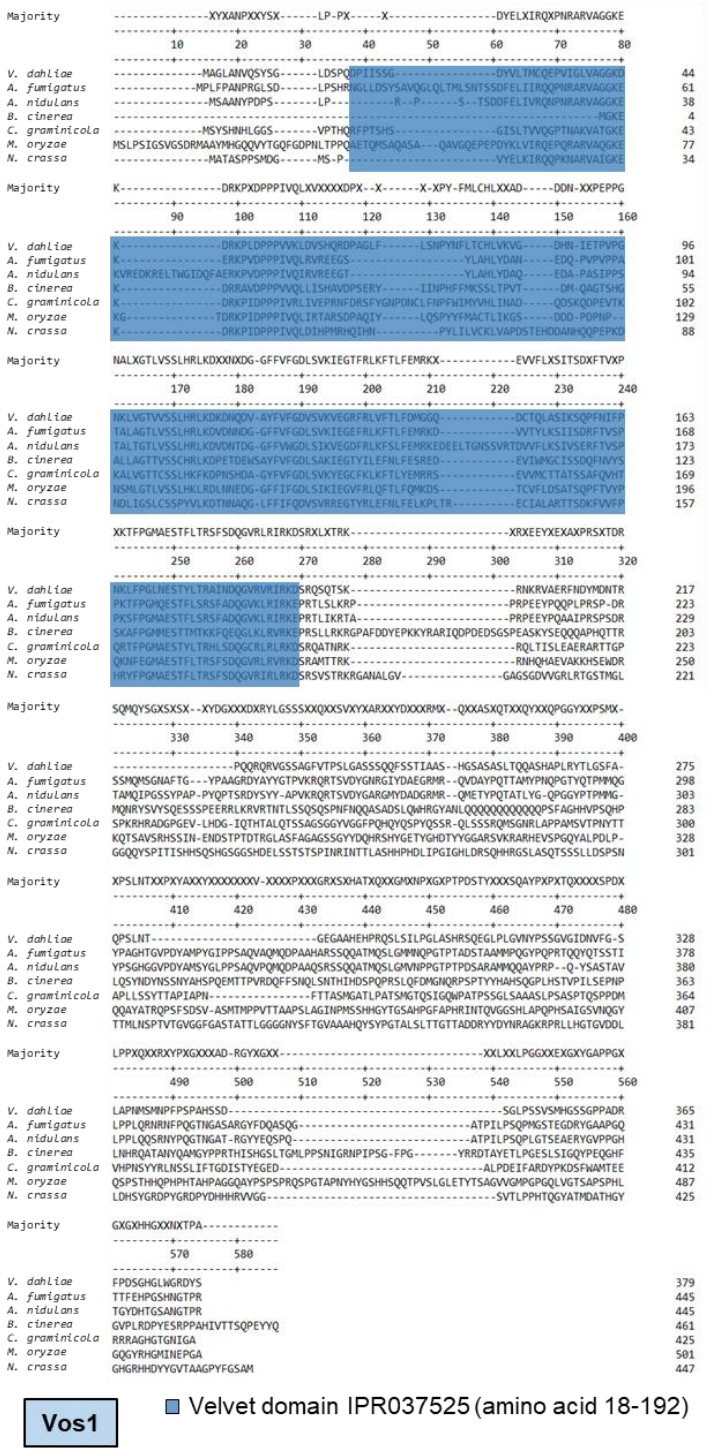

Figure A8: Comparison of Vos1-like proteins of *V. dahliae* and different fungi. Deduced proteins of *A. fumigatus* Af293, *A. nidulans* FGSC A4, *B. cinerea* BcDW1, *C. graminicola* M1.001, *M. oryzae* M68 and *N. crassa* OR74A similar to Vos1 of *V. dahliae* JR2 were aligned by MegAlignPro (DNASTAR) using ClustalW multiple sequence alignment. The sequence used for the alignment is an improved version in comparison of the prediction of VDAG_JR2_Chr3g12090a, which derived from cDNA sequencing and mass spectrometry verification of the protein. The Vos1 velvet domain predicted by InterProScan is depicted in dark blue according to IPR037525.

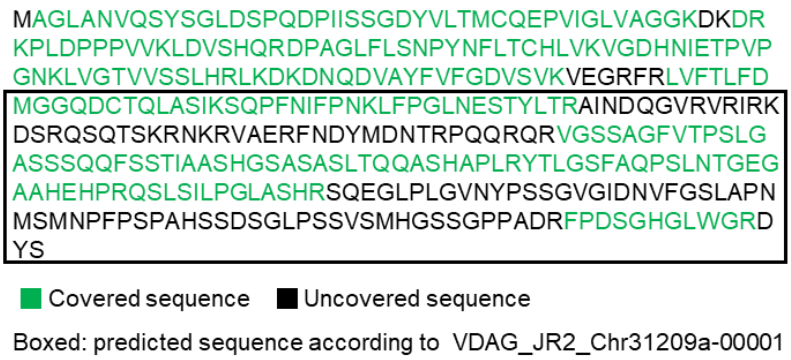

Figure A9: Amino acid sequence of Vos1 confirmed by LC-MS analysis. Amino acid sequence predicted by Ensembl Fungi is within the box, amino acids deduced from cDNA sequencing and missing in the prediction are outside of the box. The sequence highlighted in green was covered with peptides identified with LC-MS and MaxQuant 1.6.0.16 analysis. Black parts of the sequence were not covered.

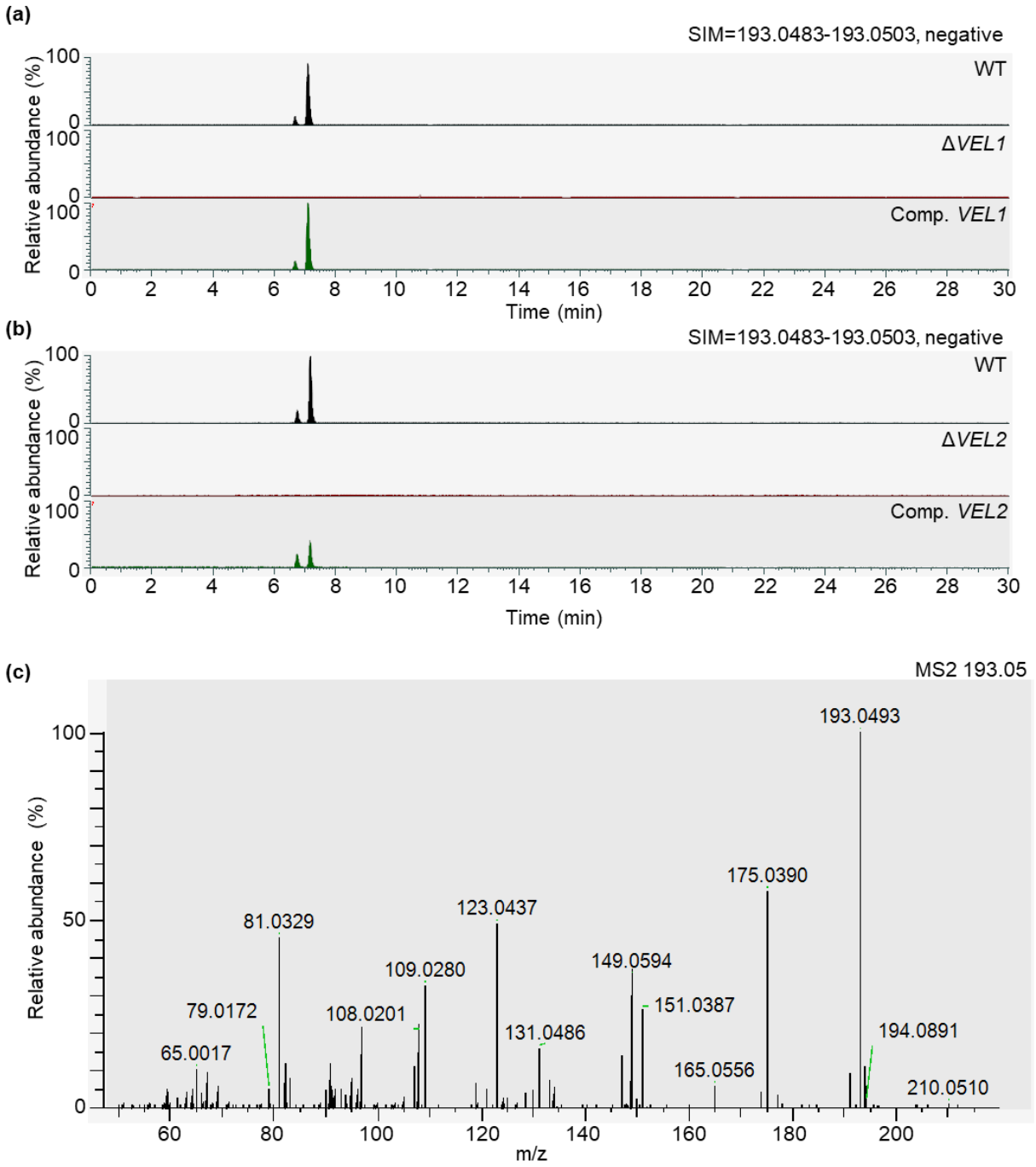

Figure A10: Single ion monitoring and MS2 spectrum for substance I from *V. dahliae* metabolite extracts. (a) and **(b)** Single ion monitoring (SIM) for substance I with m/z 193.0493 and a mass tolerance of 5.00 ppm in negative ion mode. Depicted are the wild type (WT), *VEL1* deletion strain (*ΔVEL1*) and complementation (Comp. *VEL1*) (a) as well as the wild type (WT), *VEL2* deletion strain (*ΔVEL2*) and complementation (Comp. *VEL2*) (b). **(c)** MS2 spectrum of substance I.

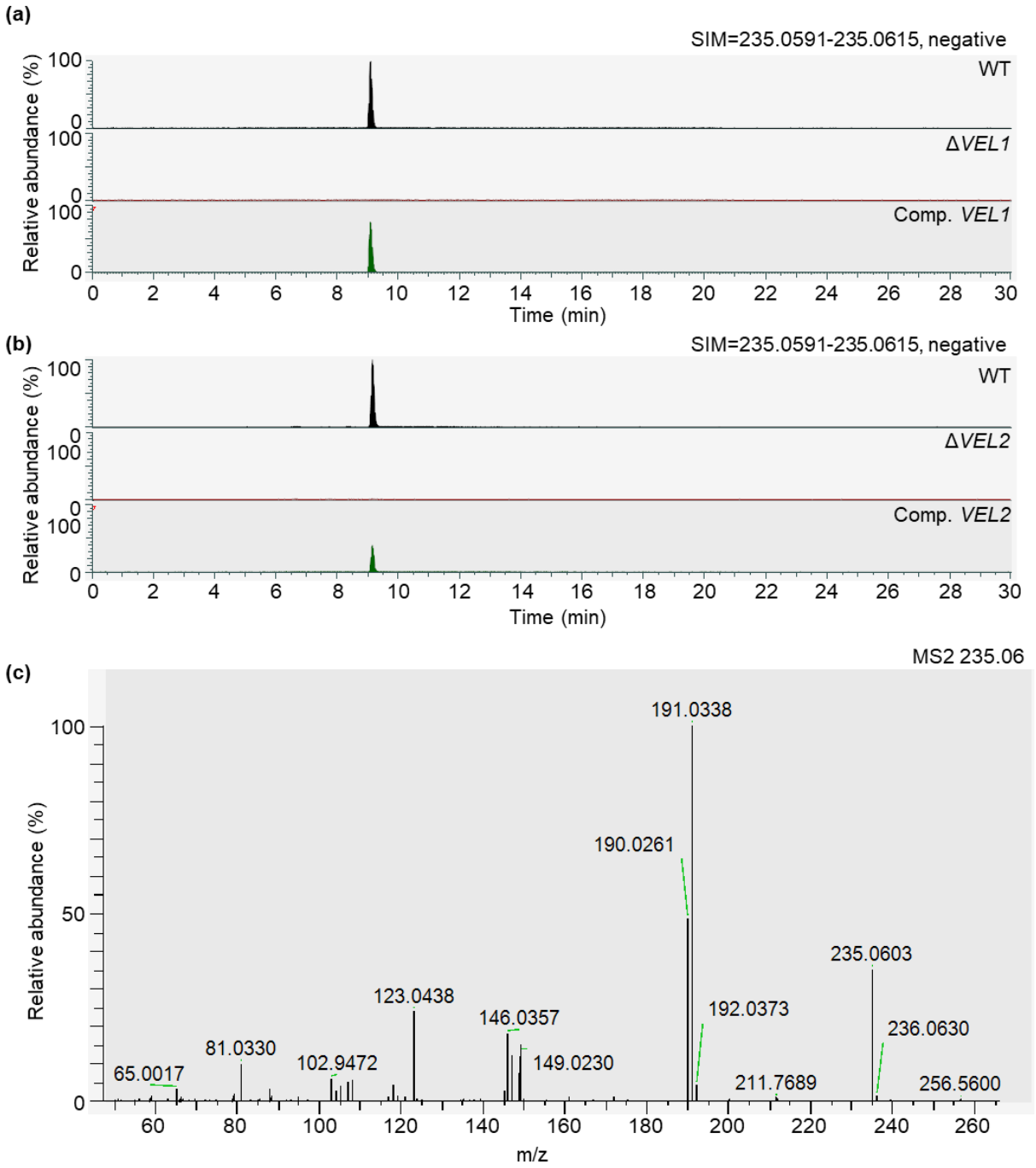

Figure A11: Single ion monitoring and MS2 spectrum for substance II from *V. dahliae* metabolite extracts. (a) and **(b)** Single ion monitoring (SIM) for substance II with m/z 235.0603 and a mass tolerance of 5.00 ppm in negative ion mode. Depicted are the wild type (WT), *VEL1* deletion strain (*ΔVEL1*) and complementation (Comp. *VEL1*) (a) as well as the wild type (WT), *VEL2* deletion strain (*ΔVEL2*) and complementation (Comp. *VEL2*) (b). **(c)** MS2 spectrum of substance II.

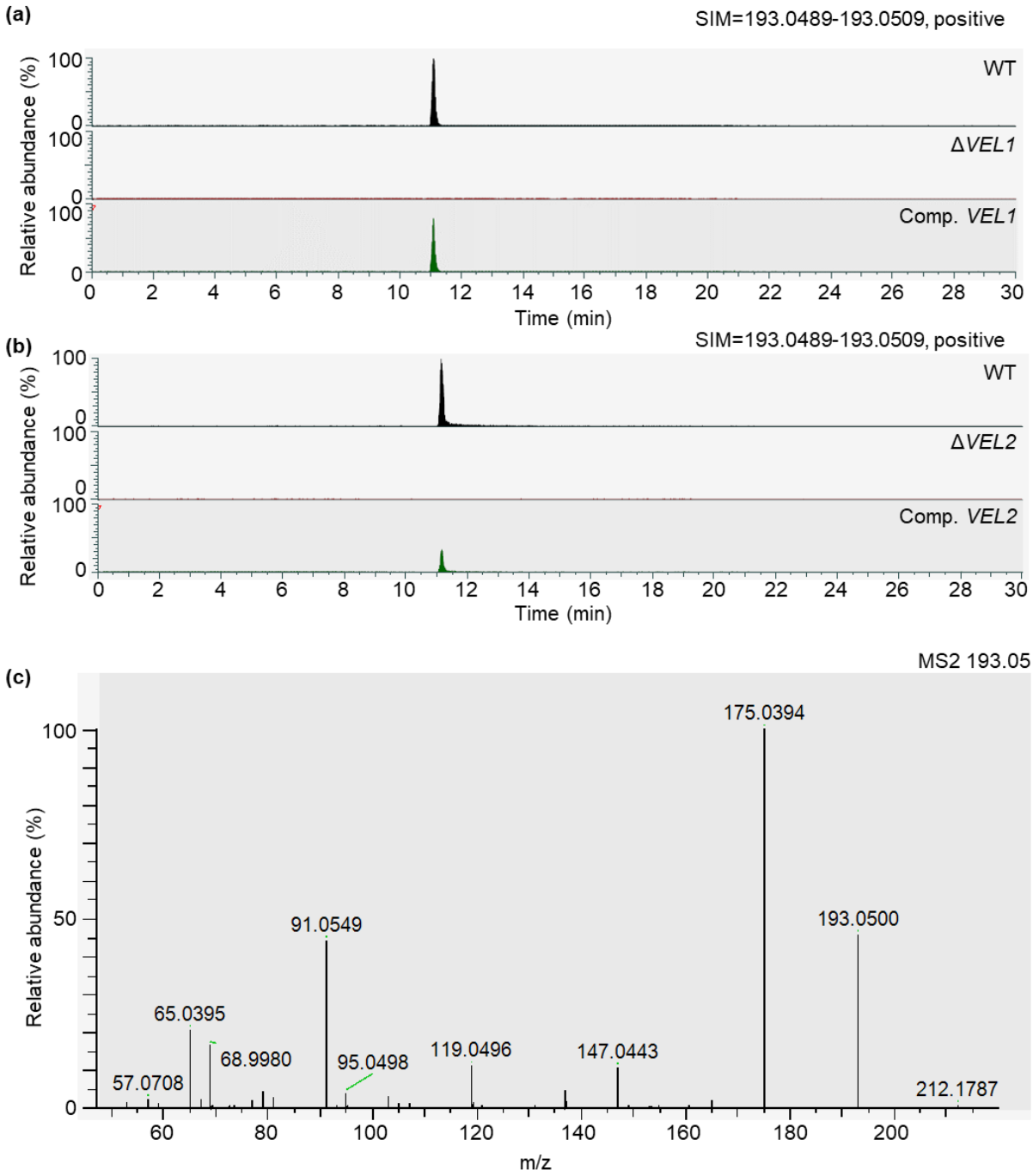

Figure A12: Single ion monitoring and MS2 spectrum for substance III from *V. dahliae* metabolite extracts. (a) and **(b)** Single ion monitoring (SIM) for substance III with m/z 193.0499 and a mass tolerance of 5.00 ppm in positive ion mode. Depicted are the wild type (WT), *VEL1* deletion strain (*ΔVEL1*) and complementation (Comp. *VEL1*) (a) as well as the wild type (WT), *VEL2* deletion strain (*ΔVEL2*) and complementation (Comp. *VEL2*) (b). **(c)** MS2 spectrum of substance III.

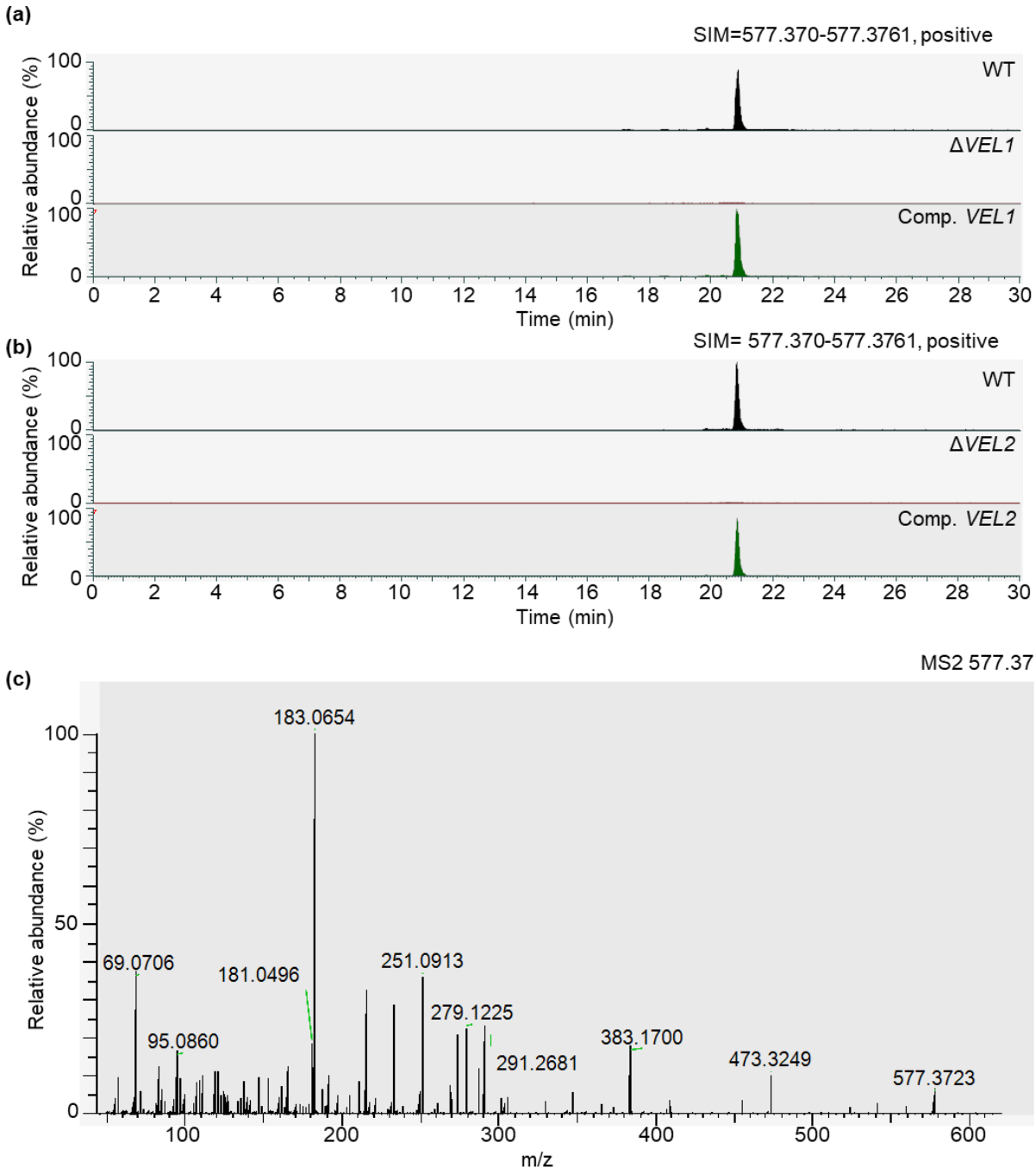

Figure A13: Single ion monitoring and MS2 spectrum for substance IV from *V. dahliae* metabolite extracts. (a) and **(b)** Single ion monitoring (SIM) for substance IV with m/z 577.3732 and a mass tolerance of 5.00 ppm in positive ion mode. Depicted are the wild type (WT), *VEL1* deletion strain (*ΔVEL1*) and complementation (Comp. *VEL1*) (a) as well as the wild type (WT), *VEL2* deletion strain (*ΔVEL2*) and complementation (Comp. *VEL2*) (b). **(c)** MS2 spectrum of substance IV.

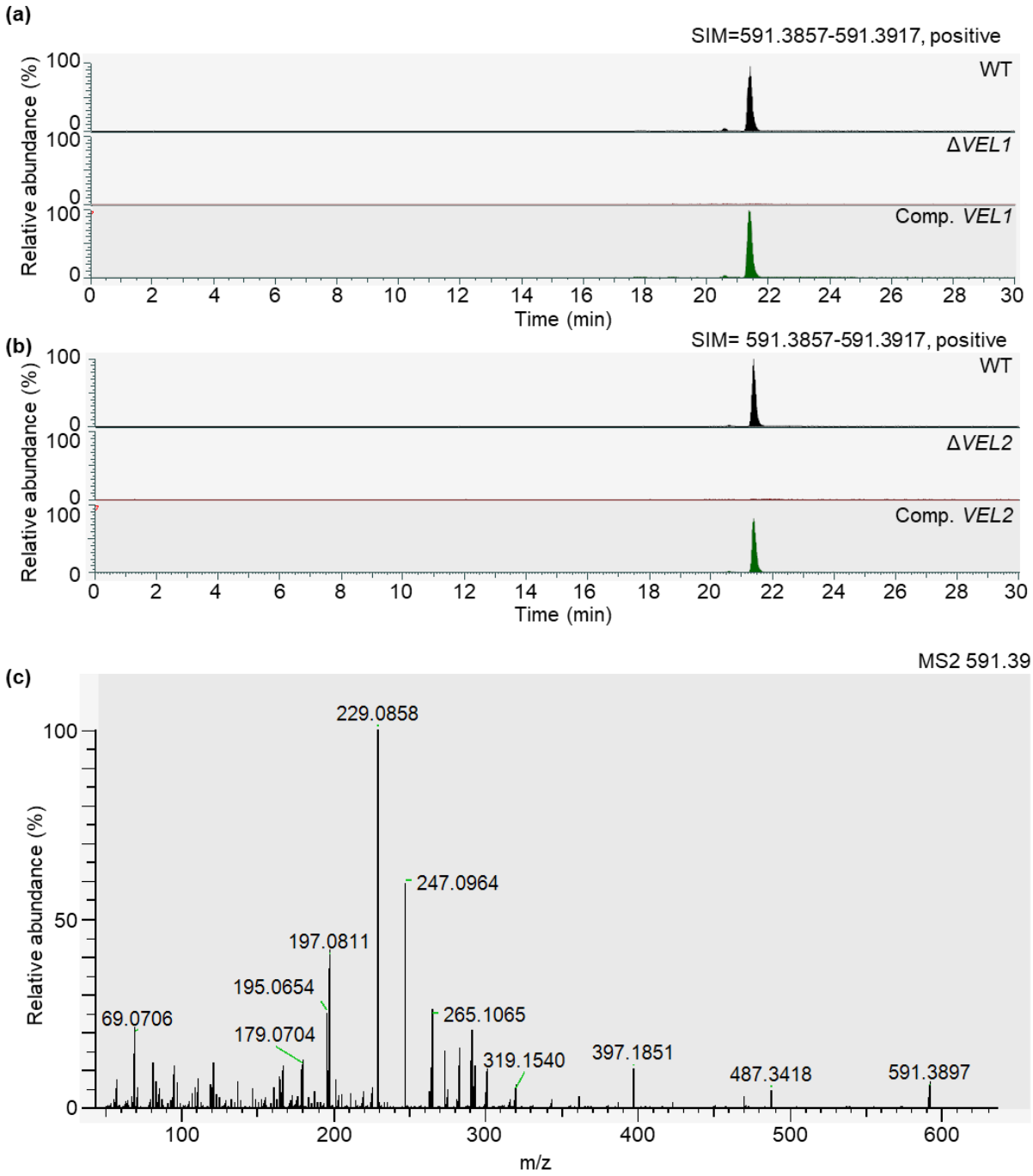

Figure A14: Single ion monitoring and MS2 spectrum for substance V from *V. dahliae* metabolite extracts. (a) and **(b)** Single ion monitoring (SIM) for substance V with m/z 591.3887 and a mass tolerance of 5.00 ppm in positive ion mode. Depicted are the wild type (WT), *VEL1* deletion strain (*ΔVEL1*) and complementation (Comp. *VEL1*) (a) as well as the wild type (WT), *VEL2* deletion strain (*ΔVEL2*) and complementation (Comp. *VEL2*) (b). **(c)** MS2 spectrum of substance V.

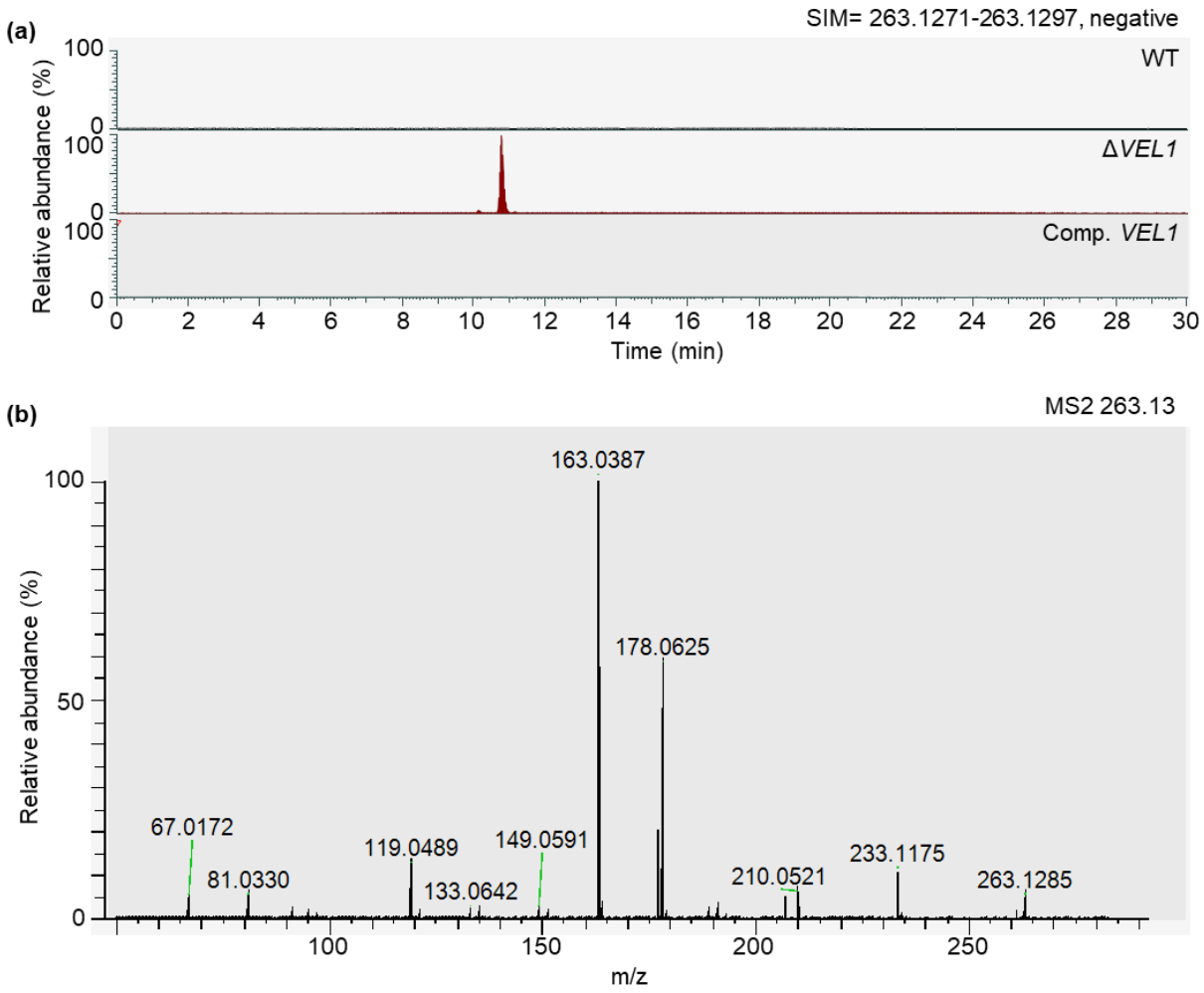

Figure A15: Single ion monitoring and MS2 spectrum for substance VI from *V. dahliae* metabolite extracts. (a) Single ion monitoring (SIM) for substance VI with m/z 263.1284 and a mass tolerance of 5.00 ppm in negative ion mode. Depicted are the wild type (WT), *VEL1* deletion strain (*ΔVEL1*) and complementation (Comp. *VEL1*). **(b)** MS2 spectrum of substance VI.

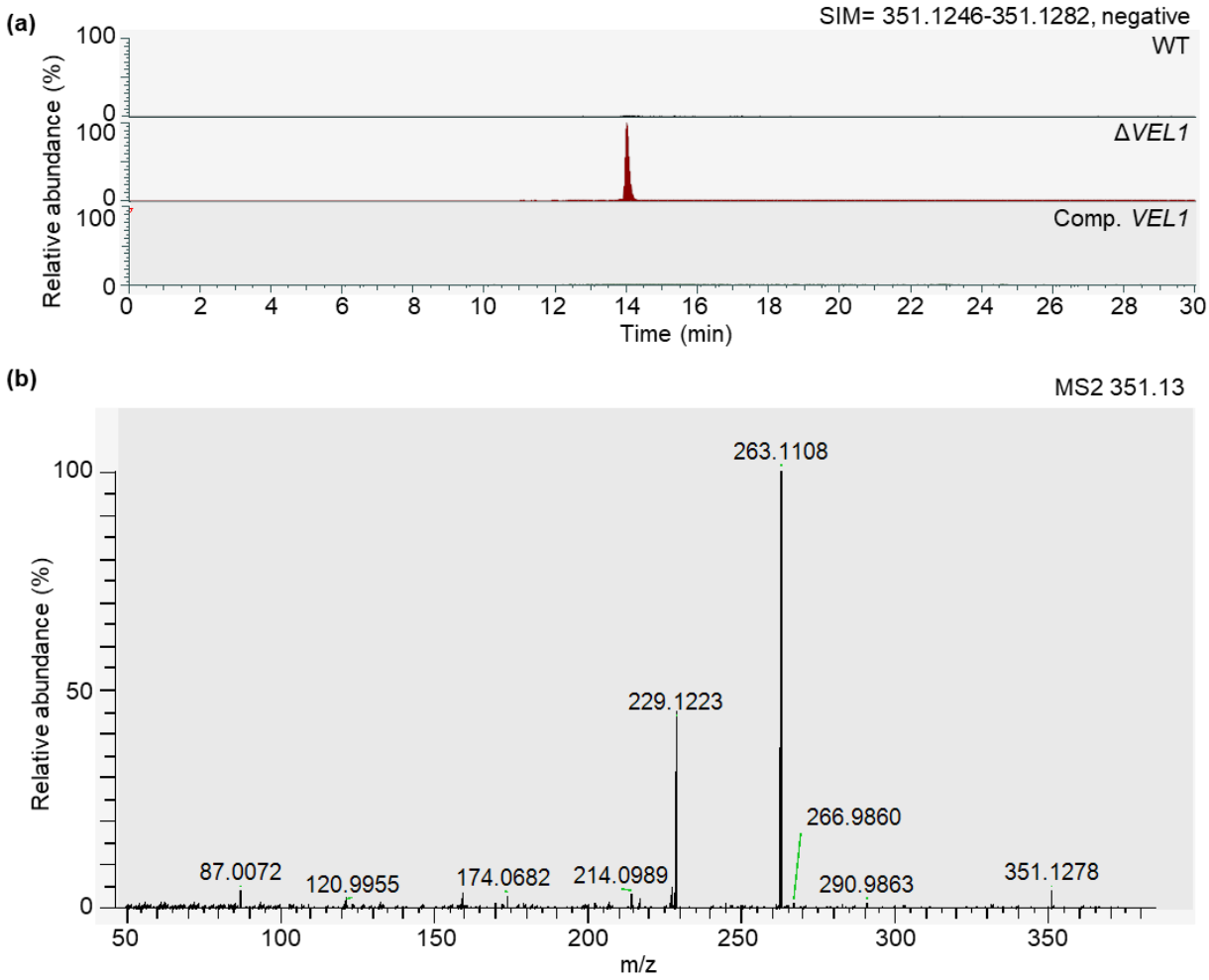

Figure A16: Single ion monitoring and MS2 spectrum for substance VII from *V. dahliae* metabolite extracts. (a) Single ion monitoring (SIM) for substance VII with m/z 351.1264 and a mass tolerance of 5.00 ppm in negative ion mode. Depicted are the wild type (WT), *VEL1* deletion strain (*ΔVEL1*) and complementation (Comp. *VEL1*). **(b)** MS2 spectrum of substance VII.

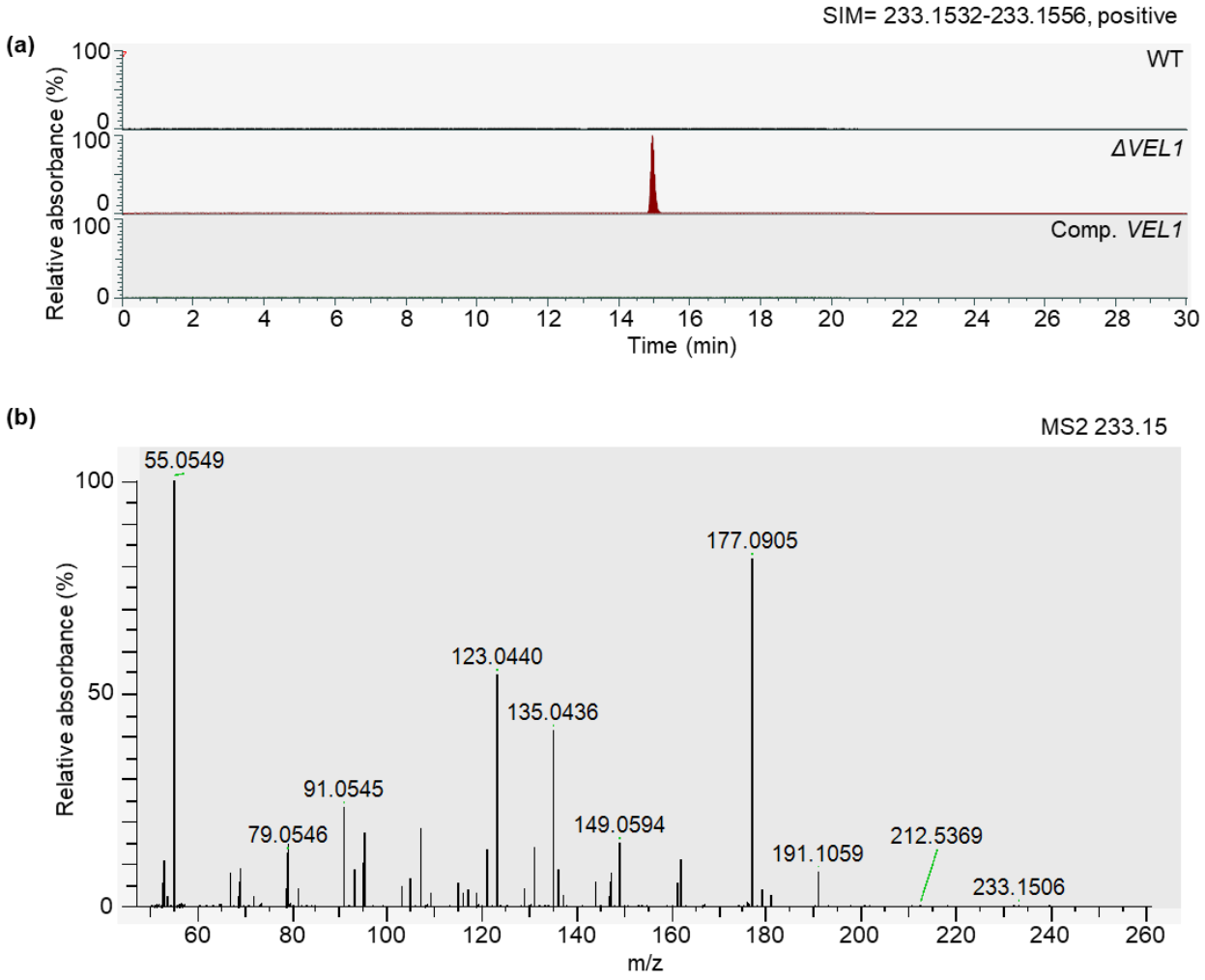

Figure A17: Single ion monitoring and MS2 spectrum for substance VIII from *V. dahliae* metabolite extracts. (a) Single ion monitoring (SIM) for substance VIII with m/z 233.1544 and a mass tolerance of 5.00 ppm in positive ion mode. Depicted are the wild type (WT), *VEL1* deletion strain (*ΔVEL1*) and complementation (Comp. *VEL1*). **(b)** MS2 spectrum of substance VIII.

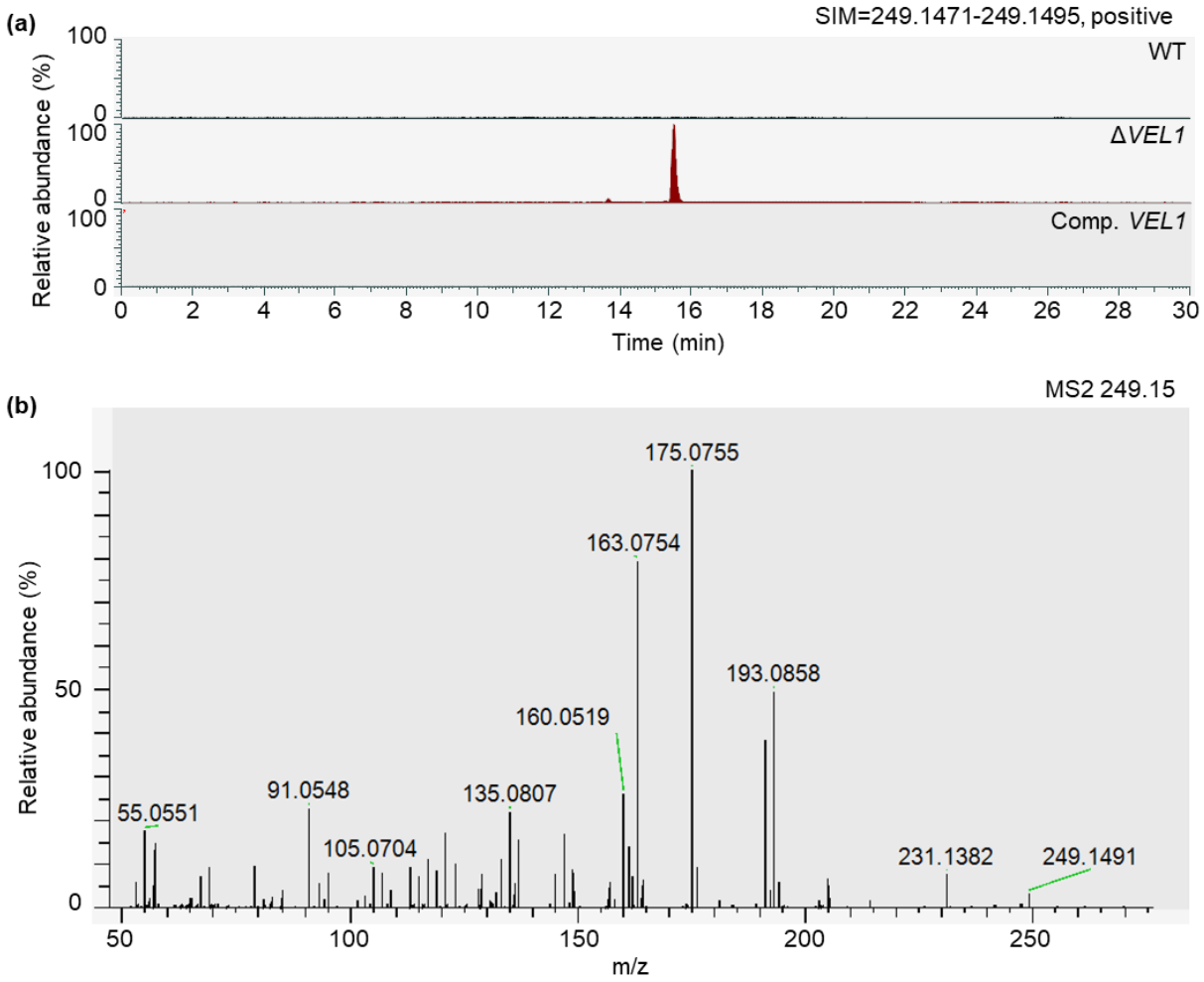

Figure A18: Single ion monitoring and MS2 spectrum for substance IX from *V. dahliae* metabolite extracts. (a) Single ion monitoring (SIM) for substance IX with m/z 249.1483 and a mass tolerance of 5.00 ppm in positive ion mode. Depicted are the wild type (WT), *VEL1* deletion strain (*ΔVEL1*) and complementation (Comp. *VEL1*). **(b)** MS2 spectrum of substance IX.

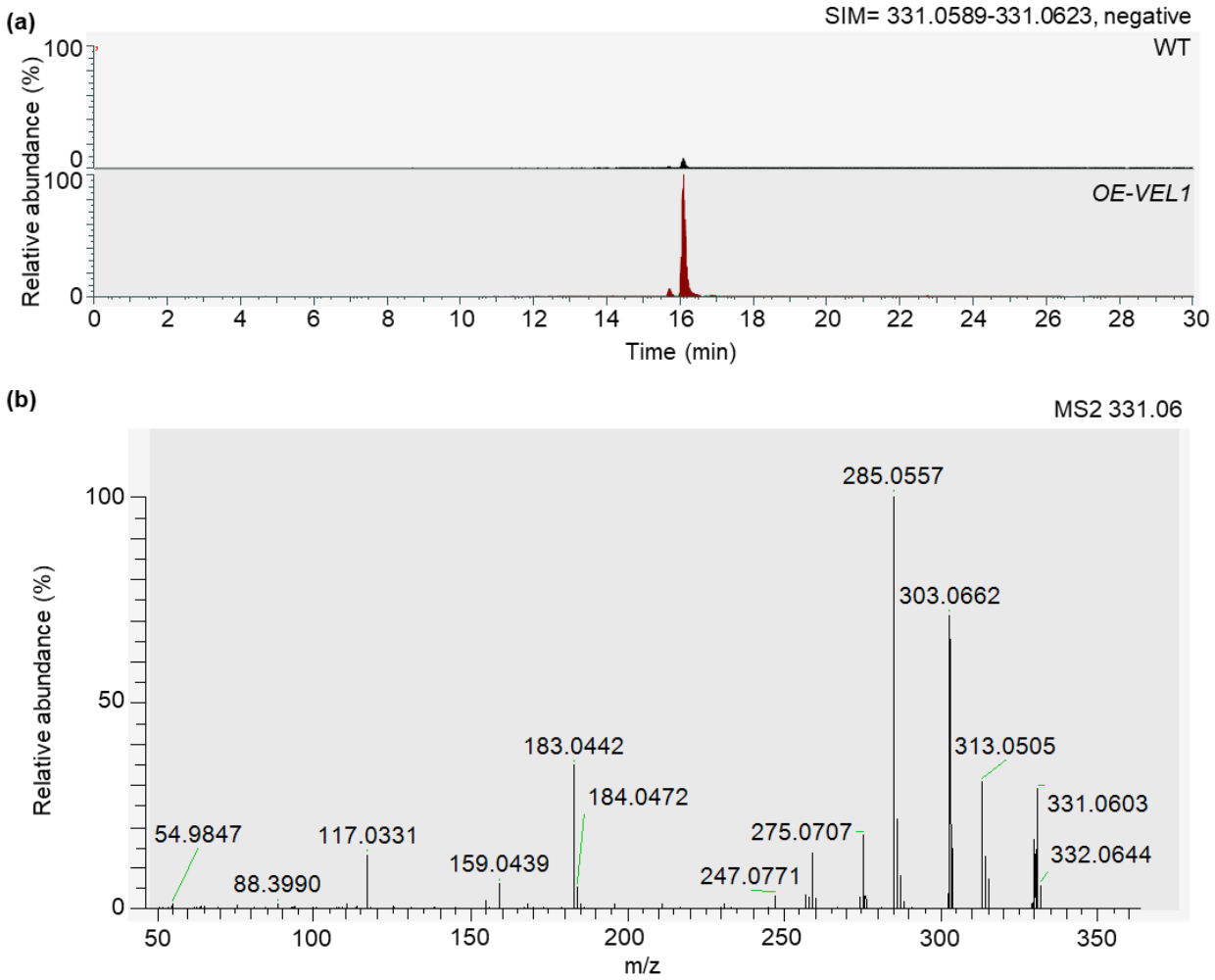

Figure A19: Single ion monitoring and MS2 spectrum for substance X from *V. dahliae* metabolite extracts. (a) Single ion monitoring (SIM) for substance X with m/z 331.0606 and a mass tolerance of 5.00 ppm in negative ion mode. Depicted are the wild type (WT) and the overexpression of *VEL1* (*OE-VEL1*). **(b)** MS2 spectrum of substance X.

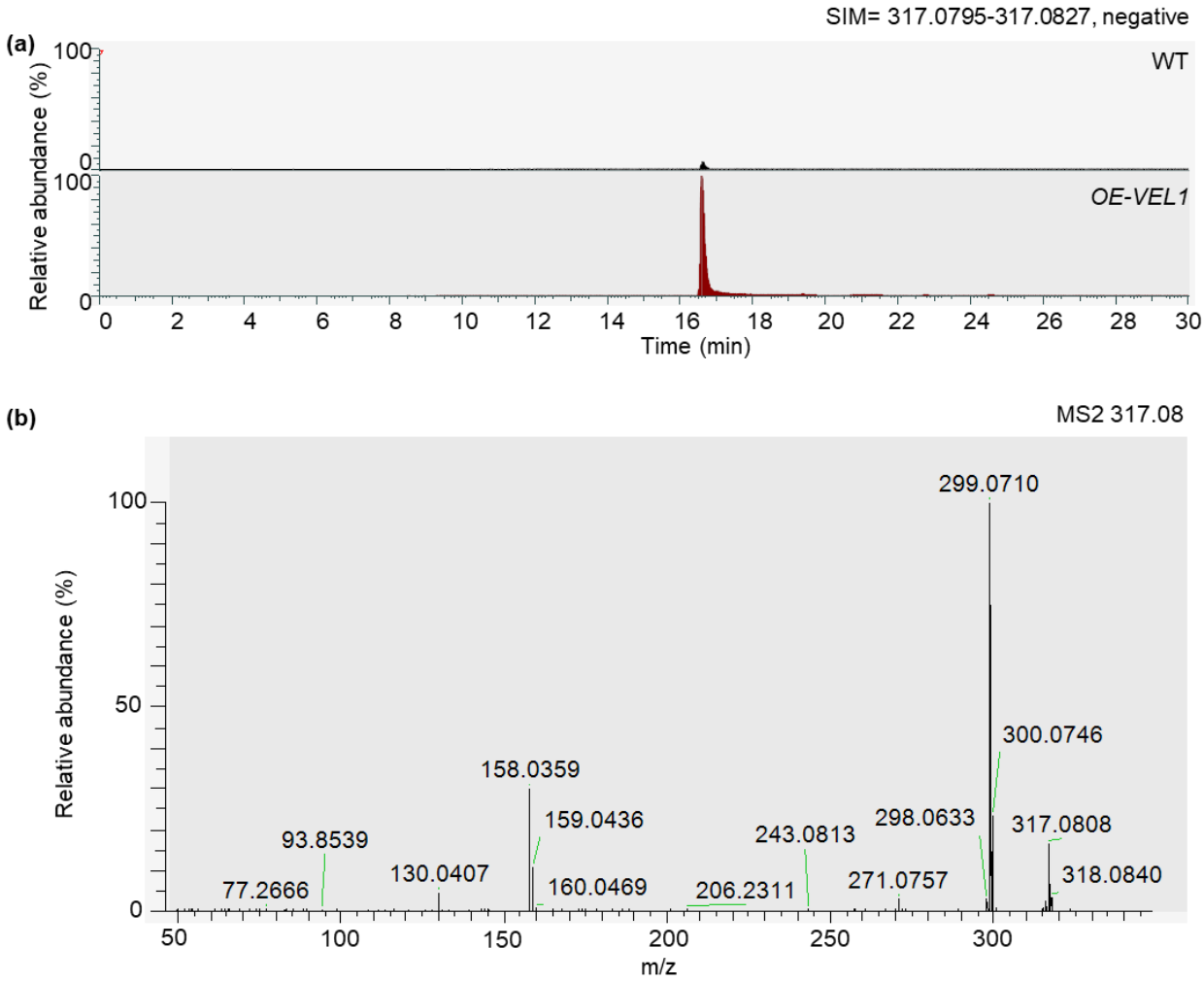

Figure A20: Single ion monitoring and MS2 spectrum for substance XI from *V. dahliae* metabolite extracts. (a) Single ion monitoring (SIM) for substance XI with m/z 317.0811 and a mass tolerance of 5.00 ppm in negative ion mode. Depicted are the wild type (WT) and the overexpression of *VEL1* (*OE-VEL1*). **(b)** MS2 spectrum of substance XI.

Table A1: Proteins significantly enriched with Vel1-GFP and their predicted domains and functions. During data analysis the command "Replace missing values from normal distribution" was repeated four times. Proteins enriched in all four repetitions are displayed as "Found in 4/4", proteins found in three repetitions are displayed as "Found in 3/4".

	Protein ID	Predicted domain	Potential function
Found in 4/4	VDAG_JR2_Chr7g00220a-00001	Cyclophilin-type peptidyl-prolyl cis-trans isomerase domain	Protein folding
	VDAG_JR2_Chr7g04890a-00001(Vel1)	Velvet domain	Development, protein folding
	VDAG_JR2_Chr7g05280a-00001	FAD/NAD(P)-binding domain	Redox metabolism
	VDAG_JR2_Chr3g06150a-00001(Vel2)	Velvet domain	Development, protein folding
	VDAG_JR2_Chr5g09190a-00001	Tetratricopeptide-like helical domain superfamily	Protein binding
	VDAG_JR2_Chr6g10140a-00001	Haem peroxidase	Redox metabolism, stress response
	VDAG_JR2_Chr7g00600a-00001	Thioredoxin domain	Redox metabolism
	VDAG_JR2_Chr1g15440a-00001	Peptidase M1	Proteolysis
	VDAG_JR2_Chr5g05440a-00001	Glycoside hydrolase, family 13	Carbohydrate metabolism
Found in 3/4	VDAG_JR2_Chr7g05650a-00001	Alpha-ketoglutarate-dependent dioxygenase AlkB-like	DNA repair, protein binding

Table A2: Significantly enriched proteins with LFQ intensities, MS/MS count, sequence coverage and unique peptides in all three replicates of Vel1-GFP in comparison to the wild type.

	LFQ intensity						MS/MS count						Sequence coverage [%]						Unique peptides						Protein ID
	wt			Vel1			wt			Vel1			wt			Vel1			wt			Vel1			
	1	2	3	1	2	3	1	2	3	1	2	3	1	2	3	1	2	3	1	2	3	1	2	3	
Found in 4/4	28,61	28,52	28,57	29,15	29,22	29,14	16	10	12	20	16	13	47,1	26,7	32,9	32,9	32,9	32,9	8	5	6	7	7	6	VDAG_JR2_Chr7g00220a-00001
	NaN	NaN	NaN	27,54	28,6	28,92	0	0	0	27	27	24	0	0	0	47,6	52,2	38,4	0	0	0	20	21	19	VDAG_JR2_Chr7g04890a-00001(Vel1)
	27,06	27,07	26,88	27,85	27,87	27,88	19	9	11	25	24	19	36,6	19,2	22,8	43,8	45	39,6	16	8	10	18	20	17	VDAG_JR2_Chr7g05280a-00001
	NaN	NaN	NaN	26,2	27,22	27,18	0	0	0	13	16	8	0	0	0	22,8	35,7	17,6	0	0	0	11	13	8	VDAG_JR2_Chr3g06150a-00001(Vel2)
	24,91	24,38	24,61	25,84	25,99	25,74	7	3	5	16	15	12	13,5	5	9	26,6	21,2	19	7	3	5	15	14	12	VDAG_JR2_Chr5g09190a-00001
	23,92	23,59	24,15	25,15	25,73	25,84	4	2	5	15	14	13	10,5	6,3	14,6	27,5	25	25,6	4	2	5	13	13	12	VDAG_JR2_Chr6g10140a-00001
	24,33	23,66	23,7	25,34	25,45	25,08	8	2	2	13	11	7	18,8	4,7	3,7	30,9	27,6	16,4	8	2	2	13	11	7	VDAG_JR2_Chr7g00600a-00001
	23,95	24	24,11	25,03	25,15	24,7	2	3	3	9	9	6	4,3	5,5	6,9	20	18,6	11,7	2	3	3	10	9	6	VDAG_JR2_Chr1g15440a-00001
	NaN	NaN	NaN	24,49	24,41	24,59	1	2	2	9	7	6	1,4	4,5	4,9	17,2	14,7	11,4	1	2	2	8	7	6	VDAG_JR2_Chr5g05440a-00001
Found in 3/4	NaN	NaN	NaN	23,97	25,35	25,57	0	0	0	3	10	11	0	0	0	6,7	18,4	22,6	0	0	0	3	9	11	VDAG_JR2_Chr7g05650a-00001

Table A3: Proteins significantly enriched with Vel2-GFP and their predicted domains and functions. During data analysis the command “Replace missing values from normal distribution” was repeated four times. Proteins enriched in all four repetitions are displayed as “Found in 4/4”, proteins found in three repetitions are displayed as “Found in 3/4”.

	Protein ID	Predicted domain	Potential function
Found in 4/4	VDAG_JR2_Chr3g06150a-00001(Vel2)	Velvet domain	Development, protein binding
	VDAG_JR2_Chr5g03080a-00001	Protein of unknown function DUF3759	
	VDAG_JR2_Chr4g06160a-00001	Citrate synthase	Carbohydrate metabolism
	VDAG_JR2_Chr7g00220a-00001	Cyclophilin-type peptidyl-prolyl cis-trans isomerase domain	Protein folding
	VDAG_JR2_Chr4g02640a-00001	Alcohol dehydrogenase	Redox metabolism
	VDAG_JR2_Chr4g06150a-00001	ATP -citrate synthase, citrate-binding domain	Carbohydrate metabolism
	VDAG_JR2_Chr5g10680a-00001	NAD(P)-binding domain superfamily, NmrA-like domain	
	VDAG_JR2_Chr2g02650a-00001	Xylulose 5-phosphate/Fructose 6-phosphate phosphoketolase	Carbohydrate metabolism
	VDAG_JR2_Chr5g01680a-00001		
	VDAG_JR2_Chr1g20590a-00001	Acyl transferase	Fatty acid metabolism
	VDAG_JR2_Chr6g02720a-00001	Acetyl-CoA carboxylase	Fatty acid metabolism
	VDAG_JR2_Chr6g01710a-00001	NAD(P)-binding domain superfamily,Short-chain dehydrogenase/reductase SDR	Redox metabolism
	VDAG_JR2_Chr1g20610a-00001	Fatty acid synthase subunit alpha, acyl carrier domain	Fatty acid metabolism
	VDAG_JR2_Chr2g07360a-00001	Pyridoxal phosphate-dependent decarboxylase	Amino acid metabolism
	VDAG_JR2_Chr7g04890a-00001(Vel1)	Velvet domain	Development, protein binding
	VDAG_JR2_Chr1g13580a-00001	Glutathione-dependent formaldehyde-activating enzyme/centromere protein V	Detoxification
	VDAG_JR2_Chr4g10440a-00001	RNA recognition motif domain	Nucleic acid binding
	VDAG_JR2_Chr7g05280a-00001	FAD/NAD(P)-binding domain	Redox metabolism
	VDAG_JR2_Chr8g10760a-00001	NADP-dependent oxidoreductase domain	Redox metabolism
	VDAG_JR2_Chr8g08780a-00001	Alpha-D-phosphohexomutase	Carbohydrate metabolism
	VDAG_JR2_Chr8g02960a-00001	Aminotransferase	Amino acid metabolism
	VDAG_JR2_Chr8g04960a-00001	Nucleotide-diphospho-sugar transferases	Carbohydrate metabolism
	VDAG_JR2_Chr4g07720a-00001	Alcohol dehydrogenase	Redox metabolism
	VDAG_JR2_Chr1g18400a-00001	Glutathione S-transferase	Redox metabolism, protein binding
	VDAG_JR2_Chr1g11550a-00001	Haloacid dehalogenase-like hydrolase	Hydrolase activity
	VDAG_JR2_Chr7g08750a-00001		
	VDAG_JR2_Chr6g06890a-00001	Melanoma-associated antigen	
	VDAG_JR2_Chr4g08190a-00001	Fatty acid desaturase domain	Fatty acid metabolism
	VDAG_JR2_Chr5g09190a-00001	Tetratricopeptide-like helical domain superfamily	Protein binding
	VDAG_JR2_Chr1g17980a-00001	Peptidase S8 propeptide/proteinase inhibitor I9	Protein folding
	VDAG_JR2_Chr6g10140a-00001	Haem peroxidase	Redox metabolism, stress response
	VDAG_JR2_Chr4g02180a-00001	NAD(P)-binding domain	
	VDAG_JR2_Chr3g03700a-00001	Sugar isomerase	Carbohydrate metabolism
	VDAG_JR2_Chr7g00600a-00001	Thioredoxin domain	Redox metabolism
	VDAG_JR2_Chr5g05440a-00001	Glycoside hydrolase, family 13	Carbohydrate metabolism
	VDAG_JR2_Chr4g07360a-00001	NADP-dependent oxidoreductase domain	Redox metabolism
	VDAG_JR2_Chr3g10860a-00001	K Homology domain, type 1	Nucleic acid binding
	VDAG_JR2_Chr4g00470a-00001	Glycosyl hydrolase, family 13	Carbohydrate metabolism
	VDAG_JR2_Chr3g01680a-00001	TspO/MBR-related protein	Transmembrane signalling
	VDAG_JR2_Chr3g12090a-00001(Vos1)	Velvet domain	Development, protein binding
	VDAG_JR2_Chr4g11880a-00001	SsuA/THI5-like	Thiamine metabolism
	VDAG_JR2_Chr8g07440a-00001	Aldehyde dehydrogenase domain	Redox metabolism
	VDAG_JR2_Chr4g09700a-00001	Homogentisate 1,2-dioxygenase	Amino acid metabolism
Found in 3/4	VDAG_JR2_Chr5g00110a-00001	Peptidase M13	Proteolysis
	VDAG_JR2_Chr3g08710a-00001	Glycoside hydrolase, family 16	Carbohydrate metabolism
	VDAG_JR2_Chr1g02490a-00001	Thiamine pyrophosphate enzyme	Thiamine metabolism
	VDAG_JR2_Chr4g08010a-00001	Class I glutamine amidotransferase-like	Amino acid metabolism
	VDAG_JR2_Chr1g18410a-00001	Ubiquitin-activating enzyme E1	Posttranslational protein modification
	VDAG_JR2_Chr3g02760a-00001	Peptidase family M49	Proteolysis
	VDAG_JR2_Chr6g00330a-00001	Peptidase M24	Proteolysis
	VDAG_JR2_Chr1g28250a-00001	FAD linked oxidase	Redox metabolism

Table A4: Significantly enriched proteins with LFQ intensities, MS/MS count, sequence coverage and unique peptides in all three replicates of Vel2-GFP in comparison to the wild type.

	LFQ intensity						MS/MS count						Sequence coverage [%]						Unique peptides						Protein ID
	wt			Vel2			wt			Vel2			wt			Vel2			wt			Vel2			
	1	2	3	1	2	3	1	2	3	1	2	3	1	2	3	1	2	3	1	2	3	1	2	3	
Found in 4/4	NaN	NaN	NaN	30,26	30,93	30,79	0	0	0	34	39	33	0	0	0	40,4	41,5	36,1	0	0	0	18	19	16	VDAG_JR2_Chr3g06150a-00001(Vel2)
	28,03	27,28	27,85	29,71	30,35	29,06	15	8	9	23	23	19	59,3	40,2	40,7	64,7	64,7	59,3	11	7	8	14	13	12	VDAG_JR2_Chr5g03080a-00001
	27,40	27,54	28,51	29,32	29,59	29,62	25	18	22	41	42	38	44,3	31,5	39,7	50,5	56,9	54,8	22	15	18	28	28	26	VDAG_JR2_Chr4g06160a-00001
	28,61	28,52	28,57	29,47	29,41	29,18	16	10	12	21	19	17	47,1	26,7	32,9	32,9	32,9	32,9	8	5	6	7	7	7	VDAG_JR2_Chr7g00220a-00001
	29,02	28,87	28,86	29,50	29,40	29,49	29	20	20	33	27	27	72,2	54,5	55,1	75,9	65,6	63,1	19	14	14	20	18	16	VDAG_JR2_Chr4g02640a-00001
	27,60	27,42	27,93	29,53	29,31	29,35	18	8	11	23	23	16	47	31,6	32,5	47,5	49,6	45,2	14	8	8	14	15	12	VDAG_JR2_Chr4g06150a-00001
	27,70	28,30	28,38	29,29	29,23	29,33	11	9	9	23	22	21	43,1	33,9	39,1	63,2	52,3	53,6	8	7	7	12	10	11	VDAG_JR2_Chr5g10680a-00001
	27,54	28,16	28,16	28,75	29,01	29,05	17	10	15	22	28	28	24,7	12,3	16,1	19,1	24,1	25,9	16	9	13	15	20	21	VDAG_JR2_Chr2g02650a-00001
	27,02	25,85	27,69	29,01	28,98	28,53	6	3	4	12	9	7	45,2	34,2	34,2	51,4	45,2	45,2	5	3	3	6	5	5	VDAG_JR2_Chr5g01680a-00001
	28,00	28,34	28,41	28,99	28,93	29,26	49	37	43	72	68	81	34,3	25,2	29,6	40	36,1	39,3	48	38	39	60	56	64	VDAG_JR2_Chr1g20590a-00001
	27,76	28,15	27,84	28,71	28,88	28,59	45	27	24	61	60	56	23,9	16,1	14,9	30,7	28,1	28,9	42	27	25	54	51	49	VDAG_JR2_Chr6g02720a-00001
	27,75	27,86	27,72	28,48	28,61	28,29	15	11	9	16	18	14	64,9	45,7	33,2	60	56,6	56,6	11	9	7	14	12	11	VDAG_JR2_Chr6g01710a-00001
	27,19	27,34	27,56	28,18	28,44	28,24	31	23	26	43	38	46	24,9	16,3	15,2	24,8	22,5	26,8	31	22	22	37	32	39	VDAG_JR2_Chr1g20610a-00001
	27,14	27,22	27,30	27,87	28,44	27,87	16	9	12	18	18	16	41,7	22,5	27,5	35,2	34,9	36,1	13	7	10	13	13	13	VDAG_JR2_Chr2g07360a-00001
	NaN	NaN	NaN	27,85	28,32	28,66	0	0	0	20	26	25	0	0	0	29,2	46	42,6	0	0	0	15	19	18	VDAG_JR2_Chr7g04890a-00001(Vel1)
	26,82	26,32	26,48	28,34	28,20	27,33	8	4	7	12	9	8	72,1	47,1	72,1	78,7	71,3	72,1	6	4	6	7	6	6	VDAG_JR2_Chr1g13580a-00001
	27,19	26,61	26,72	27,95	27,99	27,46	17	8	13	21	20	18	66,3	46,7	60,9	71	73,6	69,2	12	8	11	14	15	13	VDAG_JR2_Chr4g10440a-00001
	27,06	27,07	26,88	28,18	27,91	28,14	19	9	11	23	21	23	36,6	19,2	22,8	44	40,4	43,8	16	8	10	19	17	18	VDAG_JR2_Chr7g05280a-00001
	26,72	26,55	27,21	28,07	27,87	27,94	14	7	10	21	16	21	40,1	25,6	31,9	54,2	45,5	52,1	12	7	8	16	14	17	VDAG_JR2_Chr8g10760a-00001
	26,81	26,85	26,89	27,82	27,60	27,48	11	7	6	17	12	14	29,7	19	21,7	37,4	29,5	33,1	10	6	6	15	11	13	VDAG_JR2_Chr8g08780a-00001
	25,77	25,62	25,98	27,10	27,47	26,79	11	5	7	16	15	10	29,3	16	20,4	47,2	45,9	32,2	9	5	6	14	14	9	VDAG_JR2_Chr8g02960a-00001
	26,67	26,92	26,85	27,37	27,42	27,43	22	12	14	21	15	12	44,8	24,5	27,5	40,7	27,3	25	20	11	13	17	13	10	VDAG_JR2_Chr8g04960a-00001
	25,28	25,09	26,38	27,73	27,16	27,28	5	4	8	19	12	15	25,7	16,9	36,9	59,5	48,6	54,7	5	4	7	14	11	13	VDAG_JR2_Chr4g07720a-00001
	25,63	25,45	25,82	26,52	27,12	26,72	11	8	7	18	15	19	36,2	30,7	25,7	45,4	41,6	48,6	9	8	7	15	13	17	VDAG_JR2_Chr1g18400a-00001
	25,77	25,61	25,32	26,93	26,70	26,82	6	3	3	11	10	10	27,1	18,8	17,5	41,2	36,7	37,1	5	3	3	10	8	9	VDAG_JR2_Chr1g11550a-00001
	25,30	24,49	25,12	26,36	26,67	26,00	3	2	3	6	5	4	58,4	37,3	58,4	58,4	58,4	58,4	3	2	3	3	3	3	VDAG_JR2_Chr7g08750a-00001
	24,23	23,29	NaN	26,07	26,48	26,33	2	2	1	5	5	7	9,2	9,2	4,3	21,2	23,9	33,7	2	2	1	4	4	6	VDAG_JR2_Chr6g06890a-00001
	NaN	NaN	NaN	25,27	26,22	25,94	0	1	1	6	10	9	0	2,5	2,5	19,7	16,9	19,5	0	1	1	7	8	7	VDAG_JR2_Chr4g08190a-00001
	24,91	24,38	24,61	25,80	26,11	25,98	7	3	5	9	10	13	13,5	5	9	15,9	14,2	21,1	7	3	5	9	10	14	VDAG_JR2_Chr5g09190a-00001
	NaN	NaN	NaN	24,68	26,02	25,41	3	1	1	2	2	2	30,2	10,9	10,9	10,9	10,9	10,9	2	1	1	1	1	1	VDAG_JR2_Chr1g17980a-00001
	23,92	23,59	24,15	26,36	25,96	26,22	4	2	5	17	10	14	10,5	6,3	14,6	30,8	20,2	27,3	4	2	5	15	10	14	VDAG_JR2_Chr6g10140a-00001
	24,51	23,14	23,51	26,21	25,67	26,04	5	2	2	12	8	16	33	13,6	11,4	50,4	44,7	69,7	4	2	2	9	7	14	VDAG_JR2_Chr4g02180a-00001
	24,25	24,65	24,74	25,53	25,45	25,28	3	4	6	12	7	6	6,4	8,3	9,9	20,4	13,1	11,9	3	4	5	11	7	6	VDAG_JR2_Chr3g03700a-00001
	24,33	23,66	23,70	25,48	25,26	25,08	8	2	2	12	7	9	18,8	4,7	3,7	29,4	21,3	23,9	8	2	2	12	7	9	VDAG_JR2_Chr7g00600a-00001
	NaN	NaN	NaN	25,22	25,15	24,81	1	2	2	11	11	9	1,4	4,5	4,9	24,6	20,5	15,7	1	2	2	12	10	9	VDAG_JR2_Chr5g05440a-00001
	23,51	23,51	24,33	25,23	25,06	24,69	2	2	4	5	7	6	9	9,3	20,2	22,1	24,4	29,5	2	2	4	6	6	6	VDAG_JR2_Chr4g07360a-00001
	NaN	NaN	23,44	24,27	24,85	24,61	0	0	3	9	10	8	0	0	3,1	10,4	9,5	7,8	0	0	3	9	10	8	VDAG_JR2_Chr3g10860a-00001
	NaN	NaN	NaN	24,60	24,83	24,01	0	0	0	4	6	3	0	0	0	13,1	16,3	9,8	0	0	0	4	5	3	VDAG_JR2_Chr4g00470a-00001
	23,77	NaN	23,32	24,88	24,65	25,03	2	2	2	3	3	3	17	7,2	7,2	17	17	17	2	1	1	2	2	2	VDAG_JR2_Chr3g01680a-00001
	NaN	NaN	NaN	24,60	24,48	24,77	0	0	0	4	3	5	0	0	0	18,2	14,8	24	0	0	0	4	3	6	VDAG_JR2_Chr3g12090a-00001(Vos1)
	NaN	NaN	NaN	25,16	24,00	26,61	0	0	2	10	6	12	0	0	10,1	30,4	19,4	31,3	0	0	2	7	5	6	VDAG_JR2_Chr4g11880a-00001
	NaN	NaN	NaN	23,81	23,90	24,02	0	0	0	5	5	6	0	0	2,4	14,6	14,2	18,8	0	0	1	5	5	7	VDAG_JR2_Chr8g07440a-00001
	22,73	NaN	NaN	24,00	23,82	24,11	1	1	0	5	4	5	11,9	5,8	0	16	14,3	16	3	1	0	5	4	5	VDAG_JR2_Chr4g09700a-00001
Found in 3/4	23,05	NaN	NaN	24,43	24,40	23,41	3	0	0	3	5	3	6,7	0	0	7,4	9,9	6,1	3	0	0	4	5	3	VDAG_JR2_Chr5g00110a-00001
	NaN	NaN	NaN	23,28	24,35	24,27	2	1	1	4	7	6	7,7	3	3	11,6	22	15,8	2	1	1	4	6	6	VDAG_JR2_Chr3g08710a-00001
	NaN	NaN	NaN	23,66	23,91	23,45	1	0	1	6	5	4	2,3	0	1,9	21	13,2	11,3	1	0	1	6	5	4	VDAG_JR2_Chr1g02490a-00001
	NaN	NaN	NaN	24,23	23,87	24,07	1	0	0	4	5	3	4,5	0	4,5	21,1	16,3	19,2	1	0	1	4	4	4	VDAG_JR2_Chr4g08010a-00001
	23,29	22,14	NaN	24,64	23,77	24,21	3	1	2	9	5	7	6,8	4,3	2,3	10,7	6,5	8,2	4	2	2	7	3	7	VDAG_JR2_Chr1g18410a-00001
	22,90	NaN	NaN	23,57	23,71	23,30	2	1	0	6	4	2	3,5	1,9	0	12,4	5,3	4,4	2	1	0	6	3	3	VDAG_JR2_Chr3g02760a-00001
	NaN	NaN	NaN	23,61	23,51	23,63	1	1	1	6	4	4	2,7	3,4	6,6	20,1	11,6	11	1	1	2	6	4	4	VDAG_JR2_Chr6g00330a-00001
	NaN	NaN	NaN	23,22	23,13	23,33	0	0	1	4	3	2	0	0	2,1	11,4	7,2	5,1	0	0	1	4	3	2	VDAG_JR2_Chr1g28250a-00001

Table A5: Proteins significantly enriched with Vel3-GFP and their predicted domains and functions. During data analysis the command "Replace missing values from normal distribution" was repeated four times. Proteins enriched in all four repetitions are displayed as "Found in 4/4", proteins found in three repetitions are displayed as "Found in 3/4".

	Protein ID	Predicted domain	Potential function
Found in 4/4	VDAG_JR2_Chr6g00630a-00001(Vel3)	Velvet domain	Development, protein binding
	VDAG_JR2_Chr3g12090a-00001(Vos1)	Velvet domain	Development, protein binding

Table A6: Significantly enriched proteins with LFQ intensities, MS/MS count, sequence coverage and unique peptides in all three replicates of Vel3-GFP in comparison to the wild type.

	LFQ intensity						MS/MS count						Sequence coverage [%]						Unique peptides						Protein ID
	wt			Vel3			wt			Vel3			wt			Vel3			wt			Vel3			
	1	2	3	1	2	3	1	2	3	1	2	3	1	2	3	1	2	3	1	2	3	1	2	3	
Found in 4/4	NaN	NaN	NaN	30,82	31,04	31,30	0	0	0	47	40	35	0	0	0	54,7	52,2	49,4	0	0	0	20	21	17	VDAG_JR2_Chr6g00630a-00001(Vel3)
	NaN	NaN	NaN	27,88	25,92	27,67	0	0	0	8	4	10	0	0	0	26,4	13,5	24	0	0	0	8	4	7	VDAG_JR2_Chr3g12090a-00001(Vos1)

25 32

Log2(x)LFQ intensity

Table A7: Proteins significantly enriched with Vos1-GFP and their predicted domains and functions. During data analysis the command “Replace missing values from normal distribution” was repeated four times. Proteins enriched in all four repetitions are displayed as “Found in 4/4”, proteins found in three repetitions are displayed as “Found in 3/4”.

	Protein ID	Predicted domain	Potential function
Found in 4/4	VDAG_JR2_Chr3g12090a-00001(Vos1)	Velvet domain	Development, protein binding
	VDAG_JR2_Chr3g00030a-00001	ATP synthase	Energy metabolism
	VDAG_JR2_Chr1g18720a-00001	Isopropylmalate dehydrogenase-like domain	Carbohydrate metabolism, redox metabolism
	VDAG_JR2_Chr6g07320a-00001	Aminotransferase class-III	Amino acid metabolism
	VDAG_JR2_Chr1g16720a-00001	Eukaryotic porin/Tom40	Transport
	VDAG_JR2_Chr4g00570a-00001	Mitochondrial substrate/solute carrier	Transport
	VDAG_JR2_Chr5g09480a-00001	Ribosomal protein L32e	Protein synthesis
	VDAG_JR2_Chr8g06840a-00001	FKBP-type peptidyl-prolyl cis-trans isomerase domain	Protein folding, protein modification
	VDAG_JR2_Chr6g06940a-00001	Peptidase M16	Proteolysis
	VDAG_JR2_Chr6g00630a-00001(Vel3)	Velvet domain	Development, protein binding
	VDAG_JR2_Chr6g01510a-00001	Small GTPase superfamily, ARF/SAR type	Intracellular trafficking
	VDAG_JR2_Chr4g02360a-00001	Mitochondrial substrate/solute carrier	Transport
	VDAG_JR2_Chr3g05360a-00001	Calreticulin/calnexin	Protein folding
	VDAG_JR2_Chr3g06150a-00001(Vel2)	Velvet domain	Development, protein binding
	VDAG_JR2_Chr3g03520a-00001	Chaperone DnaJ	Protein folding, stress reponse
	VDAG_JR2_Chr7g04550a-00001	ATPase, OSCP/delta subunit	Energy metabolism
	VDAG_JR2_Chr3g01800a-00001	Cytochrome c1	Energy metabolism
	VDAG_JR2_Chr1g07570a-00001	Cytochrome c oxidase, subunit Va/VI	Energy metabolism
	VDAG_JR2_Chr7g01800a-00001	Pyruvate carboxyltransferase	Carbohydrate metabolism
	VDAG_JR2_Chr3g02140a-00001	Leucine-rich repeat	Protein binding
	VDAG_JR2_Chr3g11170a-00001		
	VDAG_JR2_Chr1g16160a-00001	Cytochrome b-c1 complex subunit 8	Energy metabolism
	VDAG_JR2_Chr8g08950a-00001	Aldehyde dehydrogenase domain	Redox metabolism
	VDAG_JR2_Chr8g08440a-00001	Pyruvate carboxyltransferase	Carbohydrate metabolism
Found in 3/4	VDAG_JR2_Chr1g24260a-00001	Cytochrome b-c1 complex subunit 10	Energy metabolism
	VDAG_JR2_Chr1g12360a-00001	NADP-dependent oxidoreductase domain	Redox metabolism
	VDAG_JR2_Chr8g04870a-00001	Band 7 domain	Membrane protein
	VDAG_JR2_Chr3g11230a-00001	Sulfite reductase flavoprotein alpha-component-like, FAD-binding	Redox metabolism
	VDAG_JR2_Chr1g14040a-00001	Anion-transporting ATPase-like domain	Transport
	VDAG_JR2_Chr1g24330a-00001	Importin-beta, N-terminal domain	Transport

Table A8: Significantly enriched proteins with LFQ intensities, MS/MS count, sequence coverage and unique peptides in all three replicates of Vos1-GFP in comparison to the wild type.

	LFQ intensity						MS/MS count						Sequence coverage [%]						Unique peptides						Protein ID
	wt			Vos1			wt			Vos1			wt			Vos1			wt			Vos1			
	1	2	3	1	2	3	1	2	3	1	2	3	1	2	3	1	2	3	1	2	3	1	2	3	
Found in 4/4	NaN	NaN	NaN	27,42	27,53	26,83	0	0	0	29	27	24	0	0	0	67	66	60,7	0	0	0	15	15	14	VDAG_JR2_Chr3g12090a-00001(Vos1)
	25,55	25,60	25,23	26,20	26,11	26,05	12	15	14	23	20	18	24,9	31,8	28,5	33,9	41,6	33,2	10	11	10	15	16	14	VDAG_JR2_Chr3g00030a-00001
	25,32	25,30	25,12	25,64	25,72	25,68	10	19	18	21	21	21	34,3	47,6	47,6	44,8	51,3	50,3	10	14	15	15	16	17	VDAG_JR2_Chr1g18720a-00001
	24,02	24,13	22,58	25,76	25,55	25,40	11	10	5	29	21	21	28,3	28,9	22,8	65,4	52,2	46,5	10	8	5	21	18	16	VDAG_JR2_Chr6g07320a-00001
	24,71	24,07	23,95	25,34	25,20	25,08	10	9	8	18	15	15	38,2	33,9	33,9	45,6	42,4	45,6	8	7	7	12	12	12	VDAG_JR2_Chr1g16720a-00001
	24,38	24,17	23,82	25,02	25,10	24,86	6	6	5	12	10	11	25,9	25,6	23,5	49,1	32,7	38	5	4	4	8	6	7	VDAG_JR2_Chr4g00570a-00001
	23,40	22,97	23,37	24,57	24,75	23,87	3	5	3	4	6	2	23,7	36,6	23,7	36,6	36,6	23,7	2	3	2	3	3	2	VDAG_JR2_Chr5g09480a-00001
	23,38	23,60	23,38	24,54	24,29	24,29	4	8	6	11	9	6	12,6	16,5	16,5	16,5	16,5	13,7	4	7	6	7	7	5	VDAG_JR2_Chr8g06840a-00001
	21,64	22,70	22,53	24,14	24,21	23,26	2	10	5	10	11	8	8,3	35,6	19,7	31,2	27,7	36	2	8	5	8	8	8	VDAG_JR2_Chr6g06940a-00001
	NaN	NaN	NaN	24,39	24,10	24,11	0	0	0	12	9	8	0	0	0	31,4	26,5	24,7	0	0	0	8	7	7	VDAG_JR2_Chr6g00630a-00001(Vel3)
	23,52	23,47	23,69	24,04	23,97	24,00	5	7	3	6	5	4	37	28,6	22,8	35,4	37	28,6	5	5	3	5	5	4	VDAG_JR2_Chr6g01510a-00001
	23,01	22,56	22,57	24,65	23,94	23,73	3	5	4	16	10	8	7,4	11	14,5	41	25,2	18,4	2	4	4	12	8	7	VDAG_JR2_Chr4g02360a-00001
	23,34	23,30	23,36	23,63	23,71	23,72	4	4	4	11	8	8	11,5	11,8	12,2	26,3	21,7	21,7	4	4	5	9	8	8	VDAG_JR2_Chr3g05360a-00001
	NaN	NaN	NaN	23,81	23,58	23,19	0	0	0	9	9	8	0	0	0	20	17,8	16,7	0	0	0	8	7	7	VDAG_JR2_Chr3g06150a-00001(Vel2)
	22,03	22,35	22,00	22,65	22,80	22,73	2	4	4	3	4	4	7,9	16,5	21,8	16,5	16,5	16,5	2	4	5	4	4	4	VDAG_JR2_Chr3g03520a-00001
	21,55	21,98	21,69	22,94	22,72	22,73	4	5	2	5	4	6	24	24	13,3	28,9	24	28,9	4	4	2	4	4	5	VDAG_JR2_Chr7g04550a-00001
	NaN	NaN	NaN	22,23	22,71	22,20	1	2	1	5	2	4	4,1	4,1	4,1	16,7	9,1	9,1	1	1	1	4	2	3	VDAG_JR2_Chr3g01800a-00001
	21,79	21,42	21,59	22,67	22,45	22,30	2	2	2	4	3	3	18,8	23,8	23,8	32,5	32,5	32,5	2	2	2	4	3	3	VDAG_JR2_Chr1g07570a-00001
	NaN	NaN	NaN	21,63	21,92	21,95	1	1	1	3	4	3	7,6	6,8	3,7	17,4	21,7	11,6	1	1	1	3	4	3	VDAG_JR2_Chr7g01800a-00001
	NaN	NaN	NaN	21,69	21,88	21,66	0	3	1	2	4	2	0	10,2	3,6	14,8	19	8,8	0	2	1	4	5	3	VDAG_JR2_Chr3g02140a-00001
	21,14	NaN	NaN	22,68	21,86	21,74	2	1	1	10	3	5	2,5	1,4	1,9	11,8	5,2	8,2	2	1	1	9	3	5	VDAG_JR2_Chr3g11170a-00001
	NaN	NaN	NaN	21,88	21,82	21,63	1	0	0	3	2	3	8,4	0	0	28,2	16,8	29,8	1	0	0	3	2	3	VDAG_JR2_Chr1g16160a-00001
	NaN	NaN	NaN	21,56	21,37	21,89	1	1	1	3	2	2	2,4	2,8	2,4	9	5,2	5,2	1	1	1	3	2	2	VDAG_JR2_Chr8g08950a-00001
	21,07	20,70	20,93	21,56	21,33	21,53	3	3	3	4	2	3	6	8	8	12,5	4,4	9,1	3	3	3	4	2	3	VDAG_JR2_Chr8g08440a-00001
Found in 3/4	NaN	21,13	NaN	22,00	21,99	21,95	1	3	1	3	5	3	15,4	61,5	15,4	34,1	62,6	62,6	1	3	1	2	4	3	VDAG_JR2_Chr1g24260a-00001
	NaN	NaN	NaN	22,07	21,88	21,92	2	2	1	5	2	3	13,3	4,6	3,2	15	7,8	10,7	3	1	1	5	2	3	VDAG_JR2_Chr1g12360a-00001
	NaN	NaN	NaN	21,67	21,71	21,55	0	1	1	3	3	2	0	8,4	6,2	19,5	19,5	11	0	1	1	3	3	2	VDAG_JR2_Chr8g04870a-00001
	NaN	20,57	NaN	21,42	21,58	21,51	0	2	0	5	5	3	0	2,9	0	6,7	7,8	5,1	0	2	0	5	5	4	VDAG_JR2_Chr3g11230a-00001
	NaN	20,87	NaN	21,66	21,49	21,62	1	3	1	2	3	3	8,6	18,3	2,7	8,6	12,4	11,2	2	4	1	2	3	3	VDAG_JR2_Chr1g14040a-00001
	NaN	NaN	NaN	21,43	21,46	21,37	1	2	1	3	4	4	1,4	2,5	1,1	4,2	5,7	5,8	1	2	1	3	4	4	VDAG_JR2_Chr1g24330a-00001

Table A9: Proteins significantly enriched with Vel2$^{\Delta IDD}$-GFP and their predicted domains and functions. During data analysis the command "Replace missing values from normal distribution" was repeated four times. Proteins enriched in all four repetitions are displayed as "Found in 4/4", proteins found in three repetitions are displayed as "Found in 3/4".

	Protein ID	Predicted domain	Potential function
Found in 4/4	VDAG_JR2_Chr3g06150a-00001(Vel2)	Velvet domain	Development, protein binding
	VDAG_JR2_Chr7g04890a-00001(Vel1)	Velvet domain	Development, protein binding
	VDAG_JR2_Chr3g00330a-00001	Clathrin, heavy chain	Transport
	VDAG_JR2_Chr1g15440a-00001	Peptidase M1, membrane alanine aminopeptidase	Proteolysis
	VDAG_JR2_Chr5g05430a-00001	Cytochrome c oxidase subunit IV family	Energy metabolism
	VDAG_JR2_Chr2g07820a-00001	Malate synthase	Carbohydrate metabolism
	VDAG_JR2_Chr2g02140a-00001	WD40 repeat	Assembly of protein complexes?
Found in 3/4	VDAG_JR2_Chr3g13120a-00001	Dienelactone hydrolase	Carbohydrate metabolism?
	VDAG_JR2_Chr1g06660a-00001	Phospholipase/carboxylesterase/thioesterase	Carbohydrate metabolism?
	VDAG_JR2_Chr5g06420a-00001	Eukaryotic translation initiation factor 3 subunit C	Translation initiation
	VDAG_JR2_Chr8g07560a-00001	MaoC-like dehydratase domain	Redox metabolism?

Table A10: Significantly enriched proteins with LFQ intensities, MS/MS count, sequence coverage and unique peptides in all three replicates of Vel2$^{\Delta IDD}$-GFP in comparison to the wild type.

	LFQ intensity						MS/MS count						Sequence coverage						Unique peptides						Protein ID
	wt			Vel2$^{\Delta IDD}$			wt			Vel2$^{\Delta IDD}$			wt			Vel2$^{\Delta IDD}$			wt			Vel2$^{\Delta IDD}$			
	1	2	3	1	2	3	1	2	3	1	2	3	1	2	3	1	2	3	1	2	3	1	2	3	
Found in 4/4	NaN	NaN	NaN	30,13	29,43	31,25	0	0	0	30	22	39	0	0	0	29,1	27,8	25,9	0	0	0	13	14	17	VDAG_JR2_Chr3g06150a-00001(Vel2)
	NaN	NaN	NaN	27,27	26,35	26,26	0	0	0	14	14	9	0	0	0	21,2	35	20,3	0	0	0	9	12	8	VDAG_JR2_Chr7g04890a-00001(Vel1)
	24,02	24,20	23,89	25,35	25,27	25,49	6	4	4	14	14	15	4,1	2,6	3,1	9,8	11,6	12,8	6	4	4	13	14	15	VDAG_JR2_Chr3g00330a-00001
	23,95	24,00	24,11	25,05	25,24	24,91	2	3	3	7	13	7	4,3	5,5	6,9	14,2	21,3	14,5	2	3	3	5	11	7	VDAG_JR2_Chr1g15440a-00001
	NaN	NaN	NaN	23,94	24,41	24,51	1	1	2	2	2	3	13	13	19	13	13	19	1	1	2	1	1	2	VDAG_JR2_Chr5g05430a-00001
	NaN	NaN	NaN	24,67	25,00	24,11	1	0	1	6	8	7	3,9	0	1,8	15,1	13,3	15,3	1	0	1	6	6	7	VDAG_JR2_Chr2g07820a-00001
	NaN	NaN	NaN	23,98	24,43	23,93	2	2	1	8	11	5	2,3	2,3	1,4	6,5	11,2	5,6	2	2	1	7	10	6	VDAG_JR2_Chr2g02140a-00001
Found in 3/4	22,93	NaN	NaN	24,06	24,11	24,52	4	1	1	3	3	4	19,8	8,3	7,5	22,2	19,8	26,2	3	1	1	3	3	4	VDAG_JR2_Chr3g13120a-00001
	NaN	NaN	NaN	23,85	23,45	23,95	0	1	1	2	3	2	0	6,4	4,1	13,9	17,3	10,5	0	1	1	2	3	2	VDAG_JR2_Chr1g06660a-00001
	NaN	NaN	NaN	24,05	24,51	23,86	2	0	0	2	6	5	3,2	0	1,3	4,5	8,7	8,9	2	0	1	2	5	5	VDAG_JR2_Chr5g06420a-00001
	NaN	NaN	NaN	24,13	23,58	23,41	1	0	0	3	4	3	4,2	0	0	20,7	22,7	17,5	1	0	0	4	4	3	VDAG_JR2_Chr8g07560a-00001

23 32

Log2(x)LFQ intensity

List of Figures

List of Tables

List of Appendices

Abbreviations

%	percent
5’	upstream flanking region
3’	downstream flanking region
α	antibody
°C	degree Celsius
Δ	deletion
λ	wavelength
µg	microgram
µl	microliter
µm	micrometer
µmol	micromol
aa	amino acid(s)
AG	Aktiengesellschaft
AG & Co. Kg	Kommanditgesellschaft auf Aktien
AMP^R	ampicillin resistance marker cassette
APS	ammonium persulfate
AS	acetosyringone
ATMT	*Agrobacterium tumefaciens*-mediated transformation
ATP	adenosine triphosphate
BLAST	basic local alignment search tool
bp	base pair(s)
CDM	Czapek-Dox medium
cDNA	Complementary DNA
CFU	colony-forming units
cm	centimeter(s)
C-terminus	carboxy terminus
DAPG	2,4-diacetylphloroglucinol
dH_2O	deionized water
DHN	1,8-dihydroxynaphthalene
DIC	differential interference contrast
DNA	deoxyribonucleic acid
d	day(s)
dpi	days post infection
DSMZ	Deutsche Sammlung von Mikroorganismen und Zellkulturen
DTT	dithiothreitol
ECL	enhanced chemiluminescence
EDTA	2,2',2'',2'''-(Ethane-1,2-diyldinitrilo)tetraacetic acid
et al.	et alii (and others)
FAD	falvin adenine dinucleotide
FGSC	Fungal Genetics Stock Center
g	gram
gDNA	genomic DNA
GEN^R	geneticin resistance marker cassette
GFP	green fluorescent protein
GmbH	Gesellschaft mit beschränkter Haftung
GOI	gene of interest
^{P}GPDA	*A. nidulans* glyceraldehyde-3-phosphate dehydrogenase promoter
H_2O_2	hydrogen peroxide
h	hours
HCN	hydrogen cyanide
HPLC	high performance liquid chromatography

HOG	high osmolarity glycerol
HYG^R	hygromycin B resistance marker cassette
IDD	intrinsically disordered domain
KAN^R	kanamycin resistance marker cassette
kb	kilobase(s)
kDA	kilo Dalton
KGaA	Kommanditgesellschaft auf Aktien
l	liter
LB	lysogeny broth
LC-MS	liquid chromatography-mass spectrometry
L-DOPA	L-3,4-dihydroxyphenylalanine
LFQ	label-free quantification
LS	lineage specific
M	molar
MAPK	mitogen activated protein kinase
mer	meros (part)
MES	2-(*N*-morpholino)ethanesulfonic acid
mg	milli gram(s)
min	minute(s)
ml	milliliter(s)
mm	millimeter(s)
mM	millimolar
mRNA	messenger RNA
ms	millisecond(s)
n	number of elements
NADP	nicotinamide adenine dinucleotide phosphate
NAT^R	nourseothricin resistance marker cassette
NES	nuclear export signal
NF-κB	nuclear factor kappa-light chain-enhancer of activated B cells
NLP	necrosis and ethylene-inducing peptide 1-like protein
NLS	nuclear localization signal
nm	nanometer
ns	non-significant difference
N-terminus	amino terminus
OD	optical density
OE	overexpression
ORF	open reading frame
PAGE	polyacrylamide gel electrophoresis
PC	positive control
PCR	polymerase chain reaction
PDA	photodiode array detection analysis
PDM	potato dextrose medium
PEST	peptide sequence rich in proline (P), glutamic acid (E), serine (S) and threonine (T)
PMSF	phenylmethylsulfonyl fluoride
PTM	posttranslational modifications
p-value(s)	probability value(s)
RFP	red fluorescent protein
RHD	Rel homology domain
ROS	reactive oxygen species
rpm	revolutions per minute
RNA	ribonucleic acid
sec	second(s)
SDS	sodium dodecyl sulfate
SIM	single ion monitoring
SISA	Simple Interactive Statistical Analysis

SOC	super optimal broth supplemented with glucose
spp.	species
SXM	simulated xylem medium
TAD	transcription activation domain
TAE	Tris-acetate-EDTA buffer
TBST	Tris buffered saline with Tween20
TEMED	N,N,N′,N′-tetramethylethan-1,2-diamine
TFA	trifluoroacetic acid
THN	tetrahydroxynaphthalene
Tris	2-Amino-2-hydroxymethyl-propane-1,3-diol
^{P}*TRPC*	*A. nidulans* tryptophane biosynthesis gene promoter
TRPC^{T}	*A. nidulans* tryptophane biosynthesis gene terminator
UV	ultra-violet
V	volt
VGB	Verticillium strain collection Gerhard H. Braus
v/v	volume per volume
WD40	structural motif of ca. 40 amino acids, ending with tryptophan-aspartic acid (W-D)
WT	wild type
w/v	weight per volume

Acknowledgements

First, I would like to thank Prof. Dr. Gerhard H. Braus for his support and guidance in the past years and especially within the last phase of my PhD thesis. I really appreciate the fruitful discussions we had, his helpful advices and expertise. In addition, I am grateful for all the conferences and meetings I could attend during my PhD studies.
Secondly, I am very thankful to my Thesis Committee Members Prof. Dr. Andrea Polle and Prof. Dr. Rolf Daniel. Both always contributed to the project with critical advices and auxiliary suggestions during our meetings.
Moreover, I want to thank Prof. Dr. Stefanie Pöggeler, Prof. Dr. Kai Heimel and PD Dr. Michael Hoppert for participation in my Examination board. I am grateful to Prof. Dr. Kai Heimel for sharing his knowledge and equipment. Furthermore, I would like to thank Prof. Dr. Stefanie Pöggeler for helpful discussions during seminars.
I am grateful for the support of the Göttingen Graduate School for Neuroscience, Biophysics and Molecular Biosciences (GGNB). The GGNB office always had everything well organized and was able to help quickly and had helpful advices when anything was unclear. The courses offered were informative and interesting. Financial support of the GGNB enabled me to attend conferences as for instance the 30th Fungal Genetics Conference in Pacific Grove in the United States of America or the 12th International Verticillium Symposium in Ljubljana, Slovenia. During my PhD studies I was part of the GGNB program Genes and Development. Within this program we had nice discussions during our meetings and retreats and I am thankful for having met PhD students from various research fields.
During the last years I had the pleasure to work with the Verticillium group including Rebekka Harting, Nicole Scheiter, Miriam Leonard, Jessica Starke, Alexandra Nagel, Isabel Maurus and Tri-Thuc Bui. I am very thankful for the time we spend together and grateful that we have met each other. Within the past years we were not just able to generate nice data and publish it, we also had nice evenings with (self-made) cocktails, BBQs with wine and nice dinners whenever we could celebrate the publication of a paper. I especially want to thank Rebekka for all the support during my thesis particularly during the last phase. Rebekka not just explained me everything about Verticillium with patience but also discussed with me my data or provided technical support during experiments. It was always a pleasure to work with her. I am thankful for the nice time we spend and for careful proofreading of my thesis. Although it is quite a while ago that Miriam and I worked together at our bench, I am happy that she has (nearly) always been by my side. Thank you for your helping hands and nice talks during incubation times. Whenever I was not working in the laboratory but in the office, I was thankful to have Jessica by my side. Thank you for informative discussions about our results and encouraging words when experiments failed. Miriam and Jessica started their PhD shortly

before me and I am thankful for all the advices they gave to me and all the solutions we found together. I would also like to thank Nicole for her excellent technical support and her outstanding and kind manner. In addition, I am thankful to Alexandra and Isabel for their support during experiments and discussions. Moreover, I am also grateful to Miriam, Jessica, Alexandra and Isabel for proofreading of my thesis. I am thankful to Thuc for sharing his expertise and protocols with me.

Furthermore, I would like to explain my gratefulness to Nils F. Aßmann, Hager Elsheikh, Gloribel Argelis Vergara Guerrero and Christian Wickbold, who joined my project either for a lab rotation or a Master thesis and helped me a lot. In particular, I would like to thank Nils F. Aßmann, who helped me a lot with the last experiments within my thesis and had critical comments whenever needed.

Kerstin Schmitt and Oliver Valerius helped me to design pull down experiments, measured the samples and introduced me into the data analysis of my results. Thank you very much for all the discussions and explanations about LC-MS analysis.

I would like to thank Jennifer Gerke for introducing me into the analysis of secondary metabolites. Thank you very much for help with the experimental design, the measurement of all my samples, the advices regarding data analysis and the patience when answering all my questions.

Moreover, I am thankful to Cindy Meister and Anna M. Köhler for not just sharing protocols but also having nice discussions and helpful advices regarding protein pull downs. I am grateful to Sabine Thieme for sharing her knowledge about the intrinsically disordered domain of VelB with me. Fruzsina Bakti and Anja Strohdiek deserve a special thank for always having an open ear for discussions or an encouraging smile whenever needed.

Susanna A. Braus-Stromeyer and Tuan Tran are gratefully acknowledged for initiating the work on velvet domain proteins in *V. dahliae*.

Moreover, I am thankful to all current and former members of the department of “Molecular Microbiology and Genetics” for the nice working atmosphere and the talks and discussions we had. Especially I am grateful to Heidi Northemann for all the administrative issues and her help whenever needed. Furthermore, I like to highlight the perfect technical assistance in the everyday lab work and management of the orderings done by Andrea Wäge, Gabriele Heinrich, Verena Große, Anna Dudek and Nicole Scheiter.

My family and friends who always supported and encouraged me deserve a special gratitude. I am thankful for always having you by my side and I am sure that all members of my family who could not stay with me always had an eye on me.

Lastly, I would like to thank my husband Sebastian for his support, patience and motivation particularly in the last year.